2018

Biofabrication of Three-Dimensional Neural Tissue Constructs from Human Induced Pluripotent Stem Cells

Tom Barsby
University of Wollongong

Biofabrication of Three-Dimensional Neural Tissue Constructs from Human Induced Pluripotent Stem Cells

A thesis submitted in fulfilment of the requirements for the award of the degree of

Doctor of Philosophy

from the

University of Wollongong

Tom Barsby

B.Sc. (Hons) Biochemistry

4931567

November 2018

Declaration

I, Tom Barsby, declare that this thesis, submitted in fulfilment of the requirements for the award of Doctor of Philosophy, in the School of Chemistry, University of Wollongong, is wholly my own work unless otherwise referenced or acknowledged. The document has not been submitted for qualifications at any other academic institution.

Tom Barsby

20th November 2018

Acknowledgements

At times such as these, it is always interesting to look back on the path that was taken, the decisions made and the contacts formed; to fully comprehend the journey as it comes to a close. To that end, I would like to gratefully acknowledge Profs. Rob Kapsa, Jeremy Crook and Gordon Wallace for giving me the opportunity to pursue this project as a member of their research teams. I would also like to thank the full ACES SBS team around Wollongong and beyond, for always offering advice and feedback on new ideas and experiments.

I am also indebted to the work and input of many post-doc researchers around St. Vincent's, namely Anita Quigley, Carmine Onofrillo, Serena Duchi, and Cathal O'Connell, who have all helped me out more times than I can count. As my PhD progressed, so increased the number of students involved in collaborative projects. For helping keep me sane, chat about ideas, and generally be a good bunch of people I would like to thank Catherine, Ita, Uma, Min, and Bijan. I wish you all the best in your projects and future endeavours!

Finally, no acknowledgements would be truly complete without mentioning Ruby, who for the past 4 years has kept me fed, lightly watered and respectably clothed through good times and bad. The submission of this work also signals the start of new and exciting adventures with her.

"And so it goes…"

-Kurt Vonnegut

Abstract

The human brain is arguably one of the most complex structures known to humankind. To understand the development, function, and dysfunction of this organ, both historical and modern neurological research methods have intrinsic limitations. Modern functional imaging and electrophysiological techniques obtain important data on the structural and functional aspects of specific brain regions but are unable to accumulate biomolecular information, whereas animal models of brain development allow for complete molecular interrogation, but show intrinsic morphological differences compared to native human brain tissue. *In vitro* modelling of human brain tissue through the differentiation of induced pluripotent stem cells (iPSCs) offers a completely novel method of studying human brain development. iPSCs can differentiate into any somatic cell derived from the three germ layers, and as such, can form cells of specific neural lineages from multiple brain regions. Furthermore, this differentiation *in vitro* follows the same principles of *in utero* brain development, and so can be used to model specific genetically-linked neurodevelopmental pathologies such as the epilepsies.

Neural cell differentiation within three-dimensional cell culture scaffolds offers a way of replicating a more *in vivo*-like microenvironment compared to standard planar culture. Therefore, the generation and optimisation of cytocompatible biomaterials to form these three-dimensional scaffolds will be integral for the future of *in vitro* neural tissue engineering.

This thesis focuses on the combination of both biomaterial engineering and iPSC-based neurological development to assess the synergy of targeted neuronal cell differentiation within three-dimensional hydrogel environments.

Comparisons between alginate-based and collagen type I-based hydrogel scaffolds (with stiffness moduli comparable to that of native brain tissue) demonstrated both scaffold types retained high cell viability of encapsulated neural cells. However, only collagen-based scaffolds were shown to be conducive to neurite extension, whereas neural cells within alginate scaffolds displayed no neuritogenesis under differentiating conditions. Alginate hydrogels modified with matrix metalloproteinase-cleavable and laminin-binding epitopes were also non-conducive to neurite extensions but did induce changes in neural-marker protein expression profiles of encapsulated neural cells relative to those within unmodified alginate and collagen hydrogels.

Human iPSCs (hiPSCs) were successfully differentiated into dorsal forebrain (excitatory) and ventral forebrain (inhibitory) neural lineages. Biomolecular analyses over the timeline of differentiation uncovered differences in the speed of neural differentiation and expression of maturation markers. Neurons derived from ventral differentiation pathways displayed enhanced functional profiles relative to neurons generated through dorsal differentiation strategies.

Neural differentiation of hiPSCs in three-dimensional collagen-based hydrogel environments enabled extensive neuritogenesis throughout the constructs. Gene expression analyses during neural induction and differentiation demonstrated significant differences in the maturation rates of hiPSC-derived neurons in three-dimensional environments relative to two-dimensional planar culture.

Finally, in order to generate more complex three-dimensional neural tissue structures using bioprinting methodologies; optimisation strategies to improve the printability of candidate biomaterials were developed. A coaxial bioprinting system was utilised by which to achieve a low stiffness “core” bioink that maintained neural differentiation and neuritogenesis, and a supportive “shell” hydrogel that generated enough structural integrity by which to bioprint multi-layered free-standing neural constructs.

In combination, the work presented in this thesis demonstrates the necessary biological assays for measuring positive markers of neural differentiation in candidate three-dimensional hydrogels and applies this knowledge to better understanding neural differentiation of hiPSCs within these environments. It also establishes a 3D coaxial bioprinting system by which to scale-up and tailor neural tissue construct design to generate *in vitro* neurological models more representative of native neural tissue.

Table of Contents

List of Figures

List of Tables

Papers in Preparation

Barsby, T., Quigley, A., Wallace, G.G. & Kapsa, R. (*In Preparation*) Neurons à la Carte: Differentiating Specific Neural Lineages from Pluripotent Stem Cells.

Barsby, T., Quigley, A., Duchi, S., O'Connell, C., Bourke, J., Crook, J., Wallace, G.G. & Kapsa, R. (*In Preparation*) Comparative Analysis of Alginate and Collagen Hydrogels as Three-Dimensional Neural Tissue Scaffolds.

Barsby, T., Quigley, A., Bourke, J., Crook, J., Wallace, G.G. & Kapsa, R. (*In Preparation*) Comparison of Forebrain Excitatory and Inhibitory Neural Differentiation from Human iPSCs in Two-Dimensional and Three-Dimensional Hydrogel Scaffolds

List of Abbreviations

2D	Two-Dimensional
3D	Three-Dimensional
Alg	Sodium Alginate
AMPAR1	α-Amino-3-hydroxy-5-Methyl-4-isoxazolePropionic Acid Receptor
ANOVA	Analysis of Variance
BDNF	Brain-Derived Neurotrophic Factor
β-III-T	Beta III Tubulin
BMP	Bone Morphogenetic Protein
cAMP	Cyclic Adenosine Monophosphate
cDNA	Complementary DNA
CGE	Caudal Ganglionic Eminence
CNS	Central Nervous System
CNTF	Ciliary Neurotrophic Factor
Coll	Collagen Type I
DAPI	4',6-Diamidino-2-Phenylindole
DAPT	N-[N-(3,5-Difluorophenacetyl)-L-alanyl]-S-phenylglycine t-butyl ester
DG	Dentate Gyrus
DKK-1	Dickkopf-1
DMEM	Dulbecco's Modified Eagle Media
DNA	Deoxyribonucleic Acid
DRG	Dorsal Root Ganglia (-on)
ECL	Cell Attachment Matrix (Entactin-Collagen IV-Laminin)
ECM	Extracellular Matrix

EDC	1-Ethyl-3-(3-dimethylaminopropyl)carbodiimide
EGF	Epidermal Growth Factor
ESC	Embryonic Stem Cell
F12	Nutrient Mixture F-12
FBS	Foetal Bovine Serum
FGF	Fibroblast Growth Factor
FACS	Fluorescence-Activated Cell Sorting
GABA	γ-AminoButyric Acid
$GABA_AR1$	GABA-A Receptor 1
$GABA_BR1$	GABA-B Receptor 1
GAD65/67	Glutamate Decarboxylase 65/67
GALC	Galactosylceramidase
GAP43	Growth Associated Protein 43
GAPDH	Glyceraldehyde 3-phosphate dehydrogenase
GAT1	GABA transporter 1
GDF	Growth Differentiation Factor
GDNF	Glial Cell Line-Derived Neurotrophic Factor
GelMA	Gelatin Methacrylate
GFAP	Glial Fibrillary Acidic Protein
h- *(prefix)*	Human
HA	Hyaluronic Acid
HAMA	Hyaluronic Acid Methacrylate
HBSS	Hank's Buffered Saline Solution
HEPES	N-(2-Hydroxyethyl) piperazine-N'-(2-ethanesulfonic acid)

HPRT1	Hypoxanthine Phosphoribosyltransferase 1
HRP	Horseradish Peroxidase
HS	Horse Serum
IGF-1	Insulin-like Growth Factor 1
iPSC	Induced Pluripotent Stem Cell
JAG-1	Jagged-1
Klf4	Kruppel-like factor 4
LGE	Lateral Ganglionic Eminence
LIF	Leukaemia Inhibitory Factor
m- *(prefix)*	Mouse/Murine
MAP2	Microtubule Associated Protein 2
MES	2-(N-morpholino)ethanesulfonic acid
MGE	Medial Ganglionic Eminence
MMP	Matrix Metalloproteinase
MN	Motor Neuron
mRNA	Messenger Ribonucleic Acid
NE	Neuroepithelia
NEP	Neuroepithelial Progenitor
NES	Neuroepithelial Stem Cell
NF-H	Neurofilament Heavy chain
NF-L	Neurofilament Light chain
NGF	Nerve Growth Factor
Ngn-2	Neurogenin-2
NIM	Neural Induction Media

NKX2.1 NK2 homeobox 1

NMM Neural Maturation Media

NMDAR1 N-Methyl-D-Aspartate Receptor 1

NPC Neural Precursor Cell

NPM Neural Proliferation Media

NSC Neural Stem Cell

Oct4 Octamer-binding transcription factor 4

Pax6 Paired box protein 6

PBS Phosphate Buffered Saline

PC12 Pheochromocytoma-12 *(Cell Line)*

PCL Polycaprolactone

PD Parkinson's Disease

PDGF Platelet-Derived Growth Factor

PDMS Polydimethylsiloxane

PEG Polyethylene Glycol

PLL Poly-lysine and Laminin

P-MAP2 Phospho-MAP2-Ser136

POL Poly-ornithine and Laminin

PPy Polypyrrole

PSC Pluripotent Stem Cell

PSD95 Post-Synaptic Density 95

Pur Purmorphamine

qPCR Quantitative Polymerase Chain Reaction

RA Retinoic Acid

RNA	Ribonucleic Acid
SAP	Self-Assembling Peptide
SATB2	Special AT-rich sequence-binding protein 2
SDIA	Stromal-cell Derived Inducing Activity
S.E.M.	Standard Error of the Mean
SFEB(q)	Serum-free Floating culture of Embryoid Body-like aggregates
SHH	Sonic Hedgehog
Sox2	SRY (sex determining region Y)-box 2
SPIE	Stromal cell derived factor 1, Pleiotrophin, Insulin-like growth factor 2, Ephrin-B1
Sulfo-NHS	Sulfo N-hydroxysulfosuccinimide
Syn	Synaptophysin
T3	Triiodothyronine
TBR1	T-box, brain, 1
TBS	Tris Buffered Saline
TBST	Tris Buffered Saline with 0.05% Tween-20
TF	Transcription Factor
TH	Tyrosine Hydroxylase
UV	Ultraviolet
VGLUT	Vesicular Glutamate Transporter
Wnt	Wingless-type MMTV integration site

Conference Presentations

Barsby, T., Quigley, A., Duchi, S., Bourke, J., Crook, J., Wallace, G.G. & Kapsa, R. (2017) Oral Presentation – "Studying the Brain Without Studying the Brain: 3D Neural Constructs from Human iPSCs" Neural Modelling Workshop, Wollongong, NSW (3 Oct 2017)

Barsby, T., Quigley, A., Duchi, S., Bourke, J., Crook, J., Wallace, G.G. & Kapsa, R. (2017) Poster Presentation – "Studying the Brain Without Studying the Brain: 3D Neural Constructs from Human iPSCs" Biomimetics, Artificial Muscles and Nano-Bio (BAMN) Conference, Wollongong, NSW (25-27 Sep 2017)

Barsby, T., Quigley, A., Duchi, S., Bourke, J., Crook, J., Wallace, G.G. & Kapsa, R. (2017) Poster Presentation – "Studying the Brain Without Studying the Brain: 3D Neural Constructs from Human iPSCs" Aikenhead Centre for Medical Discovery (ACMD) Research Week, Melbourne, VIC (7-11 Aug 2017)

Barsby, T., Quigley, A., Bourke, J., Crook, J., Wallace, G.G. & Kapsa, R. (2017) Poster Presentation – "Studying the Brain Without Studying the Brain: 3D Neural Constructs from Human iPSCs" Australasian Society for Stem Cell Research (ASSCR) Annual Meeting, Sydney, NSW (24-26 May 2017)

Barsby, T., Quigley, A., Bourke, J., Crook, J., Wallace, G.G. & Kapsa, R. (2017) Poster Presentation – "Biomaterial Optimisation for 3-Dimensional Neural Tissue Constructs" Australasian Society for Biomaterials and Tissue Engineering (ASBTE) Annual Meeting, Canberra, ACT (18-20 April 2017)

Barsby, T., Quigley, A., Bourke, J., Crook, J., Wallace, G.G. & Kapsa, R. (2017) Oral Presentation and Poster Presentation (Best Poster Prize Winner) – "Studying the Brain Without Studying the Brain: Turning Stem Cells into Brain Cells" 12th International Electromaterials Symposium, Wollongong, NSW (8-10 Feb 2017)

Barsby, T., Quigley, A., Bourke, J., Crook, J., Wallace, G.G. & Kapsa, R. (2016) Poster Presentation – "Neurons Ex Machina: 3D In Vitro Models of Neurological Development from Human iPSCs" Australasian Society for Stem Cell Research (ASSCR) Annual Meeting, Margaret River, WA (4-6 Dec 2016)

Barsby, T., Quigley, A., Bourke, J., Crook, J., Wallace, G.G. & Kapsa, R. (2016) Poster Presentation (Poster Prize Winner) – "Neurons Ex Machina: 3D In Vitro Models of Neurological Development from Human iPSCs" BioMedLink Conference, Melbourne, VIC (4 Nov 2016)

Barsby, T., Quigley, A., Bourke, J., Crook, J., Wallace, G.G. & Kapsa, R. (2016) Poster Presentation – "Neurons Ex Machina: 3D In Vitro Models of Neurological Development from Human iPSCs" Aikenhead Centre for Medical Discovery (ACMD) Research Week, Melbourne, VIC (Aug 2016)

Barsby, T., Quigley, A., Bourke, J., Crook, J., Wallace, G.G. & Kapsa, R. (2016) Oral Presentation – "Neurons Ex Machina: 3D In Vitro Models of Neurological Development from Human iPSCs" Centres of Excellence Joint Conference, Queenstown, NZ (July 2016)

Barsby, T., Quigley, A., Bourke, J., Crook, J., Wallace, G.G. & Kapsa, R. (2016) Poster Presentation – "Neurons Ex Machina: 3D In Vitro Models of Neurological Development from Human iPSCs" 11th International Electromaterials Symposium, Melbourne, VIC (10-12 Feb 2016)

Chapter 1: General Introduction

1.1 Background and Potential of Induced Pluripotent Stem Cells in Neurological Research

1.1.1 Neurons Ex Machina

The human brain is arguably one of the most complex structures known to humankind. Recent estimations of its cellular content put the total neuronal number at approximately 86 billion cells, with estimated numbers of synaptic connections between these cells well into the trillions (Pakkenberg *et al.*, 2003; Azevedo *et al.*, 2009). Studies of human brain development, function, and disease have historically been undertaken through an array of methodologies including: posthumous observation, utilising electrophysiological & non-invasive imaging techniques, and/or with the use of animal models. However, intrinsic differences between animal and human models of neurological diseases have resulted in poor rates of clinical translation and development of novel therapeutics (Matthews *et al.*, 2005; Kelava and Lancaster, 2016; Mungenast, Siegert and Tsai, 2016). To overcome this species gap *in vitro* models of brain development and disease derived from human stem cell populations offer more clinically-representative models from which to generate healthy and disease-state neural tissue for study.

Induced pluripotent stem cells (iPSCs) have revolutionised and rejuvenated the field of stem cell science since their inception just over a decade ago (Takahashi and Yamanaka, 2006). Broadly speaking, stem cells all share two basic properties; the first is the ability to self-renew through cell division and the second is to differentiate into other cell types. The number of cell types a stem cell can differentiate into is based on their "potency". For example, bone marrow, in basic terms, is a large pool of *multi*potent stem cells that replenish the diverse subtypes of blood and immune cell lineages. *Pluri*potent stem cells (PSCs) can turn into any cell type derived from the three germ layers, and as such in nature primarily exist at the very early developmental stages of viable embryos. Extraction of cells from human blastocysts and their successful culture *in vitro* was the first

stepping stone into the long term culture and use of PSCs as models of understanding pluripotency, human tissue development, and potential uses in regenerative medicine (Thomson *et al.*, 1998). These embryonic stem cells (ESCs), were and still are, an incredibly powerful type of stem cell that remain as the benchmark for *in vitro* pluripotency research. However, the necessity of harvesting them from early human embryos offered a logistical and ethical challenge to their widespread use.

ESCs remained the gold standard for *in vitro* PSC research, until a seminal paper from Takahashi and Yamanaka in 2006 showed the first induction of pluripotency in differentiated murine somatic cells through ectopic expression of four pluripotency-related factors (Takahashi and Yamanaka, 2006). From an initial twenty-four candidate genes the authors found that a combination of the factors; Oct4, Sox2, c-Myc, and Klf4 was sufficient to induce a state of pluripotency in formerly differentiated murine fibroblasts. These cells were termed induced pluripotent stem cells (iPSCs). This research was later repeated with human cell sources with the same " Yamanaka factors" (Takahashi *et al.*, 2007), and with a different cocktail of factors (Oct4, Sox2, Nanog, and Lin28) (Yu *et al.*, 2007). These human iPSCs (hiPSCs) represented an incredible breakthrough in the field of stem cell research and disseminated a logistically simple way of reprogramming somatic cell types into PSCs without the ethical concerns of utilising ESC-derived cell lines. Another striking advantage to the use of hiPSCs is the ability to induce pluripotency in cells that are genetically identical to the cell source donor, creating the potential for rejection-free tissue regenerative therapies, genetically-linked disease modelling, developmental biology studies, and pharmacological testing on a patient-specific basis *in vitro*. This wide array of possible applications has resulted in a large volume of research in only a few years

In short, the advent of this technology stands to remove a number of hurdles that had plagued stem cell research; namely issues of immune rejection, ethical concerns associated with utilising embryo-derived ESCs, and those of limited stem cell potency of somatic stem cell populations. The promise of iPSCs therefore lies in the relative ease of their generation from a spectrum of adult tissues, the promise of autologous regenerative therapies, and the lack of ethical concern with their derivation. In essence, they have the capacity to combine the advantages of both somatic stem cells and ESCs.

The advantages discussed above have also spearheaded the use of hiPSCs in neurological research. The desire to develop *in vitro* patient-specific models of neurodevelopmental and neurodegenerative disease has resulted in vast swathes of

research for dozens of disorders (Mattis and Svendsen, 2011; Israel *et al.*, 2012; Dajani *et al.*, 2013; Imaizumi and Okano, 2014; Okano and Yamanaka, 2014). In parallel to this, research into human-specific neurodevelopment from "healthy" hiPSCs has begun to shed light on how brain tissue and regional brain structures form *in utero* and allow an unprecedented view into the regulation of these processes *in vitro* (Petros, Tyson and Anderson, 2011; Anderson and Vanderhaeghen, 2014; Kelava and Lancaster, 2016). As this field of research continues to refine and expand, the potential scope for understanding numerous aspects of human neurobiology is remarkable.

That being said, no current iPSC-based neurological model is perfect, and potential limitations or problems with iPSC technology such as line-to-line differentiation variability (Hu *et al.*, 2010), epigenetic or lineage memory (K. Kim *et al.*, 2011), and chromosomal aberrations (Mayshar *et al.*, 2010) are well documented. Even so, numerous usable and statistically sound models of neurological disease have been already documented from disease-specific iPSCs (Israel *et al.*, 2012; Lancaster *et al.*, 2013; Duan *et al.*, 2014; Okano and Yamanaka, 2014; Mariani *et al.*, 2015). Care must be therefore taken to ensure that robust, reproducible and ultimately representative iPSC-derived neural cell cultures are generated for each aspect of neurobiology under scrutiny.

Each stage of iPSC-technology can be tailored to the needs of the study being undertaken. This includes the source of somatic cells for reprogramming (e.g. fibroblasts, peripheral blood progenitors or epithelial-like cells from urine samples) and the type of reprogramming vectors used to either improve reprogramming efficiency or maintain genomic integrity. Neural induction and differentiation methodologies vary from study to study, utilising diverse morphogen signalling and/or forced neuronal transcription factor expression. Each method yielding differentially heterogeneous pools of cells that can be demonstrative of the *in vivo* processes these protocols aim to mirror. Finally, culture in biomimetic 2D or 3D environments can allow enhancement of neural differentiation, promotion of neural outgrowth and modulation of cell-cell synaptic activity. Each level of this process can help to build reproducible and physiologically relevant neurological models to help elucidate the true goal of iPSC-neural modelling: unearthing the processes of neurodevelopment and the aberrations leading to neurological disease.

The ability to derive a patient-specific pluripotent cell line opens an entirely new pathway for dissecting the pathology of diseases that were either impractical or impossible to study extensively *in vivo*. This is especially true in the field of neuroscience, and most

notably in the study of neurodegenerative and neurodevelopmental conditions (Marchetto *et al.*, 2011; Mattis and Svendsen, 2011; Okano and Yamanaka, 2014). The ability to have a continuous, genetically relevant supply of neurons from patients with a specific neurological condition offers the chance to study the pathology of genetically-linked disorders throughout development *in vitro*; an impossibility in patients with late-onset conditions such as Parkinson's Disease, Alzheimer's Disease and Huntington's Disease (Imaizumi and Okano, 2014).

As well as degenerative conditions, iPSCs offer the chance to study early *in utero* developmental pathways and formation of embryological neural structures, such as human corticogenesis, which show inherent differences to animal models (Anderson and Vanderhaeghen, 2014). Understanding the formation (or malformation) of particular brain regions with the associated cytoarchitecture and neuronal diversity, will shed light on the temporal and spatial control of tissue generation, and offer insights into treatments of developmental disorders as well as human brain evolution.

1.1.2 Somatic Cell Sources and Methods of iPSC Reprogramming

This section will focus on iPSC reprogramming methodologies necessary for successful neurological development and disease modelling. Primarily, the generation of integration-free and genomically "clean" iPSC lines as well as concerns for cell type selection for reprogramming; an area often overlooked in iPSC studies but an important consideration when long term and multiple clinical samples are to be processed. A large collection of general iPSC-derivation reviews are present throughout the literature (Maherali and Hochedlinger, 2008; González, Boué and Izpisúa Belmonte, 2011; Bayart and Cohen-Haguenauer, 2013), this section will therefore represent a targeted review of the abundant sources available.

Reprogramming vectors can be broadly classified into 2 types: viral and non-viral (Fig 1-1). Viral vectors can then be sub-classified into integrating vectors, such as gamma-retroviruses (Takahashi and Yamanaka, 2006; Takahashi *et al.*, 2007; Yu *et al.*, 2007) & lentiviruses (Carey *et al.*, 2009; Chang *et al.*, 2009), and non-integrating (or transient) vectors such as adenoviruses (Stadtfeld *et al.*, 2008; Zhou and Freed, 2009) & Sendai virus (Fusaki *et al.*, 2009). Although reported reprogramming efficiencies for viral integrating vector types are higher than the non-integrating vectors, they result in random integration

of the reprogramming factors into the target genome. This has implications for neurological-focused iPSC-derived modelling where genomic integrity may be key for understanding complex neurological pathologies: ensuring no genes are disrupted for certain lineage specifications and to make certain no oncogenic gene transformations have been generated (Bayart and Cohen-Haguenauer, 2013). For any regenerative applications, the presence of tumourigenic mutations or the *in vivo* reactivation of integrated pluripotency factors could be catastrophic. Some groups have tried to reduce the impact of integrative reprogramming elements by generating an excisable vector system that after generating a stable pluripotency shift within the target cells, can then be excised from the genome (Chang *et al.*, 2009; Soldner *et al.*, 2009). While this methodology would in theory excise potentially oncogenic effects (through over-expression of genes such as c-Myc), it would still risk the generation of unforeseen recombination events that, in and of themselves, may damage the overall genomic stability of the target cell.

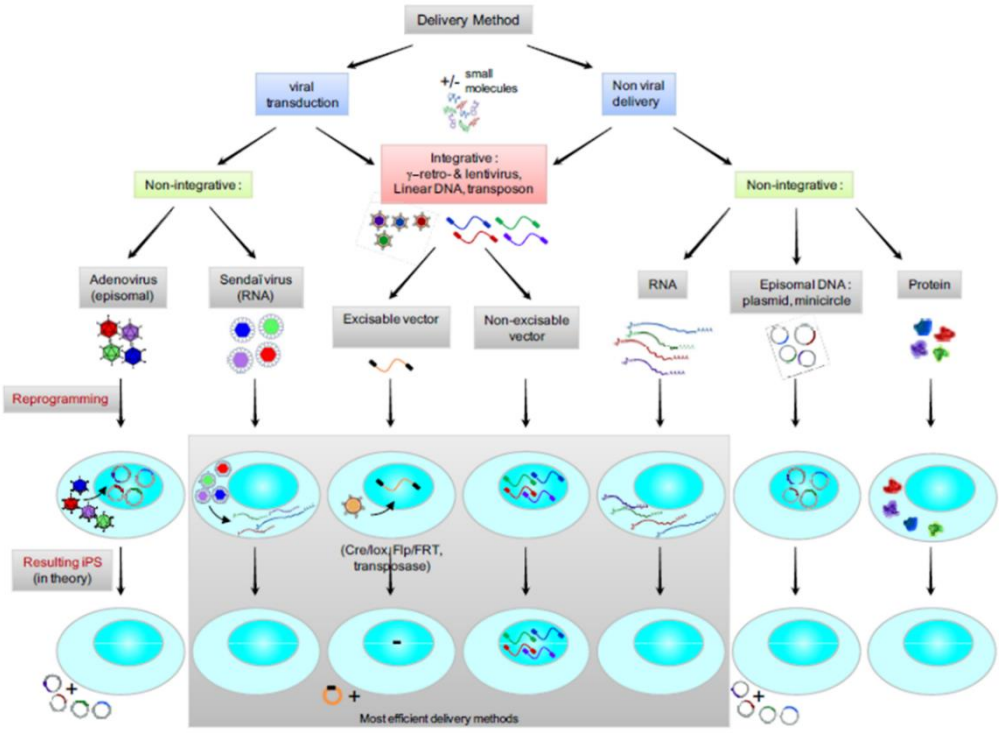

Fig 1-1: Representation of strategies used for iPSC reprogramming of somatic cell types. *Illustration from Bayart & Cohen-Haguenauer 2013*.

Non-viral vectors offer an alternative transient system of delivery for the reprogramming factors. Such vectors include the transfection of the factors encoded in plasmids (Okita *et al.*, 2008) or more stable episomal vectors (Yu *et al.*, 2009). These vectors would generate the advantageous genomically "clean" iPSC lines, but reportedly do so at a lower efficiency than retroviral vectors (Yu *et al.*, 2009). More recently, techniques have been developed to generate insertion-free iPSC lines without using DNA-based vectors. Instead they utilise either synthetic messenger RNA (mRNA) constructs of each pluripotency factor (Warren *et al.*, 2010) or the reprogramming proteins themselves (Kim *et al.*, 2009; Zhou *et al.*, 2009). The relatively high reprogramming efficiency of the mRNA-based technique makes them an appealing non-viral option for iPSC derivation. However, for multiple and ongoing iPSC banking projects, the cost of obtaining high amounts of synthetic mRNA may be a consideration. Reprogramming via use of the reprogramming proteins themselves as proof of principle is a very interesting result, however the very low efficiency of iPSC generation would not make them an ideal go-to methodology for general *de novo* iPSC banking and modelling projects (Fig 1-1).

Another concern for deriving *de novo* iPSC lines is the choice of adult cell type to undergo reprogramming. For many disease modelling studies this is a commonly overlooked consideration, with the majority (approximately 80%) of published *de novo* iPSC lines generated from dermal fibroblasts (González, Boué and Izpisúa Belmonte, 2011). This is obviously of little concern in animal studies where tissue selection does not need to represent a clinically relevant situation. However, it should be a factor for research groups hoping to generate multiple disease-specific iPSC lines from human patients. Ideally, the harvesting of cells should be relatively non-invasive and generate a large enough pool of starting cells which can be easily cultured and stored. Fibroblasts have been heavily utilised in iPSC studies because they are a robust and easily expandable cell type. To obtain human dermal fibroblasts a skin punch biopsy must be performed by a trained clinician. Although this procedure is relatively non-invasive it must be performed under local anaesthetic and is still associated with a low risk of nerve injury and infection. Minimising the discomfort of patients while maximising the speed and ease of cell collection should be a principle concern for iPSC-based disease modelling research groups. Especially when studying idiopathic and familial conditions where multiple iPSC-lines need to be generated simultaneously for broad and statistically significant experimental analysis.

Since the seminal iPSC-generation research was first published, many studies have now looked at iPSC-reprogramming of a whole host of somatic cell types, some more clinically useful than others, for obtaining a starting cell pool. Human bone marrow-derived mesenchymal stem cells (BM-MSCs) (Park *et al.*, 2008) and hepatocytes (Liu *et al.*, 2010) have been reprogrammed into iPSCs, but with the obvious disadvantage of a much more invasive harvesting process than simple skin biopsies. Dental pulp stem cells (harvested from deciduous or "baby teeth") are another source of cells that have been used in iPSC generation (Beltrão-Braga *et al.*, 2011). This may not a viable or desirable option in adult patients where the harvesting of this tissue would involve the extraction of teeth (Tamaoki *et al.*, 2010). A promising starting somatic cell pool may be keratinocytes. Although harvested in multiple studies from foreskin, keratinocytes have also been harvested and reprogrammed from hair follicles (Aasen *et al.*, 2008). Cell harvesting in this instance would simply involve a single plucked hair from which to expand the keratinocyte population. A possible issue would be the *very* limited starting cell number, but may be offset by the much higher reprogramming efficiency of keratinocytes - reportedly up to one hundred-fold more efficient and two-fold faster than fibroblast-reprogramming methodologies (Aasen *et al.*, 2008). This is also mirrored by reprogramming of dermal papillae cells (also from hair follicles) which have a reported three-fold increase in reprogramming efficiency relative to dermal fibroblasts (Muchkaeva *et al.*, 2014).

Another promising minimally-invasive method of somatic cell harvest is via peripheral blood collection (Mack *et al.*, 2011; Okita *et al.*, 2013). The obvious advantage to this methodology being that it is widely used in clinical practice for a whole spectrum of diagnostic tests. Within this framework peripheral blood could be collected from patients with no additional harvesting procedure necessary and with minimal discomfort. However, a caveat to this procedure must be the removal of mature immune cells that have undergone V(D)J rearrangements. This genomic rearrangement, although limited to adaptive immunity genes, is not ideal for production of genomically representative iPSC-lines. Hence the peripheral blood-based methodologies tend to selectively make use of CD34+ cells within the blood as a marker of a progenitor cell type that has not undergone this rearrangement.

Finally, another intriguing source of cells for iPSC generation may be those collected from urine samples (Zhou *et al.*, 2012; Xue *et al.*, 2013). Epithelial-like cells obtained through centrifugation of urine offer a completely non-invasive method of cell

harvesting. iPSC-lines derived in this way are still a recent development and as such has not been widely adopted by many research groups, however at least one research group has generated neural progenitors (and consequently mature neurons) from urine-derived somatic cells (Wang *et al.*, 2013).

1.2 Differentiation Strategies for iPSC-derived Neurons

Differentiation protocols to derive neuronal and glial cell subtypes from iPSCs have largely been based on methodologies developed from ESC-differentiation, although differences in neural lineage differentiation efficiency have been documented between the two PSC types (Hu *et al.*, 2010). Multiple varied protocols can be seen throughout the literature that result in neuronal differentiation (or more specific neuronal subtype generation) with varying efficiencies. The time frame for differentiation and neuronal maturation strategies also differs from protocol to protocol and depend on the target-cell-type.

Broadly speaking, the two main methodologies of deriving neurons from iPSCs can be defined as those that utilise developmental morphogens to trigger a step-wise differentiation into neuronal lineages, and those that employ the transfection, and consequent expression, of known neurogenic genes. An overview of the basis for morphogen-derived neuronal patterning and direct transfection of neurogenic genes are outlined below.

1.2.1 *In Vivo* Neural Tube Patterning Factors as a Basis for *In Vitro* Differentiation

Differentiation protocols based around neural tube morphogen patterning take cues from known neurodevelopmental processes and attempt to recapitulate the *in vivo* system by sequential addition of signalling factors *in vitro* to direct specific pathways of differentiation.

The neural tube is an embryonic structure that is the precursor of the central nervous system (CNS). Patterning factor gradients within this structure during development primarily form two axes; the dorsal-ventral axis and anterior-posterior axis (also referred to as the rostral-caudal axis) (Briscoe and Ericson, 2001; Petros, Tyson and Anderson, 2011; Le

Dréau and Martí, 2012). Signalling molecules form gradients within the neural tube that then act to define a precursor cell's neural fate by way of its spatial and temporal location. Different neuronal and glial subtypes will then be generated dependent on the precursor cell's location and therefore its exposure to relative amounts of specific morphogens along the two axes (Fig 1-2). Dorsal-ventral patterning is primarily derived from the interplay of three signalling pathways: Sonic Hedgehog (SHH), members of the Bone Morphogenetic Protein (BMP) family, and the Wingless-type MMTV integration site (Wnt) family. SHH is a ventralising ligand secreted from the floor plate of the neural tube and the notochord (Jessell, 2000), whereas BMPs and Wnts are released from the roof plate and trigger a dorsalising response in target cells (Le Dréau and Martí, 2012). In simple terms SHH signalling can be seen as a mechanism to derive ventral neural tube identity (and therefore ventrally-derived neuronal cell types) while BMP and Wnt signalling drive dorsal neural tube identity (and conversely a dorsally-derived neuronal lineage differentiation) (Briscoe and Ericson, 2001; Le Dréau and Martí, 2012).

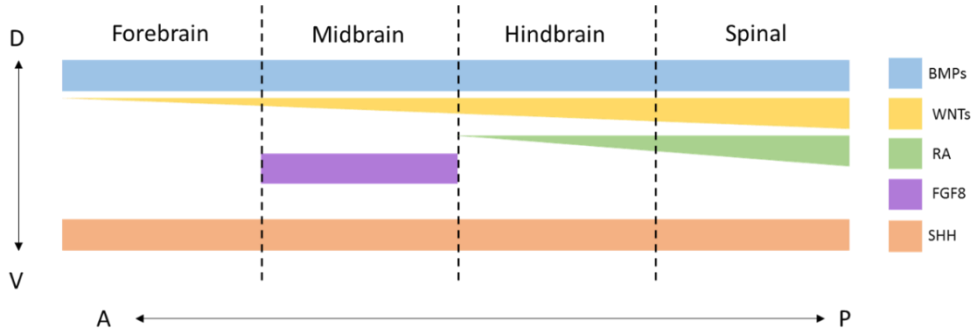

Figure 1-2: Representation of morphogen gradients in the neural tube during embryological development of the central nervous system. Combinations of factors generate a dorsal-ventral (DV) axis and anterior-posterior (AP) axis. The spatial "coordinates" derived from these gradients trigger development of specific brain areas and neural cell types. BMPs, Bone Morphogenetic Proteins; WNTs, Wingless-type MMTV integration site; RA, Retinoic Acid; FGF8, Fibroblast Growth Factor 8; SHH, Sonic Hedgehog.

The anterior-posterior axis is established predominantly by retinoic acid (RA) which is secreted from the surrounding somitic mesoderm and notochord precursors (Pierani *et al.*, 1999). Higher RA concentrations denote a posteriorising (or caudalising) signal within the neural tube and hence are associated with hindbrain and spinal neuron positional

specification of the putative CNS (Maden, 2006). Another key signalling molecule in the formation of the anterior-posterior axis is the induction of fibroblast growth factor-8 (FGF-8) signalling from the isthmic organiser. This region of the neural tube denotes the midbrain-hindbrain boundary and its signalling is integral to the formation of dopaminergic and serotonergic neurons (Goridis and Rohrer, 2002; Brodski *et al.*, 2003).

Strictly defined roles for these factors are still being elucidated and the above explanations are more of a crude overview by which *in vitro* differentiation strategies have been derived. Indeed, some of these inductive signals appear to have multiple roles: Wnt signalling has also been implicated as a posteriorising signal in developmental studies (as well as the dorsalising role explained above) (Yamaguchi, 2001). RA in differentiation studies in murine ESCs has also shown it to be a dorsalising signal as well as a posteriorising one (Okada *et al.*, 2004). Retinoids have also been shown to help induce dorsal forebrain cortical lineages from iPSCs with high efficiency (Shi *et al.*, 2012; Shi, Kirwan and Livesey, 2012).

In vitro differentiation of iPSCs into neuronal lineages using these morphogens can be broken down into a series of steps that sequentially restrict the potency of the starting iPSC colonies. Firstly, with the generation of neural precursors, then patterning these precursors to recapitulate the positional specificity of a neural subtype within the neural tube, and finally to mature and enrich the desired neuronal lineage into functional networks that can undergo further *in vitro* study.

1.2.2 Neural Induction of iPSCs *In Vitro*

The first step in the *in vitro* differentiation pathway is to trigger a neural induction within the iPSCs to generate a patterning-competent pool of neuroepithelial progenitors. Multiple strategies have been used across iPSC and ESC lines that generate neural progenitors that show consistent gene expression markers regardless of their starting PSC cell type (Falk *et al.*, 2012). There are three main strategies to induce this effect, namely; embryoid body formation, dual SMAD inhibition, and stromal cell-derived inducing activity (SDIA). As with the majority of this research, the seminal papers deal with a range of PSC types but ultimately have been utilised in iPSC differentiation strategies across the literature. It is also worth noting that not only do methodologies for neural induction vary greatly between studies, but also the nomenclature for the progenitor cell type that is initially generated

and the time course over which this cell type is propagated and matured. Studies have referred to this pool of cells as neural precursor/progenitor cells (NPCs), neuroepithelia (NE) or neuroepithelial progenitors (NEPs), neuroepithelial stem cells (NESs), and neural stem cells (NSCs). This may be a point of confusion, as although cultures of these progenitors will indeed alter their properties over time, the markers used to identify them tend to be the same across the bulk of studies, namely Nestin, Pax6 and Musashi-1 [for example (Watanabe *et al.*, 2005; Shin *et al.*, 2006; Nemati *et al.*, 2011)]. Another point of possible misunderstanding is to equate the progenitor pool derived from iPSCs to primary culture NSCs. Primary NSCs harvested from foetal or adult brain are believed to be derived from radial glia-like stem cells which when cultured as neurospheres form a renewable source of NSCs (Reynolds and Rietze, 2005). However, these primary-NSCs lack many of the characteristics of iPSC-NPCs such as intrinsic neural architecture formation and differing marker expression (Elkabetz *et al.*, 2008; Falk *et al.*, 2012; Karus, Blaess and Brüstle, 2014). iPSC-NPCs should then be seen as a more developmentally early-stage stem cell than primary NSCs and care should be taken not to confuse the two types by name alone. Therefore, for the purpose of consistency this thesis will refer to PSC-derived pools of neural precursor cells as NPCs.

1.2.3 Embryoid Body-Based Neural Induction

The first technique that will be discussed is that of neural induction via embryoid body (EB) formation, also referred to as serum-free floating culture of embryoid body-like aggregates (SFEB). This is achieved through the culture of PSC-colony fragments in suspension. The cellular aggregates self-form into tightly packed EBs which if left in iPSC media will develop markers of all three germ layer lineages. However, when the growth media is exchanged for a serum-free media, the differentiation within the EBs becomes biased towards a neuroectodermal lineage (Okabe *et al.*, 1996; Watanabe *et al.*, 2005). An improvement on this basic protocol termed SFEBq was reported by Eiraku et al., by using U-shaped wells to accelerate the formation of PSC aggregates from single cell suspensions within a few hours rather than the days needed for reaggregation in basic suspension culture (Eiraku *et al.*, 2008). When plated onto adhesive substrates these primed cells form structures termed “neural rosettes”. These can be mechanically separated and cultured independently to form a pool of multipotent NPCs which form the basis of further neural differentiation

strategies. The rosettes themselves are a self-organised two-dimensional recapitulation of the neural tube and not simply artefacts of *in vitro* NPC culture. They display apical-basal polarity (Falk *et al.*, 2012), express specific early markers of iPSC-NPCs (Elkabetz *et al.*, 2008), and even more remarkably display neural crest cell generation developing at the periphery of the rosettes; similar to the spatial separation seen *in vivo* (Karus, Blaess and Brüstle, 2014).

1.2.4 Dual SMAD Inhibition

SMAD proteins are the principal signal transducers of the Transforming Growth Factor-β (TGF-β) signalling receptor superfamily. Dual SMAD inhibition is a technique that allows for monolayer induction of NPCs from iPSCs without the need for embryoid body formation. This restriction of lineage differentiation is achieved through the selective inhibition of both BMP and Activin/Nodal/TGF-β signalling pathways. The blocking of these pathways individually had previously been shown to aid neuronal differentiation of ESCs through the use of the protein Noggin for BMP-signalling inhibition (Lee *et al.*, 2007; Elkabetz *et al.*, 2008) and the small-molecule SB431542 for inhibition of the Nodal/Activin/TGF-β pathway (Smith *et al.*, 2008). The seminal paper that brought both of these strands together showed that the dual inhibition of these pathways was sufficient to induce NPC differentiation and subsequent neuronal maturation in completely defined conditions (Chambers *et al.*, 2009).

Multiple studies have used different compounds to elicit the inhibition of each pathway. For instance, BMP signalling can be inhibited using the recombinant protein Noggin, but also by the synthetic compounds Dorsomorphin (Shi, Kirwan and Livesey, 2012; Naujock *et al.*, 2014; Stanslowsky *et al.*, 2014) and LDN193189 (Kriks *et al.*, 2011; Prè *et al.*, 2014). In general terms the NPC induction by dual SMAD inhibition is reportedly faster than that derived from the EB-based induction (Muratore *et al.*, 2014) and is generally stated to work with high efficiency. However, a recent study looking at direct comparisons of neural induction from EB-based and dual SMAD inhibition approaches in iPSCs reported a lower neural induction with the dual SMAD inhibition technique (Muratore *et al.*, 2014).

It should also be noted that these two techniques are not strictly mutually exclusive. Recent studies have reported successful neuronal differentiation via induction of NPCs through a combination of dual SMAD inhibition during EB formation (Stanslowsky *et al.*, 2014; Qian *et al.*, 2016). This is a clear demonstration that although vague divisions can be

made between stages of various differentiation protocols, this is a highly changeable sphere of frontier research and slight modifications and alterations to existing protocols are the rule and not the exception.

1.2.5 Stromal Cell-Derived Inducing Activity (SDIA)

The method of neural induction via SDIA is derived from the co-culture of iPSCs with specific stromal cell lines. These stromal cells (as a replacement for fibroblastic feeder cells in classical PSC culture) supply factors to the iPSCs that directly induce the generation of NPCs. The stromal cell lines used to trigger neuronal lineage differentiation are predominantly the PA6 (Kawasaki *et al.*, 2000) and MS-5 (Lee *et al.*, 2007) lines. Although this is still a widely used and completely valid technique, it does come with some disadvantages when applied to modern iPSC research. Firstly, it involves the use of an animal cell line, which for human iPSC regenerative research may make this technique difficult to apply clinically. Secondly, the system of induction is an undefined one and the factors necessary to drive this induction are not completely known or understood. However, some progress has been made by screening the stromal cells for elevated factors, and protocols do exist for neural induction using these so-called SPIE factors (Stromal cell-Derived Factor-1, Pleiotrophin, Insulin-like Growth Factor-2 and Ephrin-B1) (Vazin *et al.*, 2009). As with all these techniques described above, extensive characterisation of NPCs must be undertaken to ensure reproducibility between separate induction experiments. This will be integral to *in vitro* studies into disease-modelling that may hinge on subtle differences in neuronal maturation between healthy and disease-specific iPSC lines. Any irregularities in the induction of neural subtypes could therefore mask or negate any phenotypic changes present between healthy and disease-specific lines. Therefore, undefined or stochastic NPC induction protocols may result in irreproducible downstream assays or therapeutic outcomes.

1.3 Specific Neuronal Subtype Differentiation

The next step in the chain of *in vitro* neuronal differentiation is the patterning of NPCs and subsequent maturation of the desired neural subtype. As stated above, these protocols take general cues from the *in vivo* patterning of the neural tube. That being said, the time

of exposure to patterning morphogens, the combinations & concentrations of signalling molecules or agonists, and the time of maturation before experimental analysis of post-mitotic neurons differs greatly from study to study (Compagnucci *et al.*, 2014). This chapter will therefore try to bring together an overall demonstrative consensus of many neuronal differentiation studies to obtain a broad picture of subtype specific factors (Fig 1-3).

The stages of neuronal specification can be crudely broken down into; the neural induction step (covering the generation of pattern-competent NPCs); the patterning step, (in which suitable morphogens are used to recapitulate spatial location in the neural tube and therefore trigger lineage restriction); and the maturation step (where neurons are matured in media conducive to terminal differentiation and synaptogenesis) (Petros, Tyson and Anderson, 2011). This is not always the case, however, and some protocols throughout the literature do not use a pool of unpatterned NPCs, instead utilising a "pre-patterning" step that combines patterning factors with the early stages of neural induction. These protocols add patterning factors directly or soon after the start of neural induction of iPSCs and attempt to pre-determine neuronal lineage specification simultaneously with NPC generation [for example (Hartfield *et al.*, 2014)]. However, it should be noted that reported efficiencies will vary from study to study and no definitive protocols exist for subtype differentiation. An overview of specific neural subtype differentiation protocols for forebrain, midbrain and hindbrain lineages is outlined below.

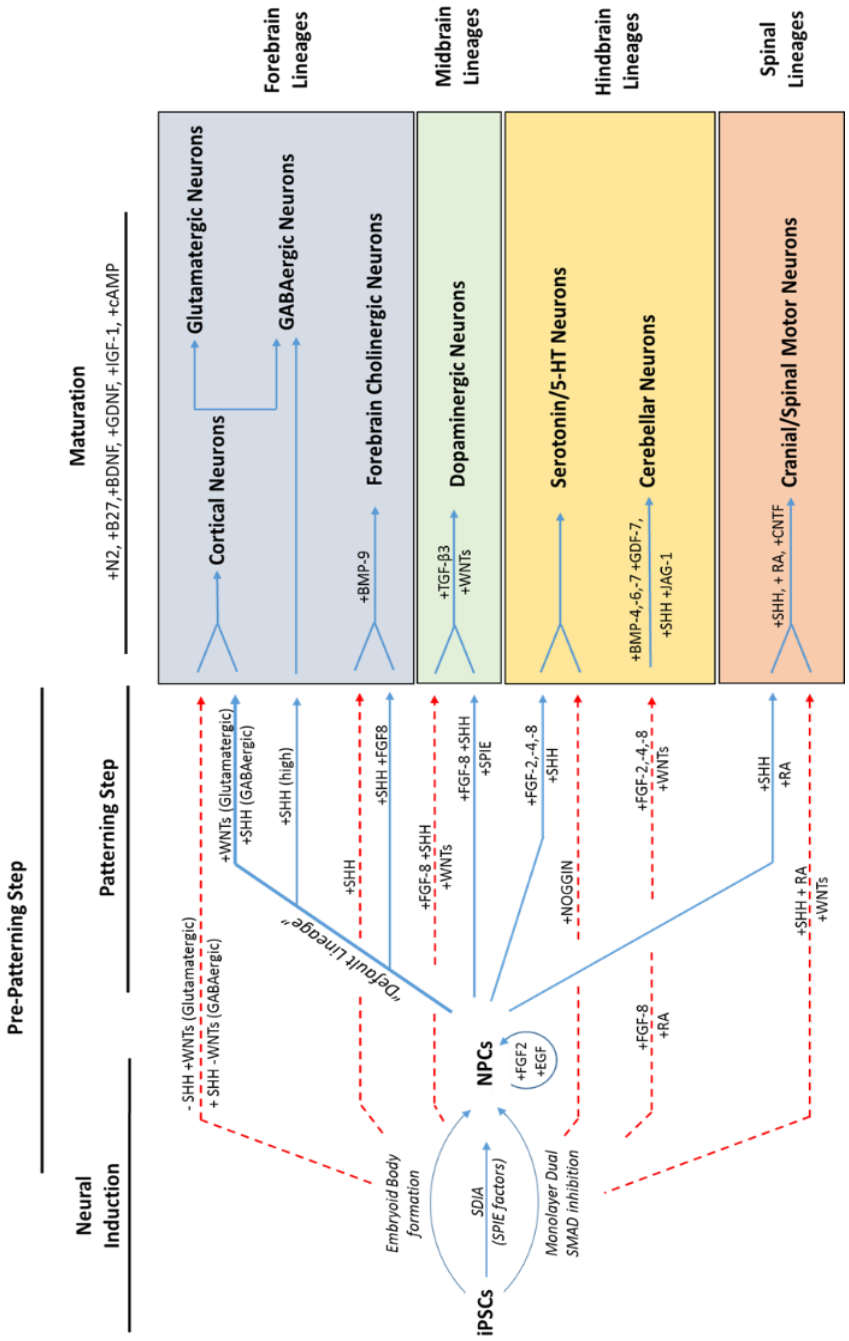

Figure 1-3: *In vitro* methods of generating Neural Progenitor Cells (NPCs) and specific neural cell lineages from iPSCs. The morphogens used are predominantly derived from known *in vivo* signalling events. Solid blue lines indicate patterning of NPCs after neural induction. Dashed red lines indicate patterning *during* the NPC induction step. SHH, Sonic Hedgehog; WNT, Wingless-type MMTV Integration site; FGF, Fibroblast Growth Factor; EGF, Epidermal Growth factor; RA, Retinoic Acid; BMP, Bone Morphogenetic Protein; CNTF, Ciliary Neurotrophic Factor; JAG-1, Jagged-1; GDNF, Glial-cell Derived Neurotrophic Factor; BDNF, Brain-derived Neurotrophic Factor; TGF-β, Transforming Growth Factor-Beta; GDF, Growth Differentiation Factor; SDIA, Stromal-cell Derived Inducing Activity.

1.3.1 Forebrain Lineages

NPCs generated via the majority of neural induction pathways listed above and cultured in a basic neural maintenance media free of any morphogens, will differentiate into mature neuronal lineages (Hansen, Rubenstein and Kriegstein, 2011). More specifically this "default pathway" directs a neural lineage specific to dorsal forebrain cortical neurons (Zeng *et al.*, 2010; J.-E. Kim *et al.*, 2011; Shi, Kirwan and Livesey, 2012). This is true across neural induction strategies in murine ESCs (mESCs), human ESCs (hESCs) and human iPSCs (hiPSCs). Therefore an "uncontrolled" or "un-patterned" differentiation will create a neuronal culture rich in glutamatergic (excitatory) and, to a lesser extent, γ-aminobutyric acid (GABA)ergic (inhibitory) neurons (Gaspard *et al.*, 2008; Li *et al.*, 2009; Espuny-Camacho *et al.*, 2013). This is an interesting point of fact as it displays a developmental bias to form anterior dorsal neural cell types in the absence of other neural tube patterning factors, and not simply a random assortment of neuronal cell lineages. This default dorsalisation effect can be further strengthened by the use of the SHH-signalling antagonist Cyclopamine, which near abolishes the presence of ventral/inhibitory neuronal subtypes (Gaspard *et al.*, 2008), or with the application of the dorsalising signalling molecule WNT-3A (Li *et al.*, 2009). This is also seen functionally where the electrophysiological properties of these "default" dorsal cultures do not alter firing properties under antagonism of GABA signalling, showing their low presence within these neural cultures (Kirwan *et al.*, 2015).

In general terms, neuronal cultures with a high proportion of glutamatergic neurons are said to have dorsal forebrain characteristics (mirroring the spatial coordinates of the neural tube from which they would be derived *in vivo*), whereas cultures with a high proportion of GABAergic neurons are said to be derived from ventral forebrain or "ventralised".

It has also been shown that the use of dorsal-ventral patterning factors can alter the percentage of excitatory and inhibitory neurons in this forebrain lineage pathway. Forebrain GABAergic interneurons account for about 20% of the neocortical neuronal cell number and develop from ventral *in vivo* structures termed the ganglionic eminences, namely the lateral ganglionic eminence (LGE), the caudal ganglionic eminence (CGE), and the medial ganglionic eminence (MGE) (Danjo *et al.*, 2011; Arber and Li, 2013; Yan Liu *et al.*, 2013). The latter also containing progenitors of forebrain cholinergic neurons (Crompton *et al.*, 2013). *In utero* these interneurons then undergo a large tangential migration into the

dorsal cortical tissues. Very high patterning concentrations of SHH (or purmorphamine – a SHH pathway agonist) have been shown to trigger GABAergic interneuron differentiation in *in vitro* PSCs (Maroof *et al.*, 2010; Danjo *et al.*, 2011; Goulburn *et al.*, 2012; Ma *et al.*, 2012; Arber and Li, 2013; Yan Liu *et al.*, 2013; DeRosa *et al.*, 2015) sometimes combined with antagonists of Wnt-based dorsalising pathways such as Dickkopf-1 (DKK-1) (Li *et al.*, 2009).

Through regulation of the concentration of ventralising signalling molecules it is possible to derive not only crude measures of GABAergic interneurons, but also define particular subsets of inhibitory NPCs derived from each of the ganglionic eminences. High concentrations of SHH (or its pathway agonists) generate pools of ventral NPCs displaying markers of the MGE and CGE neuraxis regions, whereas lower amounts instead generate medium spiny neuronal NPCs of the LGE (Danjo *et al.*, 2011; Ma *et al.*, 2012). These divisions can be further tailored by the addition of FGF-8 which increases the population of MGE-specific precursors, but is inhibited through the addition of FGF-15/19, while conversely CGE-specific precursor induction efficiencies are increased with FGF-15/19 treatment and suppressed by FGF-8 (Danjo *et al.*, 2011). Other GABAergic differentiation protocols have also found an enhancing effect of FGF-8 treatment when paired with a SHH-agonist and IWP-2 (an antagonist of the dorsalising Wnt-signalling pathway) (Kim *et al.*, 2014). Interneurons derived in this way have been successfully transplanted into murine models of induced-epilepsy and display functional integration to a level that ameliorated the seizure activity (Cunningham *et al.*, 2014). LGE-specific GABAergic NPC induction can be initiated through strict control and reduction of SHH or SHH-agonist concentration, to a level lower than is necessary for MGE and CGE differentiation, and therefore generate pools of NPCs with different marker compositions distinct from other GE and dorsal precursor cell types (Ma *et al.*, 2012).

Interestingly, similar differentiation strategies have generated cultures enriched with forebrain cholinergic neurons (Crompton *et al.*, 2013). Other strategies have combined SHH with the midbrain marker FGF-8, and further treatment with BMP-9, to generate high induction efficiencies of forebrain cholinergic neurons (Bissonnette *et al.*, 2011).

Surprisingly, other studies have reported GABAergic lineage differentiation based on NPC treatment with all-*trans*-retinoic acid (Chatzi *et al.*, 2009; Addae *et al.*, 2012) as a single factor that generates the specific ventral subtype, as well as in combination with FGF-2 (Goulburn *et al.*, 2011) although the authors postulate these cells arise from a diencephalic rather than telencephalic origin. RA, as was discussed in the context of neural

tube patterning, is used as a posteriorising signal and is predominantly associated with hindbrain and spinal cord neuronal development. The majority of motor neuron and hindbrain neuron differentiation strategies discussed below (Section 1.3.3) utilise RA as a caudalising patterning signal. It is therefore intriguing how forebrain lineages may be formed from this treatment. The concentration and timing of treatment does however differ between protocols and indeed certain levels of RA and retinoids may encourage cortical induction without caudalising the NPCs to a noticeable extent (Shi *et al.*, 2012; Shi, Kirwan and Livesey, 2012). Even FGF-2 treatment (as will be discussed below) utilised in a subset of GABAergic differentiation strategies and also a major component in many proliferation media for NPC propagation, can have caudalising effects on the NPCs themselves and can therefore generate more caudal neural subtypes (Falk *et al.*, 2012; Zhou *et al.*, 2016).

Even more surprising is the report that treatment with Activin (a member of the TGF-β signalling family) could induce the differentiation of Calretinin-expressing CGE-specific interneurons through the downregulation of SHH signalling and the upregulation of RA signalling events (Cambray *et al.*, 2012). Both components of this result appear counter-intuitive, but nevertheless highlight the esoteric nature of neural lineage differentiation both *in vivo* and *in vitro*.

Hippocampal dentate gyrus (DG) neurons are derived *in vivo* from the most dorsomedial region of the telencephalon (Yu, Marchetto and Gage, 2014). Protocols focused on the differentiation of DG neurons from PSCs are quite sparse in the literature but successful attempts have utilised a combination of WNT-3A dorsalising morphogen together with brain-derived neurotrophic factor (BDNF) (Yu *et al.*, 2014), as well as a combination of the dorsalising factors CHIR99021 (a Wnt-signalling agonist) and BMP-4 (Sakaguchi *et al.*, 2015).

It is worthy of note, that although a multitude of differentiation protocols exist for the generation of human neural subtypes through morphogen patterning as outlined above, the speed of differentiation and maturation of each cell type follows an intrinsic timeline that closely mimics that of *in utero* brain development (Espuny-Camacho *et al.*, 2013). Consequently PSC-derived cortical neural models derived from murine cell types will differentiate and mature on a much more compressed timeline than for human PSC-derived cortical neural cultures (Van den Ameele *et al.*, 2014; Kelava and Lancaster, 2016) (Fig 1-4 A). This intrinsic timing of cellular differentiation and maturation of human NPCs

also reveals *in vitro* temporal recapitulation of markers of corticogenesis indicative of *in utero* cortical lamination events (Hansen, Rubenstein and Kriegstein, 2011; Anderson and Vanderhaeghen, 2014).

Development of the human cortex into a highly organised multi-layered laminar structure generated from the pre-plate primordium occurs in a regulated temporal and spatial manner, with each neuronal layer having distinct gene expression markers. The timing of this series of precursor differentiation and maturation events of each layer identity is preserved in *in vitro* PSC differentiation studies, allowing for an exquisite view *in vitro* of the protracted time of cortical layer development (Hansen, Rubenstein and Kriegstein, 2011; Espuny-Camacho *et al.*, 2013; Anderson and Vanderhaeghen, 2014; Kelava and Lancaster, 2016). This faithful recapitulation of the inside-out nature of cortical lamination from early deep-layer neurons to later upper-layer neurons, followed by glial cell differentiation can form the basis of studying human-specific brain structures that may not be present or markedly reduced in brains of other animal models, such as the outer subventricular zone (Kelava and Lancaster, 2016) (Fig 1-4 B). Even implantation of human cortical NPCs into developing mouse brains did not accelerate the sequential maturation profile of the human cortical neurons, suggesting a level of tight control on these timing and maturation events that are not easily swayed by the cellular environment (Espuny-Camacho *et al.*, 2013). Other implantation studies of human cortical NPCs into embryonic murine cortex do show robust migration and integration into the post-natal brain, showing that even if intrinsic maturation timing is different, the human cells will still develop faithfully in an *in vivo* environment (Nagashima *et al.*, 2014).

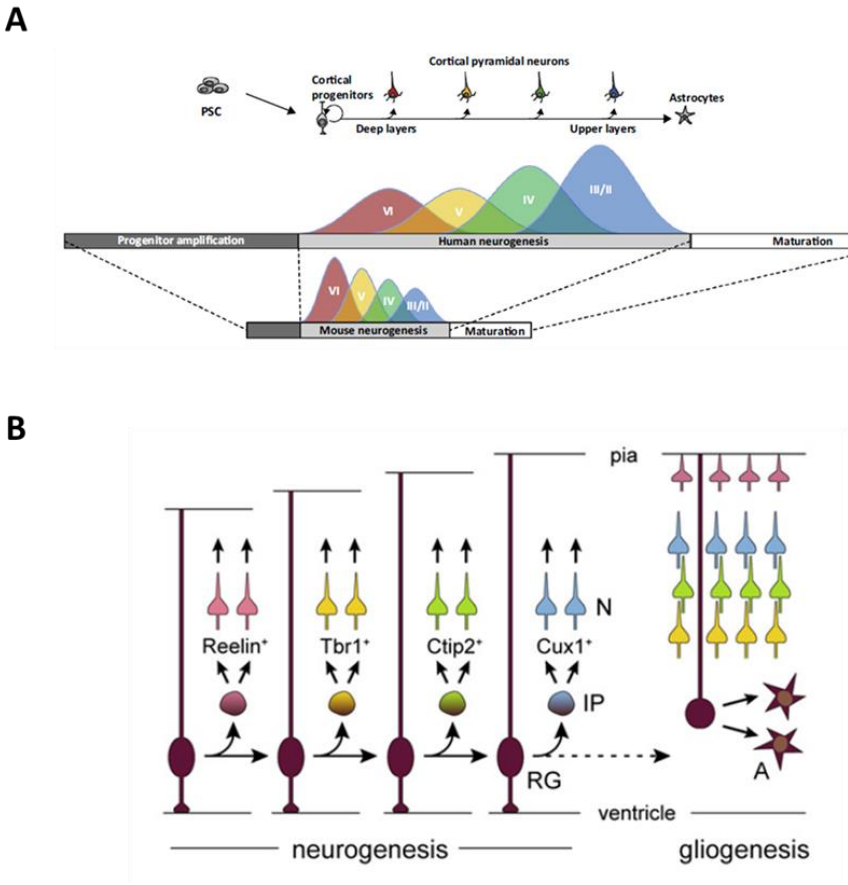

Fig 1-4: **(A)** The *in vitro* cortical differentiation of human and murine PSCs follows the same pattern of layer-specific development and intrinsic timing as is seen *in utero*. **(B)** Each cortical layer contains neurons of specific gene expression profiles that develop sequentially during the formation of the cytoarchitecture. Gliogenesis follows after the bulk of neurogenesis. *Figures adapted from Anderson & Vanderhaeghen 2014; Hansen et al. 2011*

1.3.2 Midbrain Lineages

A very high proportion of PSC-neural differentiation studies are based around midbrain dopaminergic neuron generation, compared to other neural lineages. Dopaminergic neuronal subtypes are strongly affected in Parkinson's disease (PD) pathology, and hence many research groups have focused on its lineage specification as a basis to better understand the mechanisms of PD-related neurodegeneration. These neurons *in vivo* are specified from the developing midbrain (Brodski *et al.*, 2003). A large amount of FGF-8 signalling denotes the midbrain-hindbrain boundary (the isthmic organiser) and as such,

FGF-8 treatment is a constant factor in almost all *in vitro* dopaminergic neuron differentiation strategies, together with the ventralising effect of SHH (Petros, Tyson and Anderson, 2011). Treatment with SHH triggers a strong ventralising signal which mirrors the *in vivo* discovery that true midbrain dopaminergic neurons develop from the floor plate (the most ventral mid-line portion) of the neural tube (Ono *et al.*, 2007). Successful combinations of these factors to generate neurons with dopaminergic markers have been shown in hESCs (Koch *et al.*, 2009; Kriks *et al.*, 2011) and hiPSCs (Swistowski *et al.*, 2010; Zeng *et al.*, 2010; Kikuchi *et al.*, 2011; Kriks *et al.*, 2011; Stanslowsky *et al.*, 2014) and have also been shown to be electrophysiologically active (Hartfield *et al.*, 2014). These protocols include the use of patterning and pre-patterning (or "pre-rosette") treatments with SHH and FGF-8 to obtain the target dopaminergic lineage. One of these studies showed improved *in vivo* dopaminergic marker presence and improved *in vivo* grafting of the generated neuronal pool when FGF-8 and SHH treatment was paired with canonical Wnt-signalling (Kriks *et al.*, 2011). The initial step used high amounts of SHH to ventralise the NPCs during induction into a floor-plate-like cell type which was then patterned with FGF-8 and the Wnt-signalling activator CHIR99021. As with forebrain patterning methodologies, the use of Wnt-signalling was linked with dorsalisation of the NPCs, and hence in this method the timing and use of both ventralising and dorsalising signals is necessary for improving specific dopaminergic differentiation. This then reinforces the concept of the strong interplay between morphogen gradients within the neural tube *in vivo* and the fine tuning that is capable *in vitro* to derive neuronal subtype specificity.

A large portion of dopaminergic differentiation methodologies also report successful differentiation when utilising solely the stromal cell co-culture neural induction strategy (SDIA) outlined previously (Kawasaki *et al.*, 2000; Zeng *et al.*, 2004; Parmar and Li, 2007). This leads to the conclusion that although neural induction is indeed possible with SDIA, the generated NPCs would in effect be patterned or at least biased for midbrain/hindbrain lineage differentiation. This pro-dopaminergic patterning of NPCs by SDIA has been utilised by other studies in conjunction with treatment of the patterning factors SHH and FGF8 (Perrier *et al.*, 2004), while another study showed successful dopaminergic differentiation of hESCs using the SPIE factors (Section 1.2.5) as a neural inductive signal to trigger not only patterned NPCs but also dopaminergic lineage differentiation (Vazin *et al.*, 2009).

It is also interesting to note that NPCs propagated in long term culture in the presence of FGF-2 and epidermal growth factor (EGF), will default to a midbrain/hindbrain specification instead of forebrain lineages (Falk *et al.*, 2012). This is probably due to the effect of FGF-2 which is a known caudalising signal in NPC patterning (Shi, Kirwan and Livesey, 2012; Karus, Blaess and Brüstle, 2014; Zhou *et al.*, 2016). Under these conditions, the continuously propagated NPCs will be biased towards a midbrain or hindbrain lineage specification during maturation and not the "default" cortical lineage as in protocols that involve neural induction and maturation in a single continuous process from iPSCs (Anderson and Vanderhaeghen, 2014).

1.3.3 Hindbrain and Spinal Lineages

As with *in vivo* patterning of the neural tube, the specification of hindbrain and spinal lineages *in vitro* is dependent on the presence of midbrain and/or caudalising signalling molecules during or after neural induction. Serotonergic neurons *in vivo* are generated in an area of the rostral (or anterior) hindbrain (Goridis and Rohrer, 2002) and as with dopaminergic neuron development the midbrain-hindbrain organiser is integral for this specification (Brodski *et al.*, 2003). Neural tube explant studies highlighted the necessity of not only SHH and FGF-8 signalling, but also pre-patterning with FGF-4 (probably derived from the primitive streak *in vivo*) as an inductive cocktail to drive serotonergic neuron differentiation *ex vivo* (Ye *et al.*, 1998). These factors have since been shown to successfully generate serotonergic neurons from various PSCs *in vitro* (Barberi *et al.*, 2003; Alenina, Bashammakh and Bader, 2006). Interestingly, higher serotonergic induction was reported using the MS5 SDIA induction method than with the EB-based neural induction (Alenina, Bashammakh and Bader, 2006). Another recent method of serotonergic neuronal differentiation employed a "single-step" induction of ESCs and iPSCs using only a monolayer culture of PSCs on a thick layer of Matrigel (a murine sarcoma-derived extracellular matrix product) and treatment with Noggin (a BMP-signalling antagonist) (Shimada *et al.*, 2012). It is surprising that serotonergic differentiation was derived without the exogenous use of a separate neural induction step, nor any of the classical midbrain-hindbrain signalling factors or FGF-4. A possible explanation for this may be the undefined nature of Matrigel, in terms of growth factor composition, directly influencing lineage selection.

Successful cerebellar granule neuron differentiation protocols in the literature are predominantly based around more complex and sequential addition and removal of patterning factors throughout neural induction and maturation. One of the first studies reported in the literature, using mESCs, generated Math1+ cerebellar precursor cells and L7+ Purkinje cells. The ESCs underwent a SDIA neural induction followed by treatment with BMP-4 and WNT3a resulting in the formation of cerebellar precursors. Additional treatment with FGF-8 resulted in more Purkinje cells being generated (Su *et al.*, 2006). Mature granule neurons have also been generated from mESCs through a stepwise exposure to a much wider array of morphogens through the EB-based induction method: Addition of WNT1, WNT3a, FGF-2, FGF-4, FGF-8, and RA trigger initial patterning. This in turn is followed by BMP-6, BMP-7 and Growth Differentiation Factor-7 (GDF-7) for further maturation, and then finally SHH and Jagged-1 (JAG-1) (Salero and Hatten, 2007). Functional cerebellar neurons from hESCs have also been generated with efficiencies over 75% using the same array of morphogens listed above but in a five-step sequential process over the first thirty days of induction (Erceg *et al.*, 2012). Cerebellar neural induction *in vitro* therefore seems to require tightly controlled midbrain, caudalising, early dorsalising and late ventralising signals by which to specify developmental identity.

Motor neuron (MN) lineage specification tends to rely on a strong caudalising signal (namely RA) and ventralising signal (either SHH or Purmorphamine) to promote specific differentiation. This basic concept of MN induction works consistently in mESCs (Barberi *et al.*, 2003; Soundararajan *et al.*, 2007), hESCs (Lee *et al.*, 2007; Li *et al.*, 2008; Koch *et al.*, 2009) and hiPSCs (Hu and Zhang, 2009; Karumbayaram *et al.*, 2009; Zeng *et al.*, 2010; Corti *et al.*, 2012). Successful MN differentiation with these factors does not seem dependant or inhibited by any particular method of neural induction and positive MN differentiation is seen from SDIA-based protocols (Barberi *et al.*, 2003; Lee *et al.*, 2007) and EB-based inductions (Hu and Zhang, 2009; Karumbayaram *et al.*, 2009; Zeng *et al.*, 2010). hiPSC-derived MNs differentiated in this way are reportedly electrically active and functional after 10 weeks *in vitro* (Hu and Zhang, 2009; Karumbayaram *et al.*, 2009) and have been successfully engrafted in murine models of Spinal Muscular Atrophy (Corti *et al.*, 2012).

It is also worthy of note that unlike forebrain lineage differentiation which may be inhibited in NPCs kept in long-term culture due to the caudalising effect of FGF-2, MNs can still be differentiated easily from long-term extended culture of NPCs (Koch *et al.*, 2009).

1.3.4 Glial Cell Differentiation

Glial cell differentiation, migration and maturation *in vivo* occurs predominantly after that of neuronal development and continues to do so postnatally (Barateiro and Fernandes, 2014). This pattern of delayed glial differentiation also holds true for *in vitro* neural differentiation studies (Gaspard *et al.*, 2008; Krencik *et al.*, 2011; Emdad *et al.*, 2012; Gorris *et al.*, 2015). There are many reasons why the generation of glial cell subtypes independently from neuronal lineages would be advantageous. Firstly, for improved neurological modelling, astroglial cell subtypes are known to have pro-synaptogenic properties and may aid with generating more mature and *in vivo*-like neuronal networks (Christopherson *et al.*, 2005; Hu *et al.*, 2007; Hughes, Elmariah and Balice-Gordon, 2010; Kucukdereli *et al.*, 2011; Clarke and Barres, 2013). Secondly, for disease-modelling studies, the role of glial cells may have an integral role in the pathology of the neurological condition and therefore could be studied in isolation or in tandem with neuronal populations: such as the toxic effects on hESC-derived motor neurons seen when co-cultured with astroglial cells carrying an amyotrophic lateral sclerosis-related (ALS) mutation (Di Giorgio *et al.*, 2008). Finally, for regenerative therapies, certain glial subtypes such as oligodendrocytes could be transplanted to generate autologous therapies for multiple sclerosis (Grade, Bernardino and Malva, 2013) or other CNS trauma (Nistor *et al.*, 2005), also demonstrated through astroglial-rich NPC transplantations into ALS-affected mice (Kondo *et al.*, 2014). Because of the intrinsic delayed nature of gliogenesis from PSCs undergoing neural induction, many protocols to generate both astroglial and oligodendrocyte cell types in the literature do so over a longer time frame than for neuronal subtype differentiation.

For astroglial differentiation of PSCs *in vitro*, many protocols utilise treatment with ciliary neurotrophic factor (CNTF) which has been shown to enrich Glial Fibrillary Acidic Protein-positive (GFAP+) cells (a marker of astroglial identity) in embryonic murine NSCs (Kanski *et al.*, 2014), although not as a single factor within differentiation formulations. Such an example used treatment with both CNTF and FGF-2 by which to generate astroglial cell types from PSC-derived NPCs (Emdad *et al.*, 2012). Other protocols utilise a combination of leukaemia inhibitory factor (LIF) and BMP-4 which has been shown in primary NSC culture to promote the differentiation of astroglial cells (Bonaguidi *et al.*, 2005) and which has also been successful in generating astrocyte lineages *in vitro* from hESC-derived NPC populations (Gupta *et al.*, 2012; Kondo *et al.*, 2014). A combination of

BMP-2 and CNTF was utilised in another study in the differentiation of astroglial lineages from PSCs, which also recognised heregulin (an alternative splice variant of neuregulin and member of the EGF-like ligands) as a strong inducer of astroglial cell phenotypes (Shaltouki *et al.*, 2013). Long term culture of "patterned" NPC types with individual or combinations of the dorsal-ventral and rostral-caudal morphogens FGF-8, SHH, and RA results in astroglial subtypes from various developmental regions of the neural tube and that further treatment with CNTF at later time points in differentiation can aid to increase the presence of astroglial cell types, albeit over months of differentiation (Krencik *et al.*, 2011).

Early oligodendrocyte differentiation studies employed the use of insulin and Triiodothyronine (T3) as morphogens to induce oligodendroglial lineages during extended proliferation of NPCs generated by EGF & FGF-2, which all followed NPC induction via RA treatment of hESCs (Nistor *et al.*, 2005). A similar protocol to the one above, together with a temporally controlled addition of Noggin (a BMP-signalling antagonist) increased the presence of cells displaying oligodendrocyte lineage markers (Izrael *et al.*, 2007). Yet another study utilising long term NPC expansion through FGF-2 and EGF based media, enhanced oligodendroglial precursors through the early addition of platelet derived growth factor (PDGF-AA) with a later maturation triggering signal of T3 (Kang *et al.*, 2007). The derivation of oligodendroglial cells from other patterned regions of the neural tube have also been investigated. Ventral spinal oligodendrocytes were successfully generated after patterning of hNPCs with both ventralising and caudalising morphogens; SHH and RA, prior to the addition of the oligodendrocyte maturation cytokines; PDGF-AA, insulin-like growth factor 1 (IGF-1), and T3 (B.-Y. Hu *et al.*, 2009; Hu, Du and Zhang, 2009). Interestingly, the authors show a role for FGF-2 inhibiting motor neuron generation and instead favouring the formation of early oligodendroglial precursors, but that extended FGF-2 treatment inhibits the maturation of these precursors. This further demonstrates that tailoring the temporal exposure of the same morphogen, can have stark effects on downstream NPC differentiation. This again reinforces that these processes are both biochemical and temporal in nature, and that both have equal weight in development of these protocols. Other oligodendrocyte differentiation methodologies have used similar induction cytokines as listed above (FGF-2, EGF, PDGF-AA, IGF-1, and T3), together with further glial inductive signals; CNTF (as is used in astroglial differentiation protocols), ascorbic acid (AA) (Sundberg *et al.*, 2010), and neurotrophin-3 (NT-3) (Czepiel *et al.*, 2011) but each morphogen exposure controlled via specific temporal exposure.

As a method of further refining and enriching the NPC pool from neural lineage induced PSCs, some studies have employed a fluorescence-activated cell sorting (FACS) step within the protocol. After initial neural induction, NPCs cultured in the presence of T3, RA, EGF, and FGF-2 triggered a radial glial-NPC identity, before FACS separation of cells displaying a CD133+ (prominin) plasma membrane marker. Final oligodendroglial maturation was prompted through exposure to PDGF, AA, T3, and Noggin (Gorris *et al.*, 2015).

1.4 Transcription Factor-Induced Neuronal Differentiation

Apart from the use of developmentally related morphogens to derive mature neuronal lineages from PSCs, some research groups have utilised forced expression of specific neural transcription factors (TFs) to induce precise neuronal subtype differentiation (Velasco *et al.*, 2014). The transcription factors used are ones that are known to be functional in developmentally-early neural tissue patterning and can be thought of as downstream effectors of soluble morphogen patterning. Numerous neuronal cell types from forebrain to hindbrain lineages have already been generated from these TF-based methodologies (Allodi and Hedlund, 2014).

Generally speaking, the neuronal cultures developed with this methodology reportedly have a much quicker neural identity induction time, in the scale of weeks until yielding electrophysiologically functional neurons, compared to morphogen-based protocols which may be in the scale of months (Kirwan *et al.*, 2015; Odawara *et al.*, 2016). Induction efficiencies are also consistently reported as much higher when direct forced expression of TFs drives neural differentiation; generally over 90% (Bissonnette *et al.*, 2011; Zhang *et al.*, 2013).

Some neural subtypes seem to only require one neural TF to show lineage determination, such as Neurogenin-2 (Ngn-2) which can drive PSCs and PSC-derived NPCs to an almost completely pure cortical excitatory neuronal lineage (Zhang *et al.*, 2013; Ho *et al.*, 2016). Ascl1 alone has also been shown to convert human fibroblasts into functional neurons as a single exogenous factor, although this process can be enhanced when other concurrent factors are also transfected (Chanda *et al.*, 2014). Other neuronal induction protocols require multiple neural TFs to trigger an efficient specific induction, such as

neurogenesis from hiPSCs through forced expression of both neurogenin-1 (Ngn-1) and Ngn-2 (Busskamp *et al.*, 2014). Excitatory cortical neurons have also been induced and from murine fibroblasts using forced expression of the three factors Ascl1, Brn2 and Myt1l (Vierbuchen *et al.*, 2010) and together with NeuroD triggered neuronal induction in human fibroblasts (Pang *et al.*, 2011).

Midbrain dopaminergic neurons differentiated from hiPSCs required the synergistic co-transfection of the Ascl1, Nurr1 and Lmx1a TFs (Theka *et al.*, 2013). For spinal neural lineages, a combination of Ngn2, Isl1 and Lhx3 induced spinal motor neuron differentiation in mESCs. Interestingly, the replacement of Lhx3 with Phox2a generated a pool of cranial motor neurons (Mazzoni *et al.*, 2013). This synergistic overlap between TFs is indicative of a system by which no one particular TF purely denotes each neural subtype (e.g. Ngn2 has been used both in excitatory cortical *and* motor neuron differentiation) or developmental location but instead neural tube signalling works in concert with multiple TFs in order to differentiate specific neural subtypes (Imayoshi and Kageyama, 2014).

This is also evident when TF transfections are used in conjunction with soluble morphogen patterning to try and enhance the induction efficiency of particular neural lineages. The combination of forced expression of single or multiple TFs and different patterning morphogen compositions has potent effects on the subtype and homogeneity of neural subtypes during neural induction and differentiation. Patterning of hESC-NPCs with FGF-8 and SHH, during forced expression of Lhx8 and Gbx1, generates basal forebrain cholinergic neurons (Bissonnette *et al.*, 2011; Duan *et al.*, 2014). Similar patterning morphogen treatment with FGF-8, SHH and FGF-2 but with forced expression of Lmx1a will produce dopaminergic neurons from hESCs (Friling *et al.*, 2009), but not to the high efficiency recorded in multi-TF transfection protocols. A similar protocol with the same soluble factors (but without FGF-2) and Lmx1a, expressed from a Nestin-enhancer, generated dopaminergic neurons from mESCs (Panman *et al.*, 2011). FGF-8 and SHH priming with the forced expression of Phox2a or Phox2b instead of Lmx1a in mESCs will trigger differentiation into visceral motor neurons (Panman *et al.*, 2011; Mong *et al.*, 2014), however, replacing SHH with BMP-7 but retaining forced Phox2b expression, instead generated dorsal hindbrain noradrenergic neurons (Mong *et al.*, 2014).

Patterning with both ventralising (SHH) and caudalising (RA) signals can aid with other forced expression of single TFs in ESCs. For example, Nkx2.2 expression generates

high levels of serotonergic neurons, while Olig2 expression with the same morphogens will trigger somatic motor neuron differentiation (Panman *et al.*, 2011).

While the results of these TF-based studies are striking in terms of apparent induction efficiency, subtype specificity, and speed of neuronal functionality; they must be weighed against the possible disadvantages of forced gene expression and effects related to developmental genes activated out of order, or not in correct synergy with other associated genes. This is of course not to say that neural cultures generated in this way would be unsuitable for disease modelling or developmental applications; indeed cholinergic neurons produced from TF forced expression have already been used in an Alzheimer's disease model (Duan *et al.*, 2014). Experimental methodologies that would require quick differentiation and electrophysiological analysis from a very pure and reproducible iPSC-derived neuronal subtype may very well prefer TF-based methods to slower developmentally-based morphogen protocols.

Even more intriguing is the finding that transdifferentiation of fibroblasts to neural subtypes can be achieved without ectopic expression of neural-associated TFs, and instead is possible purely from chemical induction. Induced neural stem cell-like cells (iNSLCs) were generated from murine fibroblasts after treatment with nine separate chemical factors alone (M. Zhang *et al.*, 2016).

1.5 Neuronal Subtype Enrichment

Heterogeneous cell populations are often generated when utilising neural induction protocols from hPSCs. For developmental studies this may not be an issue as the native mixed generation, maturation and connectivity of neuronal and glial cell types are the basis of the assays being undertaken, and are known to follow embryological developmental timelines (Hansen, Rubenstein and Kriegstein, 2011; Van den Ameele *et al.*, 2014; Kelava and Lancaster, 2016). Certain instances however, necessitate highly reproducible and high-yield pools of specific neural progenitors or neuronal subtypes for study. This is most evident in degenerative disease modelling where the pathology of the disease is limited (to the best current knowledge) to a particular neuronal subtype, for example, dopaminergic neurons in Parkinson's disease and motor neurons in Spinal Muscular Atrophy.

One study performing a FACS-based screen of cell surface markers of NPCs differentiated from hPSCs at different stages of induction and differentiation identified a CD184+/CD271-/CD44-/CD24+ cell population that was able to distinguish between non-induced hESCs (which do not express CD184) and non-NPC and neural crest cell contaminants (which express CD271 and CD44) thus selecting a "true" population of NPCs. After propagation and expansion of this cell pool into differentiation media the authors identified cell-surface combinations for glial pools of cells (CD184+/CD44+) and neuronal pools (CD184-/CD44-/CD15^{LOW}/CD24+) if further cell sorting and purification was necessary prior to terminal differentiation and maturation (Yuan *et al.*, 2011).

As well as cell surface markers, fluorescent protein reporters can be used to identify and sort specific neuronal lineages. When transfected either into the PSC line or NPC pool, these reporters can be driven by cell type-specific promoters or enhancers to ensure that the reporter is only expressed when the gene of interest is transcriptionally active. Examples of this technique have proven effective in identifying, sorting and enriching motor neurons via the use of a HB9-driven GFP reporter (Karumbayaram *et al.*, 2009), serotonergic neurons using a Pet-1 driven reporter (Shimada *et al.*, 2012), and GABAergic interneurons with either an Lhx6- (Maroof *et al.*, 2010), vGAT- (DeRosa *et al.*, 2015), or NKX2.1-driven fluorescent reporter (Goulburn *et al.*, 2011).

There are some important caveats to the use of these reporter constructs for neuronal enrichment protocols, namely issues of transient gene expression, non-specific expression and timing of cell selection during differentiation. The gene of interest used to drive the promoter must be specific and robust enough to a particular subtype so that other developing lineages or proliferative cells are not falsely selected. For example tyrosine hydroxylase (TH) is a well-used marker for mature dopaminergic differentiation, however, TH is also transiently expressed in other cell lineages during development (Allodi and Hedlund, 2014). Thus, a purely TH-driven promoter would enrich for both dopaminergic and non-dopaminergic cell types depending on the stage of differentiation chosen for sorting. Other dopaminergic promoter-reporter constructs based around early- (Hes5), mid- (Nurr1) and late- (Pitx3) dopaminergic markers resulted in different recovery efficiencies and cell pool enrichments. The later and mid marker-reporters (Nurr1 and Pitx3) had higher purity cultures of dopaminergic neurons after FACS-based sorting than the earlier developmental marker Hes5 (Ganat *et al.*, 2012). The trade off in using later markers rather than earlier ones is one of cell recovery efficiency and cell survival –

whereby more mature post-mitotic neurons will tend not to survive FACS-based sorting protocols.

1.6 Organoids for Studying Neurological Development and Disease

Perhaps the most striking finding in recent years within iPSC-neural modelling is the development of tissue-specific organoid cultures. Organoids are three-dimensional (3D) cellular aggregates in which the contained stem cells differentiate and self-organise into structures reminiscent of *in vivo* tissue or functional elements of mature organs (Lancaster and Knoblich, 2014; Huch and Koo, 2015). Human PSC-derived NPCs will differentiate into neuronal lineages depending on patterning factors they are exposed to *in vitro*. Incredibly however, if the hPSCs undergo neural induction as 3D aggregates they will begin to self-organise and recapitulate developmental structures indicative of early brain tissue (Karus, Blaess and Brüstle, 2014). These induced-aggregates will display neural tube-like morphology with the affiliated apical-basal polarity and gene expression patterns, and if left to develop over time will generate forebrain layered early-cortical structures (Mariani *et al.*, 2012; Kadoshima *et al.*, 2013) or cortical-spheroid structures (Paşca *et al.*, 2015). These are defined loosely by the homogeneity of the contained cells and the complexity of the derived neural cytoarchitecture. The basis of this line of research was born out of the extended SFEBq neural induction protocols used previously for PSC-based neural derivation (Eiraku *et al.*, 2008).

A single aggregate may contain multiple early-cortical-like structures, but when cultured in Matrigel droplets and cultured in a spinning bioreactor, a much more continuous neuroepithelia is generated, enabling more defined cortical regions over long term culture (Lancaster *et al.*, 2013) as well as discrete midbrain/hindbrain structural markers, and with a subset even developing retinal tissue. Organoids cultured in this way displayed discrete non-overlapping regions of cortical layering with gene expression of early- and late-born neural markers, an outer Reelin-positive layer, and even interneuron migration from ventral to dorsal regions of the organoid (Lancaster *et al.*, 2013). Even though these organoids will develop in the absence of any exogenous factors, the

organoids themselves are responsive to neural-tube patterning morphogens that alter the region of the CNS they are generating.

Ventralising of the organoids with a SHH pathway agonist triggered the enrichment of GABAergic neurons and an upregulation of adjacent LGE cell populations next to cortical-like tissue (as is seen *in vivo*) (Kadoshima *et al.*, 2013), and higher levels of MGE-like precursor pools, with concurrent lowering of LGE cell markers, was seen when the SHH agonist concentration was increased further (Kadoshima *et al.*, 2013). This follows the same pattern as is seen in equivalent two-dimensional (2D) differentiation ventralisation protocols (Ma *et al.*, 2012).

In accordance with the 2D hiPSC-NPC differentiation methods – the default development of these organoids is one of a forebrain, cortical structure. But as with the patterning of the monolayer iPSC-NPCs, these organoids can themselves be patterned to develop into structures from other developmentally-early brain regions. The generation of hPSC-derived neural midbrain organoids can be triggered through the same addition of factors necessary to generate midbrain cell identities in 2D, namely SHH and FGF-8. These mid-brain organoids also produce neuromelanin and are functionally similar to primary dopaminergic neuronal cells (Jo *et al.*, 2016). Single mESCs suspended in 3D Matrigel (or a synthetic matrix) undergoing neural induction will proliferate and form neural tube-like structures, termed neuroepithelial cysts. These cysts respond to patterning factors that both ventralise to floor plate identity and posteriorise the cysts to a more hindbrain or spinal cord identity, with the affiliated gene expression profiles (Meinhardt *et al.*, 2014). hESC-derived organoid aggregates patterned with FGF-2, FGF-19 and SDF-1, suppressed forebrain identity and enhanced endogenous FGF-8 and Wnt signalling (a property of the midbrain hindbrain boundary *in vivo*). This in turn generated markers and organoid morphology consistent with early cerebellar-like tissue (Muguruma *et al.*, 2015).

These findings combine to point to the incredible discovery that not only can individual NPCs respond to exogenous patterning to derive specific subtypes, but that early neural aggregates can respond to similar signals and self-organise into a multitude of neurodevelopmentally relevant structures. This opens the door to an incredible tool by which to analyse human brain development in a completely *in vitro* and highly reproducible way.

As well as the implications for studies on brain tissue development these organoids have already shown that they can shed light on neurological disease on a patient-specific basis. hiPSC-derived organoids from patients with a CDK5RAP2-dependent pathogenic form of microcephaly also display neural hypoplasia and generate smaller organoids than non-patient iPSC-organoids (Lancaster *et al.*, 2013). Another study generated neural organoids from patients with an idiopathic Autism Spectrum Disorder that displayed differing neural subtype compositions to control organoids. The authors even managed to track this difference down to specific aberrant gene upregulations (Mariani *et al.*, 2015). A multi-faceted approach of using forebrain, midbrain and hypothalamic organoids has recently been used to model Zika virus infection and disease pathology *in vitro* (Qian *et al.*, 2016), showing that the use of these organoids goes beyond genetically-linked neurological diseases and show promise in studying exogenous factors of brain disease and trauma.

The fact that these organoid structures have now begun to help analyse and recapitulate developmental pathways and disorders show the true power of iPSC-based neural modelling and are paving the way for future 3D neurological research. Single cell transcriptome analysis of forebrain cerebral organoids show high fidelity to expression profiles from foetal neocortex (Camp *et al.*, 2015) which further supports the paradigm of faithful recapitulation of developmental processes from these 3D *in vitro* models.

All of the models discussed in this section contain inherent technical challenges and idiosyncrasies that will need to be resolved before wide-scale implementation and translation of PSC-based brain modelling projects (Brennand *et al.*, 2015). Nevertheless, a vast amount of research has been undertaken to refine and improve both 2D and 3D neural differentiation protocols and models over a relatively short time-scale, and this is a source of optimism for the field. The combination of both stem cell biology and 3D growth environments is a fascinating area of research with untold potential for understanding embryological processes, degenerative or malformative disorders, and in unprecedented detail uncover how the brain builds itself.

1.7 Biomaterials for Neural Culture

The concept of disease modelling, or “disease in a dish”-technology, hinges on the faithful recapitulation of *in vivo* conditions in an *in vitro* model. The factors needed for accurate

neuronal maturation and survival must, by definition, recreate the *in vivo* microenvironment for disease phenotypes to be measurable. Many neurodegenerative conditions have undefined genetic components and unknown early-stage pathologies. The difference between a healthy neuronal state and a diseased one may begin as a subtle aberration. Also, measurable differences between control and disease-specific neurons may be present at the level of gene expression, synaptogenesis or detectable only with functional network formation. To simply have iPSC-derived neural cultures in a dish may not be enough to elucidate disease pathologies nor to study healthy neural development. Instead, techniques for accurately recreating *in vivo* environments by use of biomimetic constructs, may be integral for generation of pseudo-neural tissue and therefore complete disease and developmental modelling. Cell culture environments themselves can have profound effects on differentiation of stem cells, neurite outgrowth & axonogenesis, and ultimately the cytoarchitecture of neural cultures through modulation of cell-cell and cell-matrix interactions. A wide variety of methods to modulate and enhance *in vitro* neural cultures are outlined and discussed below.

1.7.1 Two-Dimensional Culture Conditions

Planar neuronal differentiation and maturation of PSC-derived NPCs requires a plating substrate conducive to cell adhesion and promotion of neurite outgrowth. Throughout the literature the most frequently used substrates are Matrigel (a murine sarcoma-derived extracellular matrix product) or a combination of poly-ornithine & laminin (POL). Both Matrigel and POL have been used successfully in many PSC-neural differentiation studies with successful NPC differentiation on both substrates (Gaspard *et al.*, 2008; Shi, Kirwan and Livesey, 2012; Naujock *et al.*, 2014). A recent side-by-side study, however, reported that when using the EB method of iPSC-neural induction, Matrigel yielded higher percentages of MAP2-positive neurons after differentiation than aggregates plated on POL (>90% vs 56%) (Muratore *et al.*, 2014). Other studies utilise non-biological growth substrates that have been modified to promote neuronal attachment and outgrowth. Poly(ester carbonate) functionalised with a laminin-derived peptide sequence resulted in higher levels of neural cell viability, neurite length and number of neurites per cell than growth on tissue culture plastic (Xing, Ma and Gao, 2014). A mix of native and synthetic elements in a hydrogel substrate composed of covalently linked Heparin and star-

polyethylene glycol (PEG), functionalised with a fibronectin-derived peptide and FGF2, enhanced murine NSC survival compared to growth on a poly-lysine substrate (Freudenberg *et al.*, 2009).

Substrate composition can also be modulated to generate growth surfaces of differing degrees of stiffness which have been shown to have strong effects on cell attachment, differentiation, and maturation (Discher, Janmey and Wang, 2005). Mesenchymal stem cells (MSCs) will favour neural differentiation when grown on soft substrates that have an elastic modulus similar to that of *in vivo* brain tissue; typically below 1kPa (Engler *et al.*, 2006). More recently, a study has reported that hPSCs cultured on soft rather than stiff substrates (700Pa vs 75kPa) will show a bias for neuronal progenitor formation and mature neuronal differentiation (Keung *et al.*, 2012). These findings are not in isolation; rat embryonic NSCs cultured on polydimethylsiloxane (PDMS) with a stiffness similar to brain tissue will extend longer neurites and have enhanced expression of pre-synaptic markers than stiffer PDMS substrates (Teixeira *et al.*, 2009), and these cultures also enhanced astrocytic differentiation. Intriguingly, another study found that cortical neurons cultured on polyacrylamide or fibrin gels of varying stiffness show strong neurite extension regardless of stiffness, but that astrocytic growth and cell spreading was *inhibited* on soft substrates (Georges *et al.*, 2006). The discrepancy between these two results may be due to the synergistic interplay of neural cells on equivalent stiffness of substrates but differing substrate compositions. Even though numerous studies implicate softer substrates in the promotion of neurite outgrowth and neural differentiation it has conversely been reported that synaptogenesis, voltage-gated calcium channel currents and neuronal networking of murine hippocampal neurons were all enhanced on stiffer rather than softer substrates (Q.-Y. Zhang *et al.*, 2014).

As well as the choice of substrate on which to differentiate neural progenitors, many studies have shown the importance of topographical features of 2D surfaces that can modulate, and to some extent control, neurite extension, arborisation and ultimately the networks formed on these surfaces (Hoffman-Kim, Mitchel and Bellamkonda, 2010). These topographies can be in the micro- to nano-scale and can be anisotropic (such as grooved surfaces or aligned fibres) or isotropic (such as nano-rough surfaces or geometrically spaced pillars) (Fig 1-5 A).

Electrospun polymer fibres are widely used to generate aligned or randomly orientated nano-scale fibres for cell-topography interaction studies (Xie *et al.*, 2010). It is

well documented that many neuronal cultures will tend to align and extend neurites in the direction of aligned fibres (Yang *et al.*, 2005; Kim *et al.*, 2008; Bourke *et al.*, 2014; Xia *et al.*, 2014). However, different neuronal subtypes will display differing outgrowth patterns depending on the level of alignment and diameter of the polymer fibre. Murine NSCs will differentiate and extend neurites along both micro- and nano-scale polylactic acid (PLA) fibres but this effect is accelerated on smaller fibre diameters (300nm vs 1.5um) (Yang *et al.*, 2005). Dorsal root ganglion (DRG) cells will tend to exclusively follow fibre alignment in a parallel fashion (Kim *et al.*, 2008; Xia *et al.*, 2014) (Fig 1-5 B) and will extend longer neurites than when grown on the same polymer in a smooth film (Mukhatyar *et al.*, 2011). This alignment becomes less strict with smaller fibre diameters (300nm) which causes a more frequent perpendicular movement of the neurite (Wang *et al.*, 2010). By contrast, embryonic rat hippocampal neurons will tend to extend processes both in a parallel fashion to the fibres, but also with regular perpendicular branching (Bourke *et al.*, 2014). Polymer fibres can be further modified to enhance substrate-cell interaction, such as mixing the pre-formed polymer with gelatin (a hydrolysed product of collagen type I) to enhance hydrophilicity and cell adhesion on the fibre mats (Alvarez-Perez *et al.*, 2010).

The results of neuronal outgrowths seen on fibre-based substrates is reflected when cells are cultured on micro-grooved surfaces. Embryonic rat hippocampal neurons grown on micro-grooved quartz will tend to extend processes parallel to wide grooves but perpendicular to narrow ones (of approximately 1µm) (Rajnicek, Britland and McCaig, 1997). However, this pattern of contact guidance differed when hippocampal cells were harvested at different stages of development: Later embryonic neural cells favoured parallel alignment to the grooves, whereas cells from developmentally earlier embryos had an increased tendency for neurite outgrowth perpendicular to grooved topography. Similar patterns were seen on micro-grooved polypyrrole (PPy, an electrically conducting polymer) surfaces; neurons polarized and defined axons faster on grooved PPy than the smooth film and orientation was both parallel and perpendicular to the grooved topography (Gomez *et al.*, 2007). Combinations of nano-rough and micro-grooved substrates also increase focal adhesion and human NSC differentiation and maturation compared to flat surfaces or each topographic feature alone (Yang *et al.*, 2014).

Isotropic micro-pillar topographies elicit differing effects on neuronal differentiation and outgrowth strictly depending on their size and spacing. Embryonic hippocampal neurons grown on micro-scale pillars will show greatest fidelity to the

geometry of the posts when the gaps between them are minimal, and generate a striking neurite growth pattern almost exclusively in strict right-angled trajectories (Dowell-Mesfin *et al.*, 2004) (Fig 1-5 C). This effect was also seen when hippocampal neurons were cultured on micro-scale PDMS conical posts (Hanson *et al.*, 2009).

As mature neural cell types are electrically active, it has long been postulated that electrical stimulation of differentiating neural cultures will have positive and enhancing effects on neuritogenesis and maturation pathways. Electrical stimulation of neuronal cultures via the electrically conducting polymer polypyrrole (PPy) was demonstrated by Schmidt et al. about 20 years ago. PC12 cells, a neural-like cell line, showed similar cell attachment to the PPy substrate and tissue culture plastic, but after electrical stimulation of the PPy substrate, generated neurite lengths double that of cells cultured on unstimulated PPy (Schmidt *et al.*, 1997). Electrical stimulation of PPy *before* cell attachment has also been shown to increase protein adsorption to the substrate from the surrounding growth media and therefore increase cell attachment and neurite outgrowth (Kotwal and

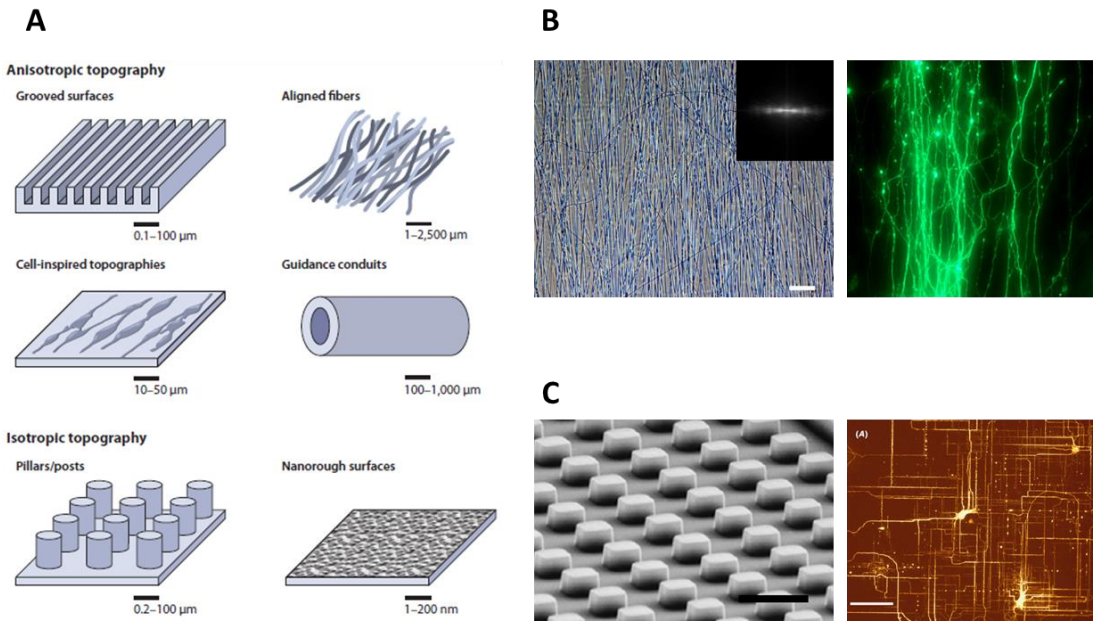

Fig 1-5: **(A)** An overview of topographies utilised on two-dimensional surfaces to modulate neural cell morphology and maturation *in vitro.* **(B)** Aligned electrospun fibres, as an example of anisotropic surface topography, trigger neurite outgrowth and alignment of dorsal root ganglion-derived cells in the direction of the fibre alignment (scale bar = 100µm). **(C)** Micro-scale pillar topography causes perpendicular patterns of neurite extension and arborisation from primary hippocampal neurons [scale bars = 4µm (black) and 100µm (white)]. *Figure adapted from Hoffman-Kim et al. 2010, Xia et al. 2014, and Dowell-Mesfin et al. 2004*

Schmidt, 2001). Electrical stimulation of this material may therefore aid outgrowth and attachment via direct interaction with the cells *and* the positive modulation of the basal PPy substrate through protein adsorption.

In addition, electrical stimulation of neural cells cultured on electrospun fibres coated with PPy induce longer and more abundant neural processes than either factor alone (Lee *et al.*, 2009), in a method that combines both topographical and electrical cues.

Further functionalization of PPy has also been tested with either the direct covalent attachment of neurotrophic factors (Gomez and Schmidt, 2007) or the doping of PPy with neurotrophic factors during polymerisation, in order to release them over time during neuronal culture (Thompson *et al.*, 2010). In both of these cases, electrical stimulation was used synergistically with the biological effect of these growth factors to promote neuronal maturation. It has also been shown that extracellular electric fields can also promote and orientate neurites. Accelerated outgrowth and higher numbers of neurites were found on the cathodal side of neurons exposed to an extracellular electric field (Patel and Poo, 1982).

Taken together; the tailored combination of biochemical, mechanical, topographical and electrical cues to a wide variety of neuronal subtypes and progenitors can generate strong, reproducible neurotrophic effects in 2D: modifying cell migration, axonal sprouting, dendritic arborisation, and even how and where neuronal networks form. The potential of combining iPSC-derived NPCs and programmable biomaterials is a powerful tool in engineering neural constructs that truly reflect more *in vivo*-like conditions, be they developmental or disease-state.

1.7.2 Three-Dimensional culture conditions

Although the level of customisation of 2D planar culture conditions is incredibly varied, it can be argued that neural cell encapsulation and growth in three-dimensional (3D) environments promote a more *in vivo*-like physiological setting. Cell-cell and cell-matrix interaction in 2D systems are confined to a single plane, with neural process outgrowths limited to two-axes and with the majority of cell surfaces exposed to the growth media. 3D cultures (with cells encapsulated within biocompatible scaffolds) allow for cell-cell contacts & neurite outgrowths in all directions, as well as complete interaction with the scaffold

matrix. Cell density can be modulated as can the composition of the matrix in order to generate a cell culture that has cytoarchitecture more representative of living tissue.

Hydrogels are a class of 3D scaffolds generated from networks of hydrophilic polymer chains. When hydrogels undergo sol-gel transitions they retain water content above 90% of their mass, and as such are highly suited to model *in vivo*-like cellular microenvironments.

The diverse list of hydrogel biomaterials used for 3D neural differentiation or maturation of progenitors includes purified proteins or extracellular matrix (ECM) protein mixes such as Matrigel (Irons *et al.*, 2008), laminin/entactin gels (Meinhardt *et al.*, 2014), collagen type I (O'Connor *et al.*, 2001), fibrin scaffolds (Montgomery *et al.*, 2015; Robinson, Douglas and Michelle Willerth, 2017), and even decellularised porcine brain (DeQuach *et al.*, 2011). Synthetic self-assembling peptides (SAPs) such as PuraMatrix have also shown promising recent use in 3D hESC-derived neural cultures (Ylä-Outinen *et al.*, 2014) and primary neural cultures (Kaneko and Sankai, 2014). As well as peptide-derived matrices the literature is also filled with polysaccharide-based hydrogels that use both mammalian polysaccharides, such as the glycosaminoglycan hyaluronic acid (HA) (Wang and Spector, 2009; Z.-N. Zhang *et al.*, 2016), and non-mammalian substrates such as chitosan (Li, Wijekoon and Leipzig, 2014), alginate (Banerjee *et al.*, 2009) and agarose (Balgude *et al.*, 2001). Results from material to material can be varied and depend on substrate composition, cell density and any modifications to the material, but as a very general rule; protein-based scaffolds tend to be more inherently conducive to neuronal differentiation and allow for more *in vivo*-like cell morphologies and cell-cell contacts than unmodified polysaccharide scaffolds.

As well as being highly used as a 2D cell adhesion matrix, Matrigel has been used extensively and successfully in 3D neuronal cell culture for neural cell lines (McMurtrey, 2014), primary cells (Irons *et al.*, 2008), NSCs (Gelain *et al.*, 2006; Koutsopoulos and Zhang, 2013) and hESC- and hiPSC-derived NPCs (Lancaster *et al.*, 2013; Moreno *et al.*, 2015). It has also formed the cell-laden structural basis for high-density 3D neural cell cultures in large-scale perfusion devices (Cullen *et al.*, 2007) and microfluidic 3D "lab-on-a-chip" perfusion devices (Moreno *et al.*, 2015). Electrophysiological analysis of neurons cultured within Matrigel scaffolds confirmed the presence of abundant cell-cell synaptic events and mature network formation (Irons *et al.*, 2008); a crucial property of biomaterials for use in neural tissue engineering.

SAPs are short synthetic peptides (usually based around a repeating core Arginine-Alanine-Aspartate-Alanine "RADA" motif) that can self-assemble under physiological pH and salt concentrations. The resulting hydrogel maintains a nanofibrous structure and porosity comparable with naturally occurring ECM structural proteins (Gelain *et al.*, 2006). Unmodified SAP-scaffolds (i.e. containing only the repeat self-assembling motif) have been shown to generate a pro-neuronal biomimetic scaffold even without native protein binding motifs: hESC-NPCs differentiated in PuraMatrix (a commercially available SAP) display more branching events and thicker dendritic processes than the same cells grown on 2D Laminin cultures (Ylä-Outinen *et al.*, 2014). Also, dopaminergic differentiation of mESCs and miPSCs was enhanced in 3D SAP scaffolds compared to 2D laminin culture and 3D Matrigel scaffolds (Ni *et al.*, 2013). This specific dopaminergic neuron increase may be due to the non-animal-derived nature of the SAP, whereby undefined growth factors within the Matrigel may promote general cell viability and neuronal differentiation [as seen in (Gelain *et al.*, 2006; Koutsopoulos and Zhang, 2013)], but may interfere to a certain degree with the patterning factors necessary for specific neuronal subtype lineage differentiation. As with 2D growth substrates, biomaterials for use in 3D scaffolds can be modified with peptide motifs with the aim of increasing cell-matrix interactions and therefore generating a truer *in vivo*-like microenvironment. SAPs have been synthesised with binding epitopes of native proteins such as laminin, fibronectin, collagens or other sequences (e.g. neuronal anti-apoptotic protein motifs) (Gelain *et al.*, 2006; Li and Chau, 2010; Koutsopoulos and Zhang, 2013; Li, Chow and Chau, 2014). These functionalised SAPs have reportedly higher neuronal differentiation efficiencies of ESCs and NSCs than basal SAP scaffolds. A different format of SAPs based around a stacking aromatic fluorenylmethyloxycarbonyl (Fmoc) group covalently functionalised with laminin-binding moieties, has shown promise in rat models of ischemic stroke recovery (Somaa *et al.*, 2017). The combination of this form of SAP together with hESC-derived NPCs allowed for an injectable delivery system into an *in vivo* model of cortical damage, that resulted in functional neural integration.

Collagen Type I (herein referred to as collagen) scaffolds are widely used throughout the literature as a go-to cell encapsulation material for numerous cell types, including neurons (Antoine, Vlachos and Rylander, 2014). Embryonic rat hippocampal neurons will show extensive neurite outgrowths and higher cell viability in collagen scaffolds than in parallel experiments with the same cell type encapsulated in agarose (O'Connor *et al.*, 2001). In contrast to this, there are examples in the literature of positive

DRG neurite outgrowth in low concentration agarose, but this finding is quite rare (Balgude *et al.*, 2001). As with SAP scaffolds, collagen can also be functionalised by covalent addition of protein-binding epitopes. DRGs cultured in collagen modified with both laminin and fibronectin motifs resulted in significantly higher MAP2 expression than unmodified collagen, the fibronectin motif alone, or a scrambled binding motif (Hosseinkhani *et al.*, 2013). Also, covalent modification of collagen with native laminin subunits resulted in greater cell survival of embedded NSCs (Nakaji-Hirabayashi, Kato and Iwata, 2012).

An interesting use of collagen scaffolds was to determine neurite outgrowth when cells were exposed to 3D stiffness or mechanical gradients. Encapsulated DRGs extend longer neurites down a stiffness gradient rather than up one. This effect is greater than when neural cells were grown in uniform stiffness (Sundararaghavan *et al.*, 2009). Also, overall DRG neurite extensions are longer in hydrogels of low collagen concentration than in higher concentration (and therefore stiffer) collagen hydrogels (Swindle-Reilly *et al.*, 2012). Collagen composite scaffolds containing a porous silk sponge as a model of cortical-like white/grey matter layering allow for more brain-like cytoarchitecture with neurons retaining function and network formation (Tang-Schomer *et al.*, 2014; Chwalek *et al.*, 2015), that was further enhanced with the addition of foetal ECM components into the collagen hydrogel (Sood *et al.*, 2016).

Neural cell electrophysiological activity is preserved in cells differentiated within collagen hydrogel matrices (O'Connor *et al.*, 2000; Ma *et al.*, 2004) and embryonic hippocampal neurons within collagen scaffolds show comparable electrophysiological profiles to those grown on 2D substrates (Xu *et al.*, 2009). By segregating cell-seeded collagen hydrogels and connecting blank-hydrogels over a multielectrode array (MEA), pathways of synaptic functionality were traced throughout a layered neural structure *in vitro* (Odawara, Gotoh and Suzuki, 2013). All of which demonstrates that collagen hydrogels are inherently conducive to neural network formation and function, and that composites or structural cues within the hydrogels can even enhance the level of these formations.

Composite scaffolds containing both Collagen and HA (either through covalent crosslinking or simply a blending of material prior to cell encapsulation) show reportedly improved results for 3D neural culture, purely from a cell morphology and neurite outgrowth point of view (Brännvall *et al.*, 2007; Wang and Spector, 2009). Also, HA scaffolds with embedded polycaprolactone (PCL) electrospun fibres (coated with laminin)

enhanced neurite lengths of SH-SY5Y cells (a human neuronal cell-line) when compared to the same fibres in 2D culture. Interestingly this increase was not found when the same fibres were utilised in a Matrigel equivalent scaffold (McMurtrey, 2014). A covalently-modified form of HA that enables UV-driven crosslinking; HA-methacrylate (HAMA), has also been shown to enable iPSC-derived neural differentiation and migration assays (Z.-N. Zhang *et al.*, 2016).

Direct comparisons between 3D NSC cultures composed of collagen, Matrigel, SAPs (RADA scaffold), and SAPs with functionalised peptide motifs, show significant differences in cell viability, differentiation and neurite outgrowth. Over long term culture, collagen scaffolds have been shown to have the lowest retention of cell viability, followed by Matrigel and then SAP scaffolds (Koutsopoulos and Zhang, 2013). Interestingly, even though long term viability was lower in Matrigel, the rate of NSC differentiation over the first 2 weeks was higher than in any of the SAP scaffolds. This may be due to the presence of undefined growth factors in this ECM-derivative promoting early cell responses (Koutsopoulos and Zhang, 2013).

As well as protein-based biomaterials for deriving scaffolds matrices, numerous polysaccharide hydrogels have shown promise in generating 3D neural cultures *in vitro*. Alginate (sodium alginate or alginic acid) is an anionic polysaccharide derived from brown algae that undergoes sol-gel transition through ionic crosslinking with divalent cations. Alginate hydrogels are a well characterised means to encapsulate cells in 3D with no significant cytotoxic effects (Andersen, Auk-Emblem and Dornish, 2015) and through generation of composite scaffolds are amenable to bioprinting technologies (Chung *et al.*, 2013). Rat NSCs encapsulated in alginate with an elastic modulus comparable to that of brain tissue show a twenty-fold higher level of β-III-tubulin expression than when differentiated in stiffer scaffolds (Banerjee *et al.*, 2009) which mirrors the known 2D effect of substrate stiffness directly affecting stem cell differentiation pathways (Engler *et al.*, 2006). Typical neuronal morphology was not directly observed in this study and cells tended to form aggregates within alginate hydrogels. This finding is not in isolation; rat DRGs embedded in alginate will show little to no neurite outgrowths, but when embedded in Matrigel show neurite outgrowths seventeen-fold longer (Novikova *et al.*, 2006). Alginate concentration and the concentration of the ionic crosslinker of each scaffold however can have stark effects on neural adhesion and morphology within the hydrogel scaffolds. For instance, “ultrasoft” alginate hydrogels, with sub-stoichiometric amounts of

calcium ion crosslinker, will allow for neurite extension in 3D scaffolds (Palazzolo *et al.*, 2015). Even on 2D alginate hydrogel substrates, neural attachment and extension are heavily dependent on lower overall calcium ion concentration and therefore the degree of crosslinking of the gel (Matyash *et al.*, 2012, 2014).

Even though mature neuronal networking is sometimes limited in unmodified alginate it has still been used as a platform for 3D neural induction protocols from mESCs (Li *et al.*, 2011; Bozza *et al.*, 2014), and hESCs & hiPSCs (Lu *et al.*, 2012; Kim, Sachdev and Sidhu, 2013) and used as a scaffold in high throughput 3D hNSC toxicity arrays (Meli *et al.*, 2014). Neural induction efficiencies are reportedly higher in these 3D structures than direct terminal differentiation in suspension culture (Lu *et al.*, 2012). It is telling however that cell aggregation and clustering are prominent in these 3D scaffolds and extensive networking beyond the boundaries of each cluster (despite having strong neural marker immunostaining) are infrequent, if present at all. Covalent functionalisation of alginate with full length-laminin or a laminin-derived binding peptide does seem to improve neural outgrowths of both hippocampal primary neurons and glial cell lines (Frampton *et al.*, 2011). A caveat may be the impressive cell densities in these constructs, which are much higher than those seen in other 3D scaffold studies. Other modified alginate constructs functionalised with an integrin-binding motif (Arginine-Glycine-Aspartate "RGD") did show enhanced adhesion and differentiation of MSCs to neural lineages within the peptide-modified alginate, but with cell seeding only after freeze-drying of the construct to generate anisotropic channels throughout the structure (Lee *et al.*, 2015).

Chitosan is a deacetylated form of chitin; a polysaccharide found within the exoskeletons of crustaceans. Its high abundance and relatively low cost make it an appealing biomaterial for tissue engineering studies. However, primary cortical cells cultured in 3D chitosan hydrogels (with elastic moduli similar to that of brain tissue) will tend to maintain a rounded cell body and extend only a single neurite. The number of cells with neurites is increased when the chitosan is functionalised with poly-lysine (Crompton *et al.*, 2007). Photo-crosslinkable methacrylamide chitosan (MAC) 3D scaffolds show poor induction of neuronal markers from rat NSCs even after functionalization with fibronectin-derived binding motifs, but can be increased through the addition of soluble or immobilized interferon-gamma (IFN-γ). As with many alginate constructs, the morphological analysis of embedded neural cells via immunostaining for neuritogenesis is not overly convincing (Leipzig *et al.*, 2011). This was also not improved by increasing the porosity of the scaffolds

by using mannitol crystals during crosslinking (Li, Wijekoon and Leipzig, 2012) or conjugation with perfluorocarbons to enhance oxygen release in the core of the gels (Li, Wijekoon and Leipzig, 2014). In both cases, NSCs displayed a rounded morphology lacking in prominent neurite extensions, even though neuronal markers were still present via immunocytochemistry. This leads to an almost counterintuitive conclusion, by which neural differentiation is still initiated in the cells throughout these scaffolds (leading to positive neuronal marker expression) but the cells themselves seem unable to generate extensive cell-cell connections outside of aggregates formed within the matrix, perhaps due to an intrinsic steric hindrance or lack of native adhesion moieties.

An intriguing solution to the lack of neurite outgrowth when neural progenitors are encapsulated in non-native matrices is the addition of protease cleavable peptides into the structure of a synthetic hydrogel (McKinnon, Kloxin and Anseth, 2013). mESC-derived motor neuron progenitors seeded in polyethylene glycol (PEG) hydrogels covalently crosslinked with matrix metalloproteinase (MMP) cleavable peptide sequences and functionalised with other binding epitopes (with moduli around 350Pa) showed robust neurite outgrowth and retained high cell viability, while stiffer moduli (>2kPa) induced almost uniform cell death. Scaffolds without the MMP-cleavable sequence showed no axonal outgrowth. This is a good demonstration that for 3D neural culture, simply having biomimetic binding motifs may not be enough to induce a true *in vivo*-like neuronal morphology and the ability for the cell to manipulate the surrounding matrix is integral to tissue-like recapitulation and development.

This directed assembly of 3D growth cultures, rather than simple scaffold-based cell encapsulation, may be able to pre-form necessary cytoarchitecture relevant for particular areas of neural tissue modelling and *in vivo*-like recapitulation. Assembly of cell-laden hydrogel “building blocks” already has precedent in the literature and can combine processes such as emulsification, photolithography, microfluidics, micromoulding, and bioprinting (Kachouie *et al.*, 2010). As well as being able to accurately arrange cell types in 3D environments it also allows the possibility of developing pseudo-vasculature in the derived 3D culture and perhaps even targeted delivery of trophic factors (Kang *et al.*, 2016). A bio-printable scaffold material formulated from alginate, carboxymethyl-chitosan, and agarose has been demonstrated to support hiPSC-derived neural differentiation within *in silico*-designed construct architectures (Gu *et al.*, 2017). Similarly, a hand-held bio-printing

technique with a peptide-functionalised gellan gum “bioink” has been able to recapitulate printed laminar structures representative of layered cortical tissue (Lozano *et al.*, 2015).

3D environments can also be generated from colloidal layering of cell-coated silica beads (45µm in diameter). Different neural subtypes attached to separate “pools” of beads will self-assemble into arrays when added into a growth chamber. In essence, each layer of beads can be tailored in composition to form highly controlled 3D arrangements, with functional synaptic connections measurable between multiple layers of cell-laden beads (Pautot, Wyart and Isacoff, 2008) that showed asynchronous patterns and differential burst firing timings than seen from basic 2D neural network formation (Frega *et al.*, 2015).

Taken all together, the array of biomaterials and fabrication technologies available for processing both 2D and 3D growth substrates for neural tissue engineering is vast (Fig 1-6). Covering all aspects of intrinsic biomaterial properties, binding moieties, substrate stiffness, topographical patterning, and functionalisation; the ability to completely tailor *in vitro* environments for any conceivable aspect of neurological modelling and combine them with additive fabrication technologies, electrode arrays and microfluidic devices will be at the forefront of the next generation of neural tissue modelling.

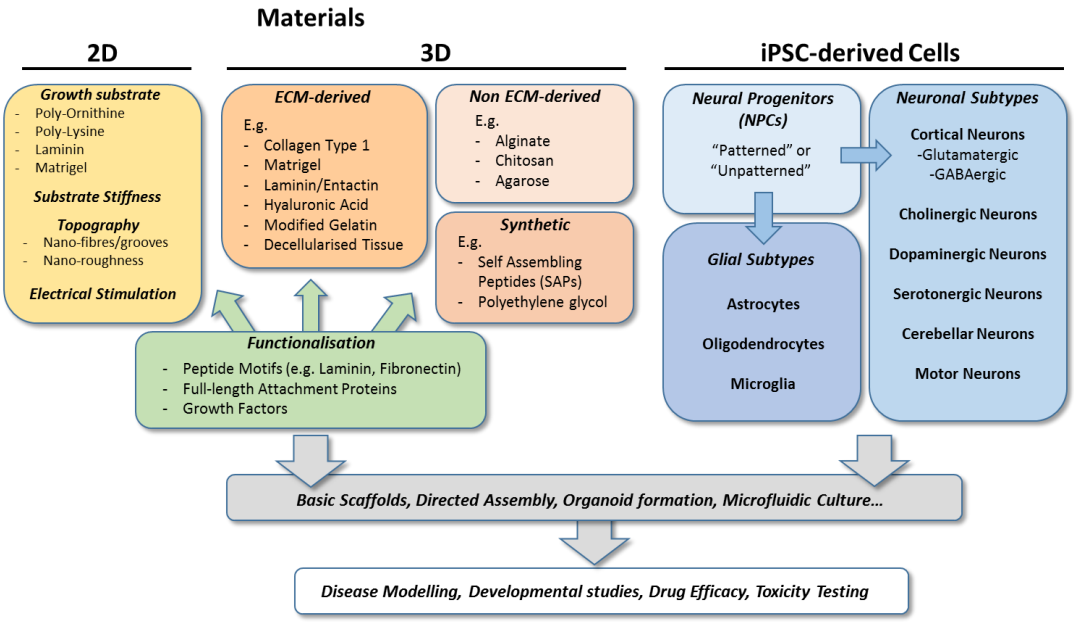

Figure 1-6: Overview of the possible material and cellular components of *in vitro* iPSC-derived neural cultures. Growth material selection may be in two- or three-dimensions and be of biological or synthetic sources. Modifications of materials can be through covalent functionalisation or the formation of composites, and can be processed into differing shapes and topographies. iPSC-derived neural cells can be patterned to specific subtypes and be combined with other neural cell lineages to develop brain-like architecture when combined with the 2D/3D scaffold materials.

1.8 Thesis Aims and Structure

Modern neurological research into human neurodevelopmental and neurodegenerative pathologies has been revitalised with the advent of induced pluripotent stem cell technology. The generation of genomically-clean, patient-specific and developmentally representative neural models *in vitro* has broad promise for not only understanding brain development and dysfunction, but to also act as a foundation stone for full regenerative therapies and drug efficacy & toxicology studies.

In addition to this, the rise of additive fabrication technologies such as 3D bioprinting within the biomedical field, holds great promise for generating more representative tissue-like constructs from an ever-increasing array of synthetic and biological materials.

The ideal *in vitro* modelling system would therefore involve the combination of iPSC-derived neural cultures differentiated within tailored 3D matrices allowing for the

development of a highly representative *in vivo*-like tissue constructs that contain specific neural cell subtypes from particular brain regions, in the appropriate cytoarchitecture, to create developmental- or disease-related network formations.

For this holistic approach to modelling brain biology to work fully and faithfully "in-the-dish", each element of its construction must be assayed; to ensure reproducible and developmentally representative neural cell differentiation from iPSCs; and to develop the appropriate assays of biomaterials from which to build the 3D *in vivo*-like environments for the derived cell types to interact with and form native cellular architecture and function.

Broadly speaking, this body of work will focus on achieving the following aims:

- To assay an array of candidate biomaterials for use as the basis for three-dimensional neural tissue scaffolds by focusing primarily on the biomolecular and biophysical responses that the matrices induce in embedded neural cells.
- To generate forebrain-specific excitatory and inhibitory neural cell populations from human iPSCs. The development of both of these cell types *in vitro* is integral for modelling not only true human forebrain development but also as the basis for disease-specific modelling of forebrain-derived pathologies such as the epilepsies.
- To compare the effect of iPSC-neural differentiation within the most promising 3D biomaterial candidate and to compare this to differentiation on 2D planar culture, in order to ascertain how differentiation strength, speed and efficiency is affected through 3D culture.
- To determine the biomaterial characteristics that maintain potential for neural cell maturation and differentiation *in vitro*, but also allow for 3D bioprinting processes that would enable more complex neural tissue-model architecture to be formed, beyond the capability of currently available bioinks.

Chapter 2 focuses on the development and assaying of candidate biomaterials for 3D neural cell culture using a neural cell-line as a proxy for hiPSC-derived neural cell cultures. The materials under investigation are alginate and collagen type I, both with and without the formation of composite gels with a Matrigel-equivalent ECM mix termed "ECL". Alginate scaffolds with covalent peptide-functionalisation with matrix metalloproteinase (MMP) cleavable motifs and laminin-derived binding moieties are also generated and tested in parallel to unmodified scaffolds. The majority of assay techniques focus on

biomaterial properties through the lens of cellular responses, and therefore positive and negative results of each scaffold are based on; retention of cell viability, conduciveness to neurite extension and native morphology, gene & protein expression of differentiation-associated markers, and comparisons to 2D differentiation benchmarks.

***Chapter 2 Hypotheses*:**

1. The neuritogenic potential of embedded neural cells in unmodified alginate hydrogels is low in comparison to collagen scaffolds, and this morphological difference is reflected in neuronal gene and protein expression.
2. Modification of alginate hydrogels with MMP-cleavable and laminin-binding peptide motifs will attenuate the morphologically restrictive nature of the hydrogel.
3. Candidate biomaterials for neural tissue engineering can be assessed through changes in neural gene and protein expression in synergy with morphological assessment of neuritogenesis

Chapter 2 Findings:

- Using aqueous carbodiimide chemistry; double-ended MMP-cleavable and laminin-binding peptide motifs can be covalently bonded to alginate polymers with high efficiency.
- Collagen type I, alginate and peptide-modified alginate hydrogels all allow for high retention of metabolic activity/cell viability of encapsulated neural cells during scaffold gelation, as well as over the time course of neural differentiation.
- Collagen type I hydrogels (both with and without ECM protein components) allow for neurite extension of encapsulated PC12 neural cells over the same time course as 2D planar differentiation.
- Low concentration alginate hydrogels are non-conducive to neuritogenesis of encapsulated differentiating PC12 neural-like cells. This effect is not ameliorated by the addition of extracellular matrix proteins.
- Peptide-modified alginate hydrogels also do not allow for neuritogenesis of encapsulated neural cells.
- The canonical neuronal protein markers β-III-Tubulin and GAP43 increase in expression over the time course of neural differentiation in 2D and 3D culture. These increases do

not reflect the neuritogenic potential of the hydrogel scaffolds and are highly expressed in alginate and alginate-peptide scaffolds which restrict neurite formation.

- Other neuronal protein markers MAP2, P-MAP2, NF-H, and NF-L do show stark differences in expression profiles during neural differentiation in the various biomaterial scaffolds. These markers therefore represent more reliable measures of neuritogenic potential of candidate biomaterials.

Chapter 3 focuses on the development of differentiation strategies of human iPSCs into both excitatory and inhibitory forebrain neuronal cell populations using neural tube patterning factors in 2D. These distinct cell populations develop separately embryologically, but following pre-natal migration, form complete forebrain-cortical structures and networks. This chapter follows the molecular timings and comparisons between distinct neural developmental pathways from hiPSCs *in vitro* and tracks the timings of subtype development, loss of pluripotency, neuronal maturation markers, synaptic machinery, and neurotransmitter receptor apparatus. As well as biomolecular markers of maturation and development, this chapter also studies the functionality of the cells through assaying of intra- and extra-cellular electrophysiological recordings of derived neural cell types. By tracking the generation of these cell types in parallel will allow for the formation of more complete and representative forebrain/cortical models.

Chapter 3 Hypotheses:

1. hiPSCs can be efficiently differentiated into mature neural cells over 60 days of differentiation and display markers of subtype specificity, forebrain regionalisation, and pre- & post-synaptic machinery.
2. Neural cell cultures can be efficiently patterned into dorsal (excitatory) and ventral (inhibitory) neuronal subtypes over a parallel time course.
3. Both dorsal and ventral neural cultures mature at equivalent rates and display equivalent molecular and functional markers of maturity.

Chapter 3 Findings:

- hiPSCs undergoing neural induction via dual-SMAD inhibition pathways generate NPCs with high efficiency over 7-14 days.
- Further maturation of NPCs without exogenous signalling morphogens will derive neuronal cells with extensive neuritogenesis after 28 days of differentiation and both neuronal and glial-lineage cell types by Day 60 of maturation.
- Neural cell cultures differentiated for 60 days will express markers of; cortical and forebrain localisation; excitatory glutamatergic neuronal subtype; pre- & post-synaptic components; and glutamate- & GABA-sensitive neurotransmitter subunits.
- Ventral patterning of NPCs, through the use of a sonic hedgehog-pathway agonist, generates mature neurons of a predominantly inhibitory GABAergic cell type after 60 days of differentiation and show heavily reduced cortical marker expression.
- Ventral-patterned neural cells show slight enrichment of neuronal associated markers at the gene and protein level in comparison to the default (dorsal) induction pathway.
- Both dorsally- and ventrally-patterned matured neuronal cells can fire an action potential under intracellular current stimulation. Multiple action potentials can be evoked from ventrally-patterned neuronal cells depending on the current stimulus level, demonstrative of a more mature phenotype than is seen in dorsally-patterned neurons.
- Transient sodium and potassium currents are both present after stimulation of dorsally- and ventrally-derived neurons. Both current levels are higher in ventrally-patterned cultures, indicative of a more mature ion channel composition phenotype. However, potassium currents in neurons from both patterning methodologies are low, showing an overall immature phenotype for all neurons assayed.

Chapter 4 will combine the differentiation pathways outlined in Chapter 3 and compare them to iPSCs differentiated within the top candidate biomaterial scaffold determined from Chapter 2. This chapter will elucidate the morphology of iPSC-derived neural cells within the scaffold and determine the rate of maturation of the 3D neural cultures when directly comparing to differentiation in 2D planar culture, using gene expression profiling. This chapter will also ascertain whether scaffold composition has an influence on the

morphogen patterning of embedded NPCs (either positively or negatively) as this may be an important factor when generating mixed neural subtype-specific 3D scaffolds.

Chapter 4 Hypotheses:

1. Differentiation of hiPSC-derived neural cells within 3D collagen type I hydrogels will enhance the speed and strength of neuronal differentiation and maturation compared to 2D culture.
2. The 3D hydrogel environment does not negatively impact the dorsal-ventral patterning of encapsulated hiPSC-derived NPCs during differentiation.

Chapter 4 Findings:

- hiPSC-derived NPCs differentiating within 3D collagen type I scaffolds undergo neuritogenesis in all three axes throughout the hydrogel over 60 days of differentiation.
- 3D encapsulated neural cultures express protein markers of post-mitotic neuronal generation as well as pre-synaptic machinery.
- Enhanced NPC marker expression was seen within ventrally-patterned neural cells but not with dorsally-patterned neural cultures when encapsulated in 3D hydrogel environments.
- 3D Ventral cultures show early peak expression of neuronal and synaptic markers significantly above the levels of 2D cultures and 3D Dorsal neural cultures.
- By later time points of differentiation: neuronal, axonal and synaptic marker expression are lower in 3D microenvironments than in 2D planar culture, suggesting an inhibition of maturation.
- Excitatory and inhibitory neuronal subtype marker expression are preserved in dorsal/ventral patterning in 3D environments, but with lower levels of expression than is seen in planar differentiation.
- Dorsal cortical localisation markers are observed in both 2D and 3D Dorsal neural cultures. In 3D scaffolds however, early-cortical markers (*REELIN, TBR1*) display expression profiles lower than in 2D differentiation, and late-cortical markers (*CTIP2, SATB2*) show enhanced expression relative to 2D Dorsal cultures.

- 3D Ventral neural cultures show significantly high expression spikes of *$GABA_BR1$*, *NMDAR1* and *AMPAR1* neurotransmitter receptor subunits, not seen in 3D Dorsal differentiation. By later time points of maturation, these markers tend to show lower expression in 3D cultures compared to 2D differentiation.
- Neuronal generation is not limited within 3D hydrogel scaffolds, but functional maturation does appear to be restricted under these experimental conditions.
- Astrocytic gliogenesis is enhanced in 3D differentiation environments compared to 2D cultures.

Chapter 5 will focus on aspects of bioprinting neural tissue and the biomaterial considerations that maintain positive neural differentiation and network formation, but balancing this with the constraints of developing bioinks that are conducive to additive fabrication technologies. Modifications and methodologies of printing neural tissue constructs from existing biomaterials utilised in Chapters 2 and 4 will be explored.

Chapter 5 Hypotheses:

1. Unmodified alginate or collagen hydrogel compositions will demonstrate low intrinsic bioprintability.
2. Combining a pro-neuritogenic collagen-based "core" bioink and a structurally robust cytocompatible alginate "shell" bioink will allow for self-supporting coaxial bioprinting suitable for neural tissue-modelling.
3. Segregation of the core and shell bioinks will be maintained under physiological conditions and maintain cell viability and neuritogenesis of encapsulated neural cells.

Chapter 5 Findings:

- Low concentration collagen and alginate hydrogel solutions show poor bioprinting traits.
- Alginate and gelatin composite bioinks show differential printing characteristics heavily dependent on concentration and ratio to each other. A 3% alginate and 5% gelatin mix was found to have promising properties for a bio-printable material.

- Coaxial printing of a collagen-based core material designed to be amenable to neural cell differentiation, and an alginate-gelatin shell bioink surrounding the core adding to the structural integrity of the scaffold, was developed.
- Core/shell separation was conserved throughout the printing process and could form two-layer *in silico* designed grid structures.
- Acellular versions of the scaffold construct could be handled manually and maintained structural integrity after storage under physiological conditions.
- Separation of core and shell biomaterial components was demonstrated through fluorescent-bead loading of the core material, which displayed continued core/shell separation after maintenance at 37^{o}C.
- Neural cell encapsulation and growth within the bioprinted core component of the coaxial scaffold demonstrated the retention of high cell viability by day four post-printing.
- Neuritogenesis was prevalent by day 7 of differentiation post-print within the coaxial scaffold. Demonstrating conduciveness to neural differentiation within the core collagen-based bioink.

Chapter 6 is the final conclusion and discussion chapter pulling together analysis from all of the previous chapters and to frame the work in the context of the field as it currently stands. It will also contain speculations and recommendations for future directions of this research as well as possible inherent limitations.

1.9 Notes on Usage

Throughout the results chapters within this thesis, the plural form of personal pronouns ("we/our" rather than "I/my") have been used as a stylistic preference to be more in line with the current format of scientific reporting.

Chapter 2: Biomaterial Optimisation for Three-Dimensional Neural Culture

2.1 Introduction

For any *in vitro* modelling of human neurodevelopment to be successful, it is critical that the growth and assay conditions of neural cell cultures accurately reflect and recapitulate the *in vivo* environment as closely as possible. To this end, many studies have focused on developing three-dimensional (3D) growth environments for neural cell differentiation and culture rather than simple planar culture. The potential advantages of this approach include; greater degrees of cell-cell interaction; enhanced paracrine effects (owing to a more restrictive diffusion rate of secreted signalling molecules); increased cell-matrix interactions allowing for cell migration, cell aggregation & self-organisation within three-dimensional space; and the responsiveness of differentiating neural cells to material moduli (and other biophysical properties) representative of native tissue (LaPlaca *et al.*, 2010).

Scaffold matrices that allow for complete encapsulation of cells and are conducive to neurite extension, is a prerequisite to one of the most important facets of *in vitro* neural tissue engineering: that of active synaptic network formation. Candidate scaffold materials must be selected on the basis of not only being permissive to this morphological development of neural cells, but possibly its enhancement to a level not demonstrated in basic two-dimensional (2D) culture.

Hydrogels are 3D scaffolds generated from networks of hydrophilic polymer chains. When transitioning into their gelled form they can retain water content above 90% of their mass, and as such, are highly suited to model *in vivo*-like cellular microenvironments (Drury and Mooney, 2003). They have been used extensively throughout the literature as scaffolds for tissue engineering of multiple tissue types (Kachouie *et al.*, 2010). Many biological and non-biological polymers can be used to form neural tissue hydrogels (see Section 1.7.2), but this chapter will focus on two commonly used natural biomaterials; alginate and collagen type I.

Alginate (sodium alginate or alginic acid) is an anionic polysaccharide derived from brown algae that undergoes sol-gel transition through divalent cation crosslinking. Alginate hydrogels have been widely used for three-dimensional neural cell culture (Banerjee *et al.*, 2009; Frampton *et al.*, 2011; Andersen, Auk-Emblem and Dornish, 2015) and as a key biomaterial in additive fabrication technologies such as bioprinting (Chung *et al.*, 2013). The use of alginate scaffolds as a basis for three-dimensional neural differentiation from murine and human pluripotent stem cells also has precedence within the literature (Li *et al.*, 2011; Lu *et al.*, 2012; Kim, Sachdev and Sidhu, 2013; Kuo and Chang, 2013; Bozza *et al.*, 2014), with differentiation efficiencies reportedly higher in these gels than parallel neural inductions in suspension culture (Lu *et al.*, 2012). Although the baseline properties of unmodified alginate hydrogels have shown promising results in upregulating levels of neuronal markers in embedded neural stem cells (Banerjee *et al.*, 2009; Meli *et al.*, 2014), the ability for neural cells within alginate scaffolds to undergo extensive neuritogenesis is restricted without ultra-low concentrations of alginate within the hydrogel and sub-stoichiometric amounts of the ionic crosslinker (Matyash *et al.*, 2012, 2014; Palazzolo *et al.*, 2015).

Greater success on this front has been reported either through covalent modification of the alginate itself or through the formation of composite gels containing blends of other biomaterials to help aid cell attachment and morphological development. For example; the enrichment of alginate hydrogels with fibronectin helped ameliorate the lack of encapsulated dorsal root ganglion (DRG) sprouting (Novikova *et al.*, 2006) and composite alginate microbeads formed with gelatin (a hydrolysed product of collagen type I) showed a higher proliferative capacity of neural stem cells (NSCs) than that seen in standard suspension culture (Song *et al.*, 2014).

Rather than simple blending of hydrogel components to form enhanced scaffolds, covalent modification of alginate with peptide motifs designed from extracellular matrix attachment epitopes can add a biomimetic element to the hydrogels not present in the basic polysaccharide structure. The covalent addition of Arginine-Glycine-Aspartic Acid (RGD) cell adhesion ligands to the alginate backbone using aqueous carbodiimide chemistry was first shown by Rowley et al. as a way of promoting cell attachment to alginate hydrogel surfaces (Rowley, Madlambayan and Mooney, 1999). This type of functionalisation with the fibronectin-derived RGD ligand however, did not improve 3D neural culture of primary neurons or glial cell lines, whereas functionalisation with either full-length laminin or a

laminin-derived binding peptide did improve neural outgrowth in alginate hydrogels (Frampton *et al.*, 2011).

The presence of rounded-cell morphology and lack of cell spreading without modification of alginate hydrogel environments (or using ultra-soft under-crosslinked compositions) has been overcome by the addition of matrix metalloproteinase (MMP)-cleavable motifs into the scaffold backbone for culture of mesenchymal stem cells (Fonseca *et al.*, 2011). Showing that not only is cell attachment integral to successful interaction with the three-dimensional environment, but that local proteolysis and the ability for cells to remodel their surroundings is key to morphological changes and cell function. This is of course combined with the synergistic factors of low hydrogel modulus, native binding epitopes, as well as overall porosity derived from limited dry mass composition and crosslinking conditions. This concept has also been successfully shown in 3D motor neuron cultures, although through modification of a synthetic polyethylene glycol (PEG) scaffold, rather than an alginate-based one (McKinnon, Kloxin and Anseth, 2013).

Type I collagen (referred to herein as "collagen") is a mammalian extracellular structural protein that can form *in vitro* hydrogel scaffolds. Collagen scaffolds have been widely used for tissue engineering purposes due to their innate cell adhesion properties, biocompatible nature and multiple hydrogel fabrication technologies (Antoine, Vlachos and Rylander, 2014). As with alginate, multiple studies have used collagen as the basis for three-dimensional neural tissue constructs (O'Connor *et al.*, 2001; Sundararaghavan *et al.*, 2009). Functionalisation with both fibronectin and laminin binding motifs, however, results in significantly higher neuronal marker expression in encapsulated dorsal root ganglion cells (Hosseinkhani *et al.*, 2013) and covalent attachment of individual laminin subunits triggers an increase in cell survival of embedded neural stem cells (NSCs) (Nakaji-Hirabayashi, Kato and Iwata, 2012).

Although much has been done to individually assess and modify both alginate and collagen scaffolds, very little has been shown that directly compares the effect of each biomaterial on the biomolecular process of neural differentiation and to directly compare different subsets of biomaterial hydrogels to each other and to 2D culture. Positive results for marker expression data may not reflect adequate neuronal outgrowth or cell-cell contact generation, and conversely, the presence of neurite morphology may not

necessarily invoke molecular changes during differentiation to a higher degree than in planar culture.

The aims of this chapter are to contrast five candidate biomaterial hydrogels: alginate (Alg); alginate composites with a Matrigel equivalent, termed "ECL" (Alg + ECL); collagen (Coll); collagen composites with ECL (Coll + ECL); and a peptide-functionalised alginate (Alg-Pep) which contains both metalloproteinase-cleavable and laminin-binding motifs representative of native extracellular matrix. These three-dimensional hydrogel-embedded neural cultures will ascertain which combination of functionalised or composite hydrogels elicit the strongest upregulation of differentiation markers and which allow the greatest degree of neurite extensions and *in vivo*-like morphology.

To streamline this process, experimental work in this chapter will be undertaken using a pheochromocytoma (PC12) neural-like cell line as a proxy for human iPSC-derived neural cells. The ability of the PC12s to mirror morphological changes of differentiating neural cells as well as expression of neuronal markers is well documented (Ohuchi *et al.*, 2002; Das, Freudenrich and Mundy, 2004; Won *et al.*, 2015). By using this cell line rather than iPSC-derived or primary neurons, a much more condensed, stable and higher-throughput molecular analysis can be used to ascertain which hydrogel configuration and composition best supports neuronal cell differentiation and thus is the most promising for downstream hiPSC-based differentiation in three-dimensional scaffolds.

Other than basic material properties such as matching moduli to native tissues and gelation conditions, the focus of this chapter will be one devoted to that of the neural tissue outcome – namely; what are the effects of each biomaterial on these differentiating neural-like cells in relation to cell viability, cell morphology, and the expression of neural gene & protein markers.

2.2 Materials and Methods

2.2.1 Cell Culture

Adherent PC12 cell cultures were maintained in a proliferation media composed of Dulbecco's Modified Eagle Media (DMEM) (Lonza), 5% Foetal Bovine Serum (FBS) (Gibco), 10% Horse Serum (Gibco), 2mM L-Glutamine (Gibco), 100U/ml Penicillin and 100µg/ml Streptomycin (Gibco). Cultures were incubated at 37^{o}C and 5% CO_2. Cells were passaged using a 0.025% Trypsin Dissociation Buffer for 5 minutes at 37^{o}C before re-plating in growth media. Differentiation of PC12s was triggered using a differentiation media composed of DMEM (Lonza), 1% Horse Serum (Gibco), 2mM L-Glutamine (Gibco), 100U/ml Penicillin, 100µg/ml Streptomycin (Gibco), and 50ng/ml Nerve Growth Factor (NGF) (Sigma). Over the course of differentiation, media was changed every 2 days. For expansion, cells were grown in 75cm^2 tissue-culture coated flasks, whereas for 2-dimensional differentiation experiments; PC12s were grown on Collagen I pre-coated 75cm^2 culture flasks (Corning). After differentiation, cells were harvested using the dissociation procedure described above and pelleted by centrifugation. Cell pellets were stored at -80^{o}C prior to molecular analyses.

2.2.2 Preparation of 3D Scaffolds

PC12s were harvested (as described above) from growth flasks at 37^{o}C for 5 minutes. Cell counts were performed using trypan blue (Thermo Fisher Scientific) staining and quantified using a haemocytometer. The cell density for each cell-laden hydrogel was 1x10^6 cells/ml.

Alginate hydrogel scaffolds were formed in sterile de-ionised water at a final concentration of 0.5% (w/v) Sodium Alginate (Sigma), 1x HEPES Buffer pH 7.4 (20mM HEPES [Sigma], 150mM NaCl [Sigma]), 15mM $CaCO_3$ (Sigma), and 30mM Gluconolactone (Sigma). Scaffolds with ECL ("+ECL") contained a final concentration of 0.05mg/ml ECL Cell Attachment Matrix (Millipore). All components listed above were mixed by pipetting prior to cell addition. The 1:2 $CaCO_3$:Gluconolactone molarity ratio ensures a balanced end pH but triggers the solubility of $CaCO_3$. 200µl of the hydrogel solution was added per well of a 48-well tissue culture plate to form each scaffold. Scaffolds underwent gelation at 37^{o}C for 15 minutes before addition of 0.5ml differentiation media per well. For peptide-

functionalised alginate (Alg-Pep) hydrogel scaffolds the process of formation was the same but final concentration of alginate solutions was split 1:1 between the MMP-modified alginate (0.25% w/v final) and the Laminin-modified alginate (0.25% w/v final) creating an overall 0.5% (w/v) alginate concentration with an even mixture of each alginate-peptide type. The process of functionalisation and characterisation of peptide modified alginate is outlined in sections 2.2.9 and 2.3.1.

Collagen hydrogel scaffolds were formed in sterile de-ionised water at a final concentration of 0.4mg/ml Collagen Type I from Rat Tail (Corning). Collagen hydrogel gelation was triggered with the addition of 0.23x of the added collagen volume of 0.1M NaOH (Sigma), and 1x HEPES Buffer pH 7.4 (20mM HEPES [Sigma], 150mM NaCl [Sigma]) before mixing with cells. Scaffolds with ECL ("+ECL") contained a final concentration of 0.05mg/ml ECL Cell Attachment Matrix (Millipore). Collagen and NaOH working volumes were mixed (to trigger neutralisation) prior to addition to buffered cell suspensions. 200µl of the hydrogel solution was added per well of a 48-well tissue culture plate to form each scaffold. Scaffolds underwent gelation at 37^{o}C for 30 minutes before the addition of 0.5ml differentiation media per well. Approximately 70% of media volume was exchanged every two days over the time course of differentiation for all hydrogel types.

2.2.3 Scaffold Digestion and Cell Retrieval

Cells from 3D differentiation experiments were harvested at Day 1, 3 and 7 for molecular analyses. Media was removed from alginate scaffold wells and the scaffold was de-gelled with the addition of 50mM Sodium Citrate (Sigma) in 1x Hank's Buffered Saline Solution (HBSS) (Gibco). Scaffolds were left at 37^{o}C for 15 minutes prior to trituration and transfer to centrifugation tubes. For Collagen-based scaffolds, differentiation media was exchanged for 0.5ml DMEM containing 0.05mg/ml Collagenase Type 1 (>125U/mg, Worthington Biochemical Corporation) per well. Scaffold digestion took place at 37^{o}C for 45 minutes prior to trituration and centrifugation of cell pellets. Cells from four scaffolds were pooled to form one pellet from each experimental setup. Cell pellets were stored at -80^{o}C.

2.2.4 Metabolic Activity and Cell Viability

Cell viability in 3D cultures was determined with an AlamarBlue (Thermo Fisher Scientific) metabolic assay. 50µl of AlamarBlue was added into each scaffold-well which contained 0.5ml of differentiation media. Experimental plates were incubated for 4 hours at 37^{o}C. 200µl aliquots were removed from each well and transferred to opaque 96-well assay plates (Corning/Sigma). Fluorescence readings were measured on a FLUOstar Galaxy Plate Reader (BMG) with an excitation wavelength of 550nm and an emission filter of 590nm. Each time point was averaged from scaffold triplicates, and each triplicate from 4 biological repeats. Statistical analysis was completed using GraphPad Prism software (version 5). For intra-scaffold data, a one way-ANOVA with Tukey's post-hoc test was used to ascertain statistical significance between time points. For inter-scaffold data, a two-way ANOVA with Bonferroni post-test was used to determine statistical significance between scaffold types at each time point.

2.2.5 Western Blot Assay

Cell pellets were resuspended in 100-200µl of M-PER Mammalian Protein Extraction Reagent (Thermo Fisher Scientific) and mixed gently at room temperature for 10 minutes. After centrifugation at 10,000x*g* for 15 minutes the supernatants were transferred to new 1.7ml microfuge tubes and stored at -80^{o}C until needed for downstream assays.

A colourmetric Bradford assay was used for total protein quantification, calibrated against a Bovine Serum Albumin (BSA) (Sigma) standard curve. 2µl of each protein sample was utilised for protein quantification together with 200µl of 1:5 diluted Bradford Reagent (Bio-Rad). Absorbance readings at 590nm were measured on a FLUOstar Galaxy plate reader (BMG).

For SDS-PAGE; protein samples were denatured at 70^{o}C for 10 minutes in the presence of NuPAGE LDS Sample Buffer (Thermo Fisher Scientific) and NuPAGE Sample Reducing Agent (Thermo Fisher Scientific). Protein samples were separated on BOLT 4-12% Bis-Tris Gels (Thermo Fisher Scientific) at 150V for 45 minutes. Molecular weight estimation was achieved with parallel loading of Precision Plus Protein Kaleidoscope Prestained Protein Standards (Bio-Rad). Protein lanes were transferred on to nitrocellulose membranes (GE Healthcare Life Sciences) using Semi-Dry Transfer (Bio-Rad) at 20V for 70

minutes in Bjerrum Schafer-Nielsen buffer (48mM Tris, 39mM glycine, 1.3mM SDS, 20% Methanol). Successful protein transfer was confirmed with Ponceau S stain (0.1% w/v) in acetic acid, and de-stained through washing in Tris buffered saline (TBS) with 0.05% Tween-20 (TBST) (50mM Tris, 150mM NaCl, pH 7.6). Membranes were blocked for 1 hour at room temperature in either 5% (w/v) low fat milk powder in TBST or 5% (w/v) BSA in TBST. Membranes were incubated with primary antibodies overnight in the block solution at 4^{o}C on a plate rocker: anti-TUJ1 (Covance MMS-435P, 1:2000), anti-GAP43 (Millipore AB5220), anti-MAP2 (Cell Signaling Technology #4542, 1:2000), anti-Phospho-MAP2-Ser136 (Cell Signaling Technology #4541, 1:2000), anti-neurofilament-H (Cell Signaling Technology #2836, 1:2000), anti-neurofilament-L (Cell Signaling Technology #2837, 1:2000) & anti-GAPDH (Cell Signaling Technology #5174, 1:5000). Membranes were washed three times in TBST prior to addition of secondary antibodies. Membranes were incubated with secondary antibodies in block solution for 1 hour at room temperature on a plate rocker: Goat-anti-Mouse-HRP (Millipore, 1:10,000), Goat-anti-Rabbit-HRP (Millipore, 1:10,000). Membranes were washed a further three times in TBST and once in TBS prior to chemiluminescent detection. Imaging of protein bands on membranes was achieved on a ChemiDoc MP system (Bio-Rad) after incubation with Western Lightning® Ultra chemiluminescence substrate (Perkin Elmer). For semi-quantitative analysis of protein expression, band intensities were recorded using ImageJ software (NIH). Protein bands of interest were calculated relative to the housekeeping gene band intensity in each lane. Statistical analysis was performed using two-way ANOVA and Bonferroni post-tests in GraphPad Prism software (Version 5). Data is shown ± standard error of the mean with significance denoted when the p-value ≤0.05. Three biological repeats were completed for each scaffold-type at each time point.

2.2.6 Gene Expression

Relative gene expression analysis was performed using quantitative polymerase chain reaction (qPCR) methodology. Firstly, RNA was purified from frozen cell pellet samples using the RNeasy Plus Mini Kit (Qiagen) as per the manufacturer's instructions into a total elution volume of 50µl nuclease free water. RNA concentration was determined using an Ultraspec 2200 Pro Spectrophotometer (GE Healthcare Life Sciences) and RNA integrity was confirmed by running samples on a 1% Agarose (w/v)-EtBR TAE gel under electrophoretic

conditions for 40 minutes at 80V followed by imaging on a ChemiDoc MP (Bio-Rad) to show sharp ribosomal RNA banding.

cDNA was generated from 1µg of each RNA using the Omniscript Reverse Transcription Kit (Qiagen) with 1µM oligo dTs (Qiagen) and 1U/ml RNase Inhibitor (Qiagen). Reverse transcription reactions took place at 37°C for 80 minutes in a 20µl reaction volume. On completion of the reaction, samples were further diluted with 20µl of nuclease free water (Integrated DNA Technologies). cDNA samples were stored at -20°C until used in qPCR reactions.

Gene Target	Catalogue Number/Dye
β-III-Tubulin (Rat)	Rn.01431594_m1 FAM (Applied Biosystems)
Gap43 (Rat)	Rn.PT.47.7307335 FAM (Integrated DNA Technologies)
MAP2 (Rat)	Rn.01401429_m1 FAM (Thermo Fisher Scientific)
NF-L (Rat)	Rn.00582365_m1 FAM (Thermo Fisher Scientific)
NF-H (Rat)	Rn.00709325_m1 (Thermo Fisher Scientific)
GAPDH (Rat)	Rn.PT.47.12624405 HEX (Integrated DNA Technologies)

Table 2-1: List of TaqMan assay probes used in PC12 gene expression analyses

qPCR analyses were completed as duplex reactions using TaqMan Gene Expression Master Mix (Applied Biosystems) in 10µl reaction volumes. The TaqMan assay probes used are listed in Table 2-1. Reactions were run on a RealPlex Mastercycler (Eppendorf) with the following parameters: 50°C for 2 minutes, 95°C for 10 minutes, followed by 40 cycles of 95°C for 15 seconds and 60°C for 1 minute. Data were analysed by the ΔΔCt method in Microsoft Excel and statistical analyses performed in GraphPad Prism (Version 5) using two-way ANOVA with Bonferroni post-test analysis. Data is shown ± standard error of the mean with significance denoted when the p-value ≤0.05. Three biological repeats were completed for each scaffold-type at each time point.

2.2.7 Rheological Measurements

Storage moduli were measured using an Anton Paar MCR 702 TwinDrive rheometer with a 25mm-diameter 2°-angle measuring cone (Anton Paar, #79039). 170µl of each scaffold

solution was used in each measurement. Crosslinking was monitored during 1Hz oscillations and 1% strain at 37^{o}C. Final storage moduli were calculated from when the rate of change of the moduli reached plateau. Rheological data is presented as mean ± standard error of the mean from three separate experiments. Statistical significance was calculated in GraphPad Prism software using one-way ANOVA with Tukey's post-test.

2.2.8 Live Cell and Immunofluorescence Microscopy

Live cell images were taken on an EVOS XL Core Cell Imaging System (Thermo Fisher Scientific) and processed on ImageJ software (NIH).

Three-dimensional scaffolds for immunocytochemistry were fixed for 1 hour at room temperature in 10% neutral-buffered formalin solution (Sigma) and permeabilised for 1 hour at room temperature in 0.5% Triton-X-100 (Sigma) in phosphate buffered saline (PBS) (137mM NaCl, 10mM Phosphate, 2.7mM KCl, pH 7.4). Samples were blocked overnight at 4^{o}C in 5% goat or donkey serum (Millipore) in PBS before incubation with primary antibodies (also in block solution) overnight at room temperature; anti-TUJ1 (Covance MMS-435P, 1:1000). Constructs were washed three times for 1 hour each in PBS before addition of secondary antibodies; goat-anti-mouse IgG AF488 (Invitrogen A11029, 1:2000) in block solution overnight at room temperature. Constructs were washed three more times in PBS before addition of DAPI (Sigma) for 1 hour, for cell nuclei visualisation.

For phalloidin staining (Texas Red-X Phalloidin, Thermo Fisher Scientific), constructs were fixed and permeabilised as described above. A working concentration of phalloidin stain was made at 1:100 dilution with PBS. Constructs were incubated with the stain overnight at 4^{o}C, before an overnight wash in PBS at 4^{o}C.

Image acquisition was performed using a Nikon Ti Eclipse microscope equipped with a fully automated A1 confocal laser (A1R, Nikon) and processed with NIS-Elements software (Nikon, version 4.20).

2.2.9 Synthetic Peptide Functionalisation

100mg of each crude peptide extract (>30% purity) (Wuxi Nordisk Biotech) were purified using reversed-phase High-Performance Liquid Chromatography (HPLC) and confirmed

using Ninhydrin stain (Sigma) and Mass Spectroscopy (see appendix 2.5.1). The purified MMP-peptide (with sequence GGYGPVGLIGGK) and the Laminin-peptide (with sequence GGSDPGYIGSRGGK) were then lyophilized and stored at -20^{o}C prior to use.

A 1% (w/v) alginate solution (Sigma) was formed in a 2-(N-morpholino) ethanesulfonic acid buffer (MES buffer) (0.1M MES [Sigma], 0.3M NaCl [Sigma], pH 6.5); buffer conditions outlined in previous peptide carbodiimide-based functionalisation protocols (Fonseca *et al.*, 2011; Ferris *et al.*, 2015). Under stirring conditions, the reaction components N-Hydroxysulfosuccinimide (Sulfo-NHS, Sigma) and N-(3-Dimethylaminopropyl)-N'-ethylcarbodiimide hydrochloride (EDC, Sigma) were added to the MES buffered alginate at a ratio of 31.1mg/g alginate and 27.4mg/g alginate respectively. This resulted in a molarity ratio of 1:2 sulfo-NHS:EDC. The solution was mixed at room temperature for 15 minutes prior to the addition of either the MMP- or Laminin-peptide at a ratio of 10mg/g alginate. The mixture was further stirred for 20 hours at room temperature. The reaction was quenched with the addition of hydroxylamine (Sigma) at a final concentration of 5mM for 10 minutes. Unreacted peptide species were removed from the reaction mix during dialysis for 4 days at room temperature using Spectra/Por 3 Dialysis Membranes (MW3500, Spectrum Laboratories). Peptide-functionalised alginates were then lyophilized and stored at -20^{o}C until use in quantification analysis and hydrogel formation.

Quantification of the degree of peptide functionalisation utilised UV-Vis absorbance of the tyrosine (Y) residues within each peptide sequence. A standard curve was generated using a 2% (w/v) alginate solution in deionised water with standard dilutions of 2.5 or 2mg/ml, 1mg/ml, 0.5mg/ml, 0.25mg/ml, and 0.0625mg/ml of each purified peptide. Absorbance was measured from 210nm to 300nm on an Ultraspec 2200 Pro Spectrophotometer (GE Healthcare Life Sciences) with base alginate as the blanking solution. Peptide-functionalised alginates were also formed in 2% (w/v) solutions for absorbance assays. The peak absorbances at 275nm of the standard curve peptides allowed for a linear regression model to be generated in GraphPad Prism software, and peptide-crosslinking efficiency was calculated from this model.

The peptide diagrams in Fig 2-1 were made using PepDraw online software (Tulane University, http://www.tulane.edu/~biochem/WW/PepDraw/index.html)

2.3 Results

2.3.1 Generation of Peptide-Functionalised Alginate

The array of both positive and negative results of unmodified alginate as a hydrogel scaffold for neural tissue engineering throughout the literature prompted the generation of a novel functionalised version of the biomaterial for direct experimental comparisons. The functionalisation outlined here utilised double-ended covalent binding of peptide motifs using aqueous carbodiimide chemistry. Two separate peptide motifs were generated, one containing an MMP-cleavable moiety (termed "MMP-peptide") and the other around a laminin-derived binding epitope (termed "Laminin-peptide") (Fig 2-1). Each peptide was crosslinked to the alginate backbone through both the peptide's N-terminal amine group and the amine group on the C-terminal lysine (K) residue side chain of each peptide.

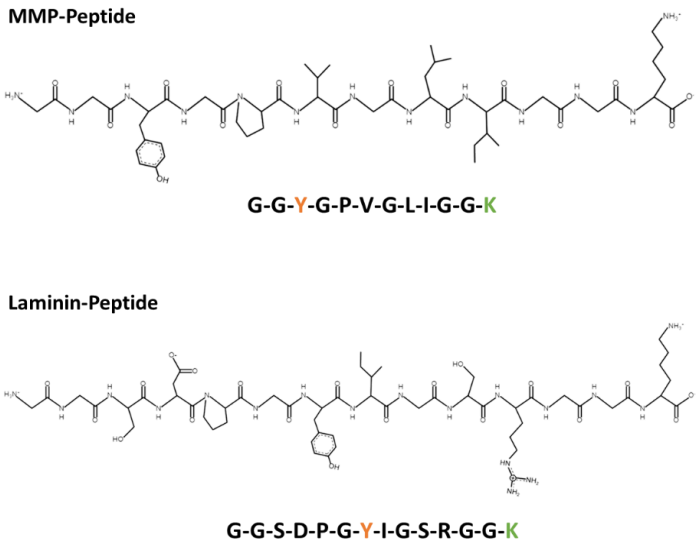

Fig 2-1: Chemical structure and amino acid sequence of the peptides used to functionalise alginate hydrogels. The MMP-peptide contains a metalloproteinase cleavable sequence (PVGLIG). The laminin-peptide contains a laminin-derived cell adhesion moiety (SDPGYIGSR). Both peptides have C-terminal lysine (K) residues (shown in green) for amine cross-linking to the alginate chains allowing for both N- and C-terminal covalent bonding. The aromatic tyrosine residues (Y, orange) allow for UV-Vis absorbance and quantification of peptide crosslinking efficiency.

The formation of chemical crosslinking events therefore utilised the carboxyl side chains of alginate polymers and the terminal amine groups of the synthetic peptides.

Peptides were also designed with an internal aromatic side chain-containing amino acid; tyrosine (Y). In the MMP-peptide this was added within a glycine spacer region to keep it separate from the MMP-cleavable domain, whereas in the laminin-peptide the tyrosine residue is a native component of the binding moiety.

The tyrosine residue allows for a UV-Vis absorption at approximately 280nm due to the aromatic side chain. As a single tyrosine residue is contained within each peptide, this then acts as a strong linear marker of peptide crosslinking and therefore of reaction efficiency. Absorbance spectra of each peptide of differing concentrations and mixed within alginate solutions showed both the absorbance at 230nm derived from peptide bond absorbance and at 270-280nm derived from the tyrosine-specific absorbance (Fig2-2 A).

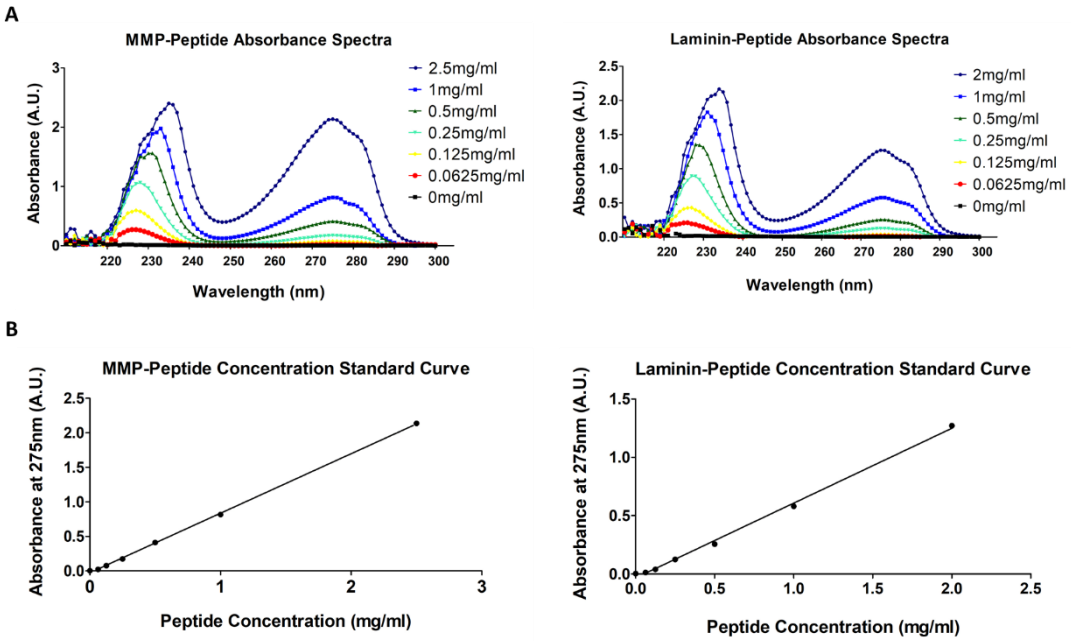

Fig 2-2: (**A**) Absorbance spectra of each peptide by which to derive concentration standard curves. Peaks around 230nm represent peptide bond absorbance. Peaks around 275nm represent Tyrosine side-chain specific absorbance. (**B**) Standard curves of peptide absorbance at 275nm for each peptide. Linear regression analysis shows strong linear agreement and basis for assessing peptide crosslinking efficiencies.

Plotting of each peptide concentration with absorbance at 275nm (the wavelength at which peak absorbance was seen) showed a strong linear relationship between absorbance and peptide concentration (Fig 2-2 B) with coefficient of determination (R^2) values calculated as 0.9995 and 0.9971 for the MMP-peptide curve and laminin-peptide curve respectively.

From this, the degree of peptide functionalisation after aqueous carbodiimide crosslinking was ascertained. For the MMP-peptide the covalent attachment conditions resulted in a degree of functionalisation of 4.05mg of peptide per 1g of alginate. This equates to a crosslinking reaction efficiency of 40.5% (Table 2-2). For the laminin-peptide the carbodiimide-derived crosslinking resulted in functionalisation of 4.68mg of peptide per 1g of alginate (Table 2-2). This had a slightly higher reaction efficiency than that of the MMP-peptide, with a calculated 46.8% crosslinking efficiency.

Peptide	Molecular Weight	Molarity in Formed Hydrogel (μM)	Peptide Functionalisation (mg/g alginate)	Reaction Efficiency (%)
MMP-peptide	1074	9.43	4.05	**40.5**
Laminin-peptide	1307	9.00	4.68	**46.8**

Table 2-2: Measures of peptide functionalisation of alginate following carbodiimide crosslinking of each peptide. Peptide molarity is based on the final 0.25% (w/v) of each modified alginate in final hydrogel scaffolds. Functionalisation degree is shown in milligrams of peptide per gram of alginate. Reaction efficiency is a measure of cross-linked peptide relative to starting peptide in the crosslinking reactions.

As well as determining mass-based figures of the crosslinking process, the overall molarity of each peptide that would be present in the final hydrogel scaffold was determined. The peptide modified alginate hydrogel scaffold (herein referred to as Alg-Pep) used in future cell experiments was formed by combining in equal measure each of the MMP- and Laminin-alginates, generating a hydrogel solution with both cell attachment and cell degradable motifs to ensure the greatest potential for positive neural cell interaction with the hydrogel scaffold. Therefore, the peptide molarities listed in Table 2-2 represent the concentration of each of the peptides in the final hydrogel solution.

2.3.2 Modulus Testing of Candidate Neural Scaffold Materials

The effect of hydrogel modulus can elicit stark morphological and biomolecular changes of attached or embedded neural cells and their precursors. Higher levels of neural differentiation have been recorded within hydrogels that have degrees of stiffness similar to those of native brain tissue (<1kPa) (Banerjee *et al.*, 2009). To ascertain whether each hydrogel composition had comparable storage moduli, rheological measurements of each biomaterial were undertaken (Fig 2-3).

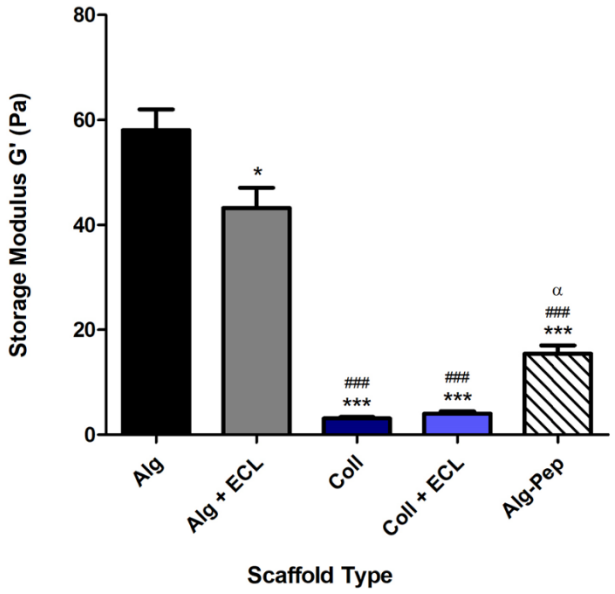

Fig 2-3: Rheological measurements of the candidate biomaterials for 3D *in vitro* neural tissue engineering. Alg, alginate; Alg + ECL, alginate composite with ECL; Coll, collagen type I; Coll + ECL, collagen type I composite with ECL; Alg-Pep, peptide-modified alginate. Data shown as mean ± standard error of the mean. Statistical significance is displayed relative to; Alg (*), Alg + ECL (#), and Coll (α). $*^{,\alpha}$ p≤0.05, $***^{,\#\#\#}$p≤0.001

The obtained storage moduli for all hydrogels were all below 60Pa, and therefore well within the limits of other neural hydrogel models with stiffness equivalent to brain tissue modulus estimates (<1kPa). Alginate scaffolds showed the highest storage modulus of 58.1Pa, which was reduced in composite gels containing the Matrigel equivalent cell attachment matrix (ECL) to 43.2Pa. This decrease reached statistical significance, showing a

consistent negative impact on hydrogel stiffness in alginate gels when formed with ECM-derived protein mixtures. In contrast, collagen scaffolds showed much lower storage moduli than either of the alginate composite hydrogels, with measurements of 3.1Pa. Conversely, collagen when blended with the ECL protein mixture showed a slight increase in scaffold modulus to 4Pa. Both of the collagen scaffolds showed significantly lower material stiffness when compared to both the alginate and composite alginate scaffolds.

The peptide modified alginate hydrogel (Alg-Pep) displayed an intermediate storage modulus, between the alginate and collagen constructs, of 15.4Pa. This drop in hydrogel stiffness following the carbodiimide-based peptide-crosslinking chemistry is not unexpected as the peptide conjugation reaction does exploit carboxylic acid groups on the polysaccharide molecule which otherwise would be utilised in the divalent cation crosslinking process. The recorded storage modulus of the Alg-Pep hydrogels was significantly lower than both alginate and alginate composite scaffolds, and significantly higher than the base collagen hydrogel.

2.3.3 Metabolic Activity and Viability of Neural Cells within 3D Scaffolds

To ascertain whether candidate biomaterials have a negative impact upon encapsulated cell survival both during the process of gelation and throughout cell culture is a key assessment of the suitability of each material to form *in vitro* tissue-like constructs.

PC12 cells fully encapsulated in each of the biomaterials were assayed for cell viability during the first 7 days of differentiation. Cell viability assays that rely on the assessment of individual cell survival using multiple fluorescent dyes and microscopy techniques are powerful tools in two-dimensional culture but become more difficult when assaying cells encapsulated within three-dimensional hydrogels, especially with epifluorescent microscopy techniques. Inherent biases in field selection, dye diffusion and background fluorescence from differing field depths make quantifiable viability assays difficult in three-dimensional constructs. To this end, this viability assay is based on metabolic activity across the whole construct as a proxy for measuring quantifiable cell survival and comparisons across each hydrogel scaffold type without such biases.

The AlamarBlue viability assay was undertaken for all cell-laden hydrogel scaffolds on the day of gelation (Day 0), and Day 1, Day 3 and Day 7 post gelation. Experiments to ensure that no acellular hydrogel interference of the assay were also performed (data not shown). No statistically significant differences in cell metabolic activity (viability) were detected between the scaffold types after the initial gelation procedures on Day 0. This was mirrored by the finding at Day 7, which also showed comparable viability levels between all of the tested constructs (Fig 2-4 A).

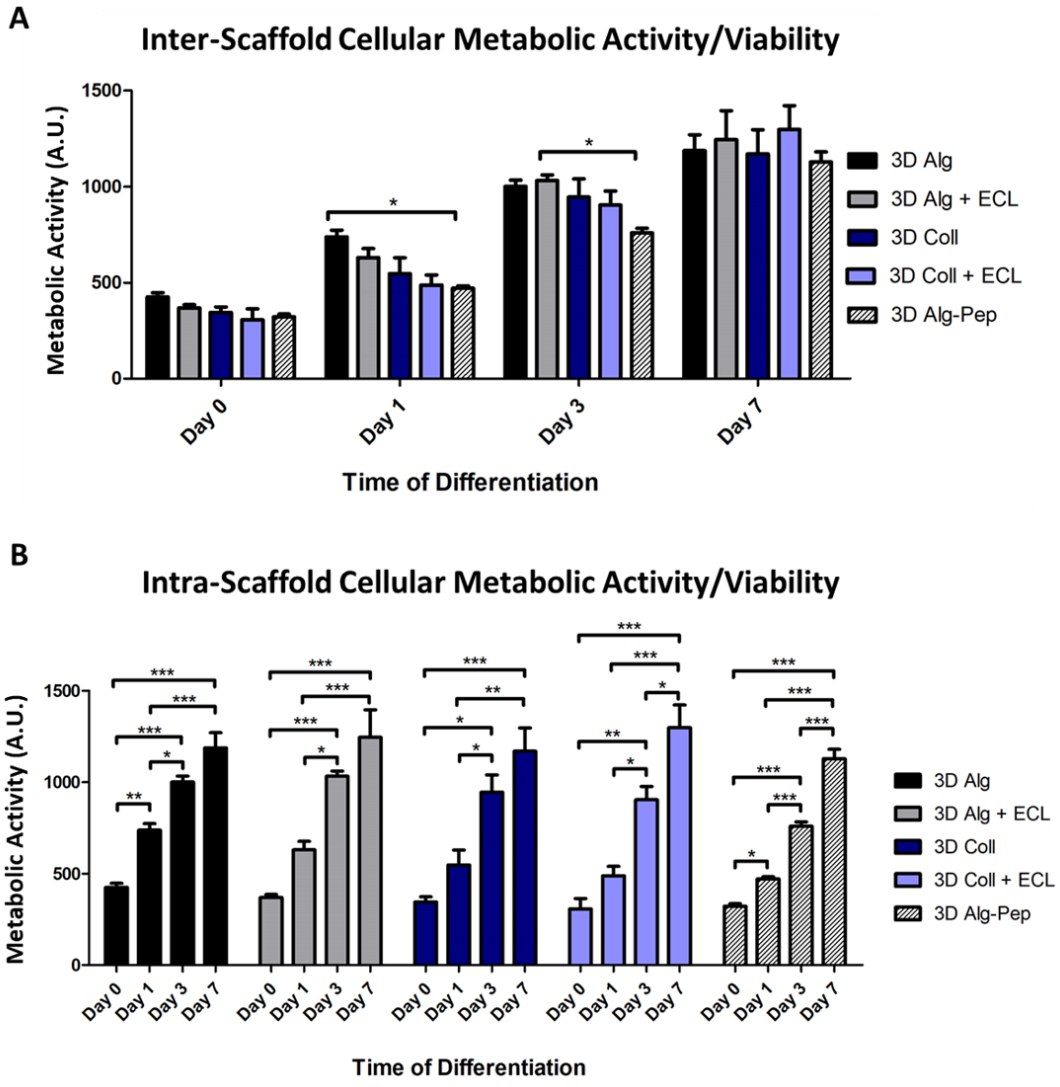

Fig 2-4: Metabolic activity/viability assays of PC12s encapsulated within each hydrogel scaffold over 7 days of differentiation. (**A**) Inter-scaffold analysis of cell viability over the time course. (**B**) Intra-scaffold analysis of cell viability over the time course. Data shown as mean ± standard error of the mean. Statistical significance denoted by *p≤0.05, **p≤0.01, ***p≤0.001

The only differences in metabolic output (as a measure of cell viability) between the hydrogel subtypes that reached statistical significance was between 3D Alg and 3D Alg-Pep constructs at Day 1 and 3D Alg + ECL and 3D Alg-Pep constructs at Day 3. In both cases the cell viability in the peptide modified hydrogel was lower than that of the base alginate and composite alginate scaffolds. All other viability measurements at Day 1 and 3 were comparable between all of the construct subtypes.

When looking at cell viability within the same scaffold type over the time course of differentiation, it is clear that metabolic activity increases to a statistically significant degree, showing that measured cell viability is not only maintained during the experimental timeline, but also significantly increases in all cases (Fig 2-4 B).

From these data, it can be demonstrated that all of the candidate hydrogel materials maintain comparable cell survival during each gelation protocol and that cell survival, proliferation, and metabolic activity increases during the process of cellular differentiation to the same degree by the end of the experimental timeline.

2.3.4 Morphological Analysis of Encapsulated Neural Cells

The success of biomaterials for use in *in vitro* neural tissue engineering is not only based on maintenance of cell viability, but also its conduciveness to allow for morphological changes such as neurite extension, cell migration and the formation of functional cell-cell contacts such as synapses.

Successful candidate biomaterials for three-dimensional neural tissue engineering should have the properties that promote equivalent cell morphology and neurite extension attained in planar culture, as well as be representative of those seen in native neural tissue. PC12s differentiated in two-dimensional culture over 7 days displayed strong morphological changes and extensive neurite extensions increasing in length and density over this time course (Fig 2-5). Rounded cell morphology is observed during the growth phase of PC12 culture (Day 0), but after the addition of differentiation triggering media PC12s rapidly undergo neuritogenesis that is visible by Day 1 with large widespread morphological changes throughout the planar culture after 7 days of differentiation.

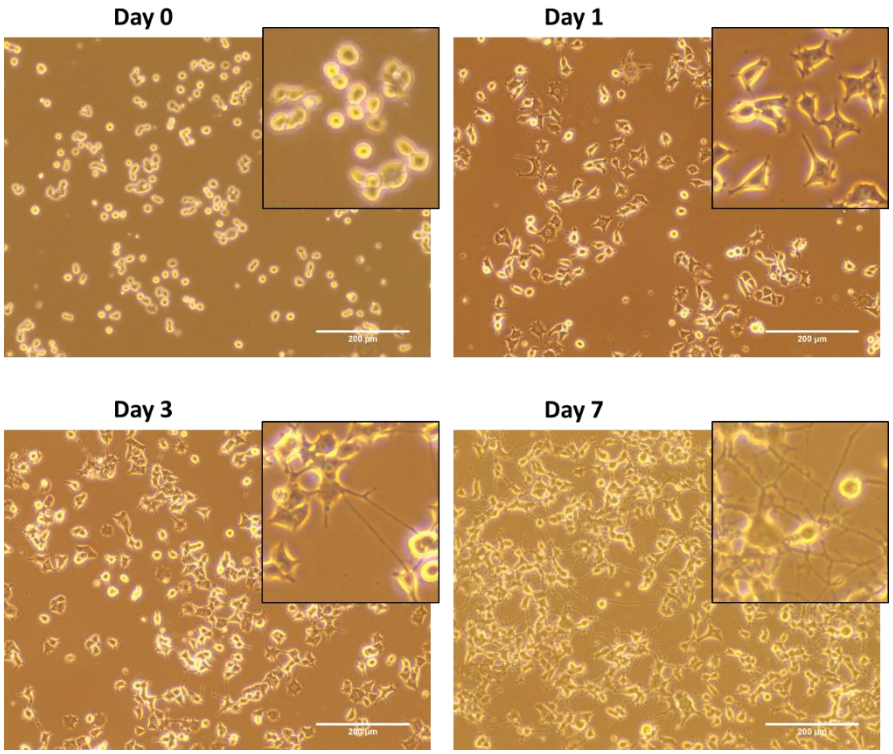

Fig 2-5: Live cell imaging of PC12s differentiating over 7 days in two-dimensional planar culture. Cell spreading and extensive neurite extensions increase during the differentiation process from very rounded cells at Day 0 to a strong neuronal morphology by Day 7. Inlays show more localised regions of interest. Scale bar represents 200µm.

Live cell imaging of PC12s encapsulated in the base and composite (+ECL) hydrogel scaffolds after differentiation showed stark contrasts between the alginate- and collagen-based scaffolds. After 7 days of differentiation within alginate hydrogels no neurite extensions were seen with any of the encapsulated cells, instead, round cell clusters were formed within the hydrogel that appear isolated from one another (Fig 2-6 A). This formation of cell aggregates without neurite extensions was also seen in the alginate composite blended scaffolds containing the ECL protein additive. In contrast, PC12s encapsulated within collagen matrices tended to show less cell clustering than cells within the alginate hydrogels and also allowed for the formation of neurite extensions into the hydrogel scaffold (Fig 2-6 A, white arrow heads). This same pattern of cell growth was also seen in the collagen composite scaffolds containing ECL.

This stark contrast in cellular morphology was also observed when investigated using fluorescent immunohistochemistry and confocal microscopy. β-III-Tubulin immunostaining of cells within alginate constructs showed tightly clustered multi-nuclear cell clusters, that although showed expression of this neuronal marker, did not display neurite extensions. This morphology was also seen after phalloidin staining, which binds strongly to filamentous actin (F-actin) fibres. Within the alginate hydrogels, PC12s displayed a strong punctate phalloidin staining pattern at the plasma membrane of the cell showing the presence of F-actin, but none that indicate neurite extension or cell morphology changes beyond the rounded morphology seen in bright field images (Fig 2-6 B).

PC12s differentiated within collagen-based hydrogels displayed pronounced morphological changes with less rounded cell morphology and highly prevalent neurite extensions into the hydrogel matrix after 7 days of differentiation (Fig 2-6 B, white and black arrow heads). β-III-Tubulin immunostaining and phalloidin staining of PC12s within collagen scaffolds again demonstrated a strong expression of the neuronal marker protein that displayed neurite extensions in all three axes of the hydrogel. The phalloidin stain showed a less punctate form than was seen in alginate-embedded PC12s, and a more continuous formation of F-actin around the cell body and within the numerous neurite extensions (Fig 2-6 B).

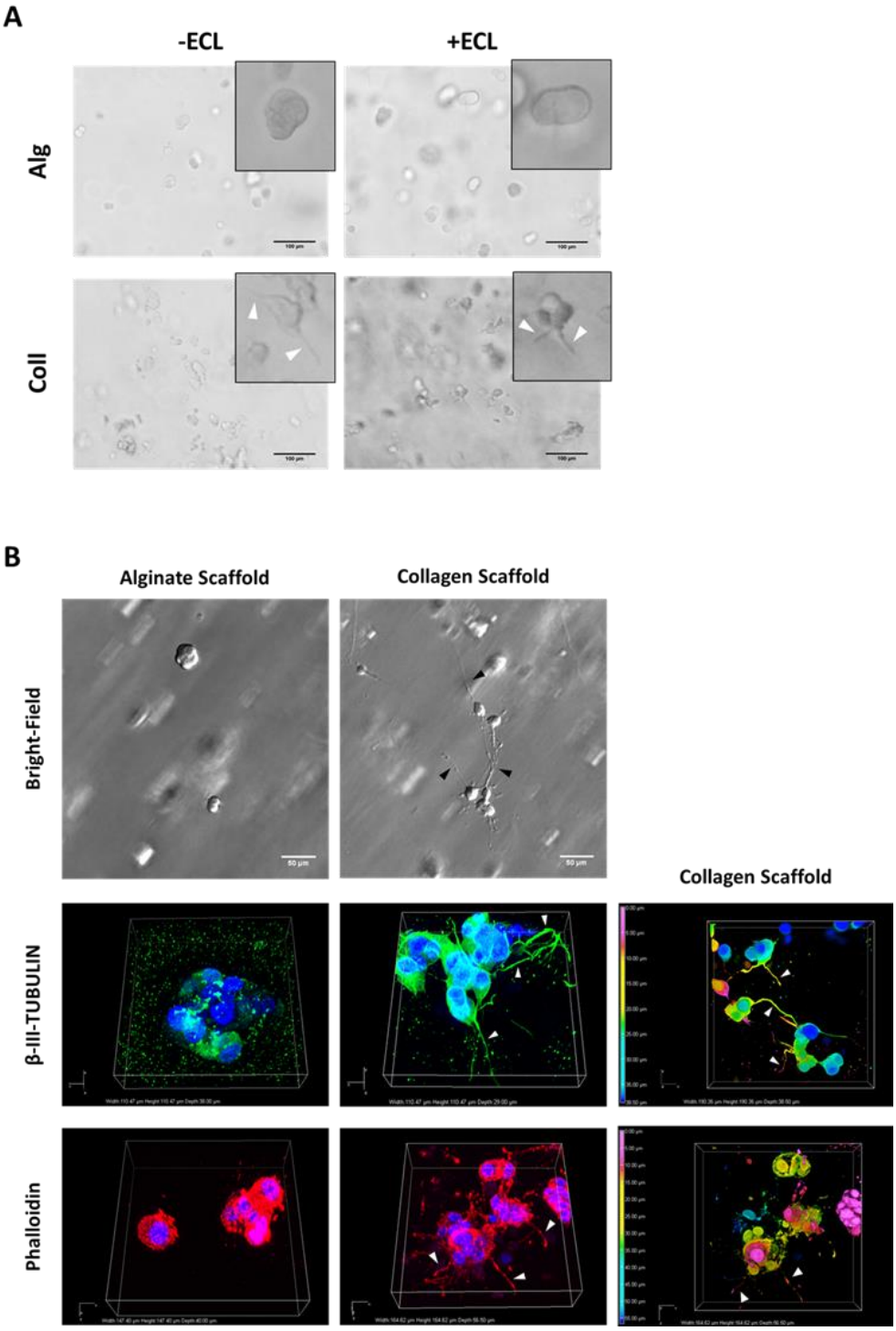

Fig 2-6: (**A**) Live cell images of PC12s in alginate (Alg) and Collagen (Coll) scaffolds after 7 days of differentiation, both with and without ECL addition. Scale bars represent 100µm. (**B**) Bright field and confocal images of PC12s embedded in alginate and collagen hydrogels for 7 days with β-III-Tubulin (green), phalloidin (red) and DAPI (blue) fluorescent staining. The right-most panel displays z-depth colour coding of the neural cells and neurite extensions. Bright field scale bar represents 50µm. Confocal images are 110µm x 110µm x 30-60µm in depth. Black/white arrowheads denote examples of neurite outgrowth.

The above data shows that the simple blended alginate hydrogels with extracellular matrix components were insufficient to overcome the inert nature of alginate hydrogels to induce a true *in vivo*-like neuronal morphology as in planar culture and in the 3D collagen scaffolds.

Using live cell imaging, direct comparisons of cellular morphology between PC12s encapsulated in alginate scaffolds and those in the peptide modified alginate (Alg-Pep) revealed similar levels of cell clustering and rounded cell morphology (Fig 2-7 A). The cell clustering within alginate and peptide-functionalised alginate was more apparent under fluorescent immunohistochemical staining of the neuronal marker β-III-Tubulin (Fig 2-7 B). Even with this degree of hydrogel modification no qualitative difference could be observed between PC12s encapsulated in the base hydrogel relative to the alginate scaffold containing MMP-cleavable and cell-adhesion moieties.

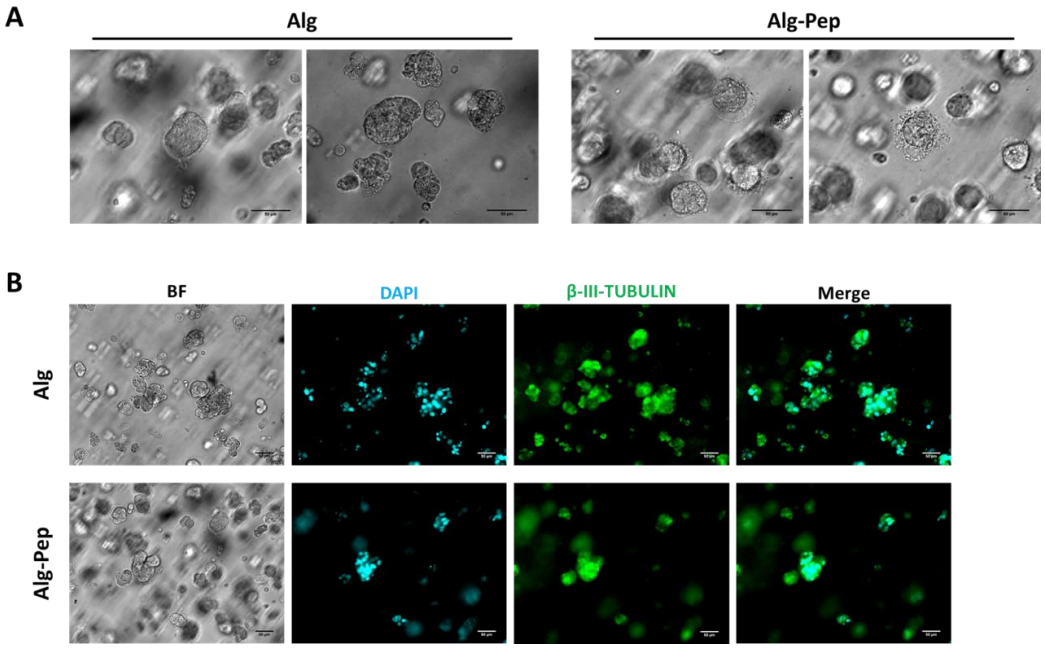

Fig 2-7: (**A**) Live cell imaging of PC12s encapsulated in alginate (Alg) and peptide-modified alginate (Alg-Pep) hydrogels after 7 days of differentiation. Scale bars represent 50µm. (**B**) Fluorescent immunostaining of β-III-Tubulin (green) and DAPI (blue) of PC12s encapsulated in each of the hydrogels after 7 days of differentiation. Scale bars represent 50µm. BF; Bright Field.

Although no gross cellular morphological changes could be seen between these two scaffold types, it is worthy of note that some clusters within the functionalised alginate

scaffold did show a halo-like effect around the cluster of cells with punctate structures visible in the hydrogel, that were seen in a lesser degree in the base alginate hydrogels (Fig 2-7 A). The presence of these elements appeared stochastically and were not accompanied with evidence of neuritogenesis, however, this phenomenon may be indicative of local proteolysis or ostensibly an enhanced cellular interaction with the peptide-modified alginate hydrogel.

2.3.5 Protein Analysis of Differentiating Neural Cells in Three-Dimensional Scaffolds

As well as morphological changes of cells within hydrogel scaffolds during neural differentiation; neuronal protein markers have been used to ascertain and quantify the strength, speed and efficacy of neural differentiation protocols and can be directly compared between two- and three-dimensional neural cell culture.

As the morphological differences were so stark between the subsets of three-dimensional scaffolds it was reasonable to assume that these differences would be reflected in molecular analyses of the PC12s during differentiation and allow for a more directly quantifiable system of elucidating the biomaterials most conducive to neuronal differentiation and directly compare this to planar differentiation.

When looking at the canonical neuronal markers β-III-Tubulin and Growth Associated Protein 43 (GAP43) from PC12s differentiated in two-dimensional culture over the course of 7-days, the relative amounts of these proteins mirrored the morphological changes induced within the cells and increased over time (Fig 2-8). It was also noticeable that a baseline constitutive expression of these markers could be seen within PC12s (expression at Day 0) even without induced differentiation and while still in a proliferative state (Fig 2-8). Surprisingly, this same pattern was seen in all five hydrogel scaffold formulations over the course of differentiation. Intriguingly, the level of expression within the alginate-based scaffolds was higher than that of the collagen hydrogels, showing upregulation of these proteins does not necessarily follow that of morphological changes and neuritogenesis, and instead are triggered via the induction of differentiation even in a sterically restrictive biomaterial scaffold.

Semi-quantitative analysis of the protein levels for these markers revealed strong differences between the differentiation of PC12s in planar culture and those differentiated in each of the hydrogel subtypes. β-III-Tubulin protein levels in PC12s from both alginate and alginate + ECL scaffolds showed a statistically significant increase in expression in comparison to two-dimensional planar differentiation and differentiation within collagen scaffolds by Day 1 (Fig 2-9). This difference lessened as time in culture increased but was still present to a statistically significant degree between the base alginate and both collagen-type scaffolds by Day 7.

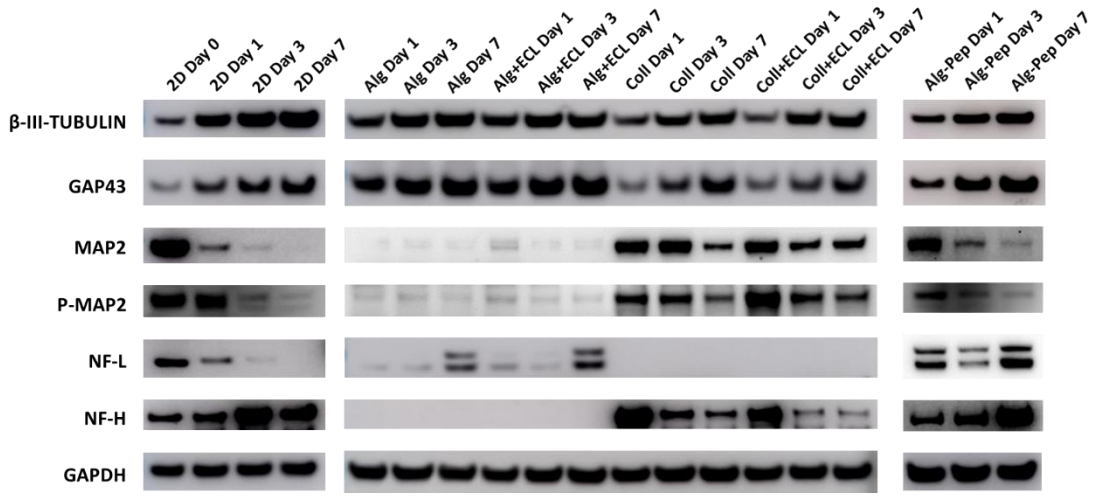

Fig 2-8: Western Blot expression data of neuronal protein markers of PC12s differentiated in two-dimensional culture (2D) and within the five hydrogel three-dimensional scaffolds (Alg, Alg+ECL, Coll, Coll+ECL, and Alg-Pep) at Day 1, 3 and 7.

It is also interesting to note that the protein expression of β-III-Tubulin from cells within Alg-Pep hydrogels more closely resembled the lower levels seen within collagen constructs, rather than the unmodified alginate hydrogels, and this difference was statistically significant at both Day 1 and Day 3 of differentiation (Fig 2-9).

A similar pattern was also observed when looking at GAP43 protein expression which showed close agreement between protein levels from planar PC12 cultures and the three-dimensional alginate ±ECL hydrogels over all time points of differentiation (Fig 2-9). These GAP43 levels showed either a strong trend or statistically significant lower intensity value in both subtypes of collagen hydrogels. As with the levels of β-III-Tubulin; GAP43 protein expression in Alg-Pep scaffolds more closely mirrored the lower levels seen in

collagen hydrogels (±ECL) rather than the expression seen in the alginate gels in the earlier time points of differentiation. This effect is reversed by Day 7, by which time the GAP43 expression level in Alg-Pep scaffolds was comparable to alginate scaffolds and statistically higher than in the collagen gels (Fig 2-9).

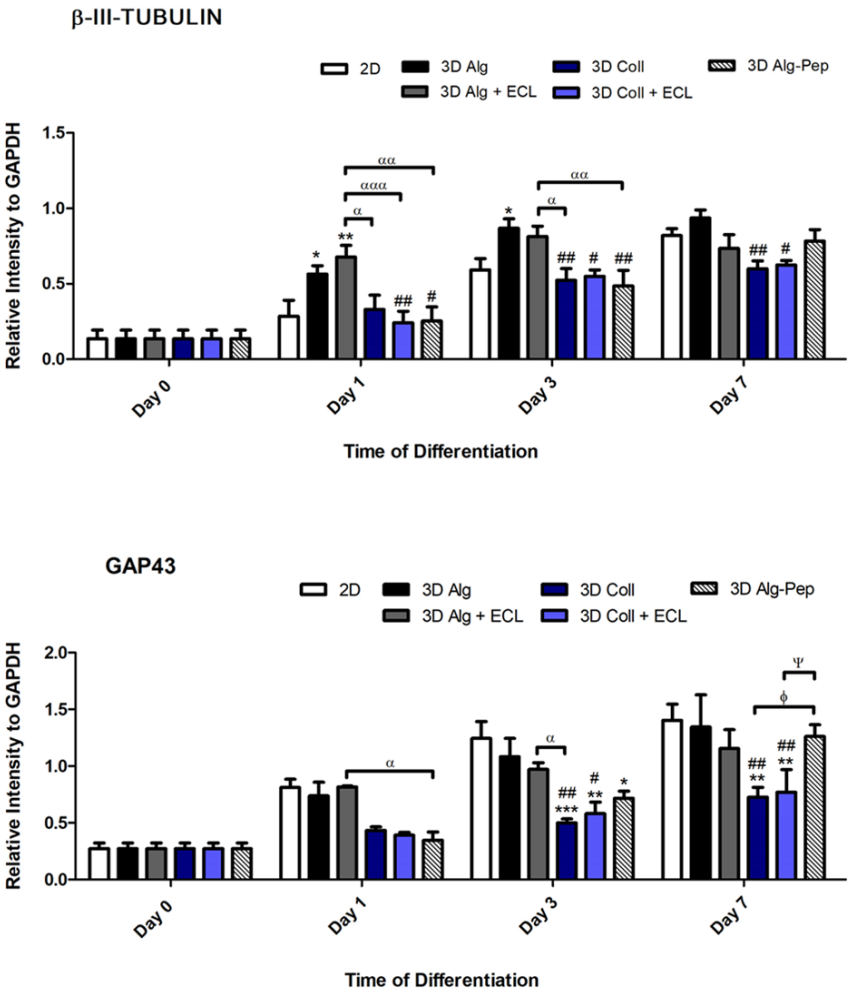

Fig 2-9: Semi-quantitative analysis of Western Blot data for β-III-Tubulin and GAP43 from PC12 cells differentiated in 2D planar culture and in 3D hydrogel scaffolds over 7 days. Data is shown as means ± S.E.M. Statistical significance is displayed relative to; 2D (*), 3D Alg (#), 3D Alg + ECL (α), 3D Coll (ϕ), and 3D Coll + ECL (ψ). $^{*,\#,\alpha,\phi,\psi}$ p≤0.05, $^{**,\#\#,\alpha\alpha,\phi\phi,\psi\psi}$ p≤0.01, $^{***,\#\#\#,\alpha\alpha\alpha,\phi\phi\phi,\psi\psi\psi}$ p≤0.001

While the protein expression patterns of both β-III-Tubulin and GAP43 showed similar expression patterns during the course of differentiation, but with a difference in the strength of expression for each scaffold type; other neuronal-associated proteins showed large differences between neural cells differentiated within hydrogel scaffold subtypes and

planar culture and offered more direct analysis of protein expression relating to neural cell morphological changes.

Microtubule-associated protein 2 (MAP2) is a dendritic protein involved in the regulation of microtubule assembly and neuritogenesis (Sánchez, Díaz-Nido and Avila, 2000). The expression pattern of the MAP2 (C/D) isoform appeared to differ strongly between neural cells differentiated in two-dimensional planar culture and those within differing hydrogel scaffolds (Fig 2-8). In planar culture, the pattern of MAP2 protein level decreased over the course of differentiation with a constitutively high expression in proliferative (Day 0) PC12s. This pattern was directly mirrored by the signal of Phospho-MAP2-Ser136 (P-MAP2), a phosphorylated form of the MAP2 protein, with high initial protein expression that declined during culture. Differential expression of both MAP2 and P-MAP2 in alginate (±ECL) versus collagen (±ECL) hydrogel scaffolds is striking, with PC12s differentiating in collagen scaffolds showing a similar but slower pattern of MAP2 and P-MAP2 decline during the time course. Neural cells within alginate scaffolds however, showed almost no expression of MAP2 or P-MAP2 from Day 1 onwards. This is the first sharp divide in protein expression seen between neural differentiation within the two scaffold types so far. Interestingly, the pattern of MAP2 and P-MAP2 expression in the peptide-functionalised alginate again followed the pattern of collagen scaffold expression rather than that of the base or ECL-composite alginate scaffolds.

Stark differences in neuronal protein marker expression between differentiating cells within hydrogel subtypes continued when looking at the regulation of the neuron-specific intermediate filaments Neurofilament-Light (NF-L) and Neurofilament-Heavy (NF-H). In the case of PC12 differentiation in two-dimensional culture, the levels of NF-L diminished over time relative to the Day 0 signal, whereas NF-H expression increased over the course of differentiation, suggestive of differential timings and roles of these filaments during the differentiation process (Fig 2-8). The collagen (±ECL) and alginate (±ECL) hydrogel cell scaffolds had clear and contrasting expression patterns of these proteins over the course of differentiation. Cells within alginate hydrogels, both with and without ECL composites, displayed a low level of NF-L signal over 7 days that increased over time, with a double-banded positive signal at Day 7. Conversely no NF-L signal was seen in cells differentiated in collagen hydrogels at any time point during the differentiation (Fig 2-8). Intriguingly, the expression pattern of NF-L from cells differentiated within Alg-Pep scaffolds showed a semi-consistent expression pattern with the double banding seen from

late time points from alginate derived samples at all time points during differentiation. So even when previous marker expression from Alg-Pep constructs more closely resembled those of collagen-derived samples, the presence of this NF-L signal was more similar to that of an alginate (±ECL) derived cell protein sample.

In contrast to NF-L protein expression, no NF-H signal was seen within differentiating PC12s within base or composite alginate scaffolds at any time point, whereas strong banding was seen from neural cells differentiated in the collagen hydrogels. The expression pattern derived from collagen scaffold samples however, did not follow the same pattern as is seen from planar differentiated samples, and instead had a peak intensity at Day 1 that declined during differentiation.

The NF-H protein expression in cells differentiated in the Alg-Pep matrices diverged from the pattern seen in the alginate and collagen scaffolds and instead displayed the pattern seen from cells in two-dimensional culture; with an increase in expression over the 7-day time course.

2.3.6 Gene Expression Analysis of Differentiating Neural Cells in Three-Dimensional Scaffolds

The large differences seen in protein expression patterns for the array of neuronal markers from PC12s differentiating in two-dimensional and three-dimensional environments seen above, raise the question of how these protein levels are regulated. Whether the regulation of these proteins expressed in environments conducive to neuritogenesis occur at the gene expression level or post-transcriptionally will allow for a better insight into how these genes and proteins work in concert over the course of neural cell differentiation.

qPCR analysis of the genes *β-III-tubulin*, *Gap43*, *Map2, Nf-l*, and *Nf-h* was completed for 7-day differentiation of PC12s in each of the five three-dimensional hydrogel scaffolds and two-dimensional planar culture to make it directly comparable to the protein expression analysis completed above.

Gene expression levels of these neuronal markers in general showed a relatively high level of constitutive expression which, for the majority of genes, showed limited up- or down-regulation when looking at fold changes of mRNA expression (Figs 2-10, 2-11).

β-III-tubulin mRNA expression displayed a general trend of slight upregulation over the time course of differentiation for the majority of 2D and 3D differentiation conditions (with the exception of Alg-Pep encapsulated PC12s, which showed a slight downregulation at Day 1). Although this upregulation never reached a 2-fold increase in expression and showed no statistically significant differences between any of the two- and three-dimensional growth conditions at any stage of differentiation.

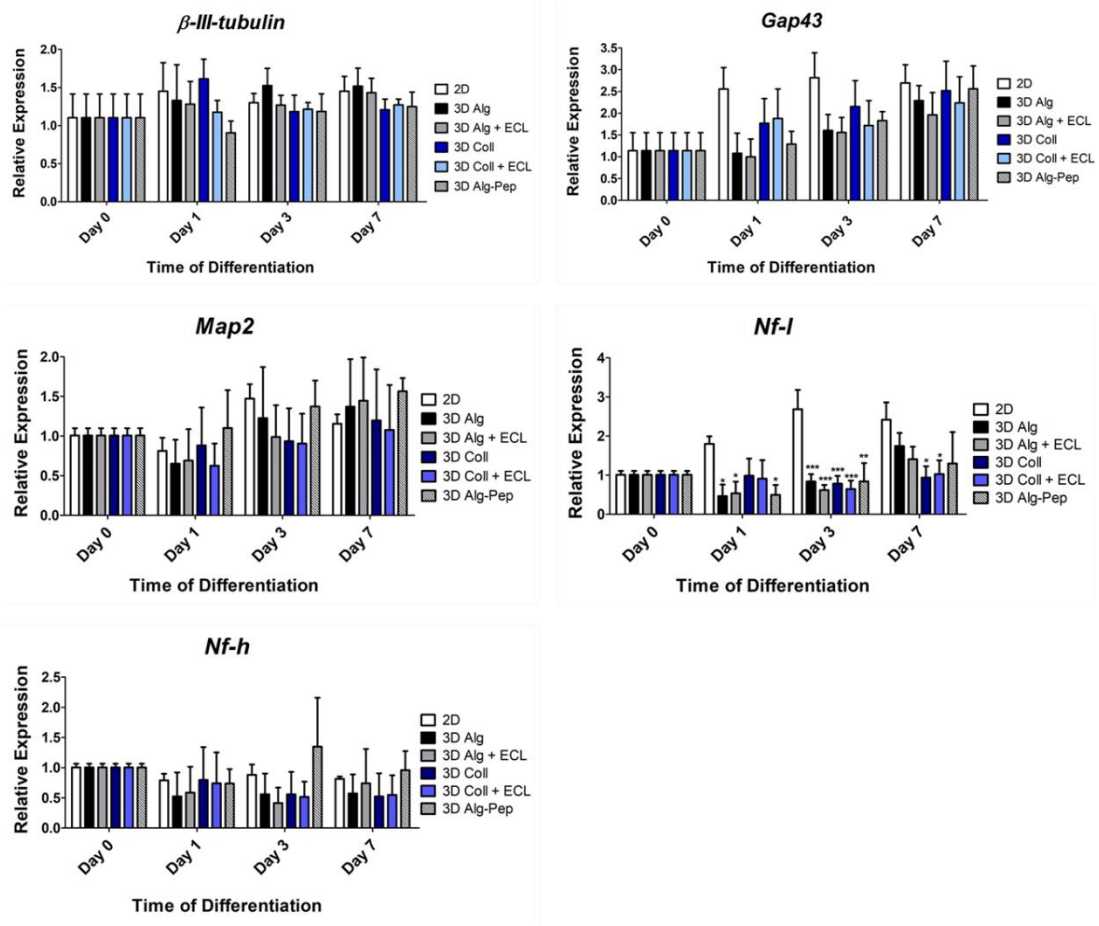

Fig 2-10: Inter-scaffold quantitative PCR (qPCR) analysis of *β-III-Tubulin*, *Gap43*, *Map2*, *Nf-l* and *Nf-h* mRNA expression in PC12 cells during differentiation in two-dimensional culture (2D), alginate hydrogels (3D Alg), alginate and ECL protein mix composite hydrogels (3D Alg + ECL), collagen hydrogels (3D Coll), collagen and ECL protein mix composite hydrogels (3D Coll + ECL), and peptide-functionalised alginate hydrogels (Alg-Pep). Data is shown as mean values ± standard error of the mean of three independent experiments. Statistical significance is denoted by * p≤0.05, ** p≤0.01, *** p≤0.001.

A similar pattern was seen for *Gap43* gene expression during differentiation, albeit with overall higher fold-changes than the Day 0 constitutive expression. In early stages of

differentiation (Days 1-3) the level of *Gap43* mRNA was highest in the two-dimensionally differentiated neural cells, followed by cells in the collagen scaffolds and then lower levels in cells from the alginate and peptide-alginate hydrogels, although none of these trends reached statistical significance (Fig 2-10). These early stage differences were also not present by Day 7 of differentiation where expression levels of *Gap43* were comparable across all 2D and 3D differentiation conditions.

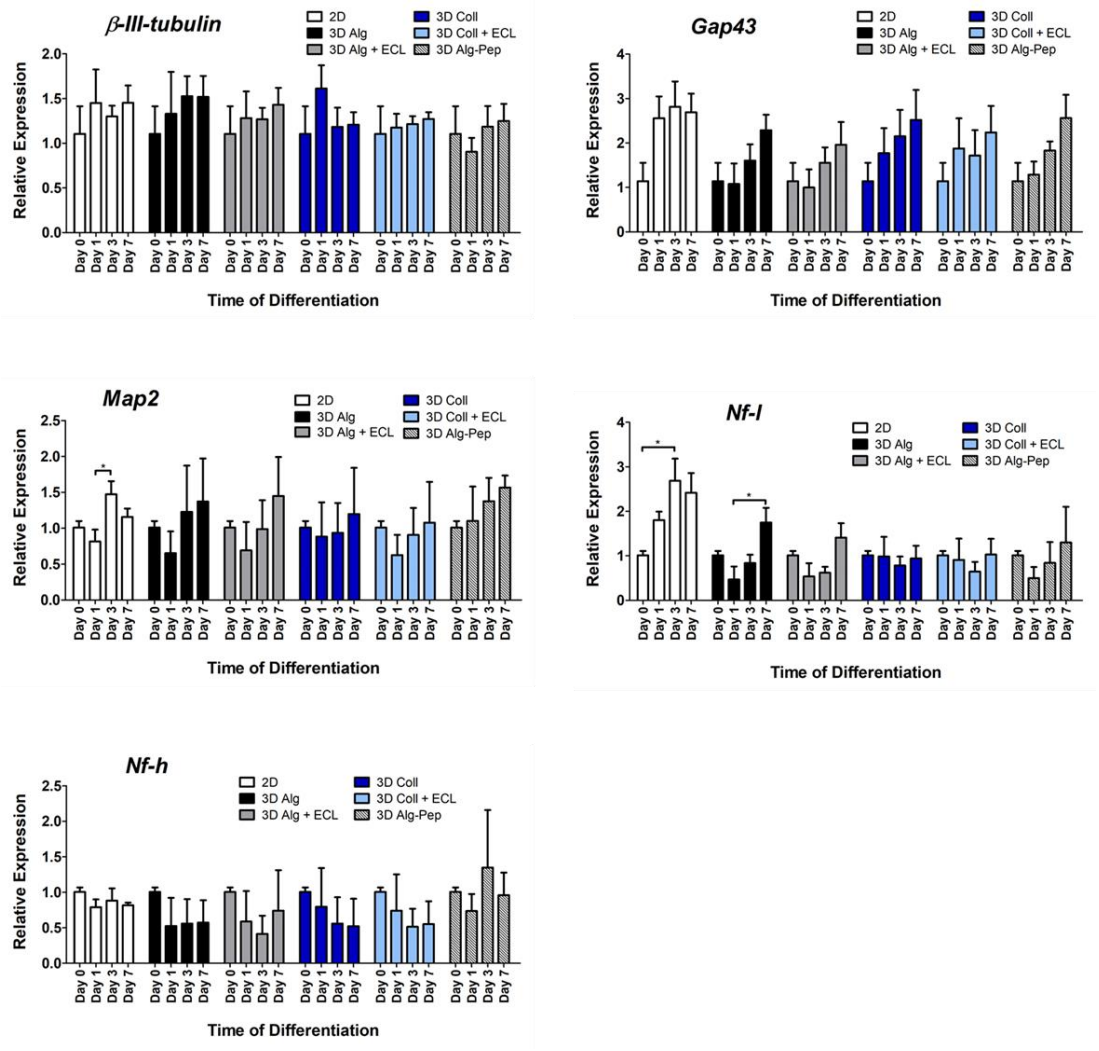

Fig 2-11: Intra-scaffold quantitative PCR (qPCR) analysis of *β-III-Tubulin, Gap43, Map2, Nf-l* and *Nf-h* mRNA expression in PC12 cells during differentiation in two-dimensional culture (2D), alginate hydrogels (3D Alg), alginate and ECL protein mix composite hydrogels (3D Alg + ECL), collagen hydrogels (3D Coll), collagen and ECL protein mix composite hydrogels (3D Coll + ECL), and peptide-functionalised alginate hydrogels (Alg-Pep). Data is shown as mean values ± standard error of the mean of three independent experiments. Statistical significance is denoted by * p≤0.05, ** p≤0.01, *** p≤0.001.

Map2 expression showed a relative drop by Day 1 of differentiation in all differentiating culture conditions which then recovered back to Day 0 levels and above by Day 3 and 7 (Fig 2-10). The only increase that reached statistical significance was the increase in *Map2* expression in two-dimensional culture between Day 1 and 3 of differentiation (Fig 2-11). Again, the fold changes seen over the course of differentiation in all culture conditions were minimal relative to the Day 0 constitutive expression and none of the differences between *Map2* expression levels at each time point showed significant differences between each planar- or hydrogel-based culture.

The gene transcript expression of *Nf-l* however, displayed the strongest difference between PC12s differentiating in planar culture versus those in three-dimensional scaffolds (Fig 2-10). By Day 1 and Day 3 of differentiation the level of expression from cells in planar culture were in all cases higher than cells within hydrogel scaffolds. This effect was less pronounced by Day 7 of differentiation but remained significantly higher than expression from cells within collagen (±ECL) scaffolds. The peak fold change seen between Day 0 *Nf-l* expression and the level of expression on Day 3 in planar culture did reach statistical significance (~2.7 fold higher) (Fig 2-11). In each of the hydrogel scaffold samples, the level of *Nf-l* was relatively consistent over the course of differentiation, after an initial downward trend. Day 7 mRNA levels of *Nf-l* from alginate hydrogels reached a peak that was statistically significant from the Day 1 fold-change (Fig 2-11).

Nf-h mRNA expression across all two- and three-dimensional differentiation conditions showed a similar pattern of slight downregulation relative to Day 0 levels (Fig 2-10, Fig 2-11), with the exception of the Alg-Pep scaffold encapsulated neural cells that showed a slight increase by Day 3 and Day 7. Overall no statistically significant differences were seen in gene expression levels of *Nf-h* either within a growth condition differentiation time course or between different growth conditions at each time point of differentiation.

2.4 Discussion and Conclusions

The techniques and challenges associated with *in vitro* neural cell culture have evolved dramatically since its inception (Millet and Gillette, 2012). Recent advances in biomaterial development and additive fabrication technologies (such as bioprinting) have put the onus on forming materials and cell growth environments that better recapitulate the cytoarchitecture and biophysical properties of native tissue. *In vitro* modelling of neural tissue forms the foundation of modern neurological research by creating a biomimetic environment to better understand human brain development, the pathology of neurological disease, to test and refine novel therapeutic agents, and eventually even form regenerative tissue applications. For this to be successful the selection and development of biological or non-biological scaffold materials that enable encapsulated cells to generate a more representative "brain-like" environment through enhanced cell-cell contact, dynamic cell-matrix interactions, and ultimately cell maturation and functionality are critical to this frontier.

Although multiple individual studies of hydrogel scaffolds for neural tissue engineering applications are present in the literature, few of them directly compare multiple scaffold subtypes to one another or compare directly to planar 2D neural differentiation. This section of research aimed to directly compare, at a material and cell biological level, the effect of the biomaterial scaffold alone on encapsulated neural cell differentiation.

Alginate and collagen type I hydrogel scaffolds have been used in a variety of neural tissue modelling research, with varying degrees of success. Collagen hydrogels are a widely used scaffold biomaterial from which to generate 3D neural tissue constructs. These scaffolds are conducive to neuritogenesis (O'Connor *et al.*, 2001; Swindle-Reilly *et al.*, 2012), show enhanced cell viability and activity when generated as composites with ECM-derived proteins (Sood *et al.*, 2016), and allow for the generation of synaptic connectivity and neural cell function (O'Connor *et al.*, 2000; Ma *et al.*, 2004; Xu *et al.*, 2009; Odawara, Gotoh and Suzuki, 2013). Alginate-based hydrogel *in vitro* constructs however, show mixed effects on embedded neural cell morphology and activity that is heavily dependent on scaffold composition and crosslinking conditions (Banerjee *et al.*, 2009; Meli *et al.*, 2014; Palazzolo *et al.*, 2015), but has shown promise in bioprinting methodologies (Chung *et al.*, 2013; Gu *et al.*, 2017).

To overcome or ameliorate this steric hindrance of neuritogenesis we generated alginate scaffolds with double-ended functionalisation peptides containing MMP2/9-cleavable motifs and laminin-derived cell binding moieties, which had shown promise in previous work with mesenchymal stem cell spreading in alginate hydrogels, and motor neurons in polyethylene glycol scaffolds (Fonseca *et al.*, 2011; McKinnon, Kloxin and Anseth, 2013). Aqueous carbodiimide crosslinking chemistry was utilised to generate the peptide-functionalised alginate (Alg-Pep) through the reaction of native carboxylic acid groups within the alginate polymer chains and the terminal amine groups of each peptide derived from the amine-terminus and a C-terminus lysine side-chain. Reaction efficiencies of 40.5% and 46.8% were achieved for the crosslinking of the MMP-peptide and the laminin-peptide respectively, resulting in MMP-peptide levels of 4.05mg/g alginate and laminin-peptide levels of 4.68mg/g alginate. The efficiencies of these modification reactions are comparable to those previously reported under similar reaction conditions (Fonseca *et al.*, 2011). This reaction chemistry generated peptide conjugates that were covalently bonded at both terminal ends of the peptides as opposed to the wider used pendant-style modification which grafts peptides using only a single terminus. The combination of both cell-binding and protease-cleavable motifs linking separate polysaccharide chains was developed in an attempt to enhance cellular interaction with a non-mammalian hydrogel scaffold whilst also limiting the steric hindrance of the alginate hydrogel on neuritogenesis, as seen in previous research (Banerjee *et al.*, 2009).

The stiffness of substrates used for *in vitro* cell culture has a strong impact on cell attachment, stem cell differentiation and cell morphology in both 2D and 3D (Engler *et al.*, 2006; Banerjee *et al.*, 2009). To optimise neural cell differentiation, the moduli of hydrogel scaffolds should be comparable to that of native brain tissue. To this end, the candidate neural tissue construct biomaterials in this work were assayed under rheological measurement to directly compare their suitability to replicate 3D brain-like soft growth conditions. The concentrations of collagen used within these hydrogels (0.4mg/ml) mirror previously reported positive results of collagen hydrogel formation for neural culture (O'Connor *et al.*, 2001). The alginate concentration used (0.5% w/v) was selected as it was the lowest concentration of polysaccharide that could generate a stable hydrogel under these culture conditions. This was an effort to engineer the lowest possible hydrogel modulus in an attempt to maximise positive neural differentiation (Banerjee *et al.*, 2009).

All crosslinked hydrogels tested displayed storage moduli below 60Pa which is well within the softness equivalent range of neural tissue (<1kPa). We observed the softest gels were generated from collagen matrices (3.1Pa) and that composite scaffolds of collagen with a Matrigel equivalent (ECL) demonstrated slightly higher moduli (4Pa). Conversely, alginate scaffolds displayed a higher storage moduli reading of 58.1Pa, which was lower in composite scaffolds containing ECL (43.2Pa). This drop may be due to the nature of the ionic crosslinking between alginate polymer chains, which may be inhibited through the presence of ECM-derived structural proteins not allowing for adequate proximity of crosslinking regions. Alg-Pep scaffolds displayed lower moduli measurements than the base and ECL-doped hydrogels (15.4Pa) owing to the fact that the carboxyl-groups utilised within ionic crosslinking become the attachment points for the peptide reactions. The double-ended nature of the peptide binding itself may also interfere on a steric level with how the alginate chains crosslink with each other and therefore lower the stiffness of the formed hydrogel during sol-gel transition. The level of peptide-crosslinking chemistry may therefore not only be used to functionalise scaffolds with biomimetic moieties, but also as a mechanism by which to tailor hydrogel moduli.

Another key criterion for the applicability of biomaterials for use in neural tissue engineering applications is the ability to maintain cell viability both during the crosslinking process and over the course of neural differentiation. The five hydrogel compositions within this study showed comparable levels of PC12 neural cell viability, both after the crosslinking process and after 7 days of differentiation. This indicates that neither crosslinking process was detrimental to cell survival and that the metabolic activity of the differentiating cells was preserved over the time course of differentiation. Only at Day 1 and 3 post-differentiation did a slight trend of lower viability in the collagen and Alg-Pep based scaffolds in comparison to the alginate (±ECL) hydrogels emerge. The fact that these differences are quite minimal, and that in all samples tested cell viability increases during the time course of differentiation, leads to the conclusion that strictly from a basis of cell survival within these constructs: all tested hydrogels show comparable cell biocompatibility profiles during neural differentiation.

Large differences were seen between the neural tissue scaffolds however, when assays of neuritogenesis and neural cell morphology were undertaken. PC12 cells show rounded cell morphologies under proliferative conditions, but quickly undergo neuritogenesis under neurotrophic treatment and display extensive morphological changes

over 7 days of differentiation [(Fig 2-4) and (Das, Freudenrich and Mundy, 2004)]. PC12s when differentiated in collagen ± ECL hydrogels also underwent neuritogenesis over a similar time frame and with neurites extending in all directions within the scaffold. No discernible positive effect on neuritogenesis was seen in collagen scaffolds containing the ECL protein mix. These morphological changes were however not seen in the alginate or ECL composite alginate scaffolds; which contained aggregates of PC12s with a rounded cell morphology. This mirrors the rounded morphology of NSCs embedded in alginate scaffolds of equivalent and higher storage moduli (Banerjee *et al.*, 2009), and the lack of dorsal root ganglia neuritogenesis also within alginate hydrogels (Novikova *et al.*, 2006). The addition of ECL as a component of the alginate hydrogel did not elicit any positive neuronal morphology changes of the PC12s in this study, although the addition of fibronectin into alginate scaffolds in previous studies has been shown to ameliorate the inhibition of neuritogenesis to a degree (Novikova *et al.*, 2006).

Strong positive neurite outgrowth of primary rat cortical neurons within unmodified but “ultrasoft” alginate hydrogels of 0.1% - 0.4% (w/v), and with sub-stoichiometric concentrations of crosslinking calcium ions, has been reported (Palazzolo *et al.*, 2015), although we were unable to generate hydrogel structures from the alginate sources used in this study at the low concentrations the authors reported (data not shown). Even at comparable storage moduli (<100Pa) we do not observe comparable levels of neurite outgrowth, suggesting that modulus alone is an incomplete marker of whether neurite outgrowth will take place. In this instance it may be that sub-stoichiometric crosslinking of alginate scaffolds, rather than low dry-mass biomaterial concentrations, elicit positive neuritogenesis through limited steric inhibition of cell movement through incompletion of the gelation process. This system of incomplete crosslinking however, would be difficult to control and would be impossible to monitor and maintain partial sol-gel transition during extended neural cell culture.

It is possible that different neural cell types respond differently to the same hydrogel environment and that PC12s and primary neurons would show different morphological trends due to intrinsic cell-line and native-neuron differences, however preliminary data showed that embryonic primary rat cortical neurons were also unable to undergo neuritogenesis within alginate scaffolds, but rapidly do so in collagen hydrogels (Appendix 2.5.2), matching the effect seen on embedded PC12s. This reinforces the concept of utilising neural cell lines as a proxy for true neuronal responses.

The differences in conduciveness to neuritogenesis between alginate and collagen-based scaffolds may be linked to the difference in storage moduli between the biomaterials (where collagen showed a much softer profile), but the recorded moduli for alginate hydrogels recorded in this study is still well within the degree of softness expected of native tissue and of equivalent successful neural tissue modelling studies (McKinnon, Kloxin and Anseth, 2013; Palazzolo *et al.*, 2015). Therefore, the apparent inhibition or enhancement of neuritogenesis may hinge on biophysical and biomimetic factors beyond simple modulus testing. This could include crosslinking fibre formation and structural elements such as porosity and polymer chain alignment and assembly, which may differ greatly between alginate and collagen hydrogels.

This lack of observable neuritogenesis seen within alginate and ECL composite alginate hydrogels is also reflected in the MMP- and laminin-peptide functionalised alginate scaffolds. Previous functionalisation of alginate scaffolds with laminin-derived binding epitopes allowed for a more *in vivo*-like glial and neuronal morphology in equivalent alginate (w/v) scaffolds (Frampton *et al.*, 2011), although in constructs of a much smaller volume and with cell densities much higher than those used in this study. It is plausible that higher cell densities may impact the gelation process and minimise the effective crosslinking of alginate chains due to the steric hindrance of the cells themselves, in a fashion similar to sub-stoichiometric crosslinking methodologies. Similar double-ended MMP-sensitive peptide functionalisation of both alginate and PEG scaffolds did show promise for embedded mesenchymal stem cell spreading and motor neuron axonogenesis (Fonseca *et al.*, 2011; McKinnon, Kloxin and Anseth, 2013). The different outcomes following peptide functionalisation of inert alginate scaffolds shown in this study may be due to multiple factors. The degree of functionalisation itself may not be at a level high enough to elicit a dense enough network of cleavable or cell-adhesive moieties for neuritogenesis and cell spreading to take place. Although reaction efficiencies were equivalent to those previously reported, the type and source of alginate used in each study (such as the content and ratio of β-D-mannuronic acid and α-L-guluronic acid monomers) have profound effects on viscosity and gelation properties that may enhance or inhibit the effects of peptide modification. Furthermore, the MMP-cleavable motif used in this study was designed to be sensitive to MMP-2 and MMP-9 secreted proteases, although a whole raft of protease-sensitive sequences can be generated, therefore it is possible that multiple sequences may enhance neuritogenesis of encapsulated differentiating neural cells

depending on their source. All of these elements could be modified in future work to try and tailor the use of alginate scaffolds for neural-tissue engineering.

The gene and protein expression profiles of PC12s within each scaffold subtype also showed stark differences over the course of neural differentiation and also when compared to standard 2D planar culture. The protein expression levels of both β-III-Tubulin and GAP43 increase during PC12 differentiation in 2D planar culture in accordance with previous studies (Ohuchi *et al.*, 2002; Das, Freudenrich and Mundy, 2004). This pattern of upregulation over 7 days of differentiation was seen across all 3D PC12 hydrogel cultures, even within the alginate (±ECL) and peptide-functionalised alginate cultures which showed no evidence of neuritogenesis. Intriguingly, this result suggests that even in matrices that restrict neural morphological development, the embedded neural cells still positively respond to signalling factors triggering differentiation-related protein expression. Equally as fascinating is the finding that at early time points (Day 1 and 3) β-III-Tubulin protein levels are significantly higher in neural cells differentiating in 3D alginate (±ECL) hydrogels than those seen at the same time points in 2D culture. This upregulation at each time point in 3D alginate scaffolds remains significantly higher than 3D collagen (±ECL) encapsulated neural cells until Day 7, and which themselves tend to match with 2D differentiation levels and the peptide-functionalised alginate hydrogels. This increase in canonical neuronal proteins from cells in 3D alginate scaffolds relative to 3D collagen scaffolds is also true of GAP43 protein expression. This finding may seem counterintuitive as higher levels of neural differentiation markers may be expected from culture conditions that allow for neuritogenesis and mature neural morphology formation. In this case however, it does appear that these particular neuronal markers although upregulated during the course of induced differentiation are unreliable markers of neuronal morphology development. The gene expression profiles of *β-III-tubulin* and *Gap43* follow a similar pattern to protein expression and are upregulated during differentiation. However, the relative increase of each gene is slight, and no upregulation in any scaffold reaches statistical significance, and the differences seen between gene expression at each time point is not statistically different from PC12s in other hydrogel scaffold types, unlike those seen for protein expression levels.

The dendritic marker MAP2 and its phosphorylated forms interact with the microtubule network within neural cells and may have a role in processes regulating cellular morphology (Sánchez, Díaz-Nido and Avila, 2000). In 2D planar differentiation,

MAP2 (C/D isoform) and the serine-136 phosphorylated form (P-MAP2) show downregulation over the course of PC12 differentiation. Robust differences are seen in MAP2 and P-MAP2 levels between PC12s differentiating in alginate and collagen scaffolds, whereby both markers are absent from PC12s in 3D alginate (±ECL) constructs but show a slower downregulation pattern mimicking the 2D differentiation samples in collagen (±ECL) constructs. Unlike the neuronal markers β-III-Tubulin and GAP43 whereby upregulation is discrete from morphological development, MAP2 and P-MAP2 show large differences between the same cell type differentiating in distinct biomaterial scaffolds. Even more surprising is the finding that the MAP2 and P-MAP2 protein expression pattern in the peptide-modified alginate scaffolds follows a similar pattern to 3D collagen and 2D planar differentiation rather than the 3D base alginate scaffolds. When looking at *Map2* gene expression however, this pattern of downregulation is not seen. Instead a high constitutive expression with an initial trend of downregulation and then upregulation over 7 days of differentiation is comparable across PC12s differentiated in all scaffold subtypes. This is an interesting disconnect between the final protein marker product and the underlying gene expression profile which suggests strong post-transcriptional regulation of the *Map2* gene depending on the cell-biomaterial interactions encountered during differentiation.

Distinct differences are also seen in the expression of the neurofilament proteins NF-L and NF-H which have been shown previously to be upregulated slightly during PC12 differentiation (Ohuchi *et al.*, 2002). In 2D planar PC12 differentiation in this study, NF-L levels decrease over time, whereas NF-H protein levels increase. This difference in expression profiles may be due to a recapitulation of developmental timings of each neurofilament with early expression of NF-L followed by a later expression pattern of NF-H (Liu *et al.*, 2004). However, within alginate hydrogels (±ECL), NF-L levels increase over time, whereas NF-H was not detected, suggesting a link between the lack of biomaterial interaction and the morphological changes within the encapsulated PC12s. The reverse of this pattern is seen in collagen hydrogels (±ECL) which do not show detectable levels of NF-L but do show positive NF-H banding, but with a different pattern to that seen from 2D planar differentiation. Interestingly, PC12s differentiated within peptide-modified alginate scaffolds show NF banding patterns indicative of both collagen and alginate hydrogel samples; with NF-L expression measurable at all time points and an upregulation of NF-H that follows the same pattern as 2D differentiation. Some NF-L probes displayed double banding within samples from the 3D alginate (±ECL) and peptide-alginate samples not seen

in 2D planar culture, which may demonstrate an effect of post-translational modification such as glycosylation and/or phosphorylation (Liu *et al.*, 2004). It has been seen in previous studies that *Nf-l* gene expression increases over the course of PC12 differentiation (Won *et al.*, 2015), which is also seen in this study in 2D planar differentiation, but to a much more static degree in PC12s within all 3D hydrogel scaffolds. This static expression profile is again seen with *Nf-h* gene levels; that display high constitutive expression that remains relatively stable over the time course of differentiation. As was the case with MAP2 gene and protein expression, these disparate patterns do not reflect the final protein patterns seen experimentally. Again, it can be concluded that strict post-transcriptional regulation of these genes must be taking place and that constant gene expression levels of these markers may be a factor of the PC12s themselves, and must be factored into any analysis involving other neural cell types.

The differing protein expression patterns of MAP2, P-MAP2, NF-L and NF-H between the hydrogel compositions and those derived from 2D differentiation highlight the complex interplay of these neural markers as PC12s undergo differentiation in environments that display different biophysical properties, that may or may not support neuritogenesis, and those that contain native-ECM binding motifs or not. From these data it appears that these protein markers are a more effective measure of cell-matrix interactions and possible neurite elongation than the canonical neuronal markers β-III-Tubulin and GAP43. It is worthy of note however, that the constitutive expression levels of many neuronal genes and proteins within PC12s in basal growth media results in a more subtle upregulation during differentiation as was discussed above, and has discounted certain markers for use in previous differentiation studies of PC12s (Das, Freudenrich and Mundy, 2004). It has also been noted that intermediate filament expression patterns (such as neurofilaments) within PC12s do diverge from patterns seen in native neural cultures (Franke, Grund and Achtstatter, 1986). This surprising gene expression disconnect from translated protein products may also be related to the reportedly high level of post-transcriptional regulation of differentiation-associated genes in PC12s (Lindenbaum *et al.*, 1988; Perrone-Bizzozero, Cansino and Kohn, 1993).

In conclusion, the striking differences between protein marker expression in PC12s within 3D hydrogels and 2D culture is a firm demonstration of cell-matrix interactions dictating cellular responses at the molecular level, even under identical differentiation inducing conditions. Even with comparable cell viability retention and scaffold stiffness

analogous to that of native brain tissue, differentiation within alginate-based hydrogels restricted neurite outgrowth and *in vivo*-like morphology, but elicited strong canonical neuronal marker expression, but differential patterns of MAP2/P-MAP2 and neurofilament protein expression than was seen in 2D planar differentiation. Conversely, collagen-based 3D hydrogel scaffolds had almost the opposite effect on the embedded neural cells; by allowing for extensive neuritogenesis together with gene and protein expression patterns more equivalent to 2D planar culture. Strikingly, peptide-modified alginate hydrogels (containing MMP-sensitive and laminin-binding motifs) although not conducive to neuritogenesis, showed protein expression patterns reflective of both alginate-embedded and collagen-embedded PC12s. This demonstrates that not only are encapsulated neural cells responding to the biophysical properties of the hydrogels themselves, but must be interacting at a biochemical level with the moieties presented within the hydrogels to regulate and modulate molecular pathways of neural cell differentiation.

2.4.1 Summary of Chapter Findings

- Using aqueous carbodiimide chemistry; double-ended MMP-cleavable and laminin-binding peptide motifs can be covalently bonded to alginate polymers with high efficiency.
- Collagen type I, alginate and peptide-modified alginate hydrogels all allow for high retention of cell viability of encapsulated neural cells during scaffold gelation, as well as over the time course of neural differentiation.
- Rheological analysis of hydrogels reveals all candidate scaffolds have storage moduli below 100Pa. Collagen hydrogels show the lowest degree of stiffness, with alginate hydrogels the highest. Peptide-modified alginate hydrogels show intermediate stiffness measurements between collagen and basal alginate scaffolds.
- Collagen type I hydrogels (both with and without ECM protein components) allow for neurite extension of encapsulated PC12 neural cells over the same time course as 2D planar differentiation.
- Low concentration alginate hydrogels are non-conducive to neuritogenesis of encapsulated differentiating PC12 neural-like cells. This effect is not ameliorated by the addition of extracellular matrix proteins.

- Peptide-modified alginate hydrogels also do not allow for neuritogenesis of encapsulated neural cells, but do show a tendency for visible “halo-like” structures around cellular aggregates, suggesting cell-scaffold molecular interactions.
- The canonical neuronal protein markers β-III-Tubulin and GAP43 increase in expression over the time course of neural differentiation in 2D and 3D culture. These increases do not reflect the neuritogenic potential of the hydrogel scaffolds and are highly expressed in alginate and alginate-peptide scaffolds which restrict neurite formation.
- Other neuronal protein markers MAP2, P-MAP2, NF-H, and NF-L do show stark differences in expression profiles during neural differentiation in the various biomaterial scaffolds. These markers therefore represent more reliable measures of neuritogenic potential of candidate biomaterials.
- Gene expression levels of the above markers in PC12s display a high constitutive expression level that show low levels of fluctuation during differentiation. These low relative changes in gene expression do not directly reflect the large differences seen with protein expression analysis. This is suggestive of a harsh post-transcriptional regulation of these genes at least within the PC12-based model.

2.4.2 Acknowledgements

We would like to thank Frosa Katsis, formerly of the St. Vincent’s Institute (SVI), for her indispensable help in the HPLC purification of crude peptide samples and mass spectrometry analysis of peptide purity. We would also like to acknowledge the help of Dr. Serena Duchi (Dept. of Surgery, University of Melbourne) for her assistance with confocal microscopy image acquisition. Finally, we would like to acknowledge Dr. Cathal O’Connell (BioFab3D, University of Melbourne) for his help and guidance in obtaining the rheological data.

2.5 Appendix

2.5.1 Peptide Functionalisation Mass Spectrometry Data

Following reversed-phase HPLC chromatography, peptide-containing aliquots were purity tested through mass spectrometry analysis. Double-charged peptide component peaks were used to determine the purest aliquots for down-stream alginate crosslinking chemistry. Some example spectra are shown below.

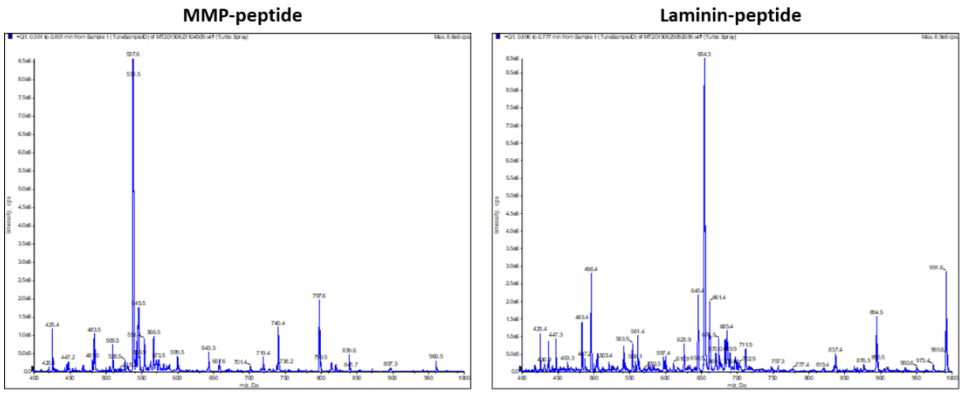

Appendix Fig 2-12: Mass spectrometry readings of aliquots of MMP- and laminin-peptide following HPLC purification. The strong peaks of the double charged peptides allowed for selection and lyophilization of pure full-length peptides.

2.5.2 Primary Rat Cortical Neural Cells within Alginate and Collagen Scaffolds

Although PC12s, a rat-derived neural-like cell line, were used as a proxy for primary or stem cell derived neuron behaviour in 3D environments, it was necessary that gross morphological changes witnessed from the PC12 3D hydrogel tissue constructs should reflect those of primary neural cultures. Embryonic (E18) rat cortical cells (kindly supplied by Dr. Justin Bourke, St. Vincent's Hospital Melbourne) were embedded in equivalent hydrogel matrices and differentiated over 7 days to ensure the inhibition or enhancement of neuritogenesis seen with PC12s in each scaffold type was recapitulated. E18 Differentiation media was composed of Neurobasal (Gibco), B27 (Thermo Fisher Scientific), N2 (Thermo Fisher Scientific), GlutaMAX (Thermo Fisher Scientific), 100U/ml Penicillin and

100µg/ml Streptomycin (Gibco). Some demonstrative images are shown below (Appendix Fig 2-13).

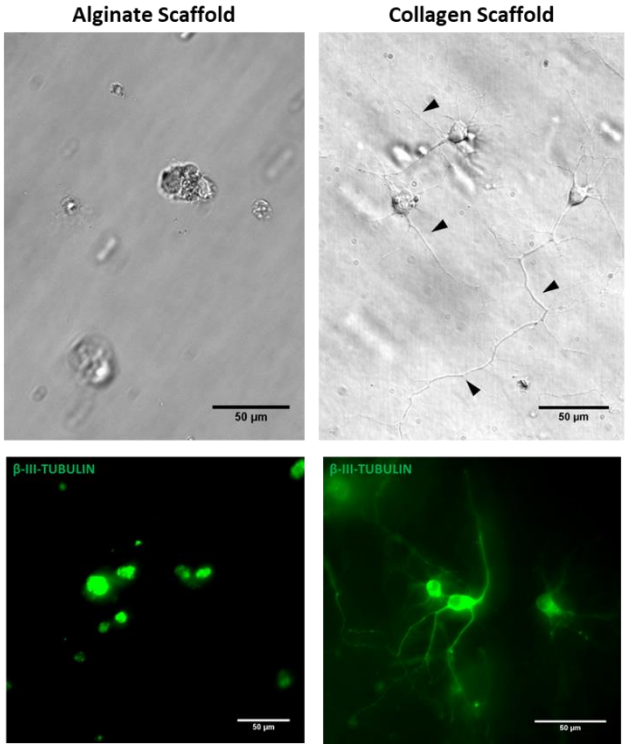

Appendix Fig 2-13: Bright field (top) and immunofluorescent (bottom) images of embryonic E18 rat cortical neurons differentiated within alginate and collagen 3D hydrogel scaffolds. β-III-Tubulin immunostaining is shown in green. As with PC12s no neuritogenesis was observed in alginate scaffolds, whereas extensive neurite branching and extension was seen from the same cells in collagen scaffolds (black arrow heads). Scale bars represent 50µm.

Chapter 3: Subtype Specific Neural Differentiation of Human Induced Pluripotent Stem Cells

3.1 Introduction

The advent of induced pluripotent stem cell (iPSC) technology has incredible potential to drive the next generation of human neurological research. Human iPSCs (hiPSCs) differentiated into neural lineages *in vitro* do so following the same developmental timings and maturation profiles as is seen *in utero*, and even more remarkably have the capacity to self-organise into multicellular substructures that are representative of early brain cytoarchitecture (Petros, Tyson and Anderson, 2011; Anderson and Vanderhaeghen, 2014; Kelava and Lancaster, 2016). This retention of *in vivo*-like properties of differentiation in the dish, combined with the fact that they can be reliably generated on a patient-specific basis, makes hiPSCs an attractive foundation for *in vitro* modelling of genetically linked neurodevelopmental and neurodegenerative pathologies (Park *et al.*, 2008; Mattis and Svendsen, 2011; Okano and Yamanaka, 2014). By differentiating human pluripotent stem cells into particular neural subtypes *in vitro* that carry mutations implicated in disease pathologies, many researchers have already begun to recapitulate and better understand such conditions as Parkinson's Disease (Soldner *et al.*, 2009; Kriks *et al.*, 2011; Miller *et al.*, 2013; Schwab and Ebert, 2015), Alzheimer's Disease (Israel *et al.*, 2012; Choi *et al.*, 2014; D. Zhang *et al.*, 2014; Duan *et al.*, 2014; Kim *et al.*, 2015; Nieweg *et al.*, 2015; Mungenast, Siegert and Tsai, 2016), Huntington's Disease (Juopperi *et al.*, 2012), Amyotrophic Lateral Sclerosis (Motor Neurone Disease) (Di Giorgio *et al.*, 2008), Spinal Muscular Atrophy (Ebert *et al.*, 2009; Corti *et al.*, 2012), Autism Spectrum Disorders (Mariani *et al.*, 2015; Marchetto *et al.*, 2017), and syndromic genetic Epilepsies such as Dravet Syndrome and Rett Syndrome (Marchetto *et al.*, 2010; Ananiev *et al.*, 2011; Cheung *et al.*, 2011; Kim, Hysolli and Park, 2011; Farra *et al.*, 2012; Yu Liu *et al.*, 2013; Dajani *et al.*, 2013; Higurashi *et al.*,

2013; Jiao *et al.*, 2013; Chen *et al.*, 2014; Williams *et al.*, 2014; Parent and Anderson, 2015; Du and Parent, 2015; Z.-N. Zhang *et al.*, 2016; Maeda *et al.*, 2016).

The strength of both *in vitro* neurological developmental- and disease-modelling is underpinned through the accurate generation of specific neural subtypes that are differentiated and matured to a level comparable to *in vivo* neural networks. Forebrain neural development *in utero* is derived from the anterior-dorsal region of the neural tube (the embryological precursor of the central nervous system). Interestingly, neural cells from this brain region represent the outcome of the default differentiation lineage of neuroectodermally induced cells from hiPSCs (Zeng *et al.*, 2010; J.-E. Kim *et al.*, 2011; Shi *et al.*, 2012), rather than stochastic differentiation of multiple neuronal subtypes from multiple neural tube regions.

However, as well as this predominantly excitatory pool of cells that form forebrain structures (such as the cortex) from this lineage pathway: approximately 20% of neocortical cell numbers are comprised of GABAergic inhibitory neural cell types (Arber and Li, 2013). These neural cell subtypes are generated from anterior-ventral regions of the neural tube and migrate tangentially into cortical regions from structures termed ganglionic eminences (Danjo *et al.*, 2011; Arber and Li, 2013). The temporo-spatial patterning of the neural tube *in utero* is derived from gradients of morphogens that define dorsal-ventral and rostral-caudal axes (Briscoe and Ericson, 2001; Le Dréau and Martí, 2012). One such morphogen is Sonic Hedgehog (SHH) which is a ventralising ligand secreted from the neural tube floorplate and notochord (Jessell, 2000). By replicating this exposure to SHH, or small-molecule agonists of the SHH-signalling pathway, many *in vitro* pluripotent stem cell-derived neural precursor cells (NPCs) can be patterned to a ventral and therefore GABAergic interneuron cell identity (Maroof *et al.*, 2010; Danjo *et al.*, 2011; Goulburn *et al.*, 2012; Ma *et al.*, 2012; Arber and Li, 2013; Yan Liu *et al.*, 2013; DeRosa *et al.*, 2015).

Therefore, to fully model human forebrain cortical development in a dish, the cellular components of the *in vitro* model must contain both dorsally-derived excitatory cells and ventrally-derived inhibitory interneurons in the appropriate ratios and combined in a developmentally relevant time frame. This will be especially important within studies of some genetic epilepsies, of which many carry mutations that specifically affect GABAergic neuronal migration and function (Noebels, 2015). Although multiple studies are present in the literature that look at single neural cell subtype differentiation and end-point

analysis, very few engage in parallel neural induction strategies that directly compare the molecular markers of differentiation, maturation and network formation.

The purpose of this chapter will be to focus on the derivation of forebrain excitatory (dorsal) neural cell types in direct timeline comparison to deriving forebrain inhibitory (ventral) GABAergic interneurons. This will shed light on the molecular processes of forebrain neural cell development and maturation, and the intrinsic differences of the process from neural cells from distinct neural tube regions triggered through morphogen patterning. As well as biomolecular markers of differentiation such as gene and protein expression, the acquisition of neuronal cell activity and function will also be studied.

All of these elements combined will help inform future models of complete forebrain development *in vitro* and will be an integral foundation stone on which to derive comparable developmental and disease-state neural tissue models. It is the processes and analyses formed within this chapter that will be used to inform future three-dimensional modelling techniques.

3.2 Materials and Methods

3.2.1 iPSC Culture

All work in this chapter utilised the commercial human iPSC lines; *ATCC-BXS0116 Human Induced Pluripotent Stem (IPS) Cells (ATCC® ACS-1030™)* derived from CD34+ bone marrow cells and *ATCC-DYS0100 Human Induced Pluripotent Stem (IPS) Cells (ATCC® ACS-1019™)* derived from foreskin fibroblasts. iPSCs were grown in feeder-free culture conditions on Vitronectin XF (Stem Cell Technologies) coated 6-well tissue culture plates in TeSR-E8 media (Stem Cell Technologies). iPSC colonies were passaged every 6-7 days with Gentle Cell Dissociation Reagent (GCDR) (Stem Cell Technologies) and were re-plated with TeSR-E8 media containing the RHO/ROCK pathway inhibitor Y-27632 (10µM, Stem Cell Technologies). Media was changed daily, except for the first day after a passage. Areas of random differentiation within colonies were removed manually. All iPSC and neural differentiation experiments used iPSCs below passage number 20.

3.2.2 Neural Differentiation

Dorsal neural induction of iPSCs was triggered using the monolayer dual SMAD-inhibition protocol using commercially available STEMdiff Neural Induction Media (NIM) (Stem Cell Technologies). Briefly, iPSCs were dissociated into single cells using GCDR (Stem Cell Technologies) and plated at densities of 1 x 10^6 cells/well of a 6-well tissue culture plate coated with poly-L-lysine (0.01%, Sigma) & laminin (20µg/ml, Sigma) (PLL) in 2ml NIM per well. Media was changed daily for the first 7 days of induction, also containing RHO/ROCK pathway inhibitor Y-27632 (10µM, Stem Cell Technologies).

After 7 days of induction, media was changed to STEMdiff Neural Proliferation Media (NPM) (Stem Cell Technologies) for another 7 days to trigger neural precursor cell (NPC) maturation. NPCs were passaged at Day 10 to allow for continued expansion and differentiation under final plating conditions onto PLL coated tissue culture plates. At Day 14 post-induction, media was changed to a final neural maturation media (NMM) which consisted of a 1:1 mix of “N2 media” and “B27 Media”. N2 media consisting of DMEM/F12 (Lonza), N-2 Supplement (1x, Thermo Fisher Scientific), GlutaMAX (1x, Gibco), Non-essential amino acid mixture (1x, Lonza), 100U/ml Penicillin and 100µg/ml Streptomycin

(Gibco). B-27 media consisting of Neurobasal (Gibco), B27 Supplement (1x, Thermo Fisher Scientific), and GlutaMAX (1x, Thermo Fisher Scientific). The combined maturation media was then supplemented with BDNF (20ng/ml, PeproTech), GDNF (20ng/ml, PeproTech), and DAPT (2µM, Stem Cell Technologies) to enhance neuronal differentiation and cell cycle synchronisation of differentiating NPCs (Crawford and Roelink, 2007; Borghese *et al.*, 2010). Maturation media was changed every 2-3 days over the course of differentiation. Ventral neural induction of hiPSCs followed the same protocol and media formulations as above but with the addition of Purmorphamine (1.5µM, Stem Cell Technologies) from Day 2 to 14 post-induction.

3.2.3 Immunofluorescence Microscopy

Samples for immunocytochemistry were fixed for 15 minutes at room temperature in 10% neutral-buffered formalin solution (Sigma) and permeabilised for 15 minutes at room temperature in 0.1% Triton-X-100 (Sigma) in phosphate buffered saline (PBS) (137mM NaCl, 10mM Phosphate, 2.7mM KCl, pH 7.4). Samples were blocked for 1 hour in 5% goat or donkey serum (Millipore) in PBS before incubation with primary antibodies (also in block solution) overnight at 4^{o}C; anti-Oct4 (Stem Cell Technologies 60093, 1:1000); anti-Pax6 (Stem Cell Technologies 60094, 1:1000); anti-Nanog (Cell Signaling Technology 4903, 1:1000); anti-Sox2 (Stem Cell Technologies 60055, 1;1000); anti-Tra-1-60 (Stem Cell Technologies 60064, 1:1000); anti-TUJ1 (Covance MMS-435P, 1:2000); anti-Nestin (Stem Cell Technologies 60091, 1:1000); anti-MAP2 (Cell Signaling Technology 4542, 1:1000); anti-GAP43 (Millipore AB5220, 1:1000); anti-Synapsin I (Abcam ab64581, 1:1000); anti-Reelin (Abcam ab138370, 1:1000); anti-TBR1 (Abcam ab31940, 1:1000); anti-CTIP2 (Abcam ab18465, 1:1000); anti-BRN2 (DSHB PCRP-POU3F2-1A3, 1:500); anti-vGLUT1 (Sigma AMAb91041, 1:1000); anti-vGLUT2 (Abcam ab101760, 1:1000); anti-GAD65+67 (Abcam ab11070, 1:1000); anti-$GABA_AR1$ (Synaptic Systems 224204, 1:1000); anti-$GABA_BR1$ (Abcam ab55051, 1:1000); anti-S100β (Sigma S2532, 1:1000); anti-GFAP (Stem Cell Technologies 01415, 1:2000). Samples were washed three times in PBS before addition of secondary antibodies in block solution for 1 hour at room temperature: goat-anti-mouse IgG AF488 (Invitrogen A11029, 1:2000); goat-anti-mouse IgG AF594 (Life Technologies A11032, 1:2000); donkey-anti-rabbit IgG AF488 (Invitrogen A21206, 1:2000); donkey-anti-rabbit IgG AF594 (Invitrogen A21207, 1:2000); donkey-anti-rat IgG AF594 (Invitrogen A12109, 1:2000);

donkey-anti-goat IgG AF488 (Abcam ab150129, 1:2000); goat-anti-guinea pig IgG AF488 (Abcam ab150185, 1:2000). Samples were washed three more times in PBS before addition of DAPI (Sigma) for 10minutes, for cell nuclei visualisation. Fluorescent images were acquired on an Olympus IX70 wide field microscope with Spot RT Slider digital camera and Spot Advanced software, version 4.8 (Diagnostic Instruments).

3.2.4 Flow Cytometry

For iPSC-based flow cytometry analysis, colonies were dissociated to single cells using GCDR (37^{o}C, 10 minutes) and trituration, prior to centrifugation (500x*g*, 5 minutes). Cells were resuspended in 10% neutral-buffered formalin solution (Sigma) for fixation for 15 minutes under mild-shaking conditions. iPSC-derived NPC cultures were dissociated with Accutase (Stem Cell Technologies) (37^{o}C, 10 minutes) and gentle trituration. The fixation procedure was the same as for dissociated iPSCs. Cell suspensions were passed through a 40µm filter (BD Falcon) to ensure the removal of large cell aggregates. All washes were preceded by a centrifugation step to pellet cells from suspension. Cells were permeabilised through 0.1% Triton-X-100 in PBS (137mM NaCl, 10mM Phosphate, 2.7mM KCl, pH 7.4) for 15 minutes at room temperature under gentle mixing. Cell suspensions were blocked in 1% Bovine Serum Albumin (BSA) (Sigma) in PBS for 1 hour at room temperature prior to the addition of primary antibodies or fluorescently labelled primary antibodies in block solution for 1 hour at room temperature: anti-Oct4 (Stem Cell Technologies 60093, 1:1000); anti-Nanog (Cell Signaling Technology 4903, 1:1000); anti-Pax6 (Stem Cell Technologies 60094, 1:1000); anti-Sox2-PerCp-Cy5.5 (BD Stemflow 561562 kit); anti-SSEA4-AF647 (BD Stemflow 562626 kit); anti-Tra-1-60-PE (BD Stemflow 562626 kit); anti-Nestin-AF647 (BD Stemflow 561562 kit); and anti-DCX-PE (BD Stemflow 561562 kit). Samples were centrifuged and washed three times with block solution. For non-fluorescently labelled primary antibody probes, a second incubation with secondary antibodies was done for 1 hour at room temperature: goat-anti-mouse IgG AF488 (Invitrogen A11029, 1:2000); donkey-anti-rabbit IgG AF488 (Invitrogen A21206, 1:2000); goat-anti-mouse IgG AF647 (Invitrogen A21236, 1:2000); goat-anti-rabbit IgG AF647 (Invitrogen A21245, 1:2000). Data acquisition and analysis was performed on the CytoFLEX Flow Cytometer with CytExpert software, version 2.0 (Beckman Coulter)

3.2.5 Western Blot Assay

For protein concentration and Western blot assays, cells were harvested with Accutase (Stem Cell Technologies) for 10 minutes at 37^{o}C and gentle trituration. Cells were pelleted under centrifugation at 500x*g* for 5 minutes and the supernatant removed. Pellets were snap frozen at -80^{o}C and stored until protein extraction.

Cell pellets were resuspended in 100-200µl of M-PER Mammalian Protein Extraction Reagent (Thermo Fisher Scientific) and mixed gently at room temperature for 10 minutes. After centrifugation at 10,000x*g* for 15 minutes the supernatants were transferred to new 1.7ml microfuge tubes and stored at -80^{o}C until needed for downstream assays.

A colourmetric Bradford assay was used for total protein quantification, calibrated against a Bovine Serum Albumin (BSA) (Sigma) standard curve. 1µl of each protein sample was utilised for protein quantification together with 200µl of 1:5 diluted Bradford Reagent (Bio-Rad). Absorbance readings at 590nm were measured on a FLUOstar Galaxy plate reader (BMG).

For SDS-PAGE: protein samples were denatured at 70^{o}C for 10mins in the presence of NuPAGE LDS Sample Buffer (Thermo Fisher Scientific) and NuPAGE Sample Reducing Agent (Thermo Fisher Scientific). Protein samples were separated on BOLT 4-12% Bis-Tris Gels (Thermo Fisher Scientific) at 150V for 45 minutes. Molecular weight estimation was achieved with parallel loading of Precision Plus Protein Kaleidoscope Prestained Protein Standards (Bio-Rad). Protein lanes were transferred on to nitrocellulose membranes (GE Healthcare Life Sciences) using a Semi-Dry Transfer Cassette (Bio-Rad) at 20V for 70 minutes in Bjerrum Schafer-Nielsen buffer (48mM Tris, 39mM glycine, 1.3mM SDS, 20% Methanol, pH 9). Successful protein transfer was confirmed with Ponceau S stain (0.1% w/v) in acetic acid, and de-stained through washing in Tris buffered saline (TBS) with 0.05% Tween-20 (TBST) (50mM Tris, 150mM NaCl, pH 7.6). Membranes were blocked for 1 hour at room temperature in 5% (w/v) low fat milk powder in TBST. Membranes were incubated with primary antibodies overnight in the block solution at 4^{o}C on a plate rocker: anti-Nanog (Cell Signaling Technology 4903, 1:2000); anti-Nestin (Stem Cell Technologies 60091, 1:2000); anti-TUJ1 (Covance MMS-435P, 1:2000); anti-neurofilament-H (Cell Signaling Technology #2836, 1:2000), anti-neurofilament-L (Cell Signaling Technology #2837, 1:2000); anti-Tau (Neuromics CH23018, 1:1000); anti-FOXG1 (Abcam ab18259, 1:2000); anti-Reelin

(Abcam ab138370, 1:1000); anti-BRN2 (DSHB, 1:750); anti-PSD95 (Abcam ab2723, 1:2000); anti-Synaptophysin (Abcam ab14692, 1:2000); anti-vGLUT1 (Sigma AMAb91041, 1:1000); anti-vGLUT2 (Abcam ab101760, 1:1000); anti-GAD65+67 (Abcam ab11070, 1:1000); anti-$GABA_AR1$ (Synaptic Systems 224204, 1:1000); anti-$GABA_BR1$ (Abcam ab55051, 1:1000); anti-NMDAR1 (Millipore AB9864R, 1:1000); anti-AMPAR1 (Abcam ab31232, 1:1000); anti-S100β (Sigma S2532, 1:2000); anti-GalC (Millipore MAB342, 1:1000) & anti-GAPDH (Cell Signaling Technology #5174, 1:5000). Membranes were washed three times in TBST prior to addition of secondary antibodies. Membranes were incubated with secondary antibodies in block solution for 1 hour at room temperature on a plate rocker: Goat-anti-Mouse-HRP (Millipore, 1:10,000); Goat-anti-Rabbit-HRP (Millipore, 1:10,000); Donkey-anti-Chicken-HRP (Millipore, 1:10,000); Goat-anti-Guinea Pig-HRP (Invitrogen, 1:10,000) Membranes were washed a further three times in TBST and once in TBS prior to chemiluminescent detection. Imaging of protein bands on membranes was achieved on a ChemiDoc MP system (Bio-Rad) after incubation with Western Lightning® Ultra chemiluminescence substrate (Perkin Elmer).

3.2.6 Gene Expression

Relative gene expression analysis was performed using quantitative polymerase chain reaction (qPCR) methodology. Cells were harvested with Accutase (Stem Cell Technologies) for 10 minutes at 37^{o}C and gentle trituration. Cells were pelleted under centrifugation at 500x*g* for 5 minutes and the supernatant removed. Pellets were snap frozen at -80^{o}C and stored until RNA extraction.

RNA was purified from frozen cell pellet samples using the RNeasy Plus Mini Kit (Qiagen) as per the manufacturer's instructions into a total elution volume of 50µl nuclease free water. RNA concentration was determined using an Ultraspec 2200 Pro Spectrophotometer (GE Healthcare Life Sciences) and RNA integrity was confirmed by running samples on a 1% Agarose (w/v)-EtBR Tris-acetate (TAE) buffered gel under electrophoretic conditions for 40 minutes at 80V followed by imaging on a ChemiDoc MP (Bio-Rad) to confirm sharp ribosomal RNA banding.

cDNA was generated from 1µg of each RNA using the Omniscript Reverse Transcription Kit (Qiagen) with 1µM oligo dTs (Thermo Fisher Scientific) and 1U/ml RNase Inhibitor (Qiagen). Reverse transcription reactions took place at 37^{o}C for 80 minutes in a

20µl reaction volume. On completion of the reaction, samples were further diluted with 20µl of nuclease free water. cDNA samples were stored at -20°C until used in qPCR reactions.

qPCR reactions were performed with SYBR Green PCR Master Mix (Qiagen) in 10µl reaction volumes with 1µM of each primer set. All primer pairs were designed using Primer-BLAST (NCBI) (Table 3-1). All amplicons were designed *de novo* to be between 50-250bp in length and have equivalent primer annealing temperatures.

Gene Target	Fwd Primer (5'-3')	Rev. Primer (5'-3')
HPRT1	AAGCCAGACTTTGTTGGATTTG	GGCGATGTCAATAGGACTCCA
OCT4	CAAAACCCGGAGGAGTCCC	AAAGCGGCAGATGGTCGTTT
PAX6	ACATCCGAGATTTCAGAGCCC	CAAAGACACCACCGAGCTGA
NKX2.1	CCAGGACACCATGAGGAACAG	GCTCATGTTCATGCCGCTC
NESTIN	CGCACCTCAAGATGTCCCTC	CAGCTTGGGGTCCTGAAAGC
ß-III-TUBULIN	AACCAGATCGGGGCCAAGTT	GGCACGTACTTGTGAGAAGAGG
TAU	ACTATCAGGTGAACTTTGAACCA	GTTCCTCAGATCCGTCCTCA
SYNAPTOPHSYIN	GGACATGGACGTGGTGAATC	AAGATGGCGAAGACCCATTG
PSD95	ACCCTAGAAGCCCCAGGATA	CCAGACCTGAGTTACCCCTT
REELIN	ACCAGCCAAAGGACTTCACA	TTGCGAGTGCTTACTAGGACGA
TBR1	GACTCAGTTCATCGCCGTCA	CAGCCGGTGTAGATCGTGTC
CTIP2	CCCAGAGGGAGCTCATCACC	AAAACCAGGATGTCCCCCAAG
SATB2	AGGCCGTGGGAGGTTTGAT	GTTCCACCTTCCCAGCTTGA
VGLUT1	CAGCCAACAGAGTTTTCGGC	CGACTCCGTTCTAAGGGTGG
VGLUT2	TCAGATTCCGGGAGGCTACA	TGGGTAGGTCACACCCTCAA
GAD67	GCTGTCGCAGAGCCGAG	CAGGTATCGTACGTTGTGGG
GAT1	CCGAGACAGCGGAGAGGTTG	TTGGAGTTGCCTCACCCTGAT
NMDAR1	GAGCGTGAGTCCAAGGCAGA	GCGGTATACAGTGGCAGCAT
AMPAR1	TTCCAAGGACAAGACAAGCG	GGAGGGTCGATGTCCGTATG
$GABA_AR1$	CCTCCTTCTGAGCACACTGAC	TTCGGTTACACGCTCTCCCAA
$GABA_BR1$	CGCCTGGAGGACTTCAACTA	TTGTAGCTGCCACCCTGAAG
GALC	ACCAGAGACCCATTACGTGG	CATCCAGCTAAATCACCTGTAACC
GFAP	CCATTCCCGTGCAGACCTTC	TAATGACCTCTCCATCCCGCATC

Table 3-1: Primer pair sequences used for qPCR analysis of human iPSC-derived neural cultures.

Reactions were run on a RealPlex Mastercycler (Eppendorf) with the following parameters: 95°C for 2 minutes, then 40 cycles of 95°C for 5s and 60°C for 10s, followed by a melt curve recording. Amplicon specificity was determined via melt curve peak analysis.

All relative expression data was normalised to *HPRT1* housekeeping gene expression. Data were analysed by the ΔΔCt method in Microsoft Excel and statistical analyses performed in GraphPad Prism using multiple unpaired T-test analyses. Data is shown ± standard error of the mean with significance denoted when the p-value ≤0.05. Four biological repeats were completed for each differentiation type (dorsal/ventral) for each time point. Robust regression analysis of fold change expression data was performed in Stata statistical software (version 15.1). Regression coefficients were maintained between ordinary least squares (OLS) regression and those of the robust regression analysis. Raw output tables are displayed in Section 4.5.1.

3.2.7 Electrophysiological Analyses

For patch clamp-based electrophysiological recordings, NPCs were seeded on 13mm glass cover slips coated with poly-L-lysine (0.01%, Sigma) & laminin (20µg/ml, Sigma) and maintained in 12-well tissue culture plates. Cell-seeded coverslips were differentiated using the same protocol as for other molecular analyses (Section 3.2.2) before patch-clamp recordings. For electrophysiological recordings, coverslips were transferred to a recording chamber fitted to an AxioExaminer D1 microscope (Carl Zeiss) and cells were superfused at 1–2 ml/min with a recording solution composed of 137mM NaCl, 5mM KCl, 10mM HEPES, 1mM $MgCl_2$, 2mM $CaCl_2$, 10mM glucose (pH 7.35; 300–305 mOsmol/kg). Neurons were visually identified by a round-to-oval soma (diameter of ~ 10 µm) and patent bipolar processes. Whole-cell patch clamp recordings were made at room temperature using borosilicate microelectrodes (2–6 MΩ; 1.0 mm O.D.; 0.58 mm I.D., Sutter) filled with an internal solution containing 115mM K-gluconate, 10mM HEPES, 7mM KCl, 0.05mM EGTA, 2mM Na_2ATP, 2mM MgATP, 0.5mM Na_2GTP (pH 7.3; 290–295 mOsmol/kg). All chemicals were purchased from Sigma unless otherwise indicated. Signals were recorded with a MultiClamp 700B amplifier (Molecular Devices), data acquisition system (Digidata 1440A, Molecular Devices), and AxoGraph X analysis software (AxoGraph Scientific). The above protocol was adapted from neurosensory cell patch clamp methodologies (Needham *et al.*, 2014). The data presented in Section 3.3.5 is representative of ventral-patterned neuronal cultures (n=9) and dorsal-patterned neurons (n=1) at Day 95 of differentiation. Preliminary data acquisition was attempted at Day 60 but limited success in patching of the cells required an extended maturation time before re-testing at Day 95 of differentiation.

3.3 Results

3.3.1 Pluripotency Validation and Quantification

To ensure robust and stable expansion and proliferation of hiPSCs prior to neural differentiation, protein markers of pluripotency such as OCT4, SOX2, NANOG and TRA-1-60 were assayed via fluorescent immunocytochemistry (Fig 3-1). Each hiPSC colony showed strong nuclear-localised staining for the pluripotency-associated transcription factors OCT4, SOX2 and NANOG. The cell-surface pluripotency marker TRA-1-60 was also present throughout cells within each hiPSC colony.

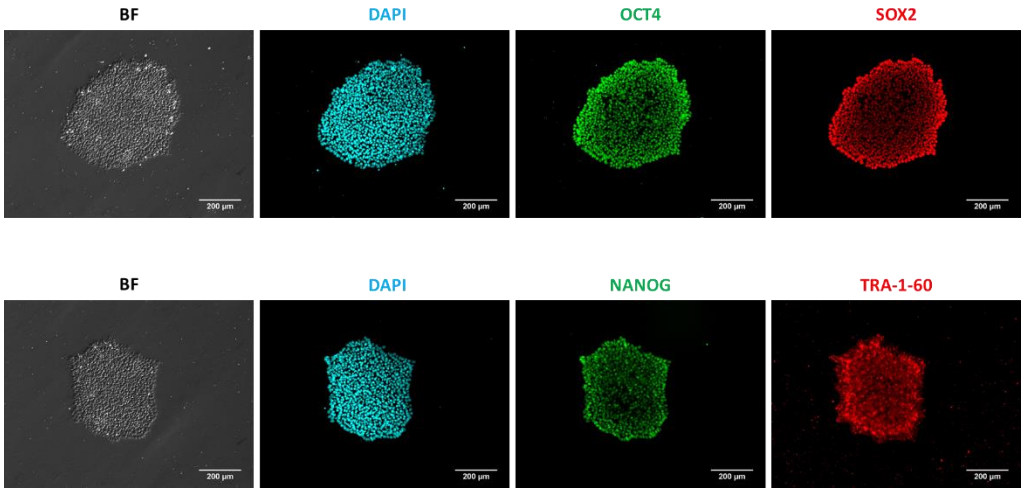

Fig 3-1: Fluorescent immunocytochemistry of pluripotency-associated protein markers in hiPSC colonies. Pluripotency-associated transcription factors OCT4, NANOG and SOX2 show strong nuclear staining, as well as the cell-surface TRA-1-60 marker. Cell nuclei are stained with DAPI. Scale bars represent 200µm. BF; bright field.

To better quantify the quality of hiPSC colonies and to determine the number of differentiated cells within a stable culture that may have lost markers of pluripotency, hiPSCs underwent flow cytometric analysis. The same markers were chosen as for the immunocytochemical analysis above, together with another cell-surface pluripotency marker, SSEA4. Dual staining of both OCT4 and NANOG showed an OCT4-positive cell population of 96.41% and a NANOG-positive hiPSC population of 95.47% within a typical culture. Co-localisation of both OCT4 and NANOG was present in 95.08% of cells (Fig 3-2 A).

This high proportion of pluripotent marker-positive cells was also observed when assaying for TRA-1-60 (95.25%), SOX2 (94.99%) and SSEA4 (99.40%) (Fig 3-2 B). Co-localisation of these markers within the hiPSCs showed high correlation with each other: TRA-1-60 & SOX2 (92.98%), TRA-1-60 & SSEA4 (95.73%), and SOX2 & SSEA4 (95.18%).

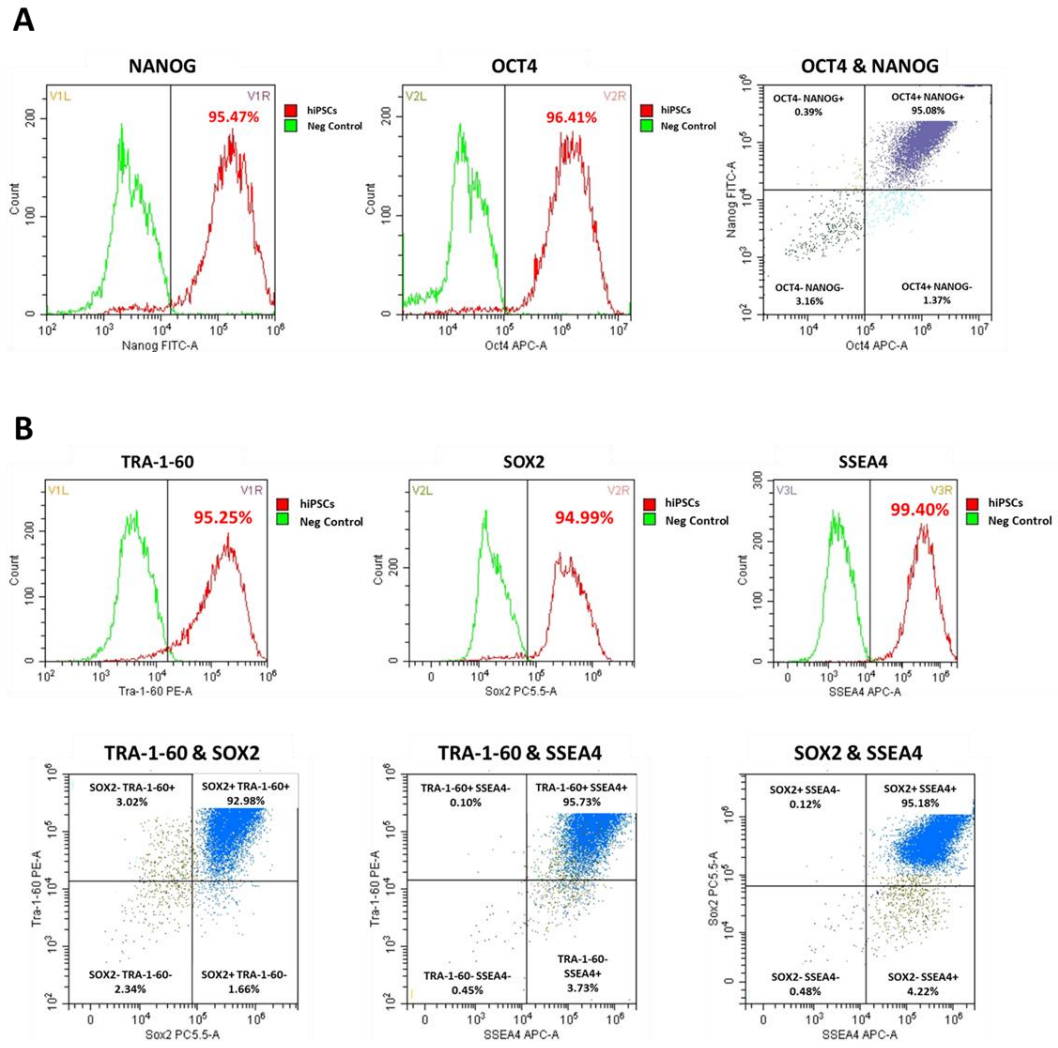

Fig 3-2: Flow cytometric analysis of undifferentiated hiPSC colonies for pluripotency-associated protein markers. (**A**) NANOG and OCT4 dual staining. (**B**) Triple-staining of TRA-1-60, SOX2 and SSEA4. hiPSC samples (red), negative controls (green).

3.3.2 Generation of Neural Precursors from hiPSCs

The first stage in neural differentiation of hiPSCs is the restriction of potency to that of a neuroectodermal or neuroepithelial lineage. In this study, initial germ layer restriction was achieved through dual-SMAD inhibition using a commercially available neural induction

media (STEMdiff, Stem Cell Technologies) (NIM). Gene expression analysis of hiPSCs dissociated as single cells and grown in monolayer in NIM for 7 days showed strong down-regulation of the pluripotency-associated gene *OCT4* (~250-fold less seen at Day 7 than Day 0), and robust upregulation of the neural precursor cell (NPC) marker *PAX6* over 7 days of neural induction (Fig 3-3 A), with an approximate 128-fold increase from Day 3 to Day 7 of differentiation. All fold change differences in gene expression reached statistical significance, with *PAX6* non-detectable in undifferentiated Day 0 hiPSCs.

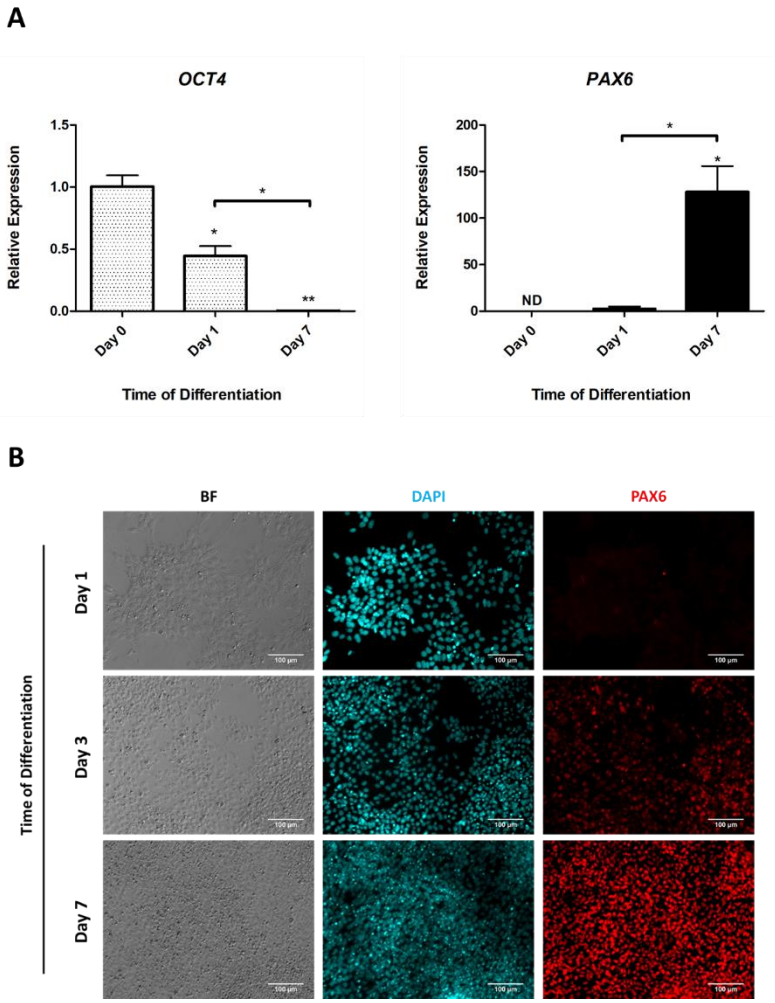

Fig 3-3: Gene and protein expression of pluripotency and neural precursor cell markers over 7 days of neural induction. (**A**) qPCR analysis of the pluripotency marker *OCT4* downregulation during differentiation, and the upregulation of the early neural precursor marker *PAX6*. Data is shown as mean values ± standard error of the mean. Statistical significance denoted by * p≤0.05, ** p≤0.01. ND; Not detected. (**B**) Upregulation of PAX6 protein expression over the same time course of neural induction. Cell nuclei are shown with DAPI staining. BF; bright field images. Scale bars represent 100µm.

Upregulation of this NPC marker transcript was also reflected at the protein level, with PAX6 protein being robustly upregulated in differentiating hiPSCs over 7 days of neural induction, as shown through fluorescent immunocytochemistry (Fig 3-3 B).

This upregulation of the early NPC marker PAX6 at both the gene and protein expression level is indicative of early forebrain neural differentiation events, together with the downregulation of *OCT4* gene expression showing the loss of pluripotent cell identity.

To better quantify the efficiency of neural induction and to track the degree of forebrain precursor marker expression and concurrent loss of pluripotency markers, differentiating cells underwent quantitative flow cytometry. Over 10 days of neural differentiation, the percentage of cells expressing OCT4 dropped from 97.26% in undifferentiated (Day 0) hiPSCs to 2.52% after 10 days of neural induction (Fig 3-4 A). The loss of pluripotency-associated markers occurred very early on in the differentiation with OCT4-positive cells accounting for 52.40% of the cell population after 1 day of differentiation, and 45.63% of cells by Day 3. After 7 days of neural induction only 3.31% of assayed cells showed OCT4 marker expression.

At later stages within the neural induction time frame, PAX6-positive cells accounted for 74.57% of the population by Day 7 and 82.46% by Day 10 (Fig 3-4 B). This high degree of neural induction efficiency is mirrored when looking at another NPC marker: the intermediate filament protein NESTIN. After 7 days of neural induction NESTIN-positive cells were present at a level of 88.90%, which remained stable at 88.32% by Day 10. However, the NPC/early neuronal protein marker DOUBLECORTIN (DCX) showed no expression in NPC cultures by Day 7 or 10, demonstrating that more extensive differentiation timelines are necessary to derive more mature NPC and neuronal markers.

To further refine the induction protocol, a second proliferative media (also commercially available) termed neural proliferation media (NPM) was studied in parallel to NIM induction alone to assay any positive or negative effects on NPC induction and marker expression. After 14 days of NIM-alone differentiation of hiPSCs, a high prevalence of PAX6-positive cells was maintained in the population, but the level of NESTIN-positive cells was more restricted in the NPC cultures and was predominantly localised to aggregated cell clusters in the monolayer induction culture (Fig 3-5). However, a stepwise neural differentiation of 7 days of NIM treatment followed by 7 days of NPM triggered NPC cultures with both a prevalent degree of PAX6-positive cells and also a much stronger and

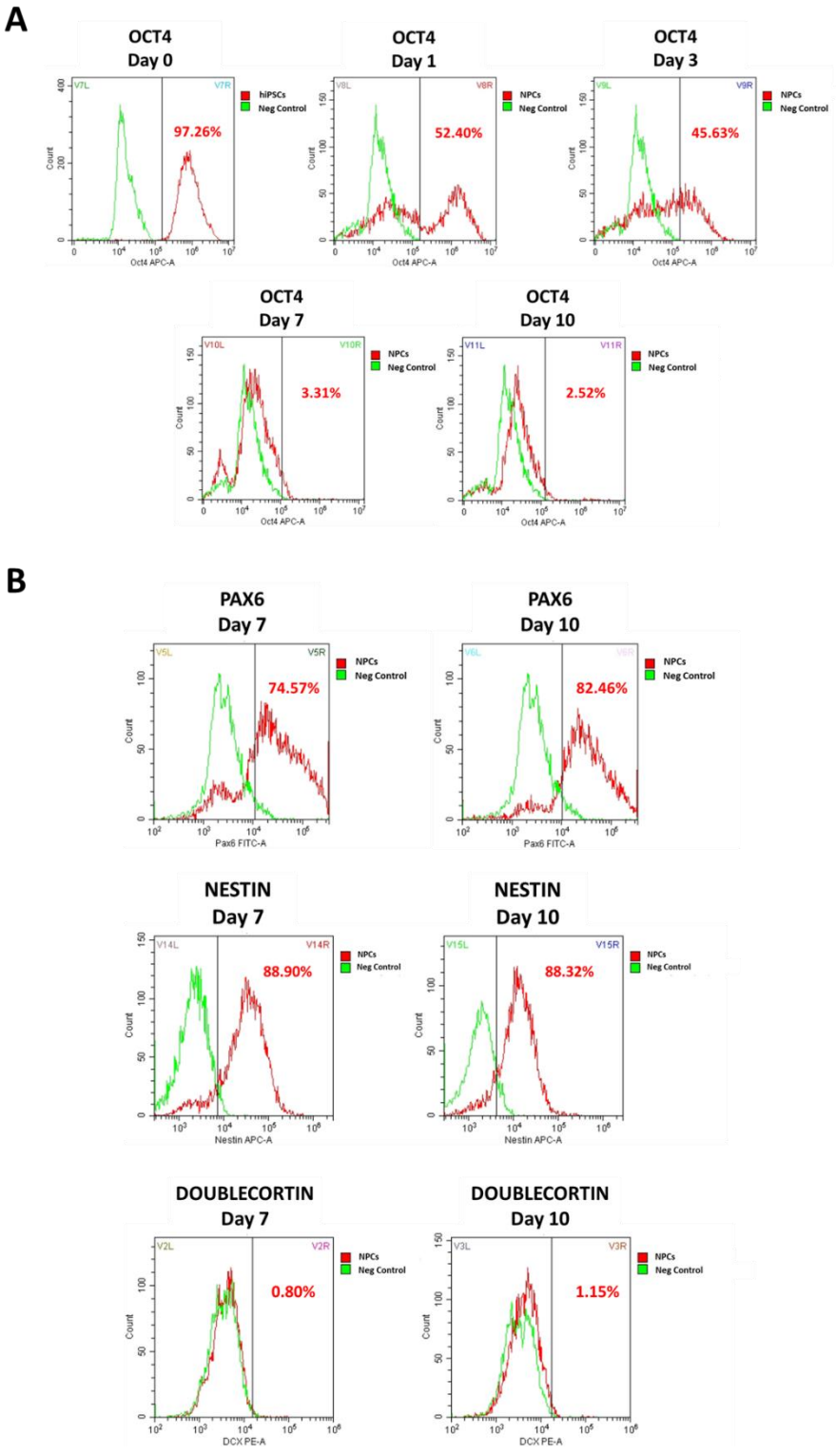

Fig 3-4: Flow cytometric analysis of pluripotency markers, neural precursor markers and early born neuronal markers in hiPSC cultures undergoing neural induction. (**A**) Levels of OCT4-positive cells during 10 days of neural differentiation. (**B**) PAX6 and NESTIN positive cells represent successful neural precursor induction by Day 7-10 of differentiation. Negative DOUBLECORTIN staining indicates no early-neuronal cells are present in the precursor pool. iPSCs/NPCs (red), negative controls (green).

widespread NESTIN signal throughout the culture. Interestingly, the size of cell nuclei also appeared to show differences under these differing culture conditions. NIM-alone treated NPCs retained smaller and more densely packed cell nuclei, whereas the NIM-NPM treated neural cultures showed bias to larger nuclei (Fig 3-5). This demonstrates that distinct differences within the differentiation pathway are occurring between these two methods resulting in higher degrees of NESTIN induction in cultures exposed to NPM following dual SMAD-inhibition methods of neural induction.

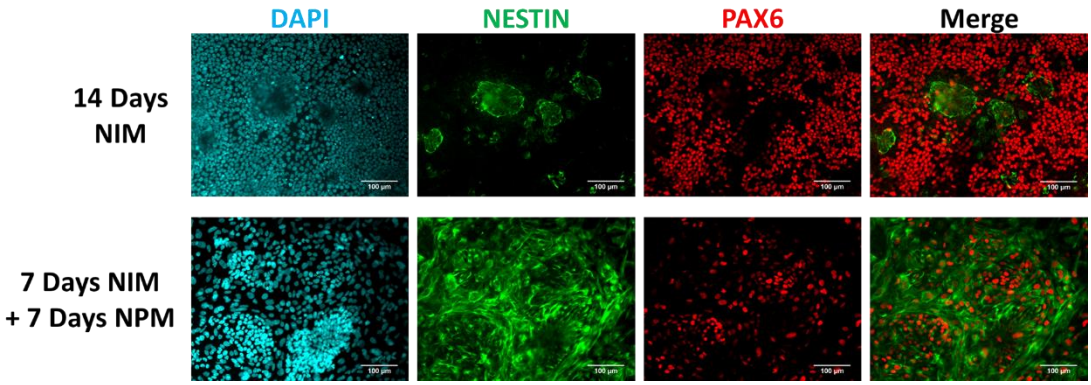

Fig 3-5: Neural precursor marker expression in hiPSCs undergoing neural differentiation over 14 days with either neural induction media (NIM) alone, or in 7 days of NIM and 7 days of neural proliferation media (NPM). Cell nuclei are visualised with DAPI stain. Scale bars represent 100µm.

To fully differentiate the NPC cultures into mature neural cells displaying typical neuronal morphology and marker expression, media composition was changed to a neural maturation media (NMM) containing N2 and B27 primary neural culture supplements as well as brain-derived neurotrophic factor (BDNF), glial cell-derived neurotrophic factor (GDNF) and the gamma-secretase inhibitor N-[N-(3,5-difluorophen- acetyl)-l-alanyl]-S-phenylglycine t-butyl ester (DAPT) (See Methods Section 3.2.2). This procedure of neural induction of hiPSCs and consequent maturation resulted in neural cell cultures displaying extensive neuritogenesis and branching, together with mature neuronal marker expression of β-III-TUBULIN after 28 days of differentiation (Fig 3-6 B). This methodology therefore was adopted for all future hiPSC neural differentiation experimental setups, with the procedure outlined in Fig 3-6 A. To retain adequate levels of cell viability during differentiation, the RHO/ROCK pathway inhibitor Y-27632 was added as a component of the NIM media.

It is interesting to note that even after 4 weeks of neural differentiation, the NPC marker PAX6 was still retained in a subset of cells, indicating the early-neuronal nature of the derived cells and the retention of NPC cell identity throughout differentiation. All of which reflects the extended timeline of differentiation and maturation seen *in utero*.

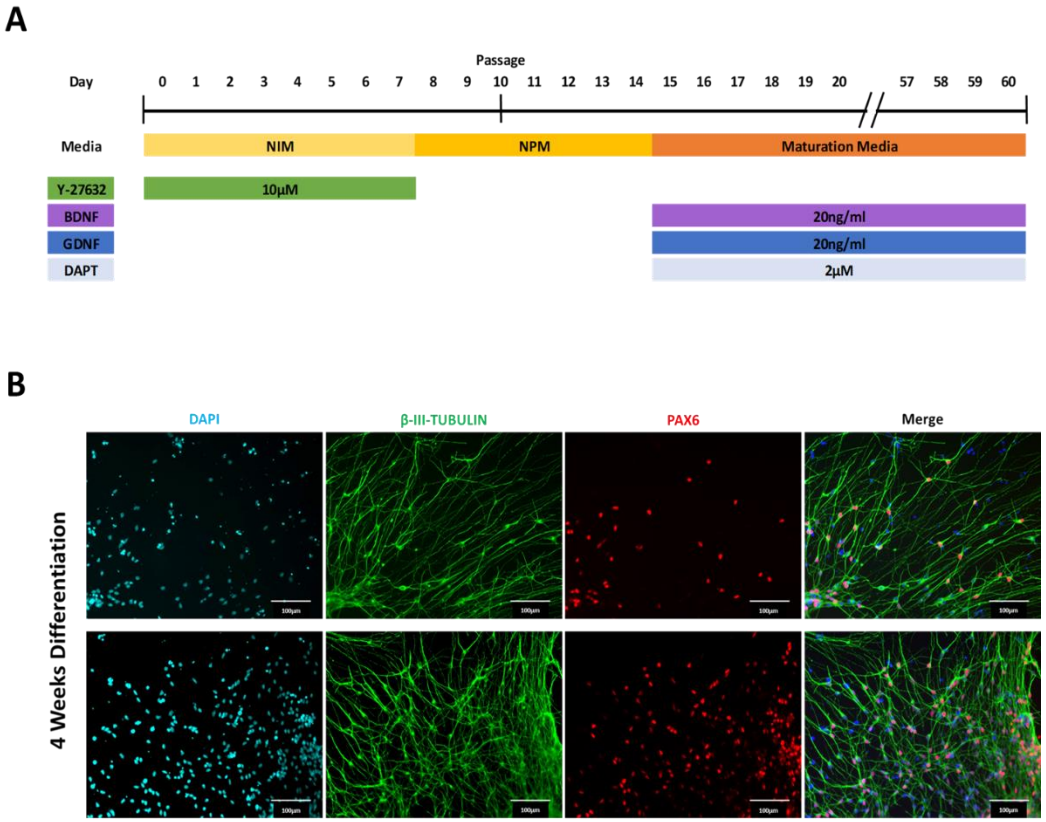

Fig 3-6: Schematic representation of neural differentiation protocol of hiPSCs and example images of derived neural cultures. (**A**) Timeline of the hiPSC-neural differentiation pathway involving stepwise treatment with neural induction media (NIM), neural proliferation media (NPM) and maturation media. The maturation media also contained the neurotrophic factors; brain-derived neurotrophic factor (BDNF), glial cell-derived neurotrophic factor (GDNF), and the Notch signalling inhibitor N-[N-(3,5-difluorophen- acetyl)-l-alanyl]-S-phenylglycine t-butyl ester (DAPT). (**B**) Fluorescent immunocytochemistry of hiPSC-derived neural cultures after 4 weeks of differentiation showing the mature neuronal marker β-III-TUBULIN and NPC marker PAX6. Cell nuclei are shown through a DAPI stain. Scale bars represent 100µm.

3.3.3 Dorsal Forebrain Differentiation and Maturation

Following the neural induction principles outlined above (Section 3.3.2), hiPSCs were differentiated towards a neural lineage for 60 days. No other patterning morphogens were added into any stage of the differentiation protocol in order to derive the default dorsal forebrain excitatory neuronal identity as is seen in other differentiation studies (Gaspard *et al.*, 2008; Zeng *et al.*, 2010; Shi *et al.*, 2012; Shi, Kirwan and Livesey, 2012). Following this extended maturation period, extensive neurite outgrowths developed in the iPSC-derived neural cultures together with positive immunostaining of both neuronal and astroglial markers (Fig 3-7).

A subpopulation of cells within the hiPSC-derived neural culture maintained NPC marker expression (PAX6 and NESTIN) even after 60 days of differentiation and maturation, showing retention of neural precursor characteristics. Widespread neural morphology in tandem with strong positive staining of the neuronal markers β-III-TUBULIN, MAP2 and GAP43 were seen throughout the iPSC-derived cultures at this time point: indicative of successful and highly efficient neural induction and maturation. Interestingly, the astroglial markers Glial Fibrillary Acidic Protein (GFAP) and S100β were also present in cells within the neural culture that did not show colocalisation with the β-III-TUBULIN neuronal marker, but robust colocalisation with each other (Fig 3-7). These cell types also had an immature cell morphology suggesting an early degree of astroglial differentiation, which does agree with *in utero* forebrain neurogenesis where glial cell differentiation follows chronologically that of neuronal differentiation (Hansen, Rubenstein and Kriegstein, 2011).

This dorsal-forebrain default neural differentiation pathway gives rise to cortical-associated structures *in vivo* and *in vitro*. To track the development of cortical generation and lamination events *in vitro* we observed markers known to localise to particular early-born (deep layer) and late-born (upper layer) cortical neurons (Fig 3-8). Reelin is an extracellular glycoprotein secreted from Cajal-Retzius cells, which form the outermost layer (Layer I) of the developing cortex (Frotscher *et al.*, 2009). REELIN immunostaining of iPSC-derived dorsal neural cultures showed diffuse but positive staining suggestive of a small proportion of neural cells of the early outer cortical plate (Fig 3-8). The transcription factor TBR1 is highly expressed within cells of the cortical preplate and within layer VI early-born (deep layer) neurons. It was also strongly expressed within a subpopulation of cells within

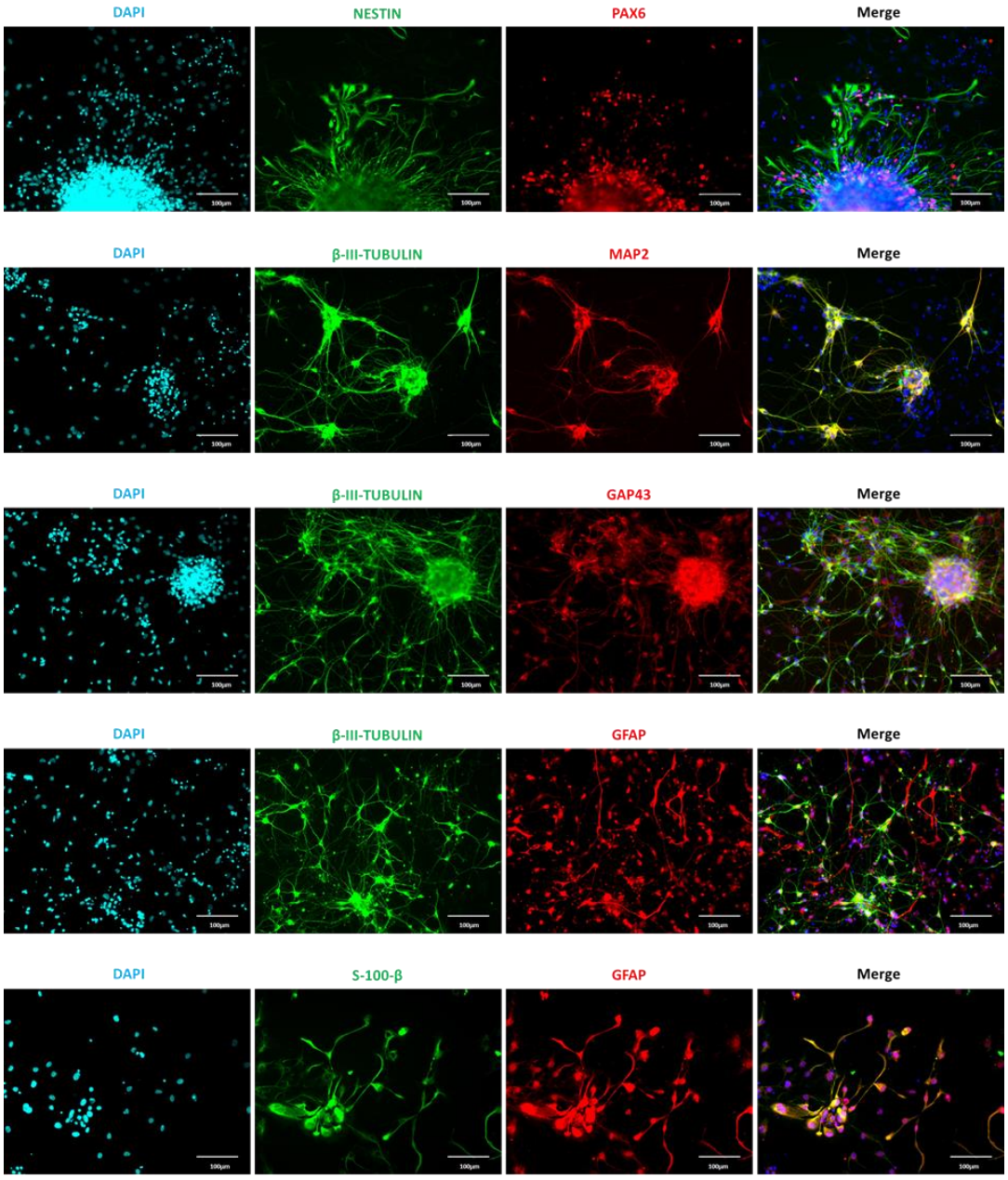

Fig 3-7: Fluorescent immunocytochemistry of hiPSC-derived neural cultures after 60 days of differentiation. A subpopulation of cells retain the NPC markers PAX6 and NESTIN, while many display the canonical neuronal markers β-III-TUBULIN, MAP2, and GAP43. Astroglial markers (GFAP and S100β) are also seen colocalised in a subpopulation of cells. Nuclei shown through DAPI staining. Scale bars represent 100µm.

these *in vitro* neural cultures, suggestive of not only cortical plate identity but also more mature deep layer cortical generation events. This is mirrored by the protein expression of CTIP2, a zinc finger transcription factor, that localises to neural cells in layer V of the developing cortex. A subpopulation of CTIP2-positive cells in these *in vitro* neural cultures is suggestive of development beyond cortical preplate generation. Late-born neurons or

upper cortical layer neurons (layers II-IV) show different protein marker expression and a well-known marker of these cell types and layer identity is BRN2. BRN2 expression within the *in vitro* iPSC-derived neural cultures at this time point was less prevalent than was seen for TBR1 and CTIP2 (Fig 3-8). As BRN2-positive neurons and upper layer cortical identity follows a more protracted timeline of development than deep layer neurons, this further shows that these neural cultures are representative of developmental timings and cytoarchitecture formation events seen *in utero*.

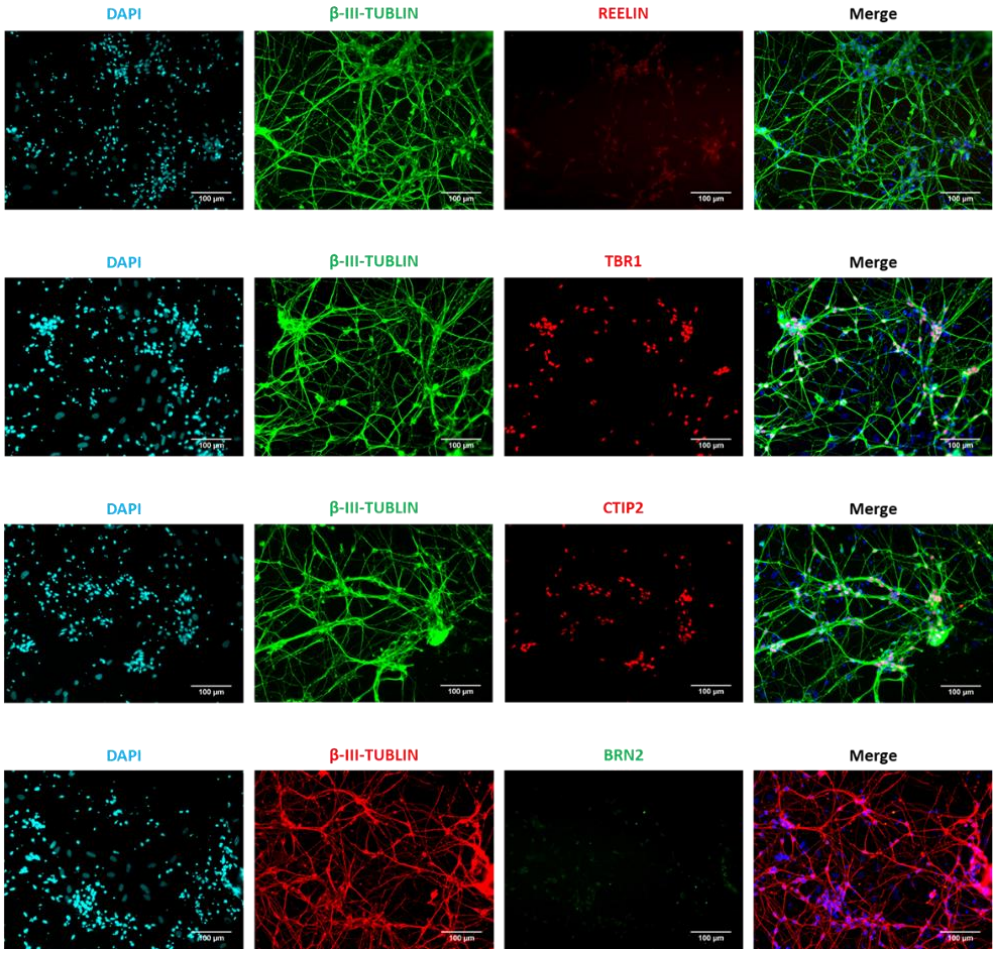

Fig 3-8: Fluorescent immunocytochemistry of cortical-associated layer markers of hiPSC-derived neural cultures. REELIN staining indicative of outer-layer (layer I) cortical identity. TBR1 associated with early-born (layer VI) and preplate cortical regions. CTIP2-positive staining representative of layer V cortical regions. BRN2 as a marker of late-born upper layer (II-IV) cortical neurons. Cell nuclei imaged with DAPI stain. Scale bars represent 100µm.

As well as localisation markers by which to describe the comparable *in vivo*-location of the differentiating neural cultures, we also aimed to describe the neuronal

subtype specificity of the derived neural cells. Dorsal forebrain differentiation reportedly derives excitatory glutamatergic pools of neuronal cells. To this end we stained for the presence of the presynaptic glutamate re-uptake transporter vGLUT2 and the glutamate decarboxylase enzymes GAD65+GAD67, present within glutamatergic neurons and GABAergic inhibitory neuronal subtypes respectively (Fig 3-9). From these data it is clear that the vast majority of derived neural types using this differentiation protocol expressed markers of excitatory glutamatergic neurons, and not of inhibitory GABAergic cell types. This fits with the known patterning effects and down-stream neural-tube derived signalling events that predispose NPCs to differing lineage subtypes as outlined in Section 3.1.

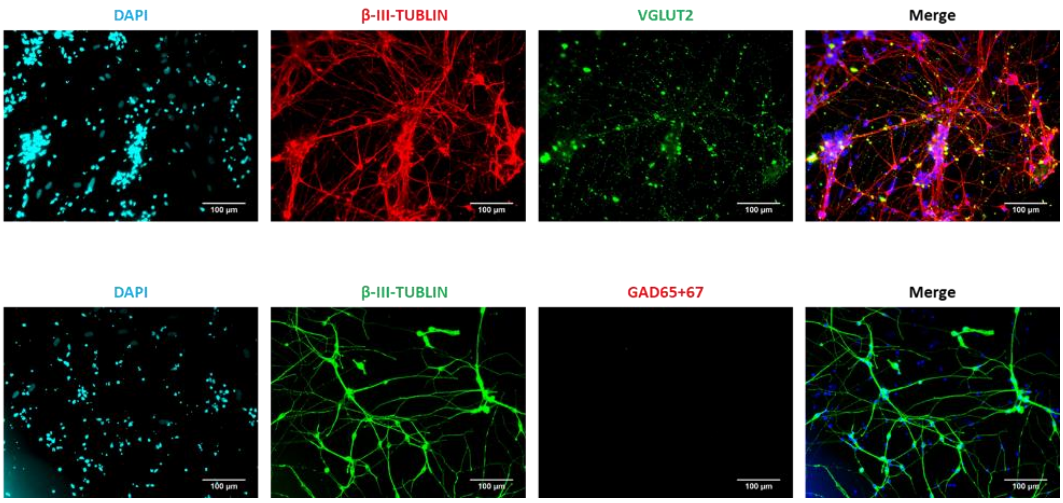

Fig 3-9: Fluorescent immunocytochemistry of excitatory and inhibitory neuronal markers of hiPSC-derived neural cultures. The excitatory glutamatergic marker VGLUT2 shows high level expression throughout the culture, whereas the GABAergic markers GAD65+67 show no expression in the derived neuronal cells. Nuclei are shown through DAPI staining. Scale bars represent 100µm.

To better track protein markers of neural differentiation and maturation over time, Western blot analysis of a panel of neural markers was undertaken to investigate the timing and maturation events of the hiPSC-derived neural cultures (Fig 3-10). The pluripotency-associated marker NANOG was highly expressed in undifferentiated hiPSC cultures but was completely absent during extended neural induction from 14 days to 60 days post induction, showing the expected loss of stem cell pluripotency after initiation of differentiation. The NPC marker NESTIN showed no expression within undifferentiated hiPSC cultures, but instead peaked at Day 14 post-neural induction following the expected timeline of NPC generation, and was also present but to a lesser degree after neural

maturation following 60 days of differentiation. β-III-TUBULIN expression was seen at Day 14 post-neural induction and continued to increase in intensity over the full time-course of differentiation, demonstrating the development and enrichment of neuronal cells within the culture. This early expression profile shows that canonical neuronal lineage markers are expressed early in the differentiation process, but other markers of neuronal differentiation, such as the axonal marker TAU and the neurofilament-light and -heavy chains (NF-L and NF-H), required more extended periods of maturation before detectable levels are seen in hiPSC-derived neural cultures *in vitro* (Fig 3-10).

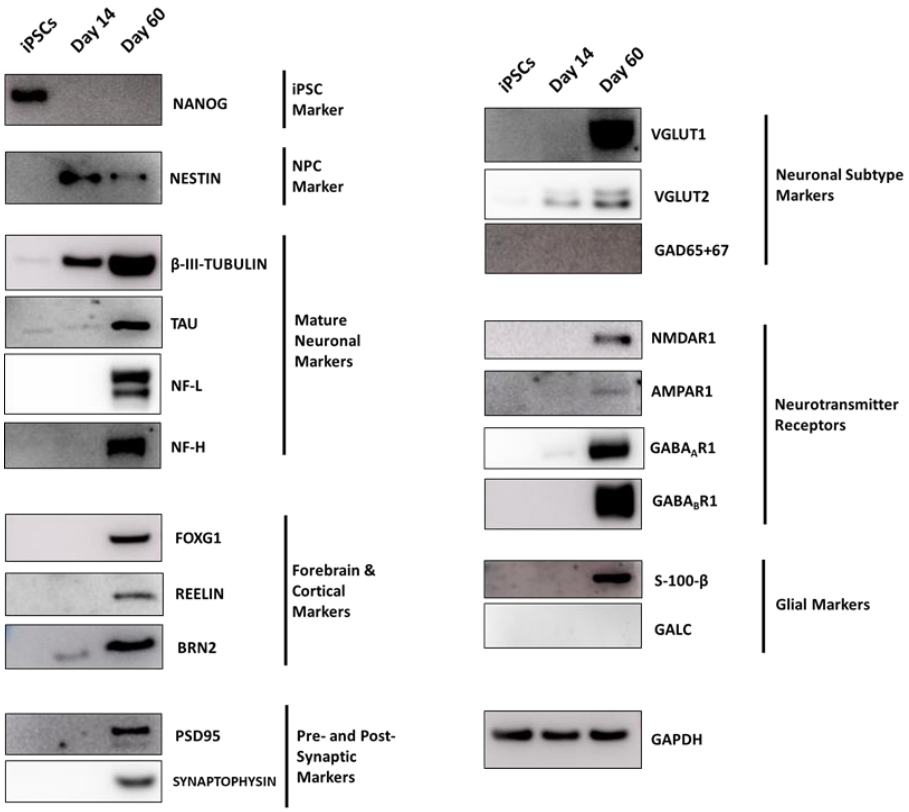

Fig 3-10: Western blot analysis for an array of neural markers present within undifferentiated hiPSCs, hiPSC-NPC cultures after 14 days of differentiation, and hiPSC-derived dorsal neural cultures after 60 days of differentiation.

The early forebrain and telencephalic marker FOXG1, as well as the early- and late-born cortical neuronal markers REELIN and BRN2 all showed protein expression by Day 60 of neural differentiation. The presence of these temporo-spatial localisation markers reinforces the finding that neural cultures differentiated in this way are biased to lineages derived from dorsal-anterior neural tube regions.

For neural networks to form *in vitro,* as they do developmentally, it is important that they express and assemble molecular machinery that form functional synaptic connections. By observing the presence of proteins involved in pre- and post-synaptic pathways it is possible to infer that neural cells in culture have the capacity to form such connections with surrounding cells. To this end the pre-synaptic marker SYNAPTOPHYSIN (SYN) and post-synaptic density marker 95 (PSD95) protein expression were both investigated. By Day 60 of neural differentiation, both SYN and PSD95 displayed detectable levels of protein expression, showing that the differentiating neurons were expressing genes relevant to pre- and post-synaptic structure formation (Fig 3-10).

For neuronal subtype identification; the glutamatergic pre-synaptic markers vesicular glutamate transporters vGLUT1 and vGLUT2 showed robust expression after 60 days of neural differentiation, with a lower expression of vGLUT2 after 14 days of differentiation. The GABAergic neuronal markers GAD65+67 were not detected in these neural cultures (Fig 3-10). Taken together, this suggests a prominent bias towards differentiation to excitatory neuronal subtypes.

Together with general synaptic machinery, the array and type of neurotransmitter receptors present within neural cultures are indicative of the maturity of the cells as well as displaying which neurotransmitters functional neural networks would respond to. The ionotropic glutamate receptors N-Methyl-D-Aspartate Receptor 1 subunit (NMDAR1, also designated as GluN1), and α-Amino-3-hydroxy-5-Methyl-4-isoxazole Propionic Acid Receptor 1 subunit (AMPAR1) both displayed protein expression by Day 60 of differentiation (Fig 3-10). The presence of both of these functional receptors would enable neuronal sensitivity and response to glutamate-based neurotransmission. The ionotropic GABA-A receptor ($GABA_AR1$ subunit) and the G-protein coupled GABA receptor subunit $GABA_BR1$ were also highly expressed within the hiPSC-derived dorsal neural cultures at later time points (Fig 3-10). The presence of all four neurotransmitter receptors at the protein level after 60 days of differentiation suggests that mature neuronal cells may be sensitive to both excitatory and inhibitory neurotransmitter signalling.

The astroglial marker S100β, was also expressed by Day 60 of differentiation, which illustrates that astrocytic lineages were also a component of neural cultures at this level of maturation. However, galactosylceramidase (GALC) a marker of mature oligodendrocytes, and lineage restricted oligodendrocyte precursors, did not display any positive signal through Western blot analysis (Fig 3-10). This either suggests a longer maturation time may

be necessary by which to generate oligodendroglial lineages, or that this pathway of lineage differentiation is intrinsically low in dorsal forebrain neural induction.

3.3.4 Molecular Comparisons of Dorsal and Ventral Forebrain Neural Lineage Differentiation

In parallel with hiPSCs differentiated towards default forebrain "dorsal" lineages, we also wanted to investigate differentiation of NPCs to "ventral" neural tube lineages through morphogen patterning via the SHH pathway agonist Purmorphamine (Pur). For direct timeline comparisons to be made, the scheme of neural induction, proliferation and maturation was kept the same as outlined in Section 3.3.3, but with the addition of Pur from Day 2 to Day 14 of differentiation (Fig 3-11).

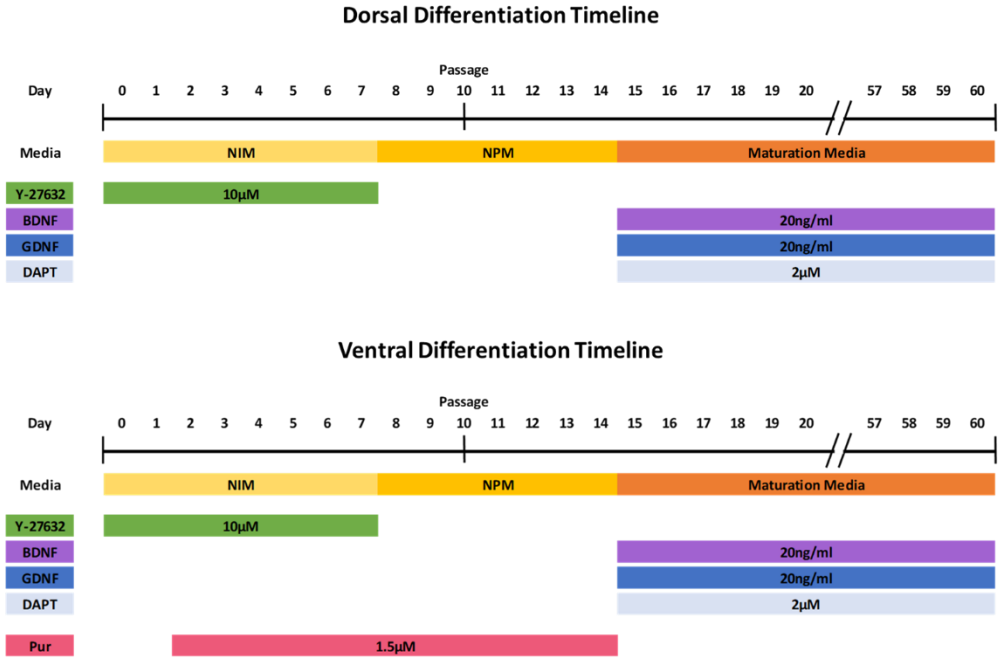

Fig 3-11: Schematic representation of the protocols for parallel differentiation of dorsal (excitatory) forebrain lineages and ventral (inhibitory) forebrain lineages from hiPSCs. Both differentiation pathways include stepwise treatment with neural induction media (NIM), neural proliferation media (NPM) and maturation media. The maturation media also contained the neurotrophic factors; brain-derived neurotrophic factor (BDNF), glial cell-derived neurotrophic factor (GDNF), and the Notch signalling inhibitor N-[N-(3,5-difluorophen- acetyl)-l-alanyl]-S-phenylglycine t-butyl ester (DAPT). In addition, the ventral differentiation pathway contained purmorphamine (Pur) a small molecule agonist of the sonic hedgehog signalling pathway.

After 60 days of differentiation following these protocols, protein marker expression was assayed through fluorescent immunocytochemistry. The early-cortical layer VI and preplate marker TBR1 showed extensive expression in dorsal neural cultures (as was seen in Section 3.3.3) but was lacking from neural cultures that underwent ventralising pathway signalling (Fig 3-12), despite having comparable levels of β-III-TUBULIN-positive neuronal cells.

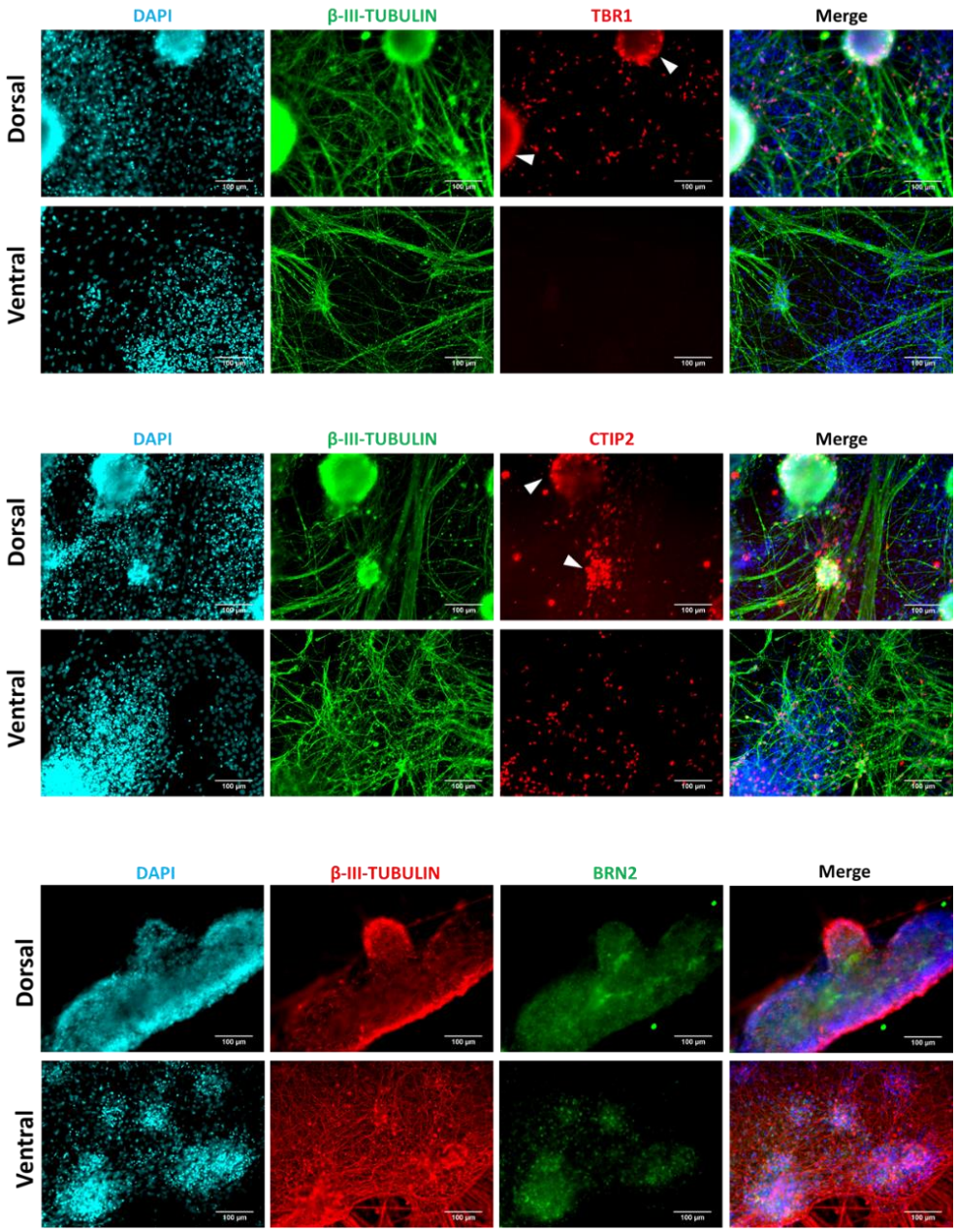

Fig 3-12: Fluorescent immunocytochemistry of early and late cortical plate markers in neural cultures differentiated from hiPSCs into dorsal and ventral forebrain lineages. All samples are stained with β-III-TUBULIN to highlight mature neuronal cell types and also markers of deep-layer and upper-layer cortical markers TBR1, CTIP2 and BRN2. Cell nuclei are imaged through DAPI staining. Scale bars represent 100µm.

As well as positive staining within nuclei of dispersed neural cells, TBR1 expression was also strongly localised to the outer layer of neural ganglia-like structures that formed within the differentiating cultures (Fig 3-12, white arrow heads). This pattern of staining is indicative of organoid-like cortical self-organisation within these cellular aggregates.

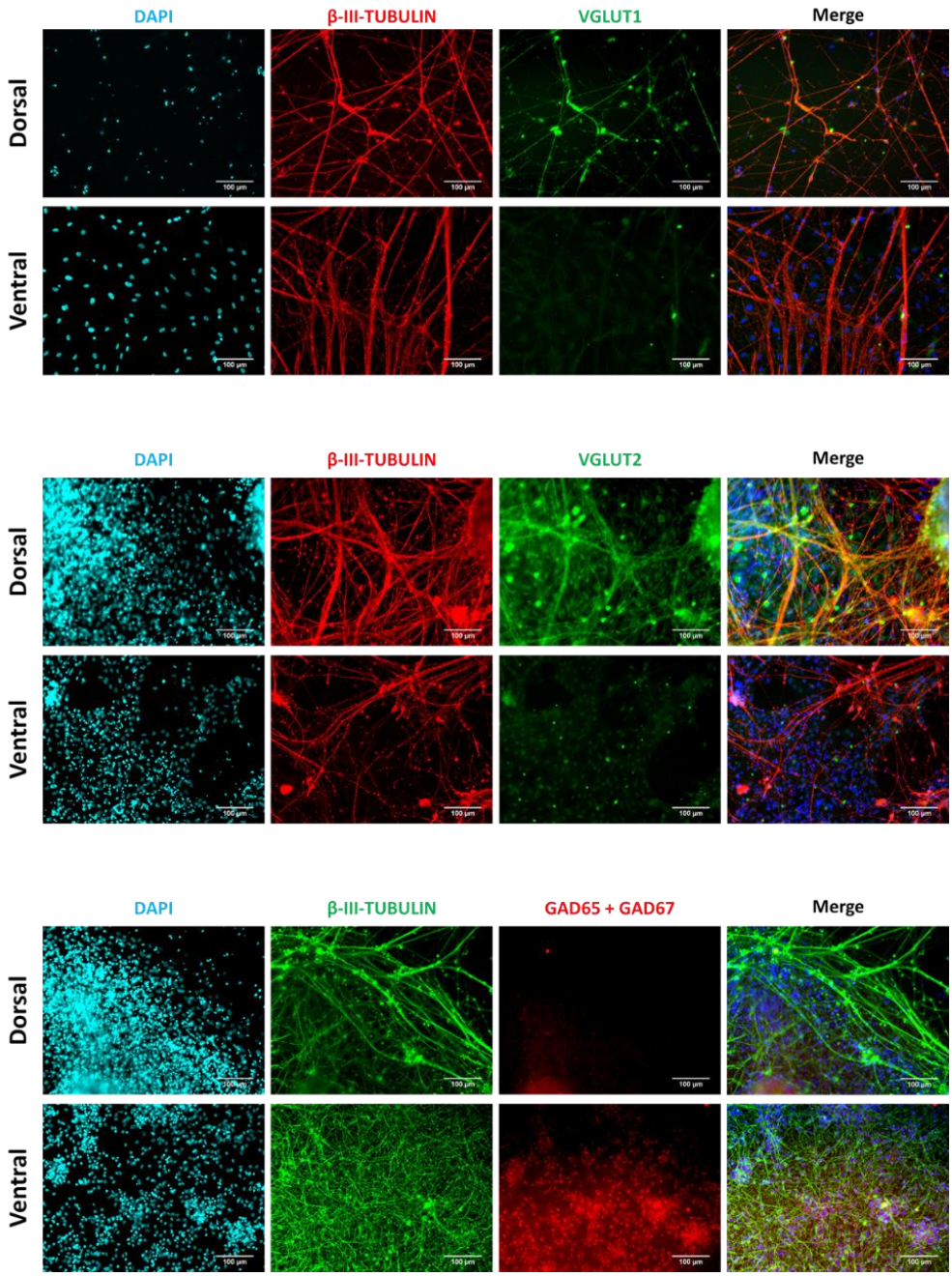

Fig 3-13: Fluorescent immunocytochemistry of excitatory and inhibitory neuronal markers in neural cultures differentiated from hiPSCs into dorsal and ventral forebrain lineages. All samples are stained with β-III-TUBULIN to highlight mature neuronal cell types with glutamatergic markers vGLUT1/2 and GABAergic markers GAD65+67. Cell nuclei are imaged through DAPI staining. Scale bars represent 100µm.

A similar pattern was also observed in dorsal cultures that displayed CTIP2-positive expression, with strong staining in the outer layer of cellular aggregates within the cultures (Fig 3-12). Unlike TBR1 however, CTIP2 staining was prevalent throughout the ventralised neural culture which suggests a role for CTIP2 within ventral neural tube neural lineage generation. The upper-layer cortical marker BRN2 showed dense staining in dorsal neural cultures which were predominantly localised and prevalent in ganglion-like aggregates. It was however, also seen to a lesser degree within ventral-patterned neural lineages.

Striking differences between markers of neuronal subtype specificity were also apparent between dorsal and ventral patterned cultures (Fig 3-13). The glutamatergic neuronal markers vGLUT1 and vGLUT2 both displayed higher degrees of staining within dorsal rather than ventral cultures. Conversely, the GABAergic markers GAD65+67 showed higher levels of expression from ventrally-patterned cell lineages.

To better understand the potential neurotransmitter responsiveness of each neural lineage subtype, we investigated the presence of the ionotropic glutamate receptor subunit AMPAR1, and the ionotropic and metabotropic GABA receptor subunits $GABA_AR1$ and $GABA_BR1$ respectively (Fig 3-14). Intriguingly, even though AMPAR1 protein expression was seen in both dorsal and ventral patterned cultures and did show colocalisation with cells expressing the neuronal marker β-III-TUBULIN, a strong presence of this glutamate receptor was also visualised in surrounding cell types, with weaker or absent mature neuronal staining. Conversely, the staining pattern for $GABA_AR1$ showed near perfect overlap with post-mitotic neuronal cells in both dorsal and ventral neural cell pools, with no apparent staining in other cells of glial or immature lineage. The G-protein coupled receptor subunit $GABA_BR1$, in contrast, only showed prevalent staining in non-neuronal cell types. Suggesting a developmental effect of this metabotropic receptor at this stage of differentiation in immature or glial cell lineages from hiPSC-derived neural cultures (Fig 3-14).

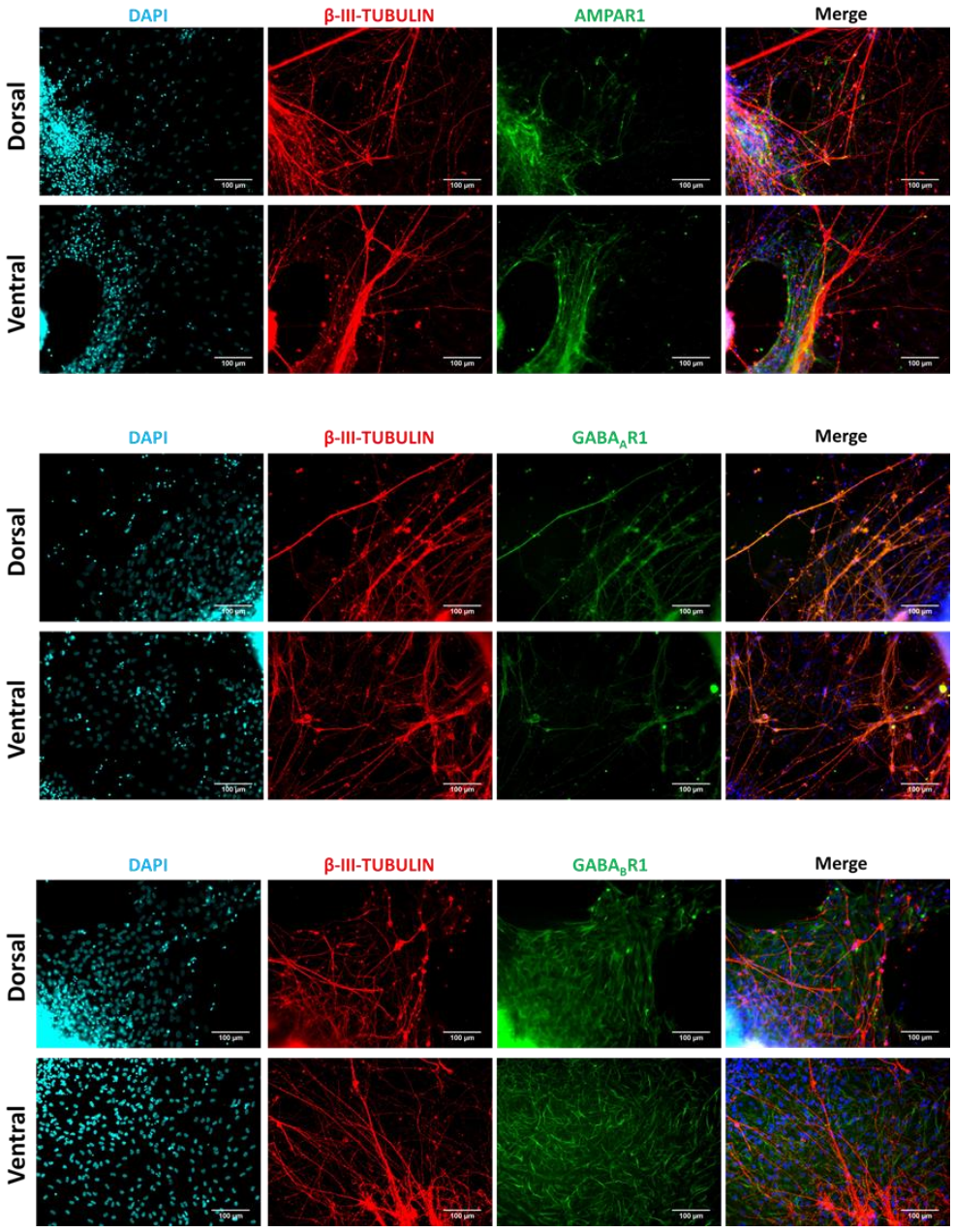

Fig 3-14: Fluorescent immunocytochemistry of neurotransmitter receptor subunit markers in neural cultures differentiated from hiPSCs into dorsal and ventral forebrain lineages. All samples are stained with β-III-TUBULIN to highlight mature neuronal cell types. Other staining displays the ionotropic glutamate receptor subunit AMPAR1, and the GABA-receptor subunits $GABA_AR1$ and $GABA_BR1$. Cell nuclei are imaged through DAPI staining. Scale bars represent 100µm.

To more accurately compare neural marker expression levels between the dorsally- and ventrally-patterned neural cultures, we undertook Western blot analysis of a wide panel of proteins related to; post-mitotic neuron identity & axonogenesis, neuronal neurotransmitter subtype, developmentally related forebrain localisation, pre- and post-synaptic machinery, and neurotransmitter receptor subunits (Fig 3-15).

Neither neural culture derived through the dorsal or ventral differentiation protocol displayed any expression of the pluripotency marker NANOG, while it was highly expressed in undifferentiated hiPSCs. The neuronal structural protein β-III-TUBULIN and axonal marker TAU showed comparable levels of protein expression in both dorsal and ventral cultures after 60 days of maturation, with a slight elevation seen within the ventrally-patterned cultures. However, neurofilament-light chain (NF-L) was seen at a much lower level in ventral cultures than the default excitatory dorsal cell populations. None of the above markers were observed in undifferentiated hiPSC cultures (Fig 3-15).

Stark and robust differences were seen at the protein expression level for identifiers of excitatory neurons and inhibitory interneurons between dorsal and ventral cultures. The glutamatergic neuronal marker vGLUT1 was only detected within dorsally-patterned neural cultures, whereas the GABAergic neuronal markers GAD65+67 were conversely only detected in ventrally-patterned differentiation cultures (Fig 3-15).

The early forebrain marker FOXG1 was strongly expressed in both dorsal and ventral cultures, indicating both retained anterior neural tube marker characteristics. However, divergence was observed when looking at the early-cortical marker REELIN and late-cortical marker BRN2, which were both expressed within dorsally-patterned neural cells but were either absent (in the case of REELIN) or reduced (in the case of BRN2) in ventrally-patterned cultures. These results highlight the dorsal-ventral cellular identity and brain regionalisation instigated respectively by these neural induction protocols.

The pre- and post-synaptic markers SYNAPTOPHYSIN and PSD95 mirror the expression of the neuronal and axonal markers, and were detected in both dorsal and ventral cultures, again with a slightly biased elevation in ventrally-patterned neural cells.

The GABAergic neurotransmitter receptor subunits $GABA_AR1$ and $GABA_BR1$, in contrast, were much more highly expressed in neural cultures undergoing ventral differentiation than dorsal patterned cultures, although they did still retain detectable levels of each receptor subunit (Fig 3-15). The glutamate receptor subunit NMDAR1 showed much more comparable levels of expression between the two methods of neural induction, albeit again with a slight elevation within ventral-patterned neural cells.

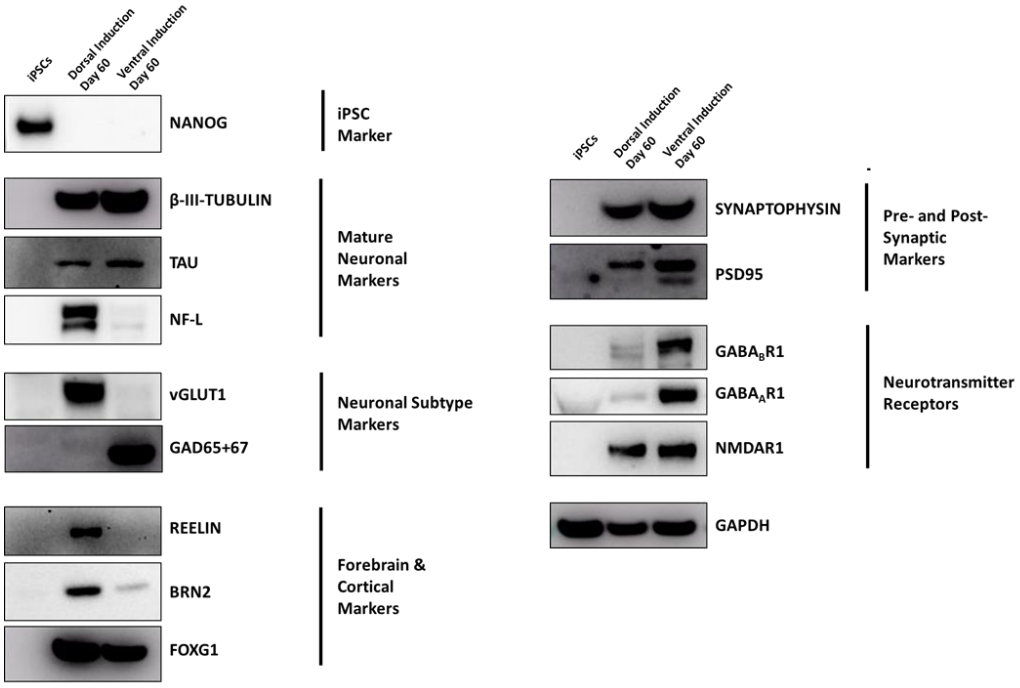

Fig 3-15: Western blot analysis for an array of neural markers present within undifferentiated hiPSCs, and dorsal- & ventral-patterned hiPSC-neural cultures after 60 days of differentiation.

To develop a greater resolution of gene regulation timings and strengths between dorsal- and ventral-patterned neural cultures; quantitative polymerase chain reaction (qPCR) analysis was used to investigate the level of gene expression in each patterned culture over the time-course of differentiation (Fig 3-16 to Fig 3-21).

The relative expression of the NPC marker *NESTIN* peaked by Day 20 in dorsal-patterned cultures, and Day 30 in ventral cultures, before reduction to lower expression levels over the remaining time course of differentiation. At all the time points assayed, the pattern of early *NESTIN* upregulation and then downregulation was followed in both dorsal and ventral cultures with no significant differences in expression level. There was a slight

trend for ventral cultures to display higher levels of expression at the later time points assayed but this difference never reached statistical significance (Fig 3-16). The dorsal-NPC marker *PAX6* followed a similar peak of expression in the early stages of neural differentiation (Day 20) before subsiding to a lower but stable level of expression. This pattern was restricted to dorsal-patterned cultures which show increased and statistically significant higher expression levels compared to *PAX6* expression within ventral-patterned cultures on Day 20, 30 and 40 of differentiation. The reverse is true of the ventral-NPC marker *NKX2.1*, which is barely detectable in dorsal-patterned cultures, but shows robust and substantially higher relative expression in ventral-patterned neural cells at all time points assayed (all of which reached statistical significance). For all three of these NPC markers; a peak of expression around Day 20 of differentiation suggests the maximal generation of neural precursors after approximately three weeks of differentiation with a gradual decrease over the following 40 days of differentiation and maturation.

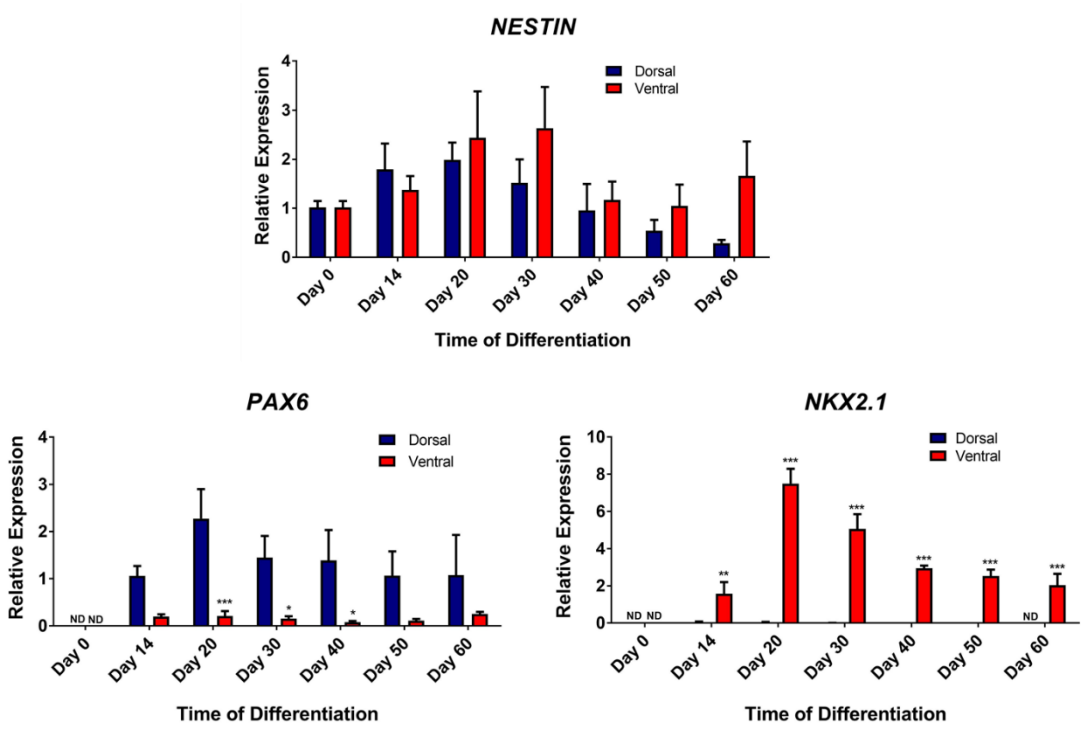

Fig 3-16: Quantitative PCR analysis for NPC markers expressed within dorsal- and ventral-patterned hiPSC-derived neural cultures over 60 days of differentiation. Data is shown as mean values ± standard error of the mean of four independent experiments. Statistical significance denoted by * p≤0.05, ** p≤0.01, *** p≤0.001 based on unpaired two-tailed t-tests.

Similar analyses were performed to observe changes in the canonical neuronal marker *β-III-TUBULIN* and axonal marker *TAU*, as well as the pre- and post-synaptic associated markers *SYNAPTOPHYSIN* and *PSD95* (Fig 3-17). *β-III-TUBULIN* expression showed a strong early expression by Day 20 in dorsal cultures, which lowered by approximately half for the remainder of the differentiation period. In contrast, ventral cultures displayed a more delayed peak of *β-III-TUBULIN* expression (Day 30) which dropped over the next 30 days of differentiation. However, expression levels in ventral cultures were significantly higher than those seen in dorsally-patterned cultures from Day 30 to 50 (~2.1-fold higher at Day 30). In addition, the axonal marker *TAU*, showed a pattern of continuous slight upregulation over the 60-day time-course of differentiation in both dorsal and ventral cultures, with a trend of higher levels of expression in ventral cultures at Day 50 and 60, however this difference did not reach statistical significance (Fig 3-17).

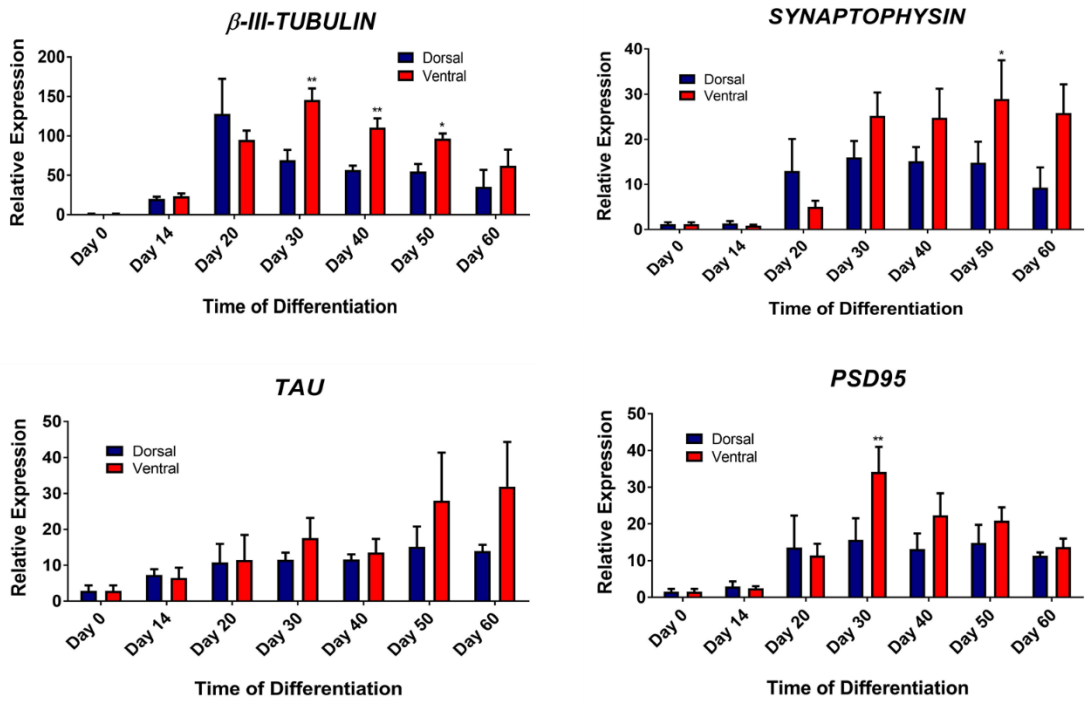

Fig 3-17: Quantitative PCR analysis for neuronal and synaptic markers expressed within dorsal- and ventral-patterned hiPSC-derived neural cultures over 60 days of differentiation. Data is shown as mean values ± standard error of the mean of four independent experiments. Statistical significance denoted by * p≤0.05, ** p≤0.01 based on unpaired two-tailed t-tests.

The pre-synaptic marker *SYNAPTOPHYSIN* showed a distinct point of upregulation after 20 days of dorsal-patterned differentiation. This level of expression was maintained within dorsally-patterned cultures for the remainder of the assayed differentiation timeline with a slight drop by Day 60. Relative to dorsal cultures, ventral cultures showed a delayed peak of expression (at Day 30 - mirroring the temporal peak of *β-III-TUBULIN* expression) and maintained a similar level of expression until Day 60. A trend for higher expression levels of *SYNAPTOPHYSIN* within these later time points in ventral cultures was seen, although statistically significant increased expression was only recorded at Day 50 between the two differentiation strategies. A similar timing peak of *PSD95* expression was also seen after 20 days of neural induction and maturation that was stable over the time course of dorsal differentiation but appeared to peak at Day 30 in ventral cultures (which represented a significant increase relative to the dorsal expression level), before lowering to dorsal-patterned equivalent expression levels (Fig 3-17).

To monitor excitatory and inhibitory neuronal maturation in either the dorsal or ventral neural patterning schemes, we also tracked gene expression levels of glutamatergic and GABAergic pre-synaptic neuronal markers (Fig 3-18). Dorsal-patterned differentiation of hiPSCs resulted in increased expression of the glutamatergic neuronal makers *vGLUT1* and *vGLUT2* after 20 days of differentiation that remained steadily expressed until Day 60. However, the GABAergic markers *GAD67* and GABA Transporter 1 (*GAT1*) displayed very low level basal expression without robust upregulation over the timeline of differentiation. In contrast to this, ventrally-patterned neural cultures showed steady upregulation of both *GAD67* (from Day 14) and *GAT1* (from Day 30) during differentiation, which by later timepoints showed statistically significant increases compared to the levels seen in dorsal cultures. In tandem with this, glutamatergic markers in ventral cultures were repressed under these patterning conditions, whereby *vGLUT1* expression was far below that seen in dorsal neural culture (Day 20-50) (Fig 3-18). This repression of glutamatergic neuronal identity was less pronounced when looking at *vGLUT2* expression, which although displayed a trend of lower expression in ventrally-patterned cultures than dorsal, these lower expression levels did not reach statistical significance. For both sets of these glutamatergic and GABAergic markers, it is apparent that there is much more robust upregulation of the non-default ventral lineage markers in the ventral-targeted differentiation than there is repression of the default glutamatergic pathway markers.

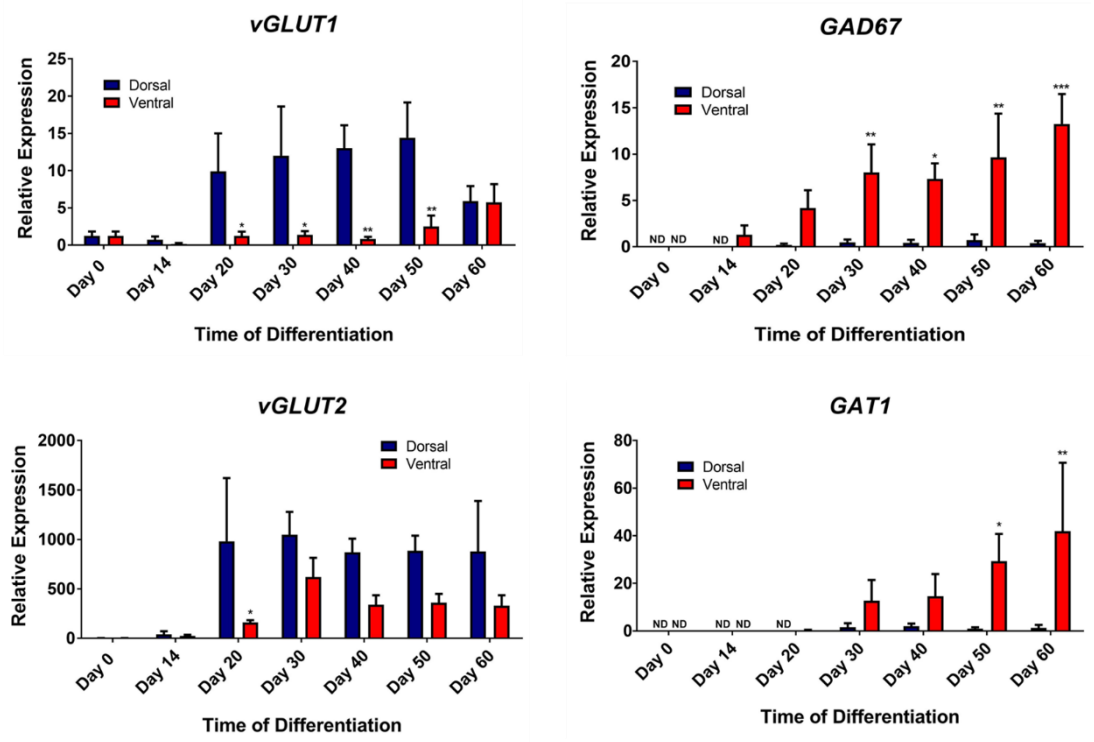

Fig 3-18: Quantitative PCR analysis for excitatory and inhibitory neuronal markers expressed within dorsal- and ventral-patterned hiPSC-derived neural cultures over 60 days of differentiation. Data is shown as mean values ± standard error of the mean of four independent experiments. Statistical significance denoted by * p≤0.05, ** p≤0.01, *** p≤0.001 based on unpaired two-tailed t-tests.

After understanding the extent of neuronal subtype divergence triggered by the patterning protocols during differentiation, we examined how markers of forebrain cortical localisation differed between the differentiation pathways. Observing the expression of the early- to late-cortical formation markers *REELIN*, *TBR1*, *CTIP2* and Special AT-rich sequence Binding protein 2 (*SATB2*) we were able to track the timing of markers relevant to deep-layer and upper-layer cortical neuronal generation *in vitro* (Fig 3-19).

Across all the cortical markers assayed, robust gene expression was seen only in dorsal-patterned cultures, with comparably lower levels seen in ventrally-induced cell populations. This is again not only suggestive of a neuronal subtype divergence triggered by each patterning methodology, but also one of brain region specification. However, it should be noted that the level of expression for the cortical localisation markers displayed high variation between biological repeats – resulting in a large spread of expression data. As each marker is suggestive of only a subset of excitatory neural types it is possible that a

stochastic generation of each subtype may strongly alter bulk mRNA expression from mixed cultures between biological repeats. Even so, strong upregulation of excitatory cortical markers was only recorded within dorsally-patterned cultures, albeit with high variance. A strong upregulation of the layer I marker *REELIN* by Day 20 and 30 post-differentiation dropped to a stable plateau for the remainder of the maturation timeline, and similar patterns are seen for both the cortical pre-plate and layer V/VI markers *TBR1* and *CTIP2* expression (Fig 3-19).

The upper-layer late-born cortical marker *SATB2* also showed slight upregulation over the course of differentiation, however the relative expression only reached just over a two-fold increase at its peak, suggestive of a baseline expression that still shows heavy bias in dorsally-patterned lineages, but which does not show a dramatic increase within the timeframe of this assay.

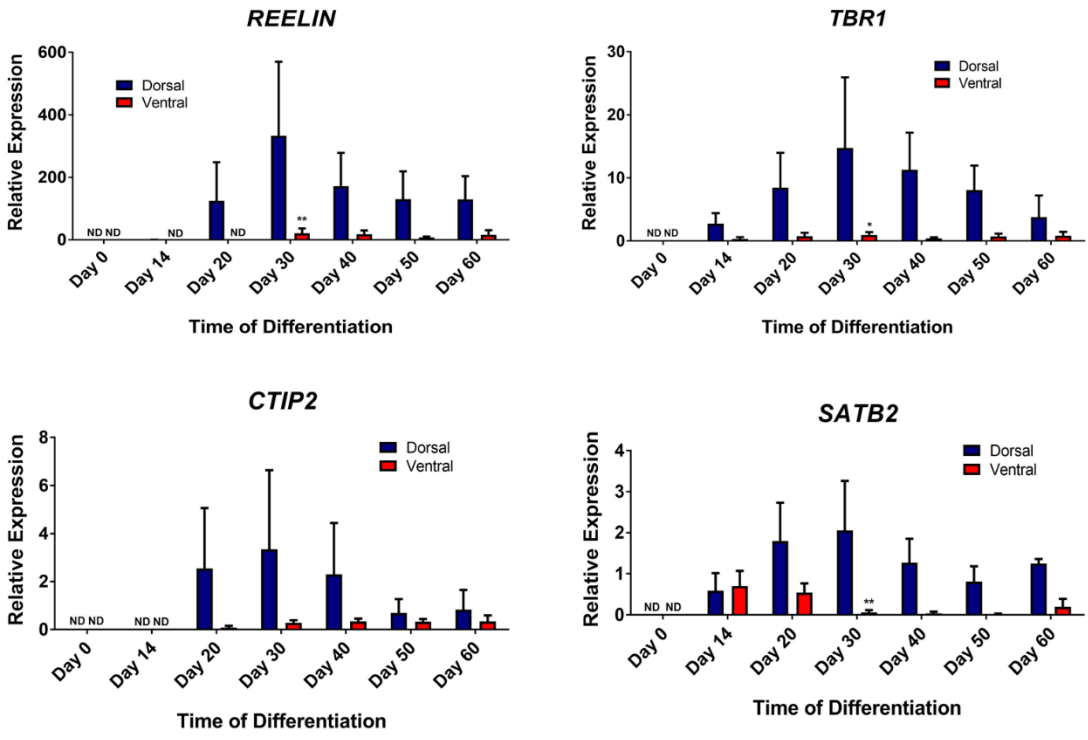

Fig 3-19: Quantitative PCR analysis for early and late cortical markers expressed within dorsal- and ventral-patterned hiPSC-derived neural cultures over 60 days of differentiation. Data is shown as mean values ± standard error of the mean of four independent experiments. Statistical significance denoted by * p≤0.05, ** p≤0.01, *** p≤0.001 based on unpaired two-tailed t-tests.

In order to further visualise the extent of the efficacy of neuronal subtype patterning we undertook robust regression analysis to compare each subtype-specific marker expression profile over the full time course of differentiation. Rather than simple point-to-point statistical comparisons this methodology seeks to compare the difference in the overall strength and pattern of expression between dorsal- and ventral-patterned neural cultures for each gene. The markers analysed were those related to dorsal neuronal identity *(vGLUT1* and *vGLUT2*), ventral neuronal identity *(GAD67* and *GAT1*), and cortical (dorsal) localisation (*REELIN, TBR1, CTIP2* and *SATB2)* (Table 3-2).

From this analysis it can be seen that a strong, statistically significant divergence is seen from both dorsal/excitatory neuronal markers when comparing dorsally-patterned and ventrally-patterned neural cultures across the 60 days of differentiation. Both *vGLUT1* and *vGLUT2* show strong significant differences in expression between the dorsal and ventral cultures when analysed using regression methodologies. This is equally mirrored with the expression pattern of the ventral neuronal markers *GAD67* and *GAT1*, which only maintain robust expression patterns within ventrally-patterned neural cultures (Table 3-2 and Fig 3-18)

Gene	Marker Type	P-value	Degree of Significance
vGLUT1	Dorsal/Excitatory neuronal cell	<0.001	***
vGLUT2	Dorsal/Excitatory neuronal cell	<0.001	***
GAD67	Ventral/Inhibitory neuronal cell	<0.001	***
GAT1	Ventral/Inhibitory neuronal cell	0.016	*
REELIN	Dorsal/Outer cortical ECM protein (Early)	<0.001	***
TBR1	Dorsal/Cortical plate (Early)	<0.001	***
CTIP2	Dorsal/Cortical Layer (Mid)	<0.001	***
SATB2	Dorsal/Cortical Layer (Late)	0.001	***

Table 3-2: Regression analysis table of dorsal and ventral neuronal identity gene markers for the time course of differentiation for dorsally versus ventrally patterned neural cultures. Statistical significance denoted by * p≤0.05, ** p≤0.01, *** p≤0.001.

The forebrain cortical localisation markers are also shown by this analysis to be statistically biased to expression predominantly within dorsally-patterned neural cultures for all of the early to late cortical marker genes (*REELIN*, *TBR1*, *CTIP2,* and the modestly expressed *SATB2*) (Table 3-2). Taken altogether this analysis confirms the divergence in

neuronal subtype differentiation that is occurring during the dorsal and ventral patterning techniques used in this chapter.

As another indicator of neuronal maturity and synaptic-associated development, we chose to observe the gene expression patterns of both the glutamatergic receptor subunits *NMDAR1* and *AMPAR1*, as well as the ionotropic and metabotropic GABA receptor subunits *GABA$_A$R1* and *GABA$_B$R1* (Fig 3-20).

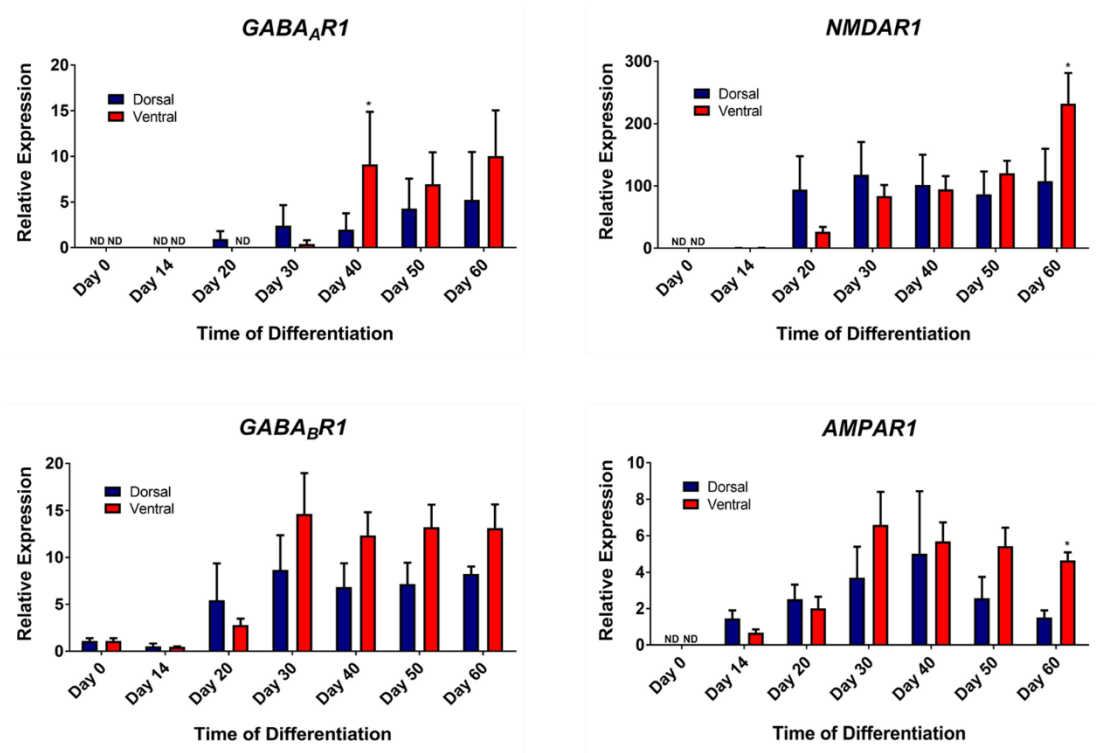

Fig 3-20: Quantitative PCR analysis for glutamatergic (*AMPAR1* and *NMDAR1*) and GABAergic (*GABA$_A$R1* and *GABA$_B$R1*) neurotransmitter receptor subunits expressed within dorsal- and ventral-patterned hiPSC-derived neural cultures over 60 days of differentiation. Data is shown as mean values ± standard error of the mean of four independent experiments. Statistical significance denoted by * p≤0.05 based on unpaired two-tailed t-tests.

The GABAergic receptor subunit *GABA$_A$R1* showed a delayed upregulation expression profile in ventral-patterned cultures (Day 40-60) relative to dorsal neural cell types, which showed a trend for lower gene expression at these later time points but an earlier onset of receptor expression. Only at Day 40 of differentiation did ventral neural cultures show a statistically significant increase of *GABA$_A$R1* expression compared to dorsal-

patterned cell types (~4.6-fold higher). A more robust, early, and stable pattern of gene upregulation was seen in both dorsal and ventral-cultures for *$GABA_BR1$* expression from Day 20 onwards. Again, there was a trend for higher relative expression in ventrally-patterned neural cells at each time point (Fig 3-20).

NMDAR1 subunit expression showed a steady expression profile in dorsal cultures from Day 20, but a gradually increasing pattern within ventral cultures, which reached a statistically significant difference at Day 60. A comparable expression profile over the timeline of differentiation was seen for *AMPAR1* gene expression in both dorsal and ventral differentiation pathways, albeit with a slight increase in ventral cell types at later time points. A peak in expression at Day 30-40 post induction was seen in both dorsal- and ventral-patterned cultures that gradually lowered over the course of maturation (Fig 3-20). However, the expression of *AMPAR1* in ventral cultures at Day 60 was significantly higher than that seen in dorsal-patterned cultures, mirroring the result of *NMDAR1*.

Finally, we wished to investigate the expression of genes related to glial cell identity over the time course of neural differentiation, and to observe whether there was a delay in the upregulation of glial-associated genes relative to neuronal markers. The astroglial marker gene *GFAP* and the oligodendroglial marker *GALC* were monitored over the same timeline of dorsal- and ventral-patterned neural differentiation (Fig 3-21).

Following the same pattern of delayed generation of astroglial cell types in CNS development *in utero* (Hansen, Rubenstein and Kriegstein, 2011), both dorsal- and ventral-patterned *in vitro* neural cultures only showed detectable levels of *GFAP* gene expression at later time points in differentiation: Day 40 in dorsally-induced cultures and Day 60 in ventrally-induced cultures. This does suggest that a more protracted timeline of differentiation and maturation would be necessary to generate an enriched population of mature astroglial cell types. Surprisingly however, *GALC* expression did show initial early upregulation and stable expression over the course of differentiation. Although *GALC* is not completely specific to oligodendroglial lineages it is highly enriched within them, and it is interesting that such robust gene expression is seen in these cultures that is not recapitulated by the protein expression from the same induction protocol (Figs 3-10, 3-21). It is possible that basal levels of *GALC* transcript are present in a subpopulation of cells within each directed neural culture, but that true oligodendroglial lineage formation and protein accumulation would take longer periods of maturation, as is seen for *GFAP*.

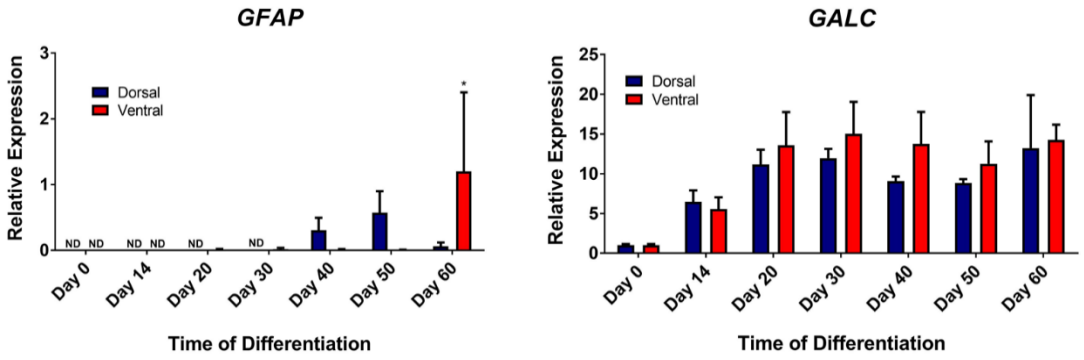

Fig 3-21: Quantitative PCR analysis for astroglial marker (*GFAP*) and oligodendroglial marker (*GALC*) expression within dorsal- and ventral-patterned hiPSC-derived neural cultures over 60 days of differentiation. Data is shown as mean values ± standard error of the mean of four independent experiments. Statistical significance denoted by * $p \leq 0.05$ based on unpaired two-tailed t-tests.

3.3.5 Electrophysiological Analyses

Tracking the differentiation and maturation of hiPSC-derived neural cultures through the molecular assays outlined above, generates a wealth of information about morphological development as well as gene and protein expression during targeted differentiation. However, electrophysiological functionality of hiPSC-derived neurons may be essential for certain aspects of *in vitro* developmental- and disease-modelling. To this end, dorsally- and ventrally-patterned neural cultures were assayed through patch clamp analysis to determine the functional maturity of cells within each neural culture generated.

Current-clamp recordings of neuronal cells from each differentiation patterning methodology after 95 days of differentiation are shown in Fig 3-22. The mean resting membrane potential of all cells assayed was -46.6mV and a capacitance of 7.1pF. In response to intracellular current injection both ventral- and dorsal-patterned neuronal cells fired action potentials (Fig 3-22 B-C). The evoked action potentials were over 100mV in both neural cell types with sharp narrow peaks. Ventrally-patterned neurons fired in between one and four action potentials at threshold stimulation, with higher numbers of action potentials initiated under lower current stimulation than supra-threshold values (Fig 3-22 B i-iii). Also, at supra-threshold stimulation levels a prolonged depolarisation was

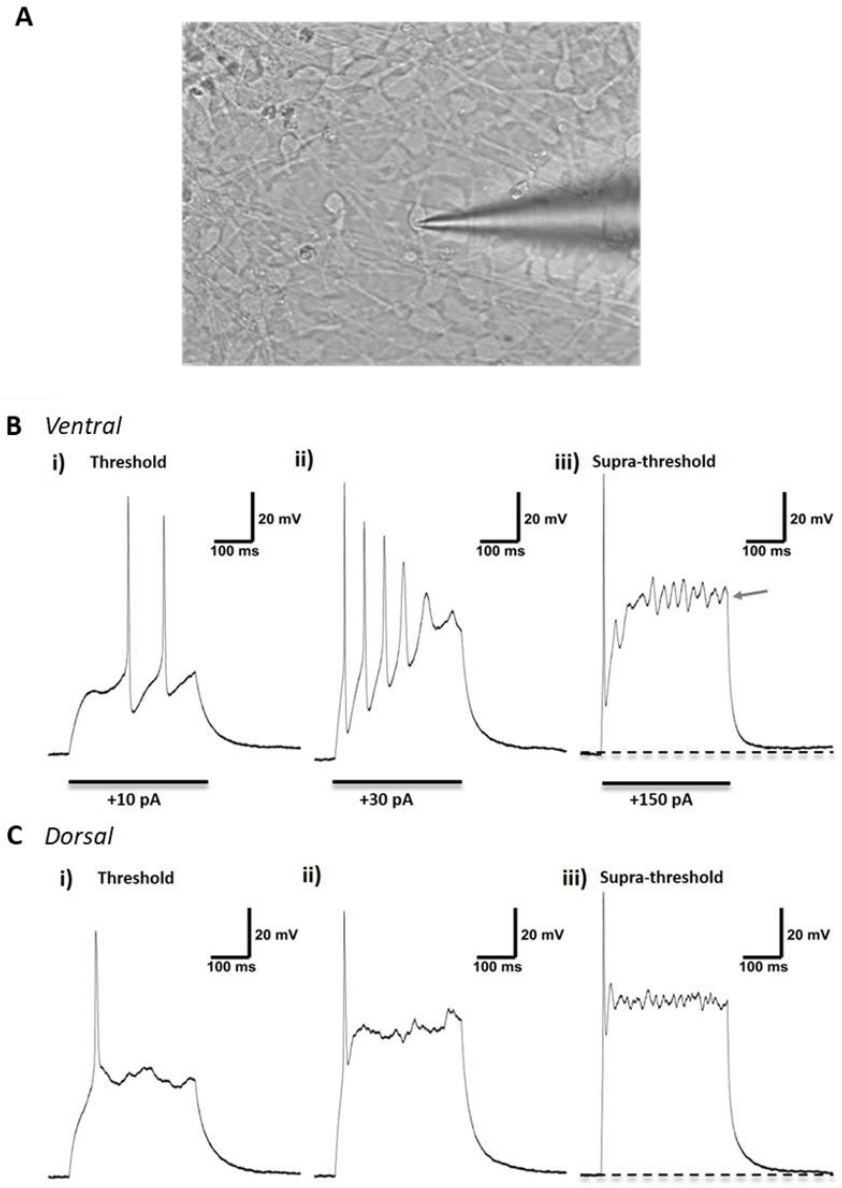

Fig 3-22: Current-clamp recordings of dorsally- and ventrally-patterned hiPSC-derived neuronal cultures. (**A**) Bright field image of a patched cell. (**B**) Ventrally-patterned neurons fired 1-4 large brief action potentials in response to current injection. Lower stimulus levels (i-ii) evoked higher numbers of action potentials than supra-threshold stimulation (iii) which elicited a sustained depolarisation before restoring holding membrane potential (grey arrow). (**C**) Dorsally-patterned neurons fired only one action potential regardless of stimulation level

recorded after the initiation of the action potential (Fig 3-22 B ii, grey arrow). Neurons from dorsally-patterned cultures however, were only capable of firing one action potential regardless of the current stimulus (Fig 3-22 C), and after firing the action potential also

displayed sustained depolarisation before returning to resting membrane potential. The action potentials seen within triggered dorsally-patterned neurons were also slightly broader than those seen from ventral neuronal cultures.

Voltage-clamp recordings of the dorsally- and ventrally-patterned neuronal cultures also showed differences in the maturation of functionality between the two differentiation pathways (Fig 3-23).

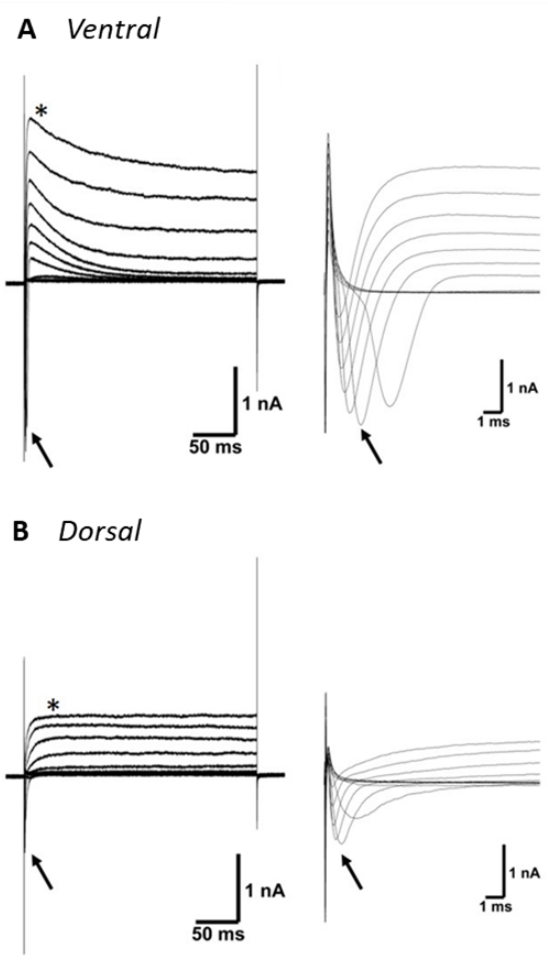

Fig 3-23: Voltage-clamp recordings of dorsally- and ventrally-patterned hiPSC-derived neuronal cultures. Both Ventral (**A**) and Dorsal (**B**) neurons displayed fast transient inwards currents following stimulation (black arrows) followed by sustained outward currents (asterisks). Both inward (sodium) and outward (potassium) currents were larger in ventrally-patterned neurons.

Neurons from both neural differentiation pathways displayed strong, transient inward sodium currents after the onset of the stimulus. This inward current flux was greater in neurons derived from ventrally-patterned cultures. Outward potassium currents were also measured following sodium depolarisation, with larger currents being seen within ventral-patterned neurons. From these data it appears as if the level of functional maturity is delayed in the iPSC-derived forebrain dorsal neuronal cultures compared to ventrally-patterned neurons.

3.4 Discussion and Conclusions

Many neural induction protocols from pluripotent stem cells have been generated for obtaining neural subtypes of dorsal-forebrain & cortical lineages (Gaspard *et al.*, 2008; Zeng *et al.*, 2010; Shi *et al.*, 2012; Espuny-Camacho *et al.*, 2013), and ventrally-derived inhibitory GABAergic interneurons (Maroof *et al.*, 2010; Danjo *et al.*, 2011; Goulburn *et al.*, 2012; Ma *et al.*, 2012; Arber and Li, 2013; Yan Liu *et al.*, 2013; DeRosa *et al.*, 2015) using signalling morphogens derived from studying *in vivo* neural tube development (Jessell, 2000). However, few studies have attempted parallel induction protocols to interrogate the timings and mechanisms of *in vitro* neurological models from distinct brain regions. Mature cortical tissue *in vivo* is derived from dorsal-anterior excitatory neural cell types combined with migrating inhibitory interneurons generated in ventral-anterior regions of the neural tube. Therefore, to fully model mature neural forebrain tissue *in vitro*, both neural cell types must be generated and combined at developmentally relevant time frames to allow for true recapitulation of neural tissue development.

We aimed to generate developmentally representative pools of excitatory cortical neural cells and inhibitory GABAergic interneurons (displaying markers of the medial ganglionic eminence transitory brain structure) from human iPSCs, and to investigate the strength of neural induction, the molecular timings of genes and proteins involved in differentiation, and the development of electrophysiological activity within the derived cultures *in vitro*.

We used commercially available hiPSC cell lines that were shown to maintain high levels of pluripotency marker expression throughout culture and expansion in a stable fashion. The dual-SMAD inhibition mechanism of neural induction triggered a rapid

reduction in pluripotency-associated cell markers, while vastly upregulating the gene and protein expression of the forebrain neural precursor marker PAX6 over the course of 7 days. Flow cytometric analysis of cells undergoing differentiation revealed induction efficiencies of >82% for PAX6-positive cells and >88% NESTIN-positive cells by Day 10. Further refinement of the differentiation protocol was investigated with the use of a neural proliferation media (NPM) and its effect on PAX6 and NESTIN expression. Stronger and more penetrant NESTIN staining was seen under NPM treatment than with dual-SMAD inhibition induction alone and was therefore adopted into the full long-term maturation protocol.

Prevalent neural morphology and post-mitotic neuronal protein expression was observed from Day 28 of the differentiation protocol. This was also studied after 60 days of neural maturation; whereby extensive neuronal and glial protein marker expression corresponded with widespread neuritogenesis. However, astroglial markers present at this time, were displayed in cells with an immature morphology. Interestingly, oligodendroglial lineage markers were not detected within neural cultures at this time point. This mirrors other findings on neurological development, by which glial differentiation and maturation is delayed relative to neuronal generation (Hansen, Rubenstein and Kriegstein, 2011; Mallamaci, 2013; Anderson and Vanderhaeghen, 2014), such marker expression therefore may be present after more protracted periods of differentiation and maturation. This "default" neural differentiation pathway also upregulated proteins associated with cortical (and therefore dorsal neural tube) neuronal cell identity. With noticeable expression of the outermost layer I marker REELIN, the deep-layer neural markers TBR1 and CTIP2, and to a lesser extent the upper-layer (II-IV) marker BRN2 in neural cultures differentiated for 60 days. This demonstrates that this level of differentiation and maturation of hiPSC-derived neural cultures display representative markers of early- and late-born markers of corticogenesis, and therefore recapitulation of neurodevelopmental processes *in vitro*.

Excitatory glutamatergic protein markers were present throughout the non-patterned differentiated neural cultures, whereas markers of GABAergic differentiation were not detected; again, suggestive of targeted dorsal-anterior cell populations. Other protein markers of neuronal maturity, pre- and post-synaptic machinery, and glutamate- and GABA-sensitive neurotransmitter receptor subunits showed high levels of protein expression after 60 days of neural differentiation but were not present during early NPC-enriched cultures nor undifferentiated hiPSCs. These results indicate a robust maturation

process occurring within iPSC-derived neural cultures after 60 days of differentiation that encompasses gene expression relevant to neurotransmitter release and response, which are the foundation stones of functional network formation.

We then attempted to "pattern" the differentiating NPC cultures to one of ventral-anterior lineages using the SHH signalling pathway agonist purmorphamine (Pur), in parallel to the default dorsal-excitatory pathway. A strong nuclear presence of the early-cortical marker TBR1 within cells in dorsal cultures, was in stark contrast to ventrally-patterned ones which showed no such positive immunostaining. The presence of TBR1 was not only localised to diffuse single cells throughout the dorsal culture, but also seen in the outer layer of neural ganglia-like structures that had formed during maturation. A similar pattern of staining was seen for the deep-layer cortical marker CTIP2 also within dorsal cultures, suggestive of a possible organoid-like self-organisation into simplified versions of early cortical structures (Kadoshima *et al.*, 2013; Lancaster *et al.*, 2013). However, CTIP2 immunostaining was also observed within subpopulations of ventrally-patterned neural cell cultures. It is possible that this effect may be due to inefficient silencing of pathways denoting default dorsal neural differentiation, and that upregulation of CTIP2 is more sensitive to this. Another possibility is the inherent presence of CTIP2 in populations of GABAergic interneurons, as has been reported *in vivo* (Nikouei, Muñoz-Manchado and Hjerling-Leffler, 2016), and therefore the use of CTIP2 alone as a cortical localisation marker should be used with caution.

Through Western blot analysis we report that the early and late cortical markers REELIN and BRN2 follow the same divergent pattern as is seen with TBR1 expression between dorsal- and ventral-patterned cultures; with the majority of protein expression of these cortical markers found within dorsal-patterned cultures. From gene expression data over the time-course of differentiation, early cortical markers peak to statistically significant elevations in dorsal-patterned neural cultures by Day 30 of differentiation, relative to ventrally-patterned cell populations. These upregulated genes continue to be expressed throughout the maturation timeline in dorsal cultures, indicating that molecular events driving early human corticogenesis can be detected as early as Day 20 of neural induction and differentiation *in vitro*. The lower relative expression levels of the upper-layer cortical marker *SATB2* over the full time-course however, does suggest that full maturation of all late-born cortical cell types has not by this time point reached completion, and that more protracted timelines of differentiation may be needed to obtain

neural cell populations representative of layers II-IV of the prenatal cortex. Interestingly, the gene expression level of *CTIP2* in ventral cultures, although lower than dorsal-patterning at all time points measured, does show a gradual increase by Day 60 in culture, which may explain the presence of the positive protein immunostaining at the end-point of differentiation seen in a subpopulation of ventrally-patterned neural cells.

For assays of neuronal subtype specificity, immunostaining and Western blot analysis of neural cultures after the full time-course of differentiation showed stark differences in expression of glutamatergic and GABAergic neuronal markers from dorsally- and ventrally-patterned cultures. vGLUT1 and vGLUT2 protein levels were far higher in dorsally-patterned cultures, whereas GAD65+67 expression showed exclusive upregulation within ventrally-patterned neural cell types. Gene expression data also displays this strong relationship to subtype marker expression and patterning methodology over the course of differentiation. However, it is worthy of note that the upregulation of non-default ventral GABAergic genes (*GAT1* and *GAD67*) show far more striking and elevated levels within differentiating ventral cultures, but still display basal levels of glutamatergic marker expression (*vGLUT1 and vGLUT2*). This is suggestive of a system by which the upregulation of non-default ventral-associated genes shows more distinct expression profiles than the complete repression of genes of the default dorsal neural-lineage pathway. Hence the lack of ventral-associated gene expression within dorsal-patterned cultures, but a “leaky” expression of dorsal-associated genes within ventral-cultures. Even so, when the pattern and strength of expression for each of these genes is assessed through robust regression analysis over 60 days of differentiation: strong statistical divergence is seen between dorsal- and ventral-patterned cultures for all of the markers assayed.

This segregation of neuronal subtype however did not disrupt comparable levels of β-III-TUBULIN and TAU neuronal protein markers between the differentiation pathways. This indicates that the timing of neuronal induction is maintained to equivalent levels between the two pathways by this timepoint in neural maturation, and that only the subtype of the neurons themselves show inherent differences. Interestingly, the intermediate filament protein NF-L did show robust upregulation within dorsal- rather than ventral-patterned neural cells, indicating a greater necessity of this gene within dorsal-patterned neural development. A slight upregulation of the canonical neuronal markers β-III-TUBULIN and TAU was seen within ventrally-patterned neuronal cultures at the transcript and protein level at most time points, which suggests a slightly more enriched

neuronal population of cells within these cultures. This pattern is also replicated when observing the expression levels of the synaptic markers SYNAPTOPHYSIN and PSD95, which again show slightly higher levels of protein expression in ventral-cultures, and a trend for upregulation at the gene transcript level at most measured time points during differentiation. These data could indicate a slightly higher proportion of mature neuronal populations within GABAergic ventral cultures, which may equate to higher degrees of glial differentiation within dorsal-patterned cell types or a higher retention of precursor cells with a slightly delayed timescale of differentiation compared to ventrally-patterned neural cells.

This postulated higher level of retention of NPCs in dorsal cultures however, is not supported by the relative gene expression profile of the NPC marker *NESTIN*. No statistically significant differences were recorded between dorsally- and ventrally-patterned neural cell cultures over the full time-course of differentiation, although there was a slight trend of higher NPC marker expression within ventral-patterned cultures. As with mature neuronal subtype markers, almost exclusive dorsal-NPC marker expression (*PAX6*) and ventral-NPC marker expression (*NKX2.1*) was recorded that agreed with each separate differentiation pathway. The statistically lower levels of *PAX6* seen within ventrally-patterned cultures may again be derived from the incomplete suppression of default differentiation, but may also be related to Pax6's role in neuroectodermal fate determination and may be due to residual expression in early-NPC cell populations (Zhang *et al.*, 2010; Goulburn *et al.*, 2011). All the NPC gene markers observed here however, show the same pattern of early high relative expression before a decrease during neural maturation. This would follow with the expected outcome of the neural differentiation pathway by which high initial levels of NPCs would be generated from lineage restricted hiPSCs which would decrease as post-mitotic neuronal differentiation takes place. Basal retention of NPCs are indicative of the protracted neurological development of human brain tissue, and are maintained throughout the differentiation culture, following intrinsic developmental cellular timings (Espuny-Camacho *et al.*, 2013).

The transcript expression of the glutamate receptor subunit *NMDAR1* showed comparable levels of expression throughout dorsal- and ventral-patterned differentiation pathways, but with increased expression in ventral cultures by Day 60 of differentiation. This increase is also reflected at the protein level. This pattern of gene upregulation in both differentiation pathways is also mimicked by the glutamate neurotransmitter receptor

subunit *AMPAR1*, which shows peak levels of expression in dorsal and ventral cultures at Day 40 and Day 30 of differentiation respectively. Surprisingly, the cellular localisation of AMPAR1 is not only within neuronal-marker-positive cell types, but also a subpopulation of surrounding cells. This points to the conclusion that upregulation of AMPAR1 may precede true post-mitotic neuronal differentiation and neuritogenesis, or that it may have other developmentally relevant uses during early neural tissue generation.

The presence of GABA-sensitive neurotransmitter subunits $GABA_AR1$ and $GABA_BR1$ did show protein level differences between dorsal- and ventral-cultures, with both of these receptor subunits showing stronger upregulation in ventrally-induced neural cells. These differences post-translationally are less pronounced when looking at gene expression levels during neural differentiation. Although relative expression levels of both subunits were consistently higher in ventrally-patterned cultures, they did not reach statistical significance over the majority of assay time-points. Intriguingly, the localisation pattern of $GABA_AR1$ and $GABA_BR1$ show stark differences in neural cultures generated from both induction pathways. $GABA_AR1$ expression was restricted to cells displaying neuronal markers and morphology, whereas $GABA_BR1$ showed strong expression within non-neuronal marker-positive cell types, to an even greater degree than was seen with AMPAR1. These results indicate that the ionotropic GABA receptor subunit $GABA_AR1$ shows a neuronal-specific expression pattern that may be indicative of maturing receptor complexes necessary for post-synaptic formation, whereas the metabotropic GABA receptor subunit $GABA_BR1$ may have a NPC-specific role in GABA sensing or in other non-neuronal cell types during neural induction and maturation.

Markers of gliogenesis, such as those found in astroglial lineages (GFAP and S100β) and oligodendroglial lineages (GALC) were assayed over the time course of neural induction and differentiation. Both astroglial markers were observed by Day 60 in dorsally-patterned neural cultures in a subpopulation of cells. These markers co-localised with each other and were separate from neuronal-marker-positive cell types. However, they displayed morphology indicative of immaturity, which does follow the delayed gliogenesis seen developmentally *in vivo* (Barateiro and Fernandes, 2014) and also from PSC-derived neural cultures *in vitro* (Gaspard *et al.*, 2008). This agrees well with the gene expression data of *GFAP* which only displays upregulation at late time points over the course of this differentiation. Oligodendroglial markers were not detected through protein analysis within Day 60 neural cultures, but gene expression data did reveal consistent expression

following NPC induction through both patterning pathways. This may be explained through the presence of *GALC* in non-oligodendroglial lineages (albeit in less enriched amounts) that were too low for detection through protein-based assays, or possibly indicate a strong post-transcriptional silencing effect before the triggered onset of gliogenesis.

Electrophysiological assays of the hiPSC-derived neural cultures also uncovered differences in functional maturation between the excitatory dorsal-patterned and inhibitory ventral-patterned neuronal subtypes. Both dorsal- and ventral-patterned neural cultures generated neuronal cells that were electrophysiologically active and could fire action potentials under current-clamp stimulation. However, dorsally-derived neurons only fired a single action potential after the onset of current stimulus whereas ventrally-derived neurons fired in between one and four action potentials depending on the level of current injection. This can be interpreted as a level of enhanced maturity of the ventrally-patterned neurons relative to dorsally-patterned neurons. This advanced level of maturation is also echoed in voltage-clamp recordings of each neuronal subtype. Larger sodium (inward) and potassium (outward) currents were seen in ventrally-derived neurons following stimulation than in the dorsally-derived counterparts. In both neuronal types however, extended periods of depolarisation after stimulus withdrawal and lower potassium currents may be indicative of a general immature neuronal phenotype relative to primary neurons. As normal human brain development takes place throughout the protracted timeline of gestation, it is plausible that true neuronal maturity and functionality of iPSC-derived neural cultures would also need to take place over the course of many months *in vitro* if the recapitulation of neurodevelopmental processes followed intrinsic timing mechanisms.

These preliminary findings show ventrally-patterned neural cultures display hallmarks of advanced maturity compared to excitatory dorsally-patterned neurons at the same time point. Although more research will be needed to verify this, it does reveal some intriguing questions about the independent developmental timings of ventrally-derived and dorsally-derived anterior neural cell types and how it would be best to combine them in *in vitro* models to develop representative models of mature forebrain. Indeed, the higher expression and protein profiles of neuronally-associated markers seen in ventrally-patterned cultures may reflect an enhanced maturing population of post-mitotic neuronal cultures, that require extended timelines to be generated from dorsal-patterned cell pools.

In conclusion, we have demonstrated that efficient neural differentiation can be elicited from hiPSCs *in vitro* and targeted to generate specific neuronal subtypes derived

from dorsal-anterior and ventral-anterior regions of the neural tube. The maturity of these patterned neuronal pools is displayed through comparable molecular markers of neuronal cell identity, synaptic machinery, and appropriate dorsal/ventral identity markers. Ventrally-patterned cells however show increased tendency for higher expression profiles of many neural-associated markers and more mature electrophysiological properties, suggestive of an accelerated maturation timeline of neural cells patterned in this way. All of these data will inform future *in vitro* models of human forebrain cortical development.

3.4.1 Summary of Chapter Findings

- hiPSCs undergoing neural induction via dual-SMAD inhibition pathways generate NPCs with high efficiency over 7-14 days.
- Further maturation of NPCs without exogenous signalling morphogens will derive neuronal cells with extensive neuritogenesis after 28 days of differentiation and both neuronal and glial-lineage cell types by Day 60 of maturation.
- Neural cell cultures differentiated for 60 days will show markers of; cortical and forebrain localisation; excitatory glutamatergic neuronal subtype; pre- & post-synaptic components; and glutamate- & GABA-sensitive neurotransmitter subunits.
- Ventral patterning of NPCs, through the use of a SHH-pathway agonist, generates mature neurons of a predominantly inhibitory GABAergic cell type after 60 days of differentiation and show heavily reduced cortical marker expression.
- Robust regression analysis of neuronal subtype marker expression confirms the efficacy of the patterning techniques and divergence of neural subtype differentiation.
- Both neural induction pathways show upregulation of canonical neuronal markers over the same timeline of differentiation.
- Ventral-patterned neural cells show slight enrichment of neuronal associated markers at the gene and protein level in comparison to the default (dorsal) induction pathway.
- Glutamate-receptor subunits show comparable expression within neural cells from both pathways of differentiation, but GABA-receptor subunits show elevated expression in ventral-patterned cultures.
- Astroglial lineage markers show highly delayed patterns of upregulation. Whereas oligodendroglial protein markers were not detected in hiPSC-derived neural cultures after 60 days.

- Both dorsally- and ventrally-patterned matured neuronal cells can fire an action potential under intracellular current stimulation. Multiple action potentials can be evoked from ventrally-patterned neuronal cells depending on the current stimulus level, demonstrative of a more mature phenotype than is seen in dorsally-patterned neurons.
- Transient sodium and potassium currents are both present after stimulation of dorsally- and ventrally-derived neurons. Both current levels are higher in ventrally-patterned cultures, indicative of a more mature ion channel composition phenotype. However, potassium currents in neurons from both patterning methodologies are low, showing an overall immature phenotype for all neurons assayed.

3.4.2 Acknowledgements

We would like to thank Dr. Karina Needham (Dept of Otolaryngology, University of Melbourne) for her indispensable help with the patch-clamp recordings of neuronal cultures, as well as assistance with data analysis and figure generation. We are also indebted to Prof. Raymond Boston (Dept of Medicine, University of Melbourne) for his aid in generating the robust regression analysis pipeline for the gene expression data displayed in this chapter.

3.5 Appendix

3.5.1 Matrigel Surface-Coatings for NPC Induction

Initial substrate testing for NPC induction and neural maturation also utilised Matrigel coating, which was reported to show high rates of neuronal marker induction in PSC-derived neural cultures (Muratore *et al.*, 2014). However, preliminary data from the hiPSCs used in this study showed high retention of NPC markers when cultivated on Matrigel substrates but with low levels of neuronal maturation and marker expression (Appendix Fig 3-24). Therefore, we chose to complete all neural induction protocols using poly-L-lysine and laminin coated surfaces that were conducive to neural maturation. Low levels of neuronal morphology and marker development after 6 weeks of differentiation discounted Matrigel coatings for assays into neural development and maturation of hiPSC-derived cultures.

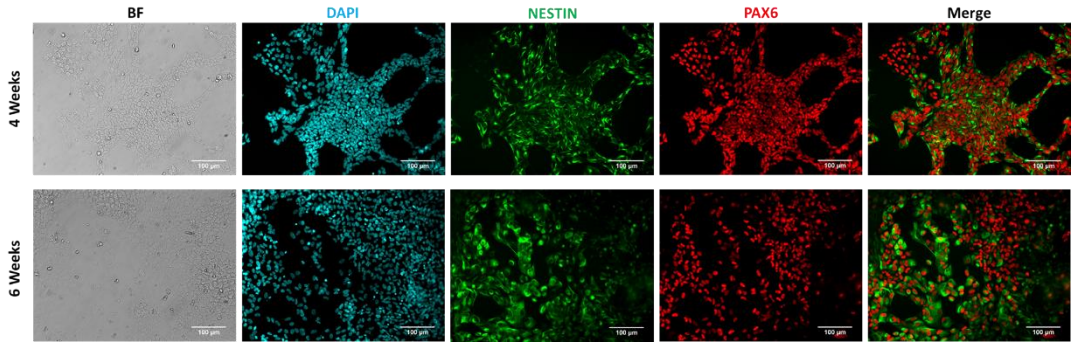

Appendix Fig 3-24: hiPSCs undergoing neural differentiation on Matrigel coated surfaces displayed limited neuronal maturation but high rates of NPC marker retention even after 4-6 weeks of differentiation. Scale bars represent 100µm.

Chapter 4: Neural Differentiation of hiPSCs in Three-Dimensional Biomaterial Scaffolds

4.1 Introduction

The generation of mature neural cultures from human iPSCs (as described in Chapter 1 and Chapter 3) follows that of embryological developmental timing and molecular signalling (Gaspard *et al.*, 2008), and can result in functional network formation (Odawara *et al.*, 2016). For the most part, these neural differentiation protocols are achieved in two-dimensional (2D) adherent cell culture environments. Even so, crude elements of self-organised developmental structures can be seen within these 2D cultures that recapitulate *in vivo*-like tissue. For example, early neural precursor structures termed "neural rosettes" are self-formed multicellular patterns that were shown to be representative of a transverse plane of neural tube cytoarchitecture (Watanabe *et al.*, 2005; Eiraku *et al.*, 2008). Further development of more mature "brain-like" structures from hiPSCs has not been recorded from planar culture but has been reported extensively since the advent of three-dimensional (3D) organoid culture. By culturing neural precursors as free-floating aggregates throughout differentiation and maturation, they generate histologically accurate representations of early brain structures beyond those seen in rosette formation (Kadoshima *et al.*, 2013; Lancaster *et al.*, 2013). The development of these 3D cerebral or brain organoid cultures has been an incredible step forward in the field of *in vitro*-based neuroscience as it illuminates not only the intrinsic timing of neural development that is preserved in hiPSC differentiation, but also an inherent ability to self-organise into region-specific complex structures (Meinhardt *et al.*, 2014; Mariani *et al.*, 2015; Muguruma *et al.*, 2015; Jo *et al.*, 2016; Qian *et al.*, 2016).

Although the potential of organoid tissue models for neurological research is remarkable, there are limitations within this methodology that may impede specific aspects of the research being undertaken. Firstly, continuous generation of single brain-like

structures within the organoids (rather than multiple pseudo-structures within the same aggregate) are dependent on high degrees of oxygen and nutrient diffusion, and therefore require the use of spinning bioreactors to enable the generation of more representative cytoarchitecture (Lancaster *et al.*, 2013; Qian *et al.*, 2016). However, this can still not overcome the presence of necrotic cores within each organoid due to lack of vasculature formation (Lancaster *et al.*, 2013; Kelava and Lancaster, 2016). Furthermore, the heterogeneity in the structure and cellular content of each organoid with high batch-to-batch variability may have repercussions in the reproducibility of experiments with more subtle phenotypic outcomes (Brennand *et al.*, 2015; Kelava and Lancaster, 2016).

Rather than free-floating organoid culture, 3D neural cultures from hiPSCs can also be generated through encapsulation of differentiating neural cells within hydrogel scaffolds that aim to mimic properties of the extracellular matrix microenvironment. The advantages of 3D neural culture over 2D planar culture are apparent, even without the use of free-floating organoid formation. The enhanced degree of cell-cell interactions allowing for *in vivo*-like cytoarchitecture and networking potential, whilst cell-matrix interactions would allow for spontaneous cell migration throughout the scaffold, together with self-organisation reminiscent of neural organoids. It is also telling that the most successful organoid culture protocols still embed cellular aggregates within droplets of hydrogel scaffolds to enhance organoid formation (Lancaster *et al.*, 2013), showing the great effect that 3D neural cell encapsulation can generate. Although the same problems of nutrient and oxygen diffusion exist in the generation of 3D encapsulated neural constructs, albeit to a lesser degree compared to those found in organoid culture, these issues can be overcome through control of cell density and scaffold geometry creation; variables that cannot be controlled during organoid formation. An overview of some of the advantages and disadvantages of 2D and 3D neural cell culture is shown in Fig 4-1.

Neural differentiation from pluripotent stem cells within 3D hydrogel environments have shown promise throughout previous studies (Li *et al.*, 2011; Lu *et al.*, 2012; Kim, Sachdev and Sidhu, 2013; Bozza *et al.*, 2014) and in some instances have been shown to enhance the efficiency and speed of neural maturation (Lu *et al.*, 2012; Z.-N. Zhang *et al.*, 2016). However, little has been shown of this effect on the biomolecular process of differentiation and maturation itself, and its effect on patterned neural subtypes that undergo differential brain-region specific pathways of differentiation and development (as outlined in Chapter 3). We have already shown the basis of generating both dorsal- and

ventral-patterned neural subtypes from hiPSCs in planar culture with time-course analyses of markers denoting post-mitotic neuronal generation, synaptic maturation, forebrain localisation, neurotransmitter receptor generation, and gliogenesis. The downstream neural maturation events of this hiPSC-derived NPC differentiation within 3D hydrogel scaffolds however, remains largely unknown.

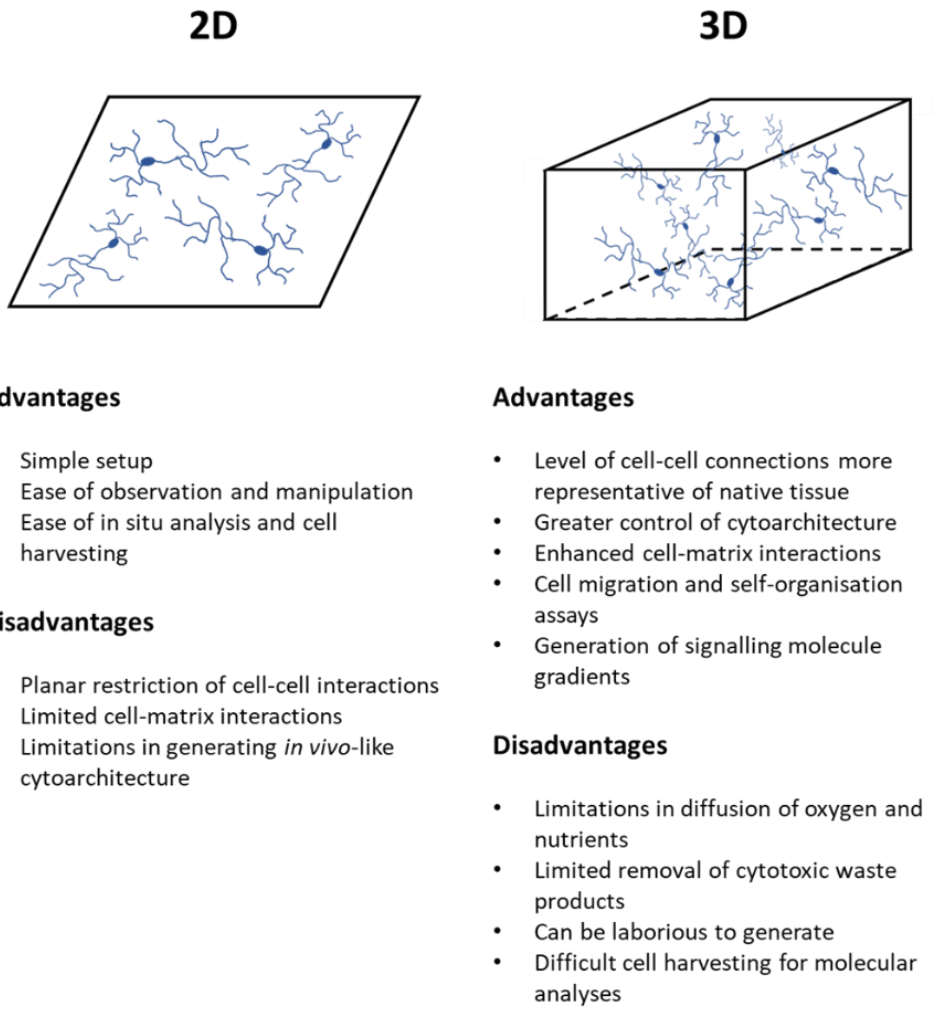

Fig 4-1: Overview of advantages and disadvantages of neural cell culture in 2D and 3D environments.

This chapter will therefore focus on the timing of the molecular processes of neural differentiation and maturation from hiPSCs *in vitro* and directly compare these markers from neural cultures grown in 2D planar culture to those grown within a neuritogenic-conducive 3D collagen hydrogel scaffold environment (as developed and assayed in Chapter 2). The results of these assays will uncover any deviation in the efficiency of derivation of dorsal- and ventral-patterned neural cultures in 3D compared to 2D environments, as well as any effect of the 3D microenvironment on neural cell maturation or neural tube patterning factors. This data will help inform future neural culture protocols and elucidate the specific advantages (or otherwise) of neural differentiation from hiPSCs within 3D hydrogel environments.

4.2 Materials and Methods

4.2.1 iPSC Culture

All work in this chapter utilised the commercial human iPSC lines; *ATCC-BXS0116 Human Induced Pluripotent Stem (IPS) Cells (ATCC® ACS-1030™)* and *ATCC-DYS0100 Human Induced Pluripotent Stem (IPS) Cells (ATCC® ACS-1019™)*. iPSCs were grown in feeder-free culture conditions on Vitronectin XF (Stem Cell Technologies) coated 6-well tissue culture plates in TeSR-E8 media (Stem Cell Technologies). iPSC colonies were passaged every 6-7 days with Gentle Cell Dissociation Reagent (Stem Cell Technologies) and were re-plated with TeSR-E8 media containing the RHO/ROCK pathway inhibitor Y-27632 (10µM, Stem Cell Technologies). Media was changed daily, except for the first day after a passage. Areas of random differentiation within colonies were removed manually. All iPSC and neural differentiation experiments used iPSCs below passage number 20.

4.2.2 Neural Differentiation

Dorsal neural induction of iPSCs was triggered using a monolayer dual SMAD-inhibition protocol using commercially available STEMdiff Neural Induction Media (NIM) (Stem Cell Technologies). Briefly, iPSCs were dissociated into single cells using Gentle Cell Dissociation Reagent (GCDR) (Stem Cell Technologies) and plated at densities of 1 x 10^6 cells/well of a 6-well tissue culture plate, coated with poly-L-lysine (0.01%, Sigma) & laminin (20µg/ml, Sigma) (PLL), in 2ml NIM per well. Media was changed daily for the first 7 days of induction, which also contained RHO/ROCK pathway inhibitor Y-27632 (10µM, Stem Cell Technologies).

After 7 days of induction, media was changed to STEMdiff Neural Proliferation Media (NPM) (Stem Cell Technologies) for another 7 days to trigger NPC maturation. NPCs were passaged at Day 10 and seeded into Collagen Type I-based hydrogel scaffolds for further differentiation and maturation within a 3D environment (see Section 4.2.3). At Day 14 post-induction, media was changed to a final neural maturation media (NMM) which consisted of a 1:1 mix of “N2 media” and “B27 Media”. N2 media consisting of DMEM/F12 (Lonza), N2 Supplement (1x, Thermo Fisher Scientific), GlutaMAX (1x, Gibco), Non-essential amino acid mixture (1x, Lonza), 100U/ml Penicillin and 100µg/ml Streptomycin (Gibco). B27

media consisting of Neurobasal (Gibco), B27 Supplement (1x, Thermo Fisher Scientific), and GlutaMAX (1x, Thermo Fisher Scientific). The combined maturation media was then supplemented with BDNF (20ng/ml, PeproTech), GDNF (20ng/ml, PeproTech), and DAPT (2µM, Stem Cell Technologies) to enhance neuronal differentiation and cell cycle synchronisation of differentiating NPCs (Crawford and Roelink, 2007; Borghese *et al.*, 2010). Maturation media was changed every 2-3 days over the course of differentiation. Ventral neural induction of hiPSCs followed the same protocol and media formulations as above but with the addition of Purmorphamine (1.5µM, Stem Cell Technologies) from Day 2 to 14 post-induction. An overview of induction protocols can be seen in Fig 4-2.

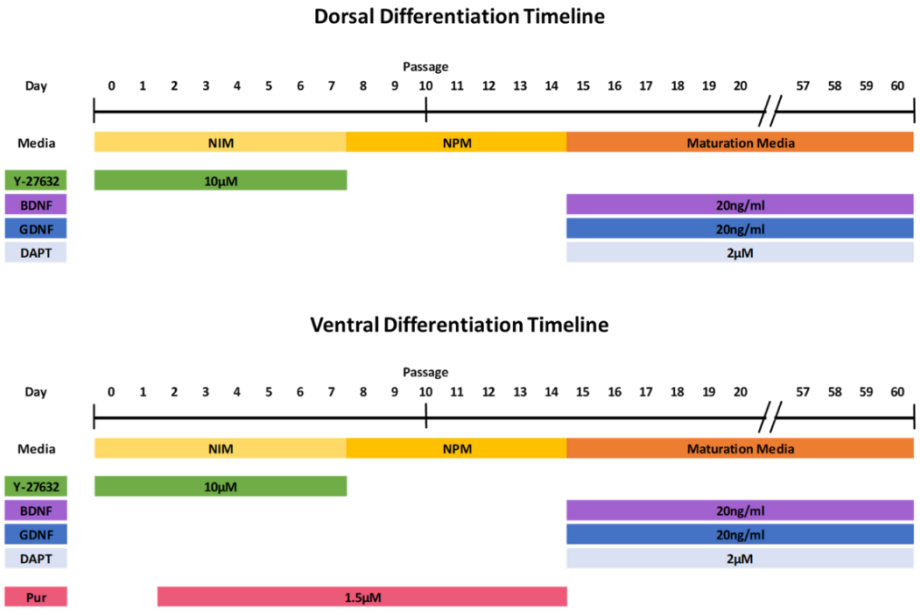

Fig 4-2: Schematic representation of the protocols for parallel differentiation of dorsal (excitatory) forebrain lineages and ventral (inhibitory) forebrain lineages from hiPSCs. Both differentiation pathways include stepwise treatment with neural induction media (NIM), neural proliferation media (NPM) and maturation media. The maturation media also contained the neurotrophic factors; brain-derived neurotrophic factor (BDNF), glial cell-derived neurotrophic factor (GDNF), and the Notch signalling inhibitor N-[N-(3,5-difluorophen- acetyl)-l-alanyl]-S-phenylglycine t-butyl ester (DAPT). In addition, the ventral differentiation pathway contained purmorphamine (Pur) a small molecule agonist of the sonic hedgehog signalling pathway.

4.2.3 Three-Dimensional Hydrogel Encapsulation of NPCs

At Day 10 post-induction, NPCs were harvested from 2D culture plates prior to 3D hydrogel encapsulation. NPCs were dissociated from the culture well surface with Accutase (Stem Cell Technologies) for 5 minutes at 37^{o}C. Cells were pelleted by centrifugation at 500x*g* for 5 minutes before resuspension in 1ml of media. Cell counts were performed using trypan blue (Thermo Fisher Scientific) staining and quantified using a haemocytometer. Final cell density for each cell-laden hydrogel was 1x10^{5} cells/ml.

Collagen hydrogel scaffolds were formed with final concentrations of 0.4mg/ml Collagen Type I from Rat Tail (Corning), 0.23x of the added collagen volume of 0.1M NaOH (Sigma), and 1x HEPES Buffer (20mM HEPES [Sigma], 150mM NaCl [Sigma] pH 7.4), and 0.05mg/ml ECL Cell Attachment Matrix (Millipore). The working volume of the collagen hydrogels was made up in sterile de-ionised water. Collagen and NaOH working volumes were mixed (to trigger neutralisation) prior to addition to buffered cell suspensions. 250µl of the hydrogel solution was added per well of a 48-well tissue culture plate to form each scaffold for molecular analyses. 500µl of cell-laden hydrogel solution was added to a 60mm x 15mm IVF One Well Dish (Falcon, Corning) for downstream fluorescent immunocytochemical and confocal microscopy analyses. Scaffolds underwent gelation at 37^{o}C for 30 minutes before addition of 0.5ml differentiation media per well, or 1ml media per dish. Approximately 70% of media volume was changed every two days over the time course of differentiation.

4.2.4 Fluorescent Immunocytochemistry and Epifluorescent/Confocal Microscopy

Three-dimensional scaffolds for immunocytochemistry were fixed for 1 hour at room temperature in 10% neutral-buffered formalin solution (Sigma) and permeabilised for 1 hour at room temperature in 0.5% Triton-X-100 in phosphate buffered saline (PBS) (137mM NaCl, 10mM Phosphate, 2.7mM KCl, pH 7.4). Samples were blocked overnight at 4^{o}C in 5% goat or donkey serum (Millipore) in PBS before incubation with primary antibodies (also in block solution) overnight at room temperature; anti-TUJ1 (Covance MMS-435P, 1:1000); anti-MAP2 (Cell Signaling Technology 4542, 1:1000); anti-GAP43 (Millipore AB5220, 1:1000); anti-Synapsin I (Abcam ab64581, 1:1000); and anti-TBR1 (Abcam ab31940,

1:1000). Constructs were washed three times for 1 hour each in PBS before addition of secondary antibodies; goat-anti-mouse IgG AF488 (Invitrogen A11029, 1:2000); donkey-anti-rabbit IgG AF594 (Invitrogen A21207, 1:2000) in block solution overnight at room temperature. Constructs were washed three more times in PBS before addition of DAPI (Sigma) for 1 hour, for cell nuclei visualisation.

Epifluorescent images were acquired on an Olympus IX70 wide field microscope with Spot RT Slider digital camera and Spot Advanced software, version 4.8 (Diagnostic Instruments). Confocal image acquisition was performed using a Nikon Ti Eclipse microscope equipped with a fully automated A1 confocal laser (A1R, Nikon) and processed with NIS-Elements software (Nikon). Prior to acquisition, 3D constructs were transferred to 35mm Nunc Glass Bottom Dishes (Thermo Fisher Scientific).

4.2.5 Gene Expression Analysis

For cell extraction from collagen scaffolds, media was exchanged for 0.5ml maturation media containing 0.05mg/ml Collagenase Type 1 (>125U/mg, Worthington Biochemical Corporation) per well. Scaffold digestion took place at 37^{o}C for 45 minutes prior to trituration and centrifugation of cell pellets. Cells from five scaffolds were pooled to form one pellet from each experimental setup. Cell pellets were stored at -80^{o}C until RNA purification.

Relative gene expression analysis was performed using quantitative polymerase chain reaction (qPCR) methodology. Firstly, RNA was purified from frozen cell pellet samples using the RNeasy Plus Mini Kit (Qiagen) as per the manufacturer's instructions into a total elution volume of 50µl nuclease free water. RNA concentration was determined using an Ultraspec 2200 Pro Spectrophotometer (GE Healthcare Life Sciences) and RNA integrity was confirmed by running samples on a 1% Agarose (w/v)-EtBR Tris-acetate (TAE) buffered gel under electrophoretic conditions for 40 minutes at 80V followed by imaging on a ChemiDoc MP (Bio-Rad) to show sharp ribosomal RNA banding.

cDNA was generated from 1µg of each RNA using the Omniscript Reverse Transcription Kit (Qiagen) with 1µM oligo dTs (Thermo Fisher Scientific) and 1U/ml RNase Inhibitor (Qiagen). Reverse transcription reactions took place at 37^{o}C for 80 minutes in a 20µl reaction volume. On completion of the reaction, samples were further diluted with

20µl of nuclease free water. cDNA samples were stored at -20°C until used in qPCR reactions.

qPCR reactions were performed with SYBR Green PCR Master Mix (Qiagen) in 10µl reaction volumes with 1µM of each primer set. *De novo* primer pairs were designed using Primer-BLAST (NCBI) (Table 4-1). All amplicons were designed to be between 50-250bp in length and have equivalent primer annealing temperatures.

Gene Target	Fwd Primer (5'-3')	Rev. Primer (5'-3')
HPRT1	AAGCCAGACTTTGTTGGATTTG	GGCGATGTCAATAGGACTCCA
OCT4	CAAAACCCGGAGGAGTCCC	AAAGCGGCAGATGGTCGTTT
PAX6	ACATCCGAGATTTCAGAGCCC	CAAAGACACCACCGAGCTGA
NKX2.1	CCAGGACACCATGAGGAACAG	GCTCATGTTCATGCCGCTC
NESTIN	CGCACCTCAAGATGTCCCTC	CAGCTTGGGGTCCTGAAAGC
β-III-TUBULIN	AACCAGATCGGGGCCAAGTT	GGCACGTACTTGTGAGAAGAGG
TAU	ACTATCAGGTGAACTTTGAACCA	GTTCCTCAGATCCGTCCTCA
SYNAPTOPHSYIN	GGACATGGACGTGGTGAATC	AAGATGGCGAAGACCCATTG
PSD95	ACCCTAGAAGCCCCAGGATA	CCAGACCTGAGTTACCCCTT
REELIN	ACCAGCCAAAGGACTTCACA	TTGCGAGTGCTTACTAGGACGA
TBR1	GACTCAGTTCATCGCCGTCA	CAGCCGGTGTAGATCGTGTC
CTIP2	CCCAGAGGGAGCTCATCACC	AAAACCAGGATGTCCCCCAAG
SATB2	AGGCCGTGGGAGGTTTGAT	GTTCCACCTTCCCAGCTTGA
VGLUT1	CAGCCAACAGAGTTTTCGGC	CGACTCCGTTCTAAGGGTGG
VGLUT2	TCAGATTCCGGGAGGCTACA	TGGGTAGGTCACACCCTCAA
GAD67	GCTGTCGCAGAGCCGAG	CAGGTATCGTACGTTGTGGG
GAT1	CCGAGACAGCGGAGAGGTTG	TTGGAGTTGCCTCACCCTGAT
NMDAR1	GAGCGTGAGTCCAAGGCAGA	GCGGTATACAGTGGCAGCAT
AMPAR1	TTCCAAGGACAAGACAAGCG	GGAGGGTCGATGTCCGTATG
$GABA_AR1$	CCTCCTTCTGAGCACACTGAC	TTCGGTTACACGCTCTCCCAA
$GABA_BR1$	CGCCTGGAGGACTTCAACTA	TTGTAGCTGCCACCCTGAAG
GALC	ACCAGAGACCCATTACGTGG	CATCCAGCTAAATCACCTGTAACC
GFAP	CCATTCCCGTGCAGACCTTC	TAATGACCTCTCCATCCCGCATC

Table 4-1: Primer pair sequences used for qPCR analysis of human iPSC-derived neural cultures in 3D matrices.

Reactions were run on a RealPlex Mastercycler (Eppendorf) with the following parameters: 95°C for 2 minutes, then 40 cycles of 95°C for 5s and 60°C for 10s, followed by a melt curve recording. Amplicon specificity was determined via melt curve peak analysis.

All relative expression data was normalised to *HPRT1* housekeeping gene expression. Data were analysed by the ΔΔCt method in Microsoft Excel and statistical analyses performed in GraphPad Prism using multiple unpaired T-test analysis. Data is shown ± standard error of the mean with significance denoted when the p-value ≤0.05. Four biological repeats were completed for each differentiation type (dorsal/ventral) for each time point from both 2D and 3D culture. Robust regression analysis of fold change expression data was performed in Stata statistical software (version 15.1). Regression coefficients were maintained between ordinary least squares (OLS) regression and those of the robust regression analysis. Raw output tables are displayed in Section 4.5.1.

4.3 Results

4.3.1 hiPSC-derived NPCs Differentiate and Undergo Neuritogenesis within Three-Dimensional Collagen Scaffolds

We demonstrated in Chapter 2 that collagen (type I) hydrogel scaffolds allowed for extensive neuritogenesis of encapsulated neural-like cells, as well as primary rat cortical neurons (Appendix 2.5.2), in contrast to neural cells within alginate hydrogel scaffolds. Therefore, we wished to observe whether these desired morphological changes in the 3D collagen environment would also allow for neurite extensions during differentiation and maturation of hiPSC-derived neural cultures.

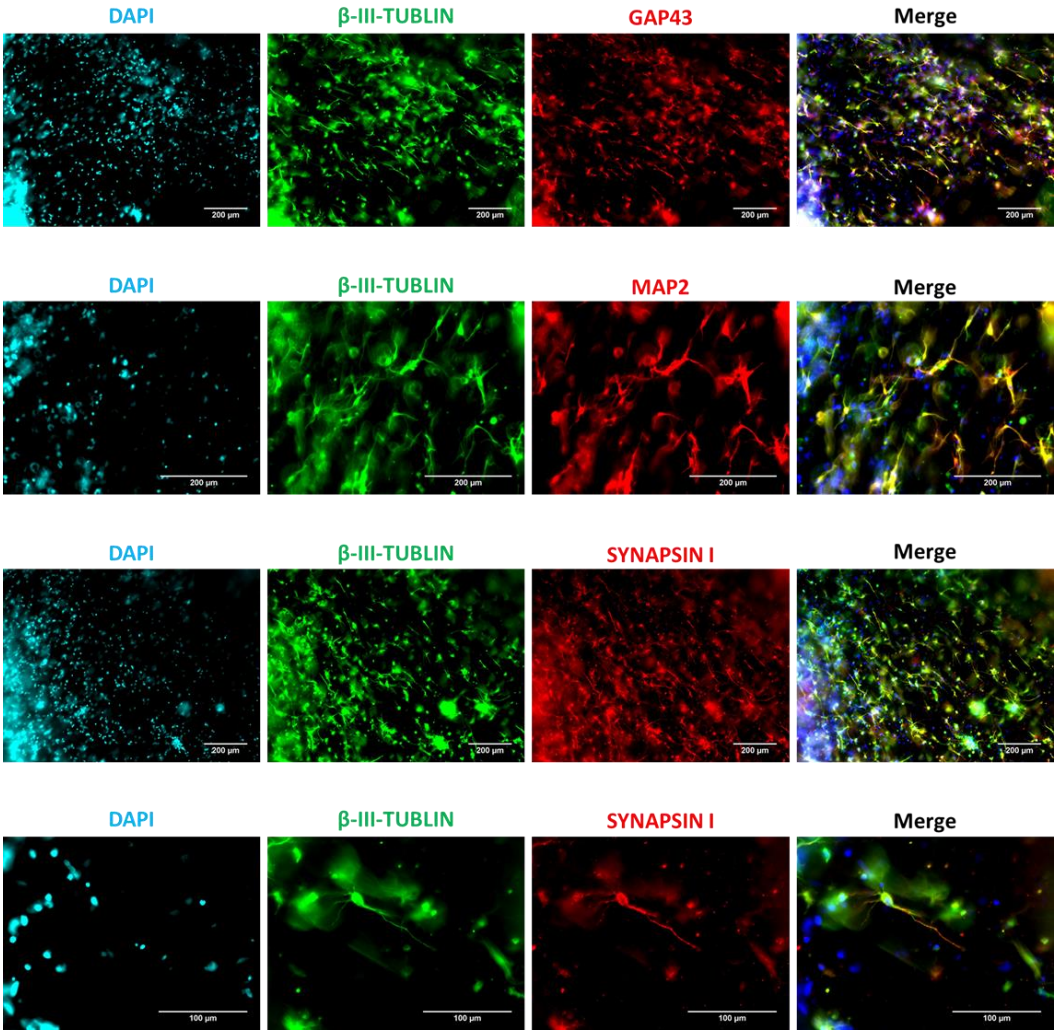

Fig 4-3: Fluorescent immunocytochemistry of neuronal and synaptic markers of hiPSC-derived neural cultures within 3D collagen hydrogel scaffolds after 60 days of maturation. Cell nuclei are visualised through DAPI staining. Scale bars represent 200µm (top three rows) and 100µm (bottom row)

To this end, hiPSC-neural precursors were derived through adherent dual-SMAD inhibition before seeding into collagen hydrogels at Day 10 of differentiation (see Methods section 4.2.3). These 3D neural constructs were matured using the same maturation protocol as 2D planar neural cultures over 60 days. Fluorescent immunocytochemical staining of the neuronal markers β-III-TUBULIN, GAP43, and MAP2 reveal widespread neuritogenesis and neuron-marker positive cells throughout the constructs (Fig 4-3). The pre-synaptic marker SYNAPSIN I is also present throughout many of the derived neuronal cells, which is suggestive of a successfully maturing neuronal population generating the machinery necessary for functional synaptic formation.

However, simple epifluorescent microscopy is unable to capture the fully 3D nature of the encapsulated cells and observed neuritogenesis. Therefore, confocal microscopy was used to acquire images to show the full range of multi-planar neuronal extension and prevalence throughout the scaffold (Fig 4-4). Dorsally-patterned neural differentiation of hiPSCs was undertaken to generate neural cultures with a high prevalence of β-III-TUBULIN-positive neuronal cells and TBR1-positive nuclei staining to better visualise the placement of cell soma and neurites within the 3D scaffold (Fig 4-4 A). Robust neuronal cell morphology and neurite extensions were observed throughout the cell-laden hydrogel showing that this formulation of collagen hydrogel is conducive to neural tissue construct formation with hiPSC-derived NPCs.

To better visualise the extent of neuritogenesis throughout the depth (Z-axis) of the hydrogel; Z-depth colour coding of the matured hiPSC-derived neural culture was generated to investigate the overall morphology of the neurite extensions and cell nuclei within 3D space (Fig 4-4 B). Image stacks of approximately 40µm in depth are sufficient to show that neurite growth occurs along all three-axes within the scaffold and that neuronal soma are also dispersed throughout the structure.

It is also worthy of mention that although loose clusters of neural cells were observed within the 3D constructs; tightly-packed ganglia-like structures seen throughout planar culture of hiPSC-derived neural cells were not observed. Also, the pattern of rounded cell aggregate formation seen within alginate hydrogels with neural cell lines (Chapter 2), were not present within these scaffolds. Another indicator of the success of this scaffold composition for allowing extensive neuritogenesis from hiPSC-derived neurons.

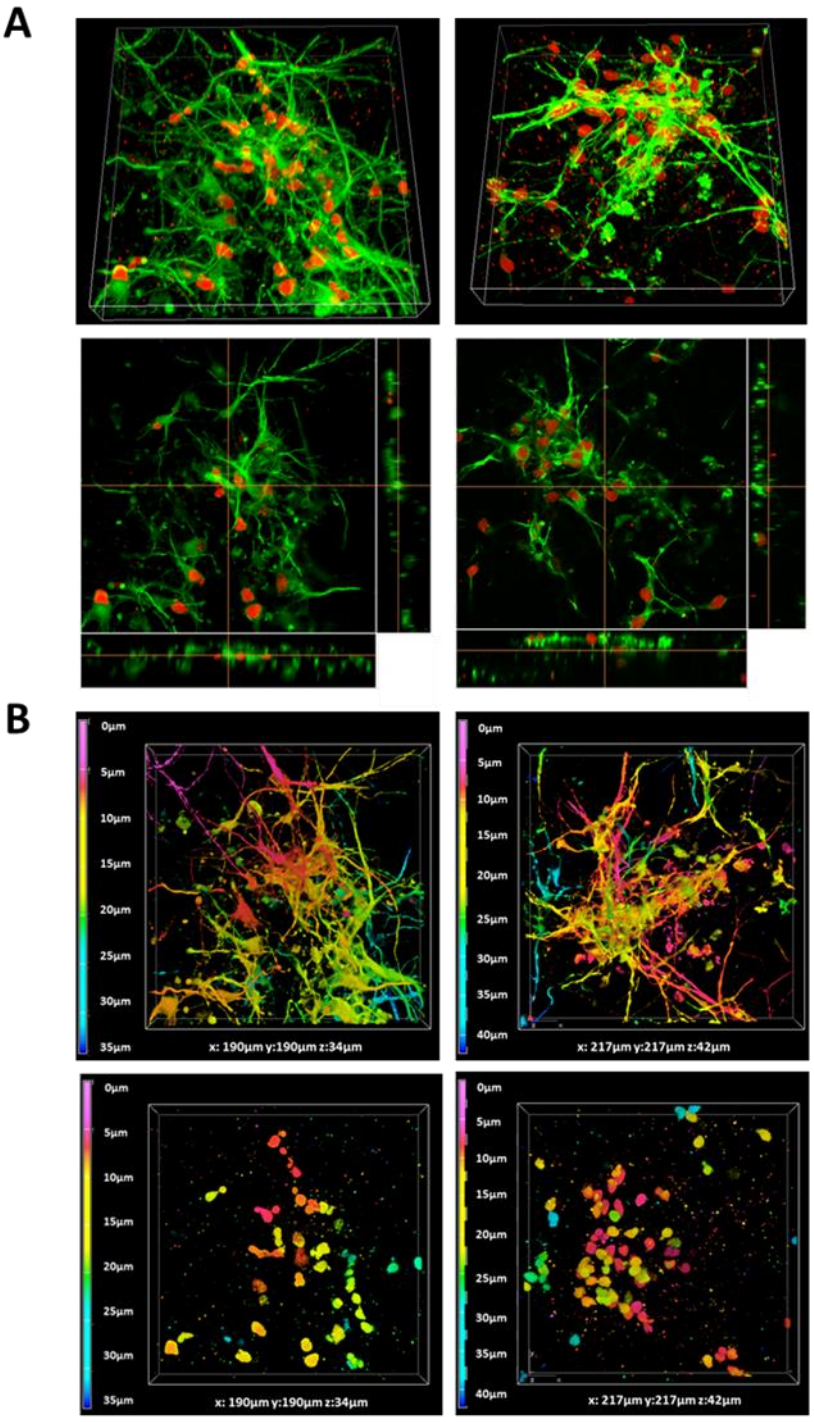

Fig 4-4: Confocal microscopy of dorsally-patterned hiPSC-derived neural cultures encapsulated in 3D collagen hydrogels. (**A**) Immunostaining with the neuronal marker β-III-TUBULIN (green) and the nuclei-localised early-cortical marker TBR1 (red). (**B**) Z-depth colour coding of the cell-laden scaffolds; β-III-TUBULIN (top row) and TBR1 (bottom row) showing neurite extension and cell soma distribution along all three axes. All image fields of view approximately 200µm x 200µm x 40µm.

4.3.2 Neural Precursor Marker Expression in 2D and 3D Hydrogel Scaffolds

To investigate whether hiPSC-derived NPCs within 3D collagen hydrogel scaffolds prompted any differences in the propagation or maturation of the precursor population over the time-course of differentiation, gene expression assays of NPC-specific markers were undertaken. These assays were done to directly compare both dorsal- and ventral-patterned neural differentiation from hiPSCs in both 2D culture (from Chapter 3) and 3D collagen hydrogel scaffolds.

The NPC marker *NESTIN* showed an early peak of expression (Day 20-30 of differentiation) in all patterned neural cell populations in both 2D and 3D culture (Fig 4-5). The levels of expression were comparable at all time points between 2D Dorsal, 2D Ventral, and 3D Dorsal cultures. Only 3D Ventral cultures showed statistically significant increases in *NESTIN* expression at Day 14 and Day 20 post-neural induction compared to the other three culture conditions. This pattern indicates that in both 2D and 3D culture conditions, early NPC marker expression occurs prior to a decrease over the time course of neuronal maturation and post-mitotic differentiation. The initial induction or preservation of *NESTIN* marker expression however, is much higher under ventral-patterning conditions within a 3D hydrogel environment.

The dorsal-forebrain precursor marker *PAX6* displays robust upregulation in 2D dorsal-patterned differentiation. This peaks at Day 20 of differentiation before slightly lower but stable expression for the rest of the maturation time course. These levels of expression were consistently and significantly higher than was seen in the ventrally-patterned neural cultures from both 2D and 3D differentiation. Interestingly, the level of *PAX6* expression within 3D Dorsal cultures did show the same early peak of upregulation, but to a much lower level than was maintained within 2D dorsal inductions. Also, this burst of *PAX6* expression was not maintained throughout maturation, suggesting that a drop in the number of dorsal-forebrain precursors may be taking place within 3D scaffolds (Fig 4-5).

The ventral-forebrain precursor marker *NKX2.1* displayed almost exclusive upregulation within ventrally-patterned neural cultures, and this ventralisation signal was unaffected through differentiation within 3D scaffolds compared to planar culture. The exception being a very high upregulation of *NKX2.1* in 3D Ventral cultures compared to 2D

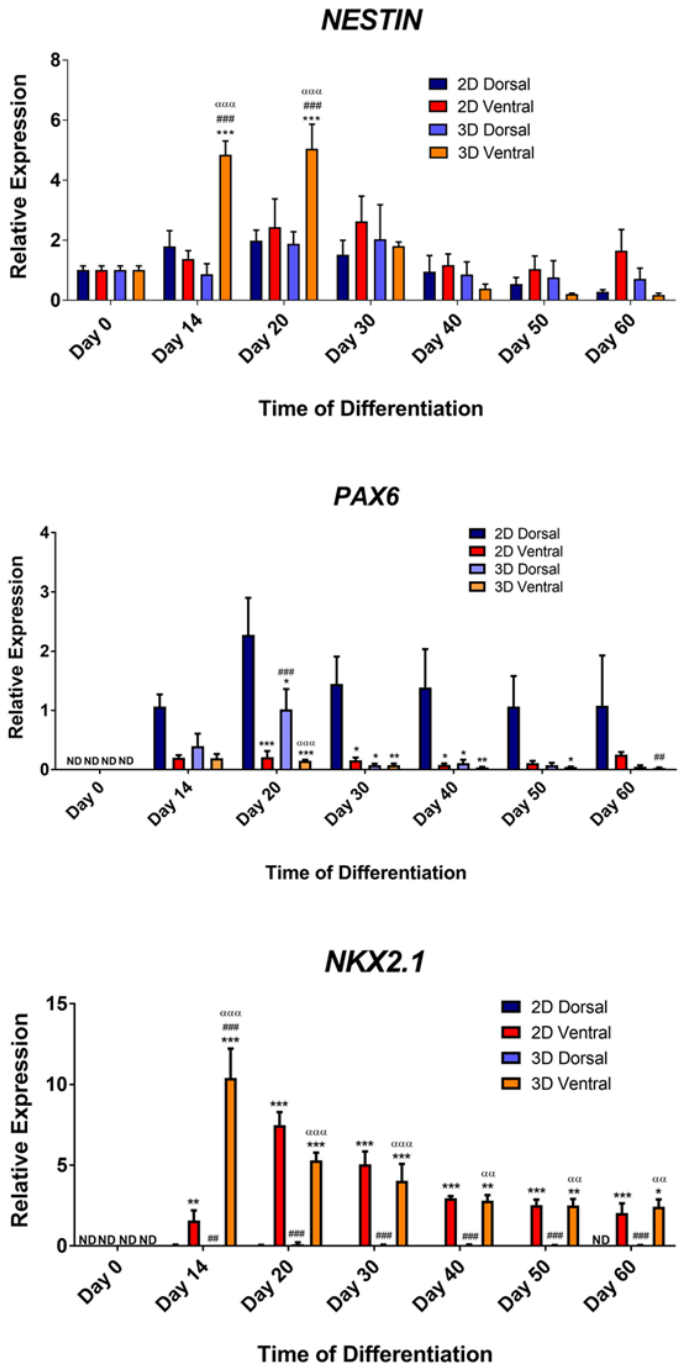

Fig 4-5: Quantitative gene expression analyses of neural precursor markers in dorsally- and ventrally-patterned hiPSC-derived neural cultures differentiated in 2D planar cultures and 3D hydrogel scaffolds over 60 days of differentiation. ND; Not Detected. Data is shown as means ± S.E.M of four independent experiments. Statistical significance is displayed relative to; 2D Dorsal (*), 2D Ventral (#), and 3D Dorsal (α). $^{*,\#,\alpha}$ p≤0.05, $^{**,\#\#,\alpha\alpha}$ p≤0.01, $^{***,\#\#\#,\alpha\alpha\alpha}$ p≤0.001 based on unpaired two-tailed t-tests.

Ventral cultures at Day 14 post neural induction (~8-fold higher), which mirrored the concurrent significant upregulation of *NESTIN* at the same point (Fig 4-5). Ventral patterning and propagation of ventral-forebrain precursors over the time course of neural differentiation for the most part was unaffected and certainly not inhibited by maturation within 3D culture environments.

4.3.3 Comparison of Neuronal and Synaptic Marker Expression Profiles in 2D and 3D Scaffolds

To further investigate and understand the effect of neural differentiation and maturation within 3D scaffold environments we next sought to observe the expression profiles of canonical neuronal and axonal markers as well as pre- and post-synaptic functional components (Fig 4-6).

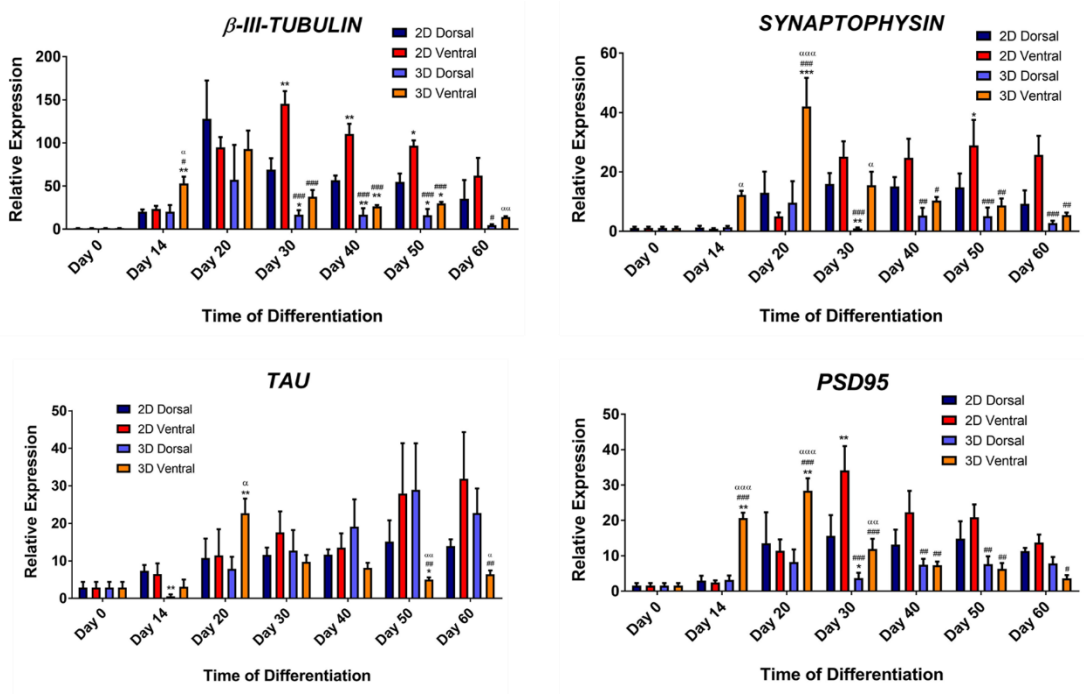

Fig 4-6: Quantitative gene expression analyses of neuronal and synaptic markers in dorsally- and ventrally-patterned hiPSC-derived neural cultures differentiated in 2D planar cultures and 3D hydrogel scaffolds over 60 days of differentiation. Data is shown as means ± S.E.M of four independent experiments. Statistical significance is displayed relative to; 2D Dorsal (*), 2D Ventral (#), and 3D Dorsal (α). $^{*,\#,\alpha}$ p≤0.05, $^{**,\#\#,\alpha\alpha}$ p≤0.01, $^{***,\#\#\#,\alpha\alpha\alpha}$ p≤0.001 based on unpaired two-tailed t-tests.

The neuronal structural marker *β-III-TUBULIN* displayed robust expression after 20 days of neural differentiation, in both 2D ventrally- and dorsally-patterned neural cultures. At later time-points this level of expression was significantly enhanced within ventral cell populations. This pattern of increased expression under ventral-patterning was also seen within the 3D encapsulated cultures, however, the overall level of expression was significantly lower in cells within hydrogel scaffolds than in planar culture by later time-points of differentiation (Day 30-60) (~3.3- to 7-fold lower) (Fig 4-6).

This difference between expression levels within 2D and 3D differentiation strategies was less pronounced at earlier time points, suggesting that the onset of post-mitotic neuronal maturation was not inhibited within 3D cultures, although further maturation or development of increased neuronal cell numbers may be negatively affected.

The axonal marker *TAU* displayed consistent upregulation over the course of differentiation in both 2D Dorsal and 2D Ventral neural cell cultures, but again with a trend for higher upregulation in ventral-patterned cultures. In contrast to the expression profiles of *β-III-TUBULIN* in 3D Dorsal cultures, which showed restricted expression compared to 2D Dorsal cultures; the level of *TAU* in 3D Dorsal culture showed a trend for constant increase over the course of differentiation. At later time points this level of expression exceeded that seen within 2D Dorsal differentiation (~1.7-fold higher at Day 60) but did not reach statistical significance. Conversely, the level of *TAU* expression within 3D Ventral differentiation displayed its highest peak of expression by Day 20 (significantly above dorsal culture conditions) before showing a gradual decreasing pattern of expression until Day 60 when it became significantly lower (~3.5-fold lower than 3D Dorsal conditions), breaking the pattern of gradual upregulation seen in other experimental conditions. This low level of *TAU* expression in 3D Ventral cultures was also significantly lower than the level of transcript obtained from 2D Ventral cultures. These data suggest that markers of axonogenesis follow a comparable pattern and level of gene expression in 2D Dorsal, 2D Ventral and 3D Dorsal neural cultures, but show divergently lower levels within 3D Ventral setups, possibly indicating an inhibitory effect of axonal generation within these cultures or retention of NPC characteristics.

The pre-synaptic marker *SYNAPTOPHYSIN* (*SYN*) from Day 30 of differentiation onwards showed stable expression within 2D Dorsal and 2D Ventral neural cell cultures, with a trend for higher expression under ventral-patterning. Overall expression levels of

SYN in 3D Dorsal cultures however, were lower than their 2D counterparts at the majority of later time points, and significantly lower at Day 30 of differentiation. From Day 30 of differentiation onwards *SYN* levels in 3D Dorsal cultures were significantly lower than those seen within 2D Ventral differentiations. After a very high peak of *SYN* expression at the early Day 20 time point in 3D Ventral cultures, that was significantly higher than that seen in any of the other experimental conditions, this too reduced to a low basal level comparable to that seen within 3D Dorsal cultures. By Day 40-60 post neural induction, *SYN* levels in both dorsal- and ventral- patterning methodologies in 3D scaffolds were significantly lower than those seen from 2D Ventral culture (Fig 4-6).

A very similar pattern was seen when assaying the post-synaptic marker *PSD95* across all 2D and 3D experimental conditions. 2D Dorsal expression levels were robustly present after Day 20 of differentiation and remained stable over the course of differentiation. This was also true of *PSD95* gene expression levels within 3D Dorsal cultures but with a relative expression level approximately half of that seen within 2D Dorsal cultures, although not to a statistically significant degree. 3D Ventral cultures showed an early expression peak of *PSD95* (Day 14-20) as was seen with *SYN* expression, but which lowered after 30 days of differentiation to levels comparable to those seen in 3D Dorsal inductions. This peak of synaptic machinery transcript expression was also seen within 2D ventrally-patterned cultures (Day 30), which may indicate a conserved upregulation of such genes in ventralised cultures compared to those undergoing dorsal patterning. Again however, significantly lower levels of relative *PSD95* expression were seen within 3D neural cultures than in 2D ventral cultures at more mature time points (Fig 4-6).

4.3.4 Preservation of Neuronal Subtype Patterning within 3D Hydrogel Scaffolds

It is possible that cell-matrix interactions occurring within 3D cell-laden hydrogel environments may have an impact on the efficacy of neural subtype patterning utilised in this study. To observe whether the 3D cellular microenvironment influenced the development of mature excitatory or inhibitory neuronal subtype markers (from dorsal-

and ventral- patterning respectively) we assayed the expression profiles of markers indicative of glutamatergic and GABAergic neuronal cell fates (Fig 4-7).

The glutamatergic marker *vGLUT1* was strongly expressed from Day 20 post neural induction in 2D Dorsal cultures demonstrating the presence of excitatory neuronal cell populations. Expression was also seen within 3D Dorsal cultures from Day 20 of neural induction although with a trend for lower expression levels than was seen from the default 2D induction pathway, but still significantly higher than both 2D and 3D ventral differentiations at Day 40-50 of maturation. Basal low-level expression of *vGLUT1* was observed within both 2D and 3D Ventral cultures showing an incomplete inhibition of the excitatory neuronal differentiation pathway, but still with significantly lower excitatory neuronal marker expression than dorsally patterned cultures. This excitatory neuronal marker was further suppressed within 3D Ventral cultures compared to the 2D Ventral differentiation pathway.

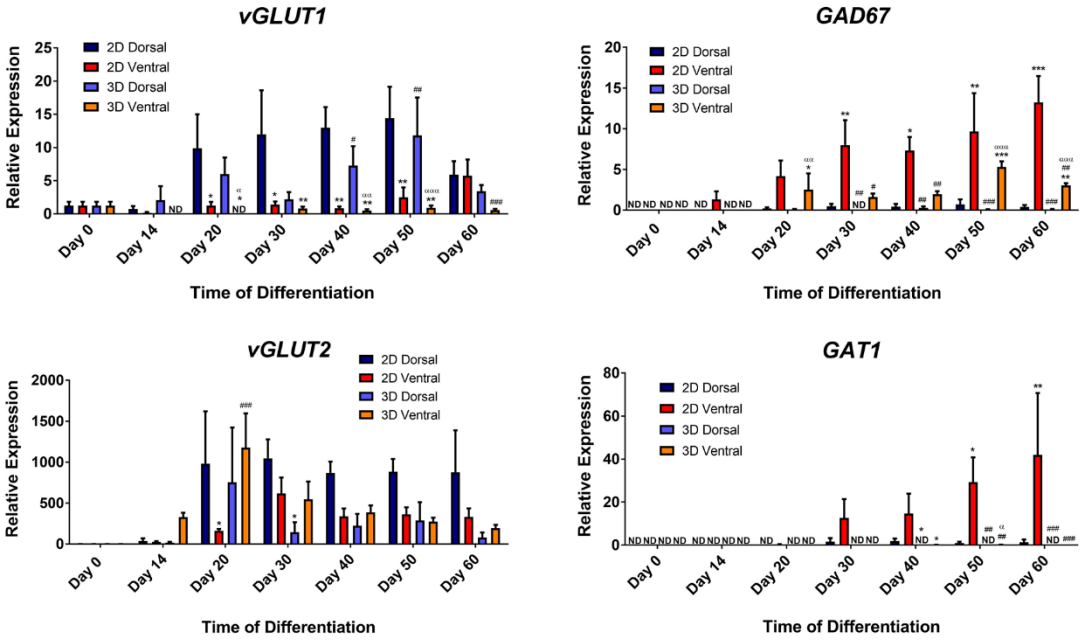

Fig 4-7: Quantitative gene expression analyses of excitatory (*vGLUT1* and *vGLUT2*) and inhibitory (*GAD67* and *GAT1*) neuronal markers in dorsally- and ventrally-patterned hiPSC-derived neural cultures differentiated in 2D planar cultures and 3D hydrogel scaffolds over 60 days of differentiation. ND; Not Detected. Data is shown as means ± S.E.M. of four independent experiments. Statistical significance is displayed relative to; 2D Dorsal (*), 2D Ventral (#), and 3D Dorsal (α). $^{*,\#,\alpha}$ p≤0.05, $^{**,\#\#,\alpha\alpha}$ p≤0.01, $^{***,\#\#\#,\alpha\alpha\alpha}$ p≤0.001 based on unpaired two-tailed t-tests.

However, adherence to this divergent pattern of expression is exhibited less in the expression level of the excitatory marker *vGLUT2*. The upregulation of this marker showed more robust segregation between 2D Dorsal-patterned and 2D Ventral-patterned cultures, with higher expression found within the former experimental condition. However, expression levels within 3D Dorsal cell populations were lower than their 2D counterparts and were more comparable to levels seen within ventrally-patterned cultures, although these lower levels of expression did not reach statistical significance. Intriguingly, the Day 20 level of expression seen within 3D Ventral cultures, was comparable to that seen within both dorsally-patterned differentiation pathways and significantly higher than the level seen within 2D ventrally-patterned cultures. However, this high spike of *vGLUT2* glutamatergic marker expression in 3D ventral cultures is not paired with an equivalent upregulation of *vGLUT1* expression (which was not detected at the same time point) (Fig 4-7). This is suggestive of either a transient upregulation of *vGLUT2* expression in ventral cultures that does not denote intrinsic pathway divergence or possibly the generation of an early glutamatergic neural subset that is not maintained throughout the culture. Overall the divergent nature of ventral- and dorsal-patterning is more apparent through *vGLUT1* expression patterns than was seen with *vGLUT2* expression.

The inhibitory GABAergic neuronal marker *GAD67* within 2D Ventral cultures displayed a steady upregulation during neural differentiation and maturation over 60 days. Upregulation was also seen within the 3D Ventral-patterned cultures, albeit to a significantly lower level than was observed in 2D (~13-fold relative expression versus ~3-fold relative expression at Day 60 of differentiation). Within both 2D and 3D Dorsal cultures the level of *GAD67* was at a consistently low basal level that was significantly lower than the expression level within the ventrally-patterned cultures throughout the latter half of the neural differentiation pathway (Fig 4-7).

GAT1 (a GABA re-uptake transporter and GABAergic marker) expression levels showed robust upregulation from Day 30 onwards of 2D ventrally-patterned neural differentiation that was not observed in either the 2D Dorsal nor 3D Dorsal differentiation pathway cultures. Unlike *GAD67* expression however, 3D Ventral cultures showed almost no *GAT1* gene expression at any time-point during the differentiation process. This more mature marker of GABAergic neuronal function may therefore be inhibited within the 3D growth conditions of this experiment.

As in the previous chapter, regression analysis of marker gene expression pattern and strength can be used to determine overall comparisons between divergent growth conditions for each marker. In this case when comparing the neuronal subtype specific markers *vGLUT1*, *vGLUT2* and *GAD67* it can be seen that between 3D Dorsal and 3D Ventral cultures a significantly divergent pattern of expression is recorded for both the dorsal marker *vGLUT1* and the ventral marker *GAD67* (Table 4-2). However, this is not true of the *vGLUT2* regression data which shows a similar pattern between 3D Dorsal and 3D Ventral cultures (mirroring the point-by-point t-test data above).

3D Dorsal vs 3D Ventral

Gene	Marker Type	P-value	Degree of Significance
vGLUT1	Dorsal/Excitatory neuronal cell	0.023	*
vGLUT2	Dorsal/Excitatory neuronal cell	0.087	ns
GAD67	Ventral/Inhibitory neuronal cell	0.004	**

Table 4-2: Table of full time-course robust regression analysis of dorsal and ventral markers for 3D Dorsal vs 3D Ventral neural cultures. Statistical significance denoted by * p≤0.05, ** p≤0.01, *** p≤0.001.

These data reinforce the conclusion that although patterning bias is preserved within dorsal and ventral 3D neural culture, the overall expression of mature neuronal subtype markers are lower in 3D growth cultures compared to 2D differentiation. This drop in overall neuronal maturation is reflected in the lower degrees of significance seen in the regression tables of 3D patterned cultures (Table 4-2) than is seen in 2D patterned cultures (Fig 4-7, Table 3-2).

To better visualise the effect of the 3D growth environment on the extent of neuronal subtype marker expression (and therefore patterned differentiation) within each neural culture; robust regression analysis was also performed on the 2D/3D Dorsal expression data (Table 4-3) and 2D/3D Ventral expression data (Table 4-4).

For dorsally-patterned differentiations there is no upregulation in ventrally associated gene expression (*GAD67*) when growth occurs within the 3D hydrogel environment compared to 2D planar culture (Table 4-3). This confirms that the hydrogel

scaffold itself does not impose any ventralising factors to the embedded cells and thereby triggering inhibitory neuronal subtype development.

2D Dorsal vs 3D Dorsal

Gene	Marker Type	P-value	Degree of Significance
vGLUT1	Dorsal/Excitatory neuronal cell	0.022	*
vGLUT2	Dorsal/Excitatory neuronal cell	<0.001	***
GAD67	Ventral/Inhibitory neuronal cell	0.451	ns

Table 4-3: Table of full time-course robust regression analysis of dorsal and ventral markers for 2D Dorsal vs 3D Dorsal neural cultures. Statistical significance denoted by * p≤0.05, ** p≤0.01, *** p≤0.001.

However, the strength of induction of dorsal-specific neuronal gene expression is inhibited within 3D Dorsal environments (Table 4-3), as is seen with the difference in expression patterns of the dorsal markers *vGLUT1* and *vGLUT2*. This difference is not derived from a breakdown in the patterning events per say, but instead is reflective of lower overall neural maturation/differentiation within this 3D environment, of which these subtype markers are also indicative (see section 4.3.3).

This is also true when comparing the patterned 2D Ventral and 3D Ventral expression data, which also preserve the same extent of dorsal-gene inhibition (i.e. the same efficacy of neural patterning) but combined with an overall significantly lower expression of ventral associated markers *GAD67* and *GAT1* (Table 4-4).

2D Ventral vs 3D Ventral

Gene	Marker Type	P-value	Degree of Significance
vGLUT1	Dorsal/Excitatory neuronal cell	0.628	ns
vGLUT2	Dorsal/Excitatory neuronal cell	0.229	ns
GAD67	Ventral/Inhibitory neuronal cell	<0.001	***
GAT1	Ventral/Inhibitory neuronal cell	0.012	*

Table 4-4: Table of full time-course robust regression analysis of dorsal and ventral markers for 2D Ventral vs 3D Ventral neural cultures. Statistical significance denoted by * p≤0.05, ** p≤0.01, *** p≤0.001.

Taken altogether this regression analysis confirms the preservation of patterning methodologies during differentiation within the hydrogel scaffolds, and that the scaffold itself does not elicit any patterning influence over the embedded cells. However, there is a strong consistent repression of neuronal subtype marker expression within both dorsal and ventral 3D cultures, which is also reflected in canonical neuronal marker expression. Therefore, under these 3D conditions; neuronal patterning is preserved but tied to inhibition of neural maturation.

4.3.5 Cortical Marker Expression Profiles in 2D versus 3D Culture

Neural morphogen patterning of hiPSC-derived NPCs does not generate specific neuronal subtypes in isolation, but instead does so by recapitulating temporo-spatial coordinates of neural tube localisation. Therefore it is necessary to uncover whether the maturation events of dorsal-forebrain identity (corticogenesis) are preserved, accelerated or altered under maturation in 3D hydrogel scaffolds. To this end, gene expression profiles of the early-to-late born cortical markers *REELIN*, *TBR1*, *CTIP2* and *SATB2* were analysed in all four neural differentiation conditions (Fig 4-8).

REELIN expression is a marker of the pioneer outer layer I of the cortex and an early marker of cortical development. The greatest upregulation of this gene was seen within 2D Dorsal cultures with peak expression after 30 days of neural differentiation but with maintenance of expression up until Day 60. It also showed upregulation within 3D Dorsal cultures although to a much lower extent. At Day 30 the relative expression in 2D was 8-fold higher than expression in 3D Dorsal cultures, but by Day 40 to 50 of differentiation this difference in expression dropped to below 2-fold. Expression of *REELIN* in both 2D and 3D ventral-patterned cultures was consistently lower than is seen in the dorsal inductions, especially after protracted periods of neural maturation, but expression was not suppressed entirely. Even within positively expressing dorsal cultures, high variability of expression between biological repeats was prevalent.

This overall pattern was repeated when observing the expression of cortical pre-plate and layer VI cortical marker *TBR1* over the course of differentiation (Fig 4-8). Robust gene expression was limited to 2D Dorsal cultures with a significant peak around 30 days of differentiation followed by a steady decrease until Day 60. Recorded expression of *TBR1* in

3D Dorsal culture was consistently lower than in 2D, ranging from approximately 8.5-fold to 5.4-fold reduced relative expression across the course of differentiation. As with *REELIN*, ventrally-induced neural cultures (both 2D and 3D) showed the lowest expression levels of *TBR1*, although did maintain a minimal expression level.

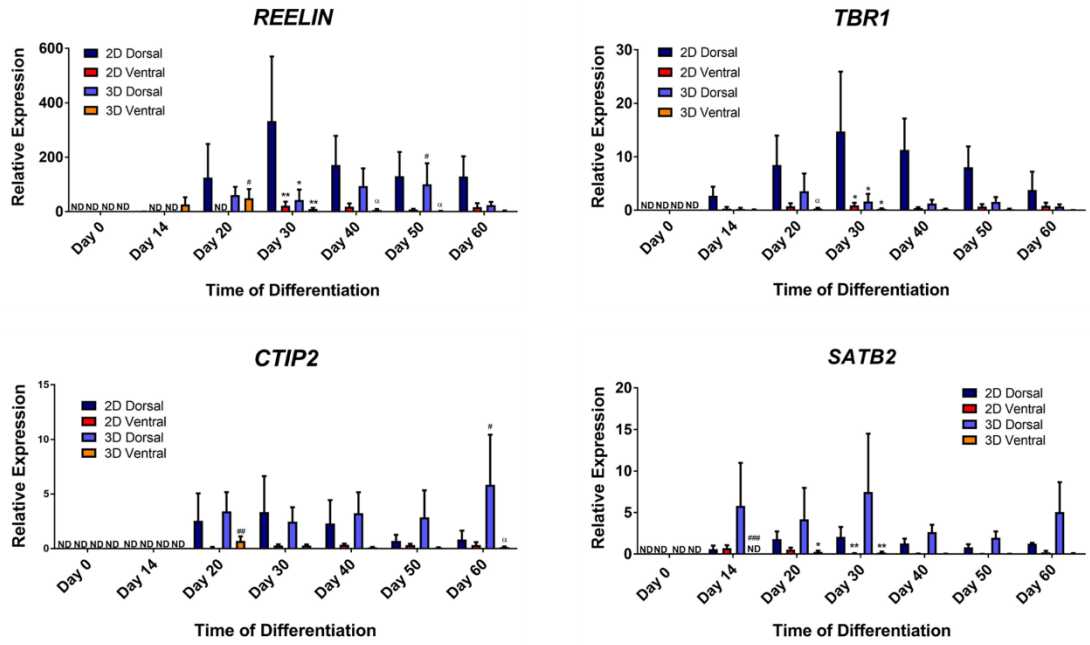

Fig 4-8: Quantitative gene expression analyses of early and late cortical-specific markers in dorsally- and ventrally-patterned hiPSC-derived neural cultures differentiated in 2D planar cultures and 3D hydrogel scaffolds over 60 days of differentiation. ND; Not Detected. Data is shown as means ± S.E.M. of four independent experiments. Statistical significance is displayed relative to; 2D Dorsal (*), 2D Ventral (#), and 3D Dorsal (α). $^{*,\#,\alpha}$ p≤0.05, $^{**,\#\#,\alpha\alpha}$ p≤0.01, $^{***,\#\#\#,\alpha\alpha\alpha}$ p≤0.001 based on unpaired two-tailed t-tests.

Intriguingly, the expression profiles of the layer V cortical marker *CTIP2* and the late-born upper layer II-IV cortical marker *SATB2* break from the pattern described above and showed enhanced levels of expression within 3D Dorsal cultures compared to the 2D Dorsal inductions (Fig 4-8).

CTIP2 expression in 2D and 3D Dorsal cultures were at approximately equivalent levels over Days 20-40 of differentiation, but increased by Day 60 within the 3D Dorsal populations to a level over 7-fold higher than that seen in 2D Dorsal cultures at the same time point. Levels of *CTIP2* gene expression within either of the ventrally-patterned culture conditions remained lower than those seen within dorsal cultures at every measured time

point. However, the low relative transcript expression increases only reached significance after 60 days of differentiation relative to 3D Dorsal cultures (Fig 4-8).

At all assayed time points the upper-layer late-born neuronal cortical marker *SATB2* displayed a trend for higher relative expression levels in 3D Dorsal rather than 2D Dorsal cultures (~2 to 4-fold higher) (Fig 4-8). No noticeable upward trend of expression level was discernible along this timeline of neural maturation that would follow with the expected timeline of late-born cortical neuron generation. As with the majority of dorsal-anterior cortical markers, the expression level of *SATB2* within both 2D and 3D Ventral cultures were barely detectable at any of the time-points assayed. The high variability of expression levels within dorsally patterned biological repeats hints at the possible stochastic nature of the development of these subpopulations of cortical cell types between differentiations. However, regardless of this spread of cortical marker strength, for all four markers analysed, all showed stronger expression profiles in the dorsally-patterned neural cultures.

To confirm the separation of cortical localisation markers between the 3D Dorsal and 3D Ventral growth environments, we once again used regression analysis of the gene expression data to compare overall pattern divergence (Table 4-5).

3D Dorsal vs 3D Ventral

Gene	Marker Type	P-value	Degree of Significance
REELIN	Dorsal/Outer cortical ECM protein (Early)	0.001	***
TBR1	Dorsal/Cortical plate (Early)	<0.001	***
CTIP2	Dorsal/Cortical Layer (Mid)	<0.001	***
SATB2	Dorsal/Cortical Layer (Late)	<0.001	***

Table 4-5: Table of full time-course robust regression analysis of cortical localisation markers for 3D Dorsal vs 3D Ventral neural cultures. Statistical significance denoted by * p≤0.05, ** p≤0.01, *** p≤0.001.

For all of the early-to-late cortical markers analysed, strong significant differences in expression pattern are maintained between 3D Dorsal and 3D Ventral cultures. All of these markers are indicative of cortical or pre-cortical neuronal localisation and dorsal forebrain development. Therefore the strong presence of these cortical markers in dorsally-patterned, but not ventrally-patterned, 2D and 3D neural cultures (Fig 4-8, Table 4-5) confirm the preservation of dorsal identity within the hydrogel environment, and that

the 3D scaffold itself does not infer any localisation specification onto the encapsulated cells.

To observe whether the 3D environment itself has a negative impact on cortical marker expression (as was seen with neuronal subtype genes in Section 4.3.4) we repeated the robust regression analysis of cortical localisation gene markers between 2D Dorsal and 3D Dorsal differentiations (Table 4-6).

2D Dorsal vs 3D Dorsal

Gene	Marker Type	P-value	Degree of Significance
REELIN	Dorsal/Outer cortical ECM protein (Early)	<0.001	***
TBR1	Dorsal/Cortical plate (Early)	<0.001	***
CTIP2	Dorsal/Cortical Layer (Mid)	0.079	ns
SATB2	Dorsal/Cortical Layer (Late)	<0.001	***

Table 4-6: Table of full time-course robust regression analysis of cortical localisation markers for 2D Dorsal vs 3D Dorsal neural cultures. Statistical significance denoted by * p≤0.05, ** p≤0.01, *** p≤0.001.

Intriguingly, the "early" cortical markers *REELIN* and *TBR1* do show significant differences in the magnitude and pattern of expression between 2D and 3D Dorsal differentiation. This is also seen with the "late" cortical marker *SATB2*. No significant difference was observed in the expression pattern of the "mid"-onset cortical marker *CTIP2*. These differences in expression pattern between 2D and 3D Dorsal inductions are not simply a reduction in each overall gene transcription, as was seen for the neuronal subtype markers. Instead the expression of the "early" markers are lower in the 3D cultures, whereas the "late" cortical marker is significantly enhanced.

To ascertain whether the repression of anterior-dorsal cortical markers is maintained in 3D encapsulated ventrally-patterned cultures, we reproduced the regression analysis above for 2D Ventral and 3D Ventral neural cultures (Table 4-7). For all of the cortical regionalisation genes, with the exception of *TBR1*, no significant differences in cortical marker upregulation is seen in the 3D Ventral cultures. The differences flagged by this analysis for TBR1 expression denotes higher expression within 2D Ventral cultures than 3D, which still confirms the conclusion that the hydrogel scaffold does not enhance dorsal gene expression patterns or limit the ventral patterning efficacy. Instead this difference,

although significant, is still based on expression levels far below those seen within planar dorsally-patterned cultures (Fig 4-8).

2D Ventral vs 3D Ventral

Gene	Marker Type	P-value	Degree of Significance
REELIN	Dorsal/Outer cortical ECM protein (Early)	0.443	ns
TBR1	Dorsal/Cortical plate (Early)	0.003	**
CTIP2	Dorsal/Cortical Layer (Mid)	0.798	ns
SATB2	Dorsal/Cortical Layer (Late)	0.803	ns

Table 4-7: Table of full time-course robust regression analysis of cortical localisation markers for 2D Ventral vs 3D Ventral neural cultures. Statistical significance denoted by * p≤0.05, ** p≤0.01, *** p≤0.001.

The combination of all cortical marker regression data does reinforce the conclusion that dorso-ventral regionalisation is strongly maintained within the 3D patterning differentiation methods utilised here. In addition to this, no evidence of repressed ventralisation within the hydrogel scaffold was observed in the pattern of cortical-specific genes. There were however differences in the magnitude of cortical gene expression from planar dorsal cultures and 3D Dorsal cultures showing that hydrogel embedding may elicit an effect on cortical cell maturation rates.

4.3.6 Effect of 3D Culture on Neurotransmitter Receptor Expression

Another aspect of neural cell maturation that may differ between planar and 3D encapsulated neural inductions is the prevalence of neurotransmitter receptor development, as a precursor to excitatory and inhibitory synaptic function.

The ionotropic GABA receptor subunit *$GABA_AR1$* showed a late-onset upregulation of expression in both 2D Dorsal and 2D Ventral neural cultures, with a bias of elevated expression within the latter (Fig 4-9). However, this pattern was not preserved with 3D Dorsal and Ventral neural inductions which displayed reduced expression in 3D Dorsal cultures relative to both 2D culture types with a 4-fold and 7.5-fold decrease in expression compared to 2D Dorsal and 2D Ventral cultures respectively. The upregulation of this receptor subunit was seen strongly within 2D Ventral inductions but were barely

detectable in 3D Ventral cell populations at any time point during differentiation (Fig 4-9). At Days 40-60 of differentiation, the *GABA$_A$R1* expression level in 3D Ventral cultures was significantly lower than that observed in 2D Ventral cultures at equivalent timepoints.

In contrast, the metabotropic GABA receptor subunit *GABA$_B$R1* displayed upregulation earlier in the time-course of neural differentiation than *GABA$_A$R1*. Consistent and robust expression of *GABA$_B$R1* was observed in both 2D Dorsal and 2D Ventral cultures with a trend for approximately double the expression within ventrally-patterned cultures than in dorsal ones from Day 30 onwards (Fig 4-9). Spikes of *GABA$_B$R1* expression at Day 14 and 20 of differentiation were seen within 3D Ventral cultures that at the latter time point were 3- to 5-fold higher than in the other three culture conditions ($p \leq 0.01$ to $p \leq 0.001$). This early increase, at the time-point indicative of initial neuronal formation, then lowered to comparable levels seen within 2D induction conditions (and even lower by Day 60). Following the same pattern of 2D Ventral and Dorsal cultures, 3D Dorsal expression of *GABA$_B$R1* was consistently lower than that seen in 3D Ventral cell populations.

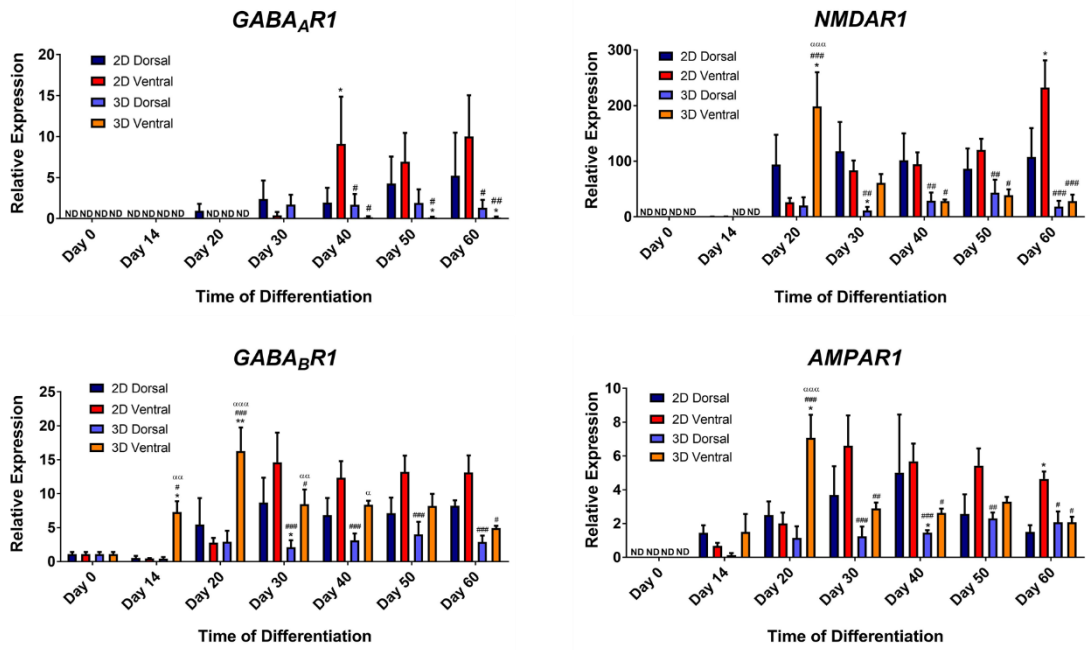

Fig 4-9: Quantitative gene expression analyses of GABA and glutamate neurotransmitter receptor subunit markers in dorsally- and ventrally-patterned hiPSC-derived neural cultures differentiated in 2D planar cultures and 3D hydrogel scaffolds over 60 days of differentiation. ND; Not Detected. Data is shown as means ± S.E.M. of four independent experiments. Statistical significance is displayed relative to; 2D Dorsal (*), 2D Ventral (#), and 3D Dorsal (α). $^{*,\#,\alpha}$ $p \leq 0.05$, $^{**,\#\#,\alpha\alpha}$ $p \leq 0.01$, $^{***,\#\#\#,\alpha\alpha\alpha}$ $p \leq 0.001$ based on unpaired two-tailed t-tests.

The overall relative expression level observed within 3D Dorsal cultures did remain steady over the course of differentiation, but at a level constantly lower than the other three neural induction conditions (Fig 4-9).

When assaying the gene upregulation of the ionotropic glutamate receptor subunits *NMDAR1* and *AMPAR1*, the same spike of high expression within 3D Ventral cultures after 20 days of differentiation is observed, similar to that seen with $GABA_BR1$ expression. For both *AMPAR1* and *NMDAR1* expression this early spike rapidly dropped over the time-line of differentiation to levels significantly below that seen in 2D culture conditions for *NMDAR1* expression, or comparable to 2D culture conditions in the case of *AMPAR1* (Fig 4-9). *NMDAR1* expression levels within 2D Dorsal cultures remained stable over every time-point from Day 20 of neural maturation, while a gradual upregulation over time was observed with 2D Ventral cultures (from 4-fold less than 2D Dorsal expression at Day 20 up to a 2-fold significantly higher expression by Day 60). 3D Dorsal expression levels of *NMDAR1* followed a similar pattern to that seen with $GABA_BR1$ expression, with gene expression levels 2- to 10-fold less than those recorded in 2D Dorsal cell populations. By Day 60 of differentiation, both 3D patterned neural cell cultures showed significantly lower expression of *NMDAR1* than 2D Ventral cultures (Fig 4-9).

This same pattern was seen with *AMPAR1* expression but less starkly than was observed in *NMDAR1* expression analyses. By Day 50-60 of differentiation, similar levels of *AMPAR1* expression was observed in 2D Dorsal, 3D Dorsal and 3D Ventral cultures, with an approximate 2-fold elevation in 2D Ventral cell populations. Earlier in the differentiation timeline (Day 20-30), the level of 3D Dorsal expression again remained stable but lower than that recorded in 2D Dorsal populations. Both 2D and 3D Ventral patterned cultures displayed slight trends for elevated *AMPAR1* glutamate receptor expression than neural populations undergoing dorsal-patterning.

4.3.7 Gliogenesis within 3D Scaffolds

Gliogenesis *in utero* is delayed relative to neuronal differentiation, and this pattern is recapitulated in neural differentiation pathways from pluripotent stem cells *in vitro*. To study whether neural differentiation of hiPSCs within 3D hydrogel environments affects the induction strength of astroglial and oligodendroglial cell lineages, or the timing of such

molecular events relative to 2D, we studied the gene expression profiles of the astrocytic marker *GFAP* and oligodendroglial lineage marker *GALC* (Fig 4-10).

The astrocytic marker *GFAP* did indeed display a robust delay of upregulation in comparison to the neuronal-specific markers analysed above, with detectable expression levels only later in the maturation timeline (Day 50 to 60 of differentiation). The level of *GFAP* expression was increased within both 3D Dorsal and 3D Ventral cultures relative to both 2D neural induction cell populations, with statistically significant higher levels of expression in 3D Ventral cultures. By Day 60, 3D Dorsal neural populations displayed significantly higher levels of *GFAP* expression compared to 2D dorsally-patterned cell types.

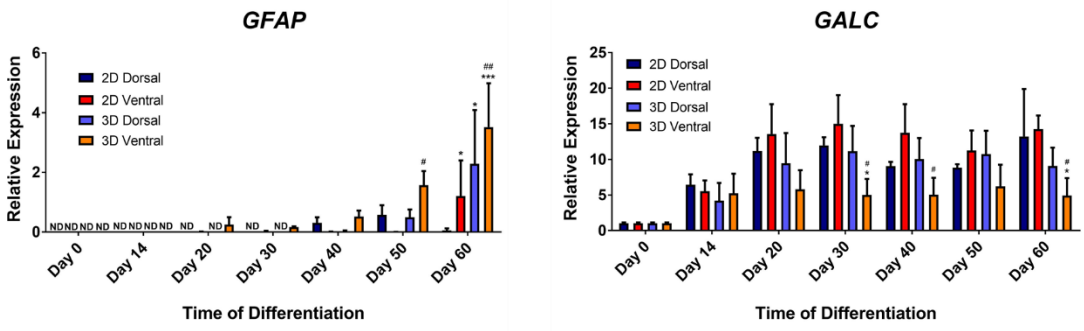

Fig 4-10: Quantitative gene expression analyses of astroglial (*GFAP*) and oligodendroglial (*GALC*) markers in dorsally- and ventrally-patterned hiPSC-derived neural cultures differentiated in 2D planar cultures and 3D hydrogel scaffolds over 60 days of differentiation. ND; Not Detected. Data is shown as means ± S.E.M. of four independent experiments. Statistical significance is displayed relative to; 2D Dorsal (*), 2D Ventral (#), and 3D Dorsal (α). $*^{,\#,\alpha}$ p≤0.05, $**^{,\#\#,\alpha\alpha}$ p≤0.01, $***^{,\#\#\#,\alpha\alpha\alpha}$ p≤0.001 based on unpaired two-tailed t-tests.

Interestingly, the expression of the oligodendroglial lineage marker *GALC* did not appear to be affected by neural differentiation strategies in either 2D or 3D environments and showed relatively stable expression levels over the full time-course of differentiation (Fig 4-10). Only in 3D Ventral cultures did the level of *GALC* expression show maintenance at significantly lower levels than 2D differentiation pathways. This is surprising, as the development of oligodendrocytes would logically follow the same pattern as astroglial generation, with a protracted (and intrinsic) delay following neuronal differentiation. However, this stable expression profile may represent basal levels of *GALC* within non-oligodendroglial cell types (including neurons), and extended maturation times may be

necessary to show strong gene upregulation indicating true oligodendrocyte formation. The trend of overall lower levels of expression in 3D Ventral cultures may indicate an increased population of neuronal rather than glial subtypes compared to other differentiation strategies, or an inhibition of oligodendroglial precursor identity within the 3D culture.

4.4 Discussion and Conclusions

To fully model neurological development and *in vivo*-like cytoarchitecture *in vitro*, many studies have focused on the generation of various 3D environments for neural cell encapsulation. These aim to mimic the biophysical and biochemical properties of native neural tissue. The reported advantages of such 3D neural cell culture systems would allow for enhanced cell-cell contacts (e.g. synapse formation) along all three axes, as well as greater degrees of cell-matrix interaction allowing for cell migration and possible self-organisation (LaPlaca *et al.*, 2010). Differentiation of iPSCs into neural lineages in various 3D hydrogel environments has been linked with enhanced markers of differentiation, and has been successfully used for migration-defect modelling of neurons from neurological pathologies (Z.-N. Zhang *et al.*, 2016; Gu *et al.*, 2017). However, direct comparisons of neural differentiation between 3D and 2D planar culture, and the effect of 3D hydrogel environments on dorsal- and ventral-patterned encapsulated NPCs in parallel, has not been explored.

In this chapter we have shown that hiPSC-derived NPCs differentiated in 3D collagen hydrogel scaffolds undergo extensive neuritogenesis. This is consistent with the finding detailed in Chapter 2; with neurite formation from neural-like cells encapsulated within collagen scaffolds. These neurites extend in all three-axes of the hydrogel environment and display markers of post-mitotic neuronal identity and pre-synaptic molecular machinery. Previous studies have shown that neural cell electrophysiological activity is preserved within collagen hydrogel matrices (O'Connor *et al.*, 2000; Ma *et al.*, 2004), so such neuritogenesis as described here is integral for the maturation of functional synapses between neuronal cells in this microenvironment.

The NPC marker *NESTIN*, shows comparable levels of expression when hiPSC-derived neural cultures are differentiated in 2D Dorsal, 2D Ventral and 3D Dorsal environments over 60 days. However, *NESTIN* expression early in differentiation (Day 14-

20) within 3D Ventral cultures is significantly higher than is observed in all other experimental conditions (~3.6-fold higher at Day 14 and ~2.4-fold higher at Day 20). This suggests a higher level of NPC induction within 3D encapsulated ventrally-patterned neural cultures. This early spike of NPC induction is reflected by higher levels of the ventral forebrain precursor marker *NKX2.1* at early time points within 3D Ventral cultures relative to 2D Ventral conditions. This pattern is not seen for dorsal-patterned cultures, in which *PAX6* levels are not enhanced within cells cultured in a 3D environment. This suggests that this 3D environment enhances ventral NPC generation, but does not enhance default dorsal precursor cell pools. Importantly, the effect of 3D collagen encapsulation did not appear to alter the patterning of encapsulated cells. That is to say, the effect of the patterning molecule purmorphamine is not inhibited through cell growth and differentiation in hydrogels. Also, the biophysical composition of the hydrogel itself does not appear to adversely affect the dorsal/ventral NPC developmental pathway. This is in opposition to primarily Matrigel-based hydrogel scaffolds that can alter downstream neuronal subtype composition through inherent signalling molecule content (Shimada *et al.*, 2012; Ni *et al.*, 2013).

When observing markers of neuronal maturation such as *β-III-TUBULIN*; 2D and 3D growth environments appear to elicit comparable levels of this marker at early time points of neural differentiation (Day 14-20). However, this level drops to significantly lower levels in both 3D Dorsal and Ventral cultures relative to 2D inductions for the remainder of neural maturation. This may be due to either an inhibition of maturation of post-mitotic neuronal cells within the 3D environments or a possible inhibition of the NPC-to-neuronal transition event, leading to a retention of immature NPC characteristics. This 2D and 3D segregation is less defined when looking at the axonal marker *TAU*, in which only 3D Ventral cultures show lower expression levels by later timepoints of maturation. Interestingly, the pre- and post-synaptic markers *SYN* and *PSD95* display early peaks within 3D Ventral cultures (Day 14-20) that dissipate over the remainder of neural maturation to levels below those recorded in 2D culture. This may be indicative of an initial acceleration of ventral neural differentiation in 3D culture that is not maintained for the time course of differentiation and maturation. This effect, however, is limited to ventrally-patterned 3D cultures as no such early peak (or indeed elevation) of neuronal or synaptic markers is observed in 3D Dorsal neural cultures at any assayed time point. It may then be possible that these 3D hydrogel environments may elicit both enhancing and diminishing effects on hiPSC-derived

neural maturation dependant on the early patterning and neural tube regionalisation of the starting NPC pool.

As with NPC patterning specificity, dorsal- and ventral-derived forebrain localisation markers are also preserved within 3D hydrogel environments. The early- and late-born cortical markers *REELIN*, *TBR1*, *CTIP2* and *SATB2* are all present in 2D and 3D Dorsal cultures. *REELIN* and *TBR1* expression levels however, were lower in 3D Dorsal cultures compared to 2D differentiation, whereas *CTIP2* and *SATB2* (late born cortical markers) showed higher expression profiles. Limited expression of these dorsal markers was seen in either 2D or 3D Ventral neural cultures. The segregation of these dorsal-associated cortical markers between the dorsal and ventral patterned cultures is also confirmed through regression analysis of each pattern of marker expression for the whole time-course of differentiation. It is interesting to note that the raw patterning segregation of these dorsal regionalisation markers is preserved within 3D dorsally-patterned cultures, but that differences in early- and late-born cortical markers are apparent. It is possible that the enhanced upregulation of *CTIP2* and *SATB2* within 3D microenvironments may be due to biophysical interactions with the hydrogel itself, or a possible acceleration of late-born cortical neurogenesis at the expense of prolonged early-born cortical cell identity (*REELIN* and *TBR1*). In either case, the patterning of dorsal and ventral neural cell localisation identity appears preserved within this 3D hydrogel system.

Excitatory and inhibitory neuronal subtype patterning was also shown to be unaffected by differentiation within the hydrogel environment through robust regression analysis of marker gene expression patterns between all of the growth conditions. The excitatory neuronal subtype marker *vGLUT1* is highly expressed in 2D Dorsal neural culture but shows more restricted expression within neural cells in 3D Dorsal culture. Even so, the level of expression in dorsally-patterned neural cultures is still higher than that observed under ventral patterning, showing the preservation of excitatory/dorsal neuronal identity. This is also reflected in the upregulation of the GABAergic ventral neuronal marker *GAD67*, which shows steady upregulation in 2D Ventral cultures during maturation. *GAD67* expression is also observed within 3D Ventral neural cultures although, as with *vGLUT1*, to a lower level than is recorded from 2D planar culture. This is much more apparent with the GABAergic marker *GAT1* which shows significantly lower levels of expression in 3D Ventral cultures compared to 2D. A possible explanation of this finding may be related to ideas discussed above, by which the 3D environment appears to be having an inhibitory effect on

the rate of neural maturation. This may be due to an interaction with the biomaterial itself, or possibly an issue related to relative cell densities between 2D and 3D environments. Cell seeding densities within this study were selected on the basis of maximising construct size without generating scaffolds that would have a negative impact on cell viability through restrictive diffusion of oxygen and nutrients. However, a truer *in vivo*-like developmental environment would require higher cell densities to be more neural tissue-like, which may positively impact neural cell differentiation. To overcome this, other studies have utilised restricted construct size to counterbalance cell death from high cell densities (Frampton *et al.*, 2011), cultured 3D constructs within perfusion devices to keep pace with the metabolic demands of encapsulated cells (Cullen *et al.*, 2007), and generated 3D bioprinted constructs that enable higher surface area exchange of oxygen and nutrients (Gu *et al.*, 2017).

This restriction of maturation within 3D environments was also observed when looking at molecular markers of neurotransmitter sensitivity. By later time points of neural differentiation and maturation, cells cultured within both 3D environments displayed generally lower levels of the neurotransmitter receptor markers *$GABA_AR1$*, *$GABA_BR1$*, *NMDAR1*, and *AMPAR1*. Although this restriction was most pronounced in the expression profiles of *$GABA_AR1$* and *NMDAR1*. Interestingly, after 20 days of differentiation, 3D Ventral cultures displayed the same strong peak of expression for *NMDAR1*, *$GABA_BR1$* and *AMPAR1* as was seen for *SYN* and *PSD95* expression. It is surprising that both pre- and post-synaptic machinery transcripts seem to be preferentially upregulated in 3D Ventral environments rather than 3D Dorsal ones early in neural differentiation. This initial burst of expression may be related to an accelerated differentiation profile, before cessation during more protracted timelines of differentiation, and one that appears specific to ventrally-patterned NPCs within 3D hydrogels. However, this does not hold true for markers of neurotransmitter generation and uptake (*GAD67* and *GAT1*) which conversely show more restricted expression in 3D Ventral environments than 2D Ventral counterparts. It may be concluded therefore that 3D encapsulation in biomaterial scaffolds can have differential effects on separate elements of neural differentiation and maturation, rather than complete enhancement of all neural differentiation markers. This effect also appears dependent on the type of patterned NPC pool, as ventrally- and dorsally-patterned precursors responded differently to the same 3D environment.

Finally, the generation of astrocytic glial lineages does appear to be influenced through 3D hydrogel encapsulation compared to planar culture. Both 3D Dorsal and Ventral neural cell types displayed higher levels of the astrocyte marker *GFAP* by Day 60 of differentiation than is seen in either 2D culture. It is also possible that the 3D environment elicits a pro-glial environment for NPC differentiation, or may even accelerate intrinsic developmental timings that regulate the gliogenesis *in vivo*.

In conclusion, we have shown that 3D collagen hydrogel environments are conducive to neural cell neuritogenesis of encapsulated hiPSC-derived NPCs. Neural differentiation and maturation markers are expressed during this 3D differentiation, but in many cases, are directly comparable or reduced relative to 2D planar differentiation. 3D Ventral differentiation did appear to show accelerated markers of neural maturation through early expression spikes of canonical neuronal and synaptic markers, that were not seen in 3D Dorsal culture. From these data, it appears as though differentially patterned pools of NPCs demonstrate differing effects on gene expression from growth in the same 3D environment. This would impact the formation of neural tissue constructs derived from dorsal and ventral lineages within these 3D scaffolds, with such discrepancies influencing the formation of any representative native tissue cellular composition.

The lack of sustained expression of maturation markers observed may be due in part to lower cell densities within the 3D culture system resulting in reduced overall cell-cell contact number than when compared to dense 2D neural cultures. Thus, high cell densities may be key to recapitulate and enhance neural differentiation in 3D but must overcome limitations in maintaining cell viability through restricted diffusion of oxygen and nutrients. Therefore, methods of generating bioprinted neural-tissue constructs (using biomaterials utilised in Chapters 2 and 4) that can maintain high neural cell densities, will be the focus of the next chapter.

4.4.1 Summary of Chapter Findings

- hiPSC-derived NPCs differentiating within 3D collagen type I scaffolds undergo neuritogenesis in all three axes throughout the hydrogel over 60 days of differentiation.

- 3D encapsulated neural cultures express protein markers of post-mitotic neuronal generation as well as pre-synaptic machinery.
- Neural differentiation in 3D collagen hydrogel scaffolds does not affect the efficacy of patterning morphogens to generate dorsal- and ventral-derived neural lineages.
- Enhanced NPC marker expression was seen within ventrally-patterned neural cells but not with dorsally-patterned neural cultures when encapsulated in 3D hydrogel environments.
- 3D Ventral cultures show early peak expression of neuronal and synaptic markers significantly above the levels of 2D cultures and 3D Dorsal neural cultures.
- By later time points of differentiation: neuronal, axonal and synaptic marker expression are lower in 3D microenvironments than in 2D planar culture, suggesting an inhibition of maturation.
- Excitatory and inhibitory neuronal subtype marker expression are preserved in dorsal/ventral patterning in 3D environments, but with lower levels of expression than is seen in planar differentiation.
- Dorsal cortical localisation markers are observed in both 2D and 3D Dorsal neural cultures. In 3D scaffolds however, early-cortical markers (*REELIN, TBR1*) display expression profiles lower than in 2D differentiation, and late-cortical markers (*CTIP2, SATB2*) show enhanced expression relative to 2D Dorsal cultures.
- The ionotropic GABA-receptor *$GABA_AR1$* shows limited expression in both 3D Dorsal and 3D Ventral neural cultures.
- 3D Ventral neural cultures show significantly high expression spikes of *$GABA_BR1$*, *NMDAR1* and *AMPAR1* neurotransmitter receptor subunits, not seen in 3D Dorsal differentiation. By later time points of maturation, these markers tend to show lower expression in 3D cultures compared to 2D differentiation.
- Neuronal generation is not limited within 3D hydrogel scaffolds, but functional maturation does appear to be restricted under these experimental conditions.
- Astrocytic gliogenesis is enhanced in 3D differentiation environments compared to 2D cultures.

4.4.2 Acknowledgements

We would like to acknowledge and thank Dr. Serena Duchi (Dept. of Surgery, University of Melbourne) for her assistance in confocal microscopy imaging. We are also indebted to Prof. Raymond Boston (Dept of Medicine, University of Melbourne) for his aid in generating the robust regression analysis pipeline for the gene expression data displayed in this chapter.

4.5 Appendix

4.5.1 Robust Regression Analysis Output Tables

To further statistically verify the segregation of neural subtype patterning markers between dorsally-patterned and ventrally-patterned cultures (in both 2D and 3D) we undertook robust regression analysis for the pattern and magnitude of each subtype marker gene (Sections 3.3.4, 4.3.4, and 4.3.5). The raw output statistical tables for each pair-wise comparison and each gene marker are displayed in the figures below.

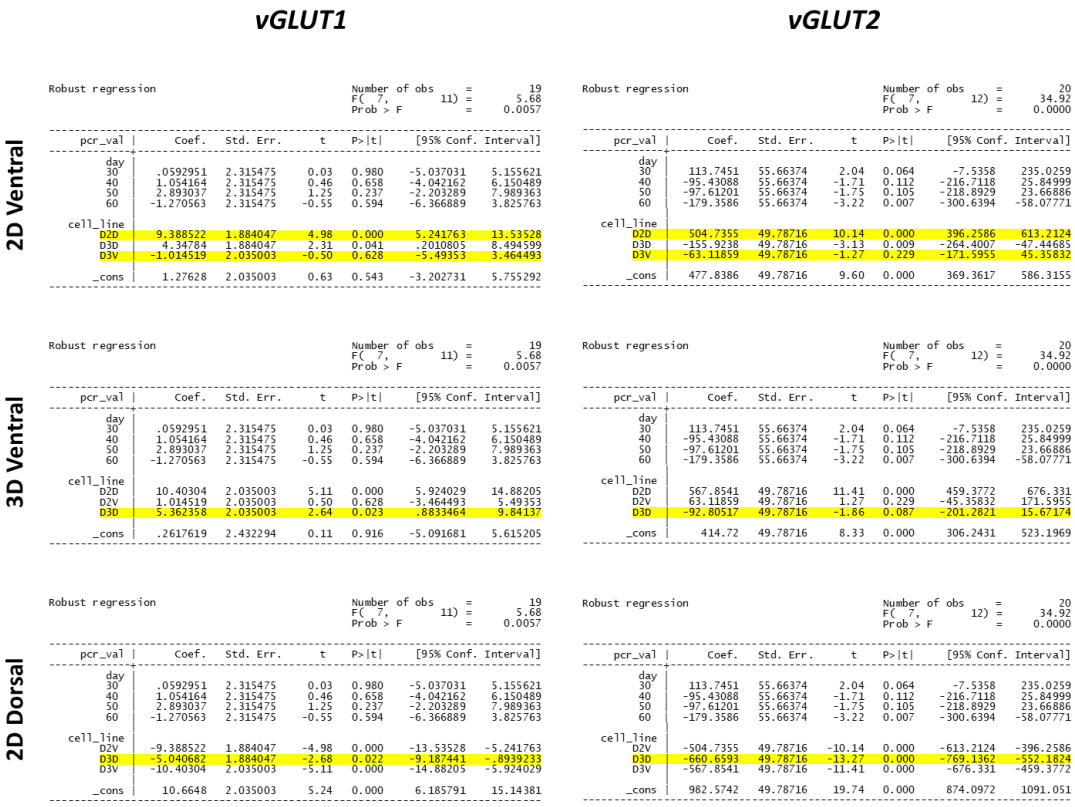

Appendix Fig 4-11: Robust regression analysis output tables for glutamatergic (dorsal) neuronal cell identity genes *vGLUT1* and *vGLUT2*. Data set being compared to in each table is displayed on the left-hand side. Highlighted rows contain outputs used in compiled results tables in Chapters 3 and 4.

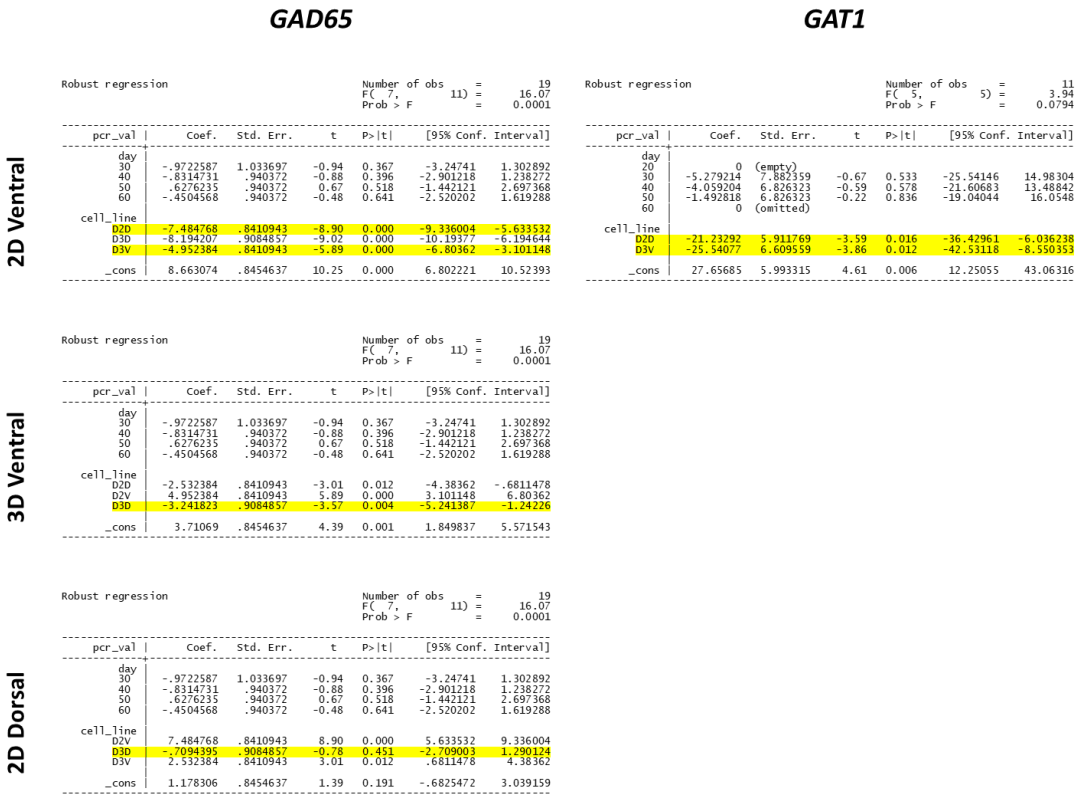

Appendix Fig 4-12: Robust regression analysis output tables for GABA-ergic (ventral) neuronal cell identity genes *GAD67* and *GAT1*. Data set being compared to in each table is displayed on the left-hand side. Highlighted rows contain outputs used in compiled results tables in Chapters 3 and 4.

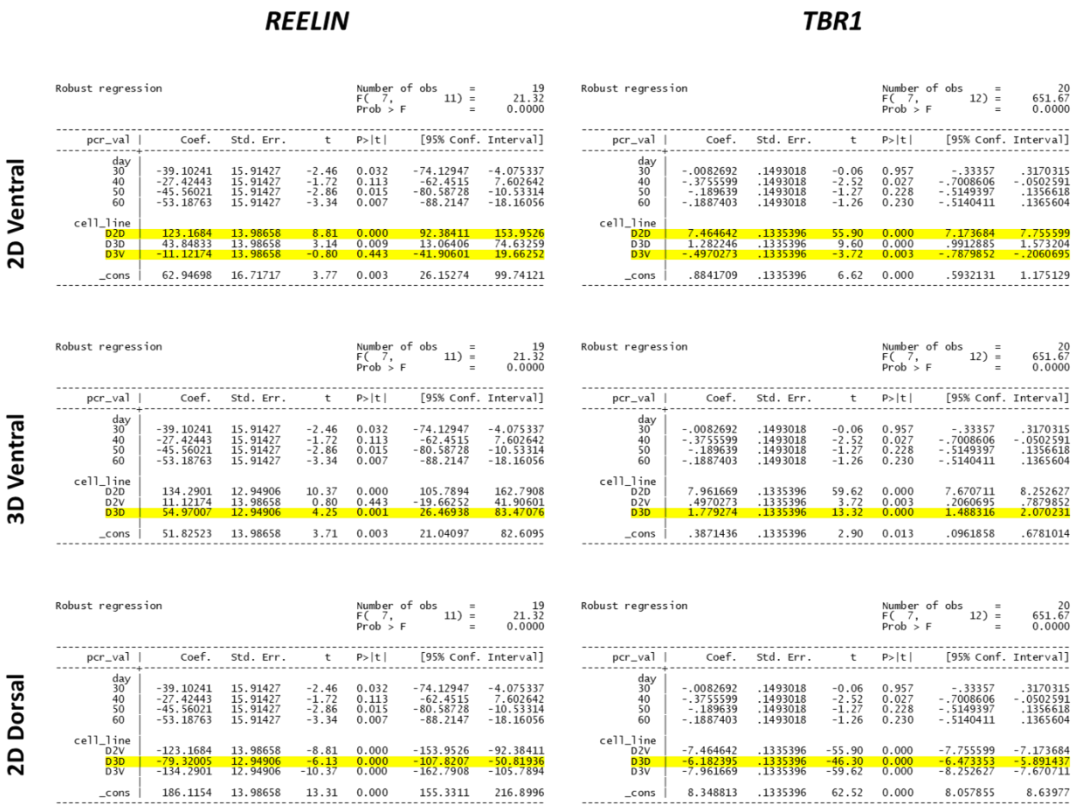

Appendix Fig 4-13: Robust regression analysis output tables for early cortical-specific regionalisation (dorsal) neuronal cell identity genes *REELIN* and *TBR1*. Data set being compared to in each table is displayed on the left-hand side. Highlighted rows contain outputs used in compiled results tables in Chapters 3 and 4.

CTIP2 ***SATB2***

2D Ventral

Robust regression — Number of obs = 20; F(7, 12) = 45.56; Prob > F = 0.0000

pcr_val	Coef.	Std. Err.	t	P>|t|	[95% Conf.	Interval]
day						
30	-.8436695	.3411974	-2.47	0.029	-1.587075	-.1002641
40	-.5682955	.3411974	-1.67	0.122	-1.311701	.1751099
50	-.7567948	.3411974	-2.22	0.047	-1.5002	-.0133895
60	-.7089576	.3411974	-2.08	0.060	-1.452363	.0344477
cell_line						
D2D	4.036067	.3051763	13.23	0.000	3.371145	4.700989
D3D	3.450851	.3051763	11.31	0.000	2.785929	4.115773
D3V	-.0797032	.3051763	-0.26	0.798	-.7446251	.5852188
_cons	1.092048	.3051763	3.58	0.004	.427126	1.75697

Robust regression — Number of obs = 20; F(7, 12) = 81.47; Prob > F = 0.0000

pcr_val	Coef.	Std. Err.	t	P>|t|	[95% Conf.	Interval]
day						
30	-.3272918	.3913078	-0.84	0.419	-1.179878	.5252947
40	-.7034486	.3913078	-1.80	0.097	-1.556035	.149138
50	-.9349984	.3913078	-2.39	0.034	-1.787585	-.0824119
60	-.8384204	.3913078	-2.14	0.053	-1.691007	.0141661
cell_line						
D2D	1.471246	.3499964	4.20	0.001	.7086698	2.233823
D3D	7.084743	.3499964	20.24	0.000	6.322166	7.84732
D3V	-.0893053	.3499964	-0.26	0.803	-.8518819	.6732713
_cons	.8865298	.3499964	2.53	0.026	.1239532	1.649106

3D Ventral

Robust regression — Number of obs = 20; F(7, 12) = 45.56; Prob > F = 0.0000

pcr_val	Coef.	Std. Err.	t	P>|t|	[95% Conf.	Interval]
day						
30	-.8436695	.3411974	-2.47	0.029	-1.587075	-.1002641
40	-.5682955	.3411974	-1.67	0.122	-1.311701	.1751099
50	-.7567948	.3411974	-2.22	0.047	-1.5002	-.0133895
60	-.7089576	.3411974	-2.08	0.060	-1.452363	.0344477
cell_line						
D2D	4.115771	.3051763	13.49	0.000	3.450849	4.780693
D2V	.0797032	.3051763	0.26	0.798	-.5852188	.7446251
D3D	3.530554	.3051763	11.57	0.000	2.865632	4.195476
_cons	1.012345	.3051763	3.32	0.006	.3474228	1.677267

Robust regression — Number of obs = 20; F(7, 12) = 81.47; Prob > F = 0.0000

pcr_val	Coef.	Std. Err.	t	P>|t|	[95% Conf.	Interval]
day						
30	-.3272918	.3913078	-0.84	0.419	-1.179878	.5252947
40	-.7034486	.3913078	-1.80	0.097	-1.556035	.149138
50	-.9349984	.3913078	-2.39	0.034	-1.787585	-.0824119
60	-.8384204	.3913078	-2.14	0.053	-1.691007	.0141661
cell_line						
D2D	1.560552	.3499964	4.46	0.001	.7979751	2.323128
D2V	.0893053	.3499964	0.26	0.803	-.6732713	.8518819
D3D	7.174048	.3499964	20.50	0.000	6.411472	7.936625
_cons	.7972245	.3499964	2.28	0.042	.0346479	1.559801

Robust regression — Number of obs = 20; F(7, 12) = 45.56; Prob > F = 0.0000

pcr_val	Coef.	Std. Err.	t	P>|t|	[95% Conf.	Interval]
day						
30	-.8436695	.3411974	-2.47	0.029	-1.587075	-.1002641
40	-.5682955	.3411974	-1.67	0.122	-1.311701	.1751099
50	-.7567948	.3411974	-2.22	0.047	-1.5002	-.0133895
60	-.7089576	.3411974	-2.08	0.060	-1.452363	.0344477
cell_line						
D2V	-4.036067	.3051763	-13.23	0.000	-4.700989	-3.371145
D3D	-.5852166	.3051763	-1.92	0.079	-1.250139	.0797054
D3V	-4.115771	.3051763	-13.49	0.000	-4.780693	-3.450849
_cons	5.128115	.3051763	16.80	0.000	4.463193	5.793037

Robust regression — Number of obs = 20; F(7, 12) = 81.47; Prob > F = 0.0000

pcr_val	Coef.	Std. Err.	t	P>|t|	[95% Conf.	Interval]
day						
30	-.3272918	.3913078	-0.84	0.419	-1.179878	.5252947
40	-.7034486	.3913078	-1.80	0.097	-1.556035	.149138
50	-.9349984	.3913078	-2.39	0.034	-1.787585	-.0824119
60	-.8384204	.3913078	-2.14	0.053	-1.691007	.0141661
cell_line						
D2V	-1.471246	.3499964	-4.20	0.001	-2.233823	-.7086698
D3D	5.613497	.3499964	16.04	0.000	4.85092	6.376073
D3V	-1.560552	.3499964	-4.46	0.001	-2.323128	-.7979751
_cons	2.357776	.3499964	6.74	0.000	1.5952	3.120353

Appendix Fig 4-14: Robust regression analysis output tables for late-born cortical-specific regionalisation (dorsal) neuronal cell identity genes *CTIP2* and *SATB2*. Data set being compared to in each table is displayed on the left-hand side. Highlighted rows contain outputs used in compiled results tables in Chapters 3 and 4.

Chapter 5: Development of Bioinks for Neural Tissue Bioprinting

5.1 Introduction

Many potential advantages of *in vitro* neural tissue development within 3D culture systems have been outlined above (Chapter 4) and are well documented across other sources (LaPlaca *et al.*, 2010). The construction of natural or synthetic cellular microenvironments, such as those within hydrogel scaffolds, allow for the recapitulation of *in vivo*-like spatial geometry, cell-cell communication and cell-matrix interactions. However, the use of simple hydrogel encapsulation of neural cells has implicit limitations. Cell densities within the constructs must not exceed the rate of oxygen and nutrient diffusion available, and therefore the more "tissue-representative" the cellular content, the smaller the size of the construct must be to avoid cell death. As is seen in Chapter 4, this critical cell density may be necessary for adequate neural cell maturation and development of function. Certain techniques have been utilised to overcome this limiting factor through the use of perfusion devices (or so-called "brain-on-a-chip" devices) by which to maximise the available concentrations of nutrients and the removal of metabolic waste products (Cullen *et al.*, 2007; Pamies, Hartung and Hogberg, 2014; Moreno *et al.*, 2015).

As well as issues with controlling nutrient diffusion, the cytoarchitecture within hydrogel scaffolds is difficult to modify manually, with the cells, in many cases, distributed evenly throughout the construct prior to gelation. Therefore, controlled deposition or assembly of different cellular pools is extremely difficult in basic encapsulation methods. Neural organoid culture can show incredible recapitulation of early-neurological structures derived from intrinsic self-organisation, and do so strongly when embedded within hydrogel scaffolds (Lancaster *et al.*, 2013; Kelava and Lancaster, 2016), however, the same issue of low diffusion rates of nutrients (even within bioreactors) leads to the formation of necrotic cores and inherent size limitations of each organoid.

To retain the intrinsic advantages of 3D neural cell culture, but to overcome the disadvantages of limited nutrient diffusion (or small construct size) and tighter control over

cell subtype segregation and placement, many research projects are now focused on the development of additive fabrication technologies to generate neural tissue *in vitro* (Thomas and Willerth, 2017; Knowlton *et al.*, 2018). This process, termed "bioprinting", is based around the use of 3D-printing technology by which to accurately generate 3D cytocompatible tissue-like structures in a controlled temporo-spatial manner.

The scaffolds used for such bioprinting techniques are termed "bioinks", which may also be a class of hydrogels, but are distinguished through the bioink's ability to form and retain a filamentous morphology during the printing process. The ability to retain such shape fidelity allows for the design of custom topologies and complex structural elements. Unlike simple hydrogel encapsulation, which may only form a solid block of tissue-like scaffold, bioprinting can generate complicated geometries, may be formed from multiple bioinks, and contain structural elements to enhance the construct's tissue-like properties (Kang *et al.*, 2016). Certain aspects of cell positioning and placement within simple hydrogel *in vitro* neurological models, such as the layering of the cortex using hydrogel moulds and microfluidic devices, have been elegantly accomplished (Kunze *et al.*, 2011; Odawara, Gotoh and Suzuki, 2013). However, the level of tailoring of construct parameters through these methods suffers from low resolution and require long periods of development. Scaffold designs for bioprinting, on the other hand, can be developed *in silico* and re-designed extremely quickly. An example of an *in silico* designed output and a 3D-printed product can be seen in Fig 5-1.

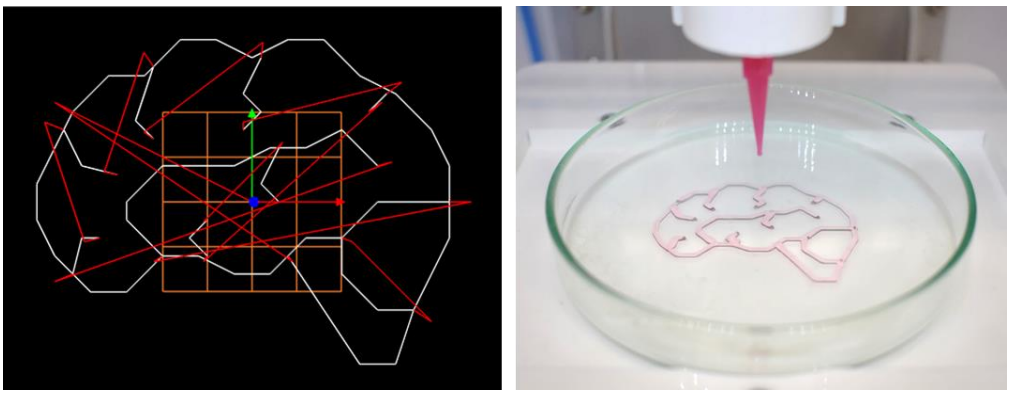

Fig 5-1: An example of an *in silico* 3D-printable design (*left*) that can generate complex structures from hydrogels through 3D printing technology (*right*).

By creating specific geometries within the bioprinted construct, it is also possible to generate patterns of pseudovasculature that not only allow for improved access of encapsulated cells to oxygen and nutrients, but by doing so, allow for the scaling-up of hydrogel scaffolds into sizes relevant for human tissue research or regenerative therapy (Kang *et al.*, 2016). The use of bioprinting therefore combines the advantages of basic 3D hydrogel culture with the ability to generate larger and more cell-dense *in vitro* models.

A critical aspect of any bioprinting methodology is the selection (and potential modification) of bioinks to make them amenable to the 3D-printing extrusion process as well as being tolerated by encapsulated neural cells. Cytocompatibility is of paramount importance when generating 3D cell-laden constructs and so not only in the base state must a bioink be non-cytotoxic to cells, but any associated cross-linking gelation processes must also be non-damaging (Knowlton *et al.*, 2018).

Methacrylate groups are a common additive to polymer backbones as a way of inducing controlled covalent crosslinking and gelation of hydrogels. This process predominantly utilises photoinitiator compounds that generate free radicals under exposure to ultraviolet (UV) light that consequently react and chemically-bond adjacent methacrylate moieties. Such crosslinking has been used extensively with the biomaterials methacrylated gelatin (GelMA) (Thomas and Willerth, 2017) and hyaluronic acid (HAMA) (Z.-N. Zhang *et al.*, 2016). Hydroxyphenylpropionic acid (HPA) conjugated gelatin (GelHPA) also crosslinks in the presence of free radicals, but rather than UV-activated photoinitiators, can be catalysed through the reaction products of hydrogen peroxide and horse radish peroxidase (M. Hu *et al.*, 2009). Care must be taken however when optimising the exposure of cell-laden bioinks to UV irradiation and free radical generation as both are known to have pronounced cytotoxic effects (Williams *et al.*, 2005; Mironi-Harpaz *et al.*, 2012). Bioinks derived from non-mammalian polysaccharides also have precedent as scaffolds for bioprinted neural tissue engineering, with ionic crosslinking either following or as a continuous process during bioprinting (Lozano *et al.*, 2015; Gu *et al.*, 2017), with no discernible negative effect on encapsulated cell types.

As well as the cytocompatibility of biomaterials for 3D tissue-engineering, bioinks should display an array of physical characteristics, that in broad terms, combine to define the “printability” of the material. Multiple methodologies of biomaterial printing have shown promise in generating cell-laden biomaterial scaffolds, although the main three techniques are inkjet-based printing, laser-assisted printing, and extrusion printing

(Knowlton *et al.*, 2018). By far the most common however, is extrusion-based printing. This involves the mixing of cells and bioink prior to deposition through pressurised nozzles or needles. This fabrication technique allows for the rapid and large-volume deposition of cell-laden and/or acellular biomaterial scaffolds. For extrusion-based bioprinting to be successful, the printability of bioinks is dependent on various material characteristics. The physical traits necessary for the generation of extrudable bioink formulations include; appropriate viscosity; non-Newtonian shear-thinning or thixotropic qualities; and retention of filament fidelity prior to crosslinking.

The viscosity of bioinks allows for the retention of design fidelity following extrusion from the nozzle. Therefore, extrudable bioinks must have viscosities that are high enough to maintain a free-standing shape, as well as being necessary for multiple layers to be printed and stacked on top of each other to generate 3D topographies. Candidate bioinks with too low a viscosity will lose shape resolution and be unable to form true 3D scaffolds. Another desired trait of extrudable-bioinks is for the biomaterial to display shear-thinning or thixotropic qualities. This is a non-Newtonian pseudoplastic behaviour by which viscosity decreases under shear strain. In essence, this can be seen as transitioning the bioink to a more liquid-like state during the pressure-driven extrusion process, but after deposition, rapidly regains highly viscous characteristics. A bioink with high degrees of shear-thinning will result in lower levels of shear stress being generated under extrusion, which is advantageous for cell-laden bioinks, where high degrees of shear stress can have negative effects on cell survivability (Blaeser *et al.*, 2016). Bioink compositions can also be modified to alter properties of viscosity; such as the addition of glycerol to modify the extrusion characteristics (Kang *et al.*, 2016); as well as controlling the temperature of extrusion apparatus which can directly affect bioink printability (Chung *et al.*, 2013).

This Chapter will focus on the development of bioinks and bioprinting techniques that allow for extrusion-based bioprinting of neural cells. The biomaterials used as a basis for these bioinks will be those assayed previously in Chapters 2 and 4, namely alginate and collagen type I. From Chapter 2 we demonstrated that neural cells encapsulated in alginate scaffolds retain high cell viability, but restricted neuritogenesis, whereas collagen type I hydrogels were conducive to neuritogenesis and hiPSC-derived neural differentiation (Chapter 2 and 4). This section of research will explore methods of utilising alginate within acellular components of a neural construct, with collagen forming the cell-laden and neuritogenic-conducive elements of the bioprinted scaffolds. After preliminary

development of biomaterial formulations, we also investigate the use of coaxial bioprinting as a mechanism of segregating structural and cell-laden components of the bioink scaffold. This mechanism of coaxial bioprinting is based on previously reported hand-held bioprinting of precursor cartilage tissue (Duchi *et al.*, 2017).

This Chapter therefore aims to combine the findings from all previous chapters and to derive a usable neural-conducive bio-printable scaffold system by which to generate neural-tissue constructs from *in silico* designs.

5.2 Materials and Methods

5.2.1 Preparation of Bioinks

The biomaterials used in this chapter are; Sodium alginate (Sigma); Collagen Type I (Millipore); Hyaluronic acid (HA, Xi'an Rongsheng Biotechnology); Gelatin from bovine skin (Sigma); and CELLINK Start (CELLINK) as a "gold standard" extrusion printable material. For acellular extrusion assays, all dry-mass biomaterials were reconstituted in distilled water with percentages denoting w/v measurements. Samples were kept at 37^{o}C until fully dissolved and mixed through trituration to ensure even dispersal. Fully dissolved materials were stored at 4^{o}C until used. Acellular collagen bioinks were composed of a 0.4mg/ml final concentration derived from a commercially available stock solution, working concentrations were generated through dilution in distilled water.

5.2.2 Bioprinting

Bioprinting design G-Code was written *de novo* in a basic word processing software and visualised using an online G-Code simulator (https://nraynaud.github.io/webgcode). All bioprinting utilised the INKREDIBLE+ printer system from CELLINK (Fig 5-2). Bioinks were loaded into 3cc dispensing cartridges and extruded through a 25-gauge (0.25mm internal diameter) nozzle tip (Nordson EFD).

Fig 5-2: Image of the INKREDIBLE+ Bioprinter utilised for all bioprinting experimental work outlined in this chapter.

Extrusion pressure for each bioink formulation was adjusted to maximise a smooth extrusion of material. Extrusion pressures varied from 5kPa for low viscosity materials up to 140kPa for highly viscous bioinks. All materials were printed at room temperature, with the bioinks allowed to equilibrate to room temperature prior to printing. The printing substrate surfaces used were 25mm x 75mm standard microscope slides, as a simple way to handle and image the printed structures. All macroscopic images were captured with a Nikon D3400 DSLR camera and processed in ImageJ software (NIH).

Shape fidelity assays were qualitative assessments of each bioink to recapitulate an *in silico* spiral design (20mm x 16mm) and therefore a measure of the viscosity and bio-printable qualities of each bioink. String test assays were used as an indirect measure of printability by examining not only the base bioink viscosity, but also the cohesive nature of the material relating to shape fidelity (Schuurman *et al.*, 2013). Biomaterials that formed a droplet under extrusion were said to have failed the test, whereas materials that formed strings over 10mm long during extrusion were more likely to generate better formed printed constructs. The layer stacking test is another measure of a biomaterial's ability to stack upon itself following extrusion, as a precursor to fully realised multi-layer 3D scaffold printing. Bioinks that failed to adequately stack layered filaments of a 15mm x 15mm square were discounted from further testing.

5.2.3 Coaxial Bioprinting

For coaxial bioprinting, a specialised coaxial extrusion nozzle, previously developed for cartilage tissue engineering (Cornock *et al.*, 2014; O'Connell *et al.*, 2016; Duchi *et al.*, 2017) was utilised. This nozzle was attached to two of the 3cc bioink cartridges used above, and was then fastened to the INKREDIBLE+ print stage. An image of the coaxial system used is seen in Fig 5-8.

For the shell material, a mixture of alginate (3%): gelatin (5%) was found in mono-axial tests to generate a bioink with acceptable shape fidelity, string printability and filament stacking attributes under acceptable extrusion pressures. Both components were mixed together vigorously within a 5ml syringe (BD Biosciences) attached to the 3cc bioink cartridge, after warming to 37^{o}C to minimise viscosity. The cell laden core material was composed of final concentrations of 0.4mg/ml collagen type I (neutralised with 0.23x of the added collagen volume of 0.1M NaOH, Sigma), 1% (w/v) HA, and 1x HEPES (20mM HEPES

[Sigma], 150mM NaCl [Sigma] pH 7.4). The remaining volume was composed of growth media containing neural cells. Final cell density within the core bioink was $2x10^6$ cells/ml. For acellular core/shell testing, the cells were replaced with fluorescent red latex beads (0.5µm) (Sigma) used at 10µl per ml of core material, and with DMEM (Gibco) used in place of growth media. All manipulation of materials was done under aseptic conditions in tissue-culture facilities and sterile laminar flow hoods. Extrusion pressures for core and shell material components were 12kPa and 50kPa respectively.

The crosslinking of alginate components of the shell material was done post-print with a sterile 200mM $CaCl_2$ solution (Sigma). Scaffolds were left to crosslink at room temperature for 3 minutes, prior to scaffold transfer to 6-well tissue culture plates with 3ml of growth media per well. Cells were then cultured at 37°C and 5% CO_2 in standard cell culture incubators. Differentiation within the printed scaffolds was monitored over 7 days, with differentiation media changed every 2 days.

5.2.4 Cell Culture

The murine NSC-34 neural cell line (obtained courtesy of the Intelligent Polymer Research Institute) was used for the assessment of cell survival and neural differentiation within bioprinted structures generated in this chapter. The short time-frame of induced differentiation enabled rapid assessment of the cell-laden bioprinted structures. Briefly, cells were cultured in a proliferation media composed of DMEM (Gibco), 10% FBS (Gibco), 2mM L-Glutamine (Gibco), 100U/ml Penicillin and 100µg/ml Streptomycin (Gibco). Cells were cultured in 75cm^2 tissue culture coated flasks and were passaged using a 0.025% Trypsin Dissociation Buffer for 5 minutes at 37°C. Differentiation of NSC-34s was triggered using a differentiation media composed of DMEM (Gibco), 2% Horse Serum (Gibco), 2mM L-Glutamine (Gibco), 100U/ml Penicillin and 100µg/ml Streptomycin (Gibco),

For cell harvesting prior to addition to the core bioink, cells were harvested through trypsin dissociation (as above) and pelleted at 400x*g* centrifugation for 5 minutes. Cells were resuspended in 1ml proliferation media, with an aliquot utilised for manual cell count estimation using trypan blue dye (Thermo Fisher Scientific) on a haemocytometer.

5.2.5 Viability Assay

For assays of cell viability, the fluorescent dyes Calcein-AM (Life Technologies) and Ethidium Homodimer (Life Technologies) were used to establish the proportion of living and dead cells respectively, within printed cell-laden scaffolds. Briefly, media around the constructs was exchanged for DMEM containing 1µM Calcein-AM and 1µM Ethidium Homodimer. The constructs were left to incubate at 37^{o}C and 5% CO_2 for 1 hour. The dye-laden media was then exchanged for differentiation media prior to imaging.

5.2.6 Fluorescent and Live Cell Imaging

Live cell imaging was achieved through visualisation on an EVOS XL Cell Imaging System (Thermo Fisher Scientific), with images processed with ImageJ software (NIH).

Imaging acquisition of fluorescent bead-loaded core constructs and fluorescently-labelled cell viability assays was performed on an Olympus IX70 wide field microscope with Spot RT Slider digital camera and Spot Advanced software, version 4.8 (Diagnostic Instruments).

5.3 Results

5.3.1 Assessment of Unmodified Alginate and Collagen Hydrogels as Bioinks

Previous work has shown that neural cells encapsulated within collagen hydrogels of low mass content, will undergo extensive neuritogenesis during differentiation (Chapters 2 and 4). Cell-laden alginate hydrogel scaffolds retain many cytocompatible characteristics, display storage moduli comparable to native neural tissue, but are non-conducive to neurite extensions under assayed conditions (Chapter 2). However, the generation of a multimodal neural tissue construct whereby the support structure is supplied by one biomaterial and the cell-laden component by another, would allow for more complex scaffolds to be formed.

Using unmodified alginate and collagen in the concentrations known to be cytocompatible with encapsulated neural differentiation in cast-gel scaffolds, these biomaterial formulations were assayed for their printability in comparison to a commercially available 3D printable water-soluble ink.

Compared to the programmed print design, both alginate and collagen candidate bioinks at these formulations failed to maintain any filament integrity during the printing process (Fig 5-3). Each biomaterial displayed a viscosity similar to that of water, and as such, after printing were unable to maintain a filamentous shape, and instead combined into an amorphous pool of biomaterial. When compared to the Cellink Start material, which demonstrated high pattern fidelity and retention of filament shape, these basic alginate and collagen formulations would be unsuitable for the generation of free-standing neural tissue scaffolds.

Under extrusion from the bioprinting nozzle, both the alginate and collagen hydrogels formed only droplets, whereas the viscous cohesive nature of the Cellink Start generated a flowing “string” that reached over 10mm in length. This string test has been used previously as a qualitative measure of a bioink’s propensity to form free-standing filamentous structures (Schuurman *et al.*, 2013). Under these assay conditions, again the alginate and collagen formulations evaluated here would fail to demonstrate appropriate printability markers as usable bioinks.

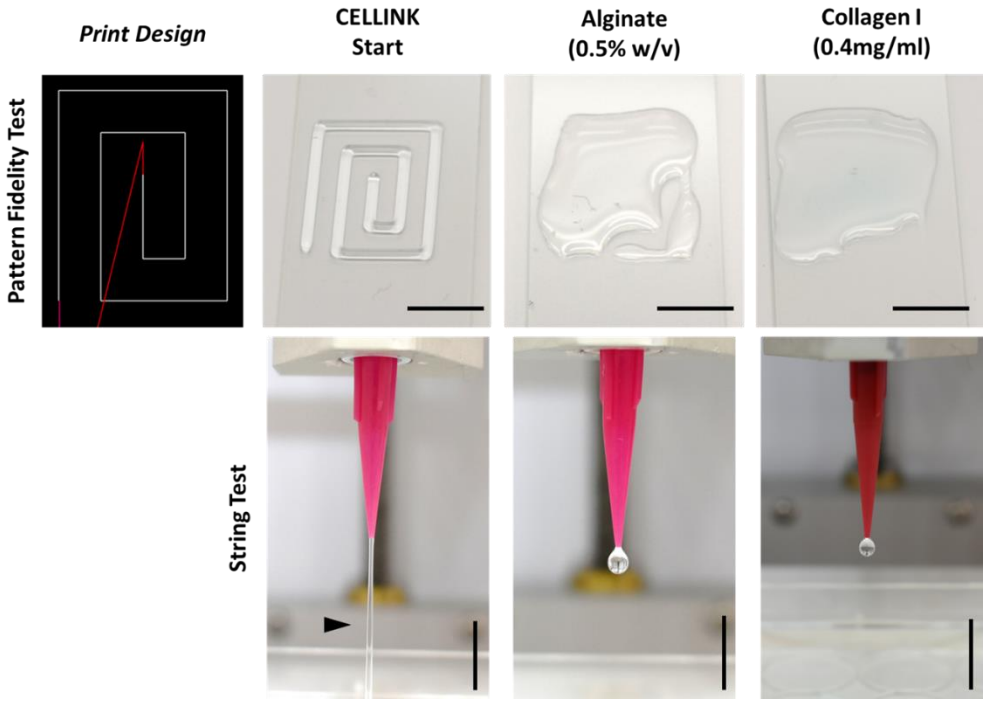

Fig 5-3: Pattern fidelity and string test assays of collagen and alginate bioinks at low concentrations. When compared to the Cellink Start material, both alginate and collagen hydrogels fail to retain the printed filamentous design or generate flowing "strings" under extrusion (black arrow head). Scale bars represent 10mm.

As well as shape fidelity and string formation, another useful assay is the demonstration of multi-layer stacking properties of bioinks.

An *in silico* designed 15mm x 15mm four-layered square was used as a basic assay of filament stacking properties. The Cellink Start ink formed a strong recapitulation of the programmed design shape, and demonstrated the ability to stack filaments in ordered layers (Fig 5-4). However, as with the pattern fidelity assays, both collagen and alginate hydrogels at these concentrations failed to form not only the basic shape pattern, but could not stack on themselves vertically, akin to other non-viscous fluids (Fig 5-4).

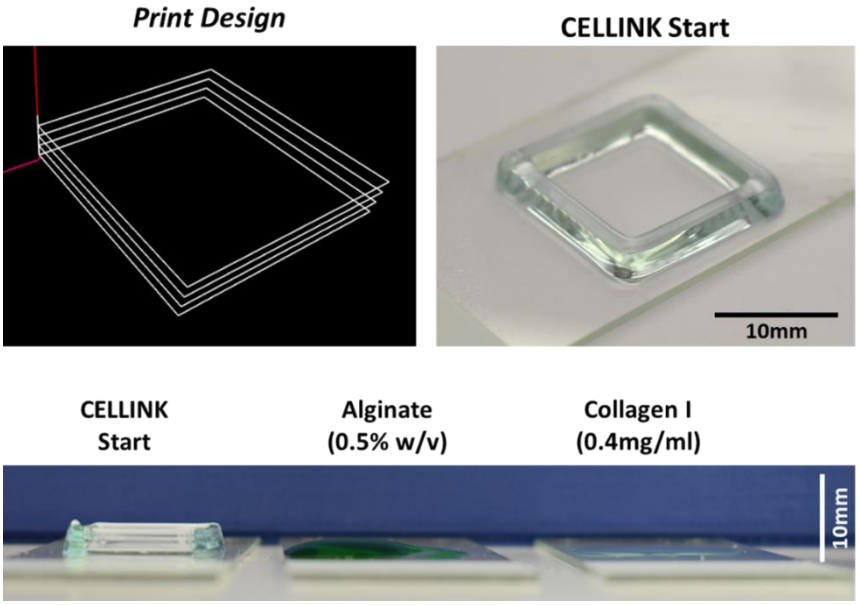

Fig 5-4: Layer stacking assay of collagen and alginate bioinks at low concentrations. Cellink Start-based inks form a faithful recapitulation of input design (top panel) and allow for true 3D stacking of multiple printed layers. Collagen and alginate hydrogels simply pool after printing and do not display any layer stacking properties. Scale bars represent 10mm.

5.3.2 Modification of Alginate and Collagen Bioinks to Improve Printability

We have shown above that collagen and alginate bioinks in the formulations necessary for *in vitro* neural tissue formation in solid cast-gel formats, are unsuitable for bioprinting purposes. However, certain concentrations and formulations of these inks may have positive effects on printability characteristics without negatively impacting cytocompatibility and permissiveness to neural tissue generation.

Using alginate as simply a structural support hydrogel in downstream neural tissue construct fabrication would utilise its strengths of cytocompatibility and inert cellular interactions, but not rely on encapsulated neural cell differentiation and neuritogenesis. For this reason, multiple alginate concentrations were assayed for the printability assays outlined in the previous section. Alginate hydrogels at 2% (w/v) displayed higher viscosities than the lower 0.5% (w/v) concentrations and as such maintained a better, although still poor, filamentous pattern fidelity after extrusion printing (Fig 5-5). However, this concentration of alginate still failed to generate a “string” under free-standing extrusion.

When concentrations of alginate were increased to 8% (w/v) the recapitulation of the printed pattern design was far greater than was seen with lower concentrations. However, even at this very high alginate hydrogel solution, an incomplete string formation was observed and layer stacking tests tended to collapse shortly after printing has completed (Fig 5-5). It is also worth noting that manipulations of this high concentration alginate hydrogel were difficult due to its high level of viscosity as a solution, hence increasing alginate concentrations beyond 8% (w/v) was not possible.

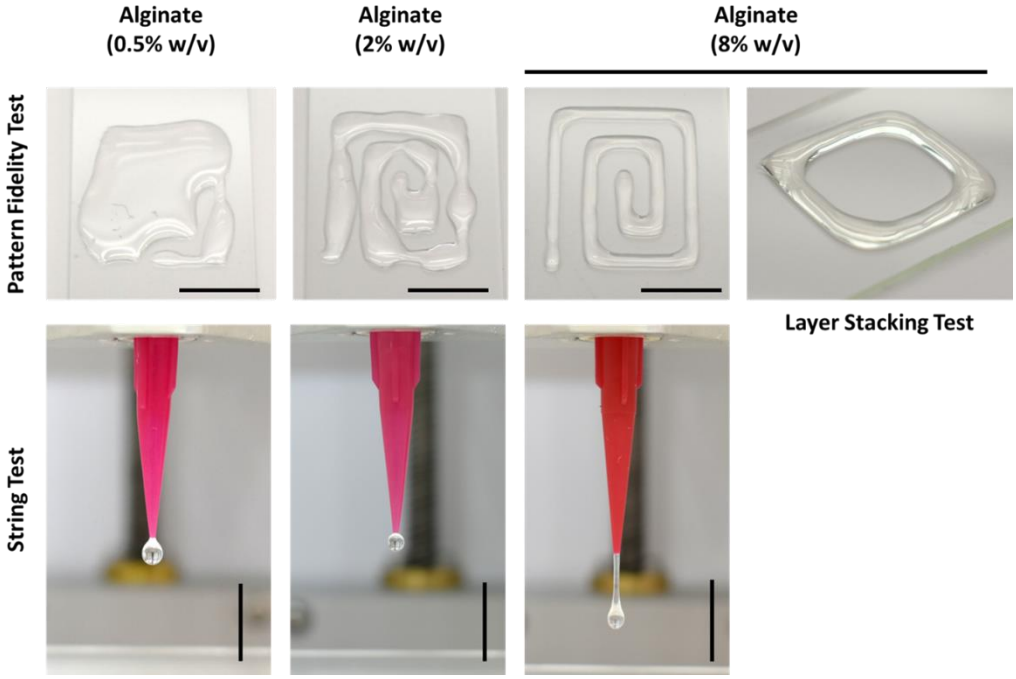

Fig 5-5: Pattern fidelity, string test, and layer stacking assays of multiple alginate hydrogel concentrations. Increasing concentrations of alginate have positive effects on pattern fidelity, but are unable to form continuous strings or stack adequately during printing. Scale bars represent 10mm.

Collagen scaffold production with increased levels of collagen concentration may allow for enhanced bioprinting characteristics, however, these higher concentrations may have detrimental effects on neural differentiation and neuritogenesis within the scaffolds, as reported previously (O'Connor *et al.*, 2001). Composite hydrogels formed from other soluble mammalian polymers however, may allow for the formation of a bioprinted construct but elicit a non-damaging effect on encapsulated neural cells and the gelation of the collagen fibrous network.

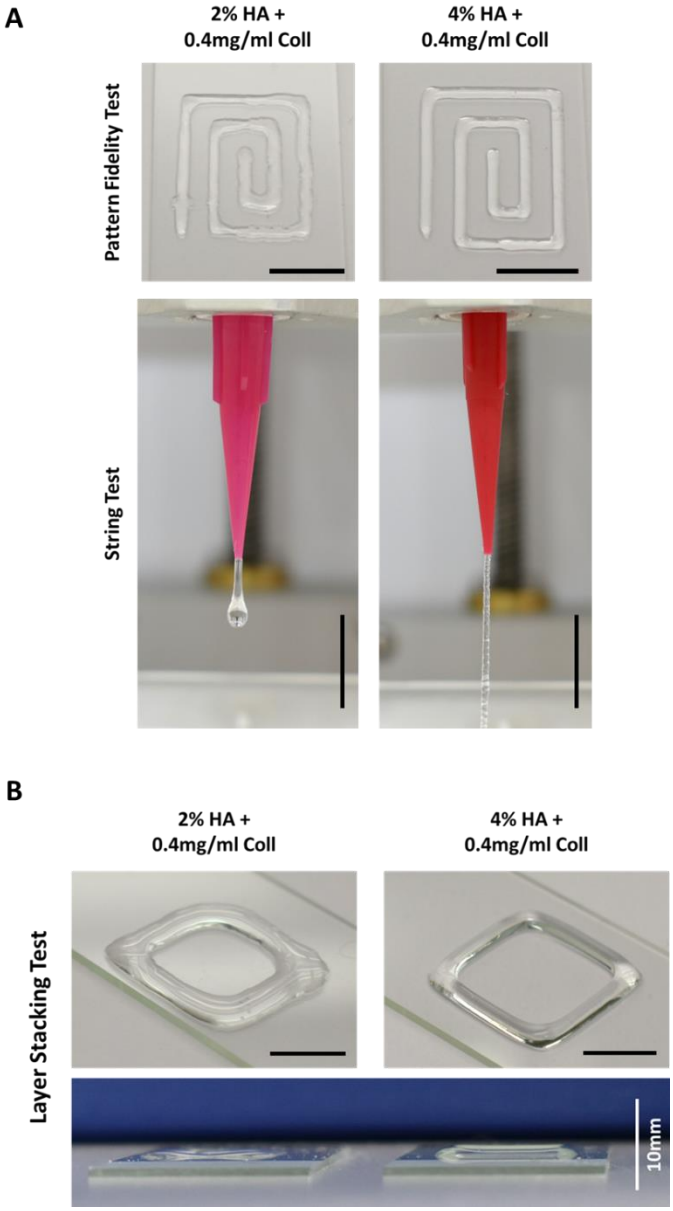

Fig 5-6: Pattern fidelity, string test and layer stacking assays of hyaluronic acid (HA) and collagen composite hydrogels. (**A**) Increasing the concentration of HA generates greater shape fidelity and string formation compared to base collagen hydrogels. (**B**) Layer stacking even with higher concentrations of HA shows limited height and compression of printed layers. Scale bars represent 10mm.

The addition of the mammalian anionic glycosaminoglycan hyaluronic acid (HA) to collagen hydrogels did dramatically increase all measures of printability (Fig 5-6). Composite hydrogels of 2% (w/v) HA and collagen showed much stronger pattern fidelity than was seen with collagen hydrogels alone, although such a blend did not generate an extruded string of over 10mm and retained droplet-like morphology during extrusion. When the

concentration of HA was increased to 4% (w/v), a noticeable increase in the sharpness of the printed pattern was seen and the extruded bioink did form a free-standing string (Fig 5-6 A).

Layer-stacking of multiple filament layers was also improved by the addition of higher concentrations of HA (Fig 5-6 B), although neither of these formulations generated stacked structures to the same degree as was seen with Cellink Start ink (Fig 5-4). Printed structures derived from HA and collagen hydrogel composites are a promising source of modifying collagen bioinks to make them more amenable to bioprinting technologies. However, the non-crosslinked and soluble nature of the HA component of the ink, together with low stacking characteristics would necessitate the use of a secondary structural element by which to contain and protect and collagen scaffold undergoing gelation in an aqueous environment.

As base alginate bioinks, even at high concentrations, have poor string formation and layer stacking qualities, other strategies must be developed to generate printable forms of this biomaterial. As HA was used to modify the viscosity and printing characteristics of collagen hydrogels, we next demonstrated the use of gelatin composites within alginate hydrogels to modify bioink traits (Fig 5-7). Gelatin is a hydrolysed form of collagen type I, and the use of gelatin as a component of bioinks, has widespread precedent throughout the literature (Chung *et al.*, 2013). Even small amounts of gelatin were shown to have profound effects on bioink printability and the extrusion pressure necessary to print the bioinks. 2% alginate and 2% gelatin composite inks showed low pattern fidelity and droplet formation during extrusion, but both parameters were slightly improved when alginate concentration was increased to 4% (Fig 5-7 A). The pressures necessary to extrude these materials increased only slightly from 8kPa to 13kPa. A vast improvement in print fidelity and string formation was seen with bioinks composed of 4% alginate and 4% gelatin, although with considerable lag in the extrusion deposition of the material and lag after the ceasing of the extrusion pressure. This was seen by the absence of bioink filament in the lower left point of the spiral design (the print origin point) and the slight pooling of material in the centre of the spiral design (the print endpoint) (Fig 5-7 A). This increase in bio-printable characteristics with increased gelatin concentration was also accompanied with an increased necessary extrusion pressure (56kPa).

Further increasing the gelatin concentration to 6% with 2% alginate did increase the resolution of the printed design, and demonstrated string formation during extrusion.

However, this bioink lost characteristics of smooth filament formation and demonstrated traits of over-gelation that required high extrusion pressures to print (~140kPa). This stiff gel-like bioink did perform very well in the layer stacking assay (Fig 5-7 B), but its inability to print smoothly and consistently would be disadvantageous in downstream neural tissue engineering applications. A composite blend of 3% alginate and 5% gelatin bioink demonstrated high print pattern fidelity, string formation and relatively good layer stacking properties, and as such was chosen as the candidate structural alginate bioink formulation for a component of coaxial neural tissue bioprinting.

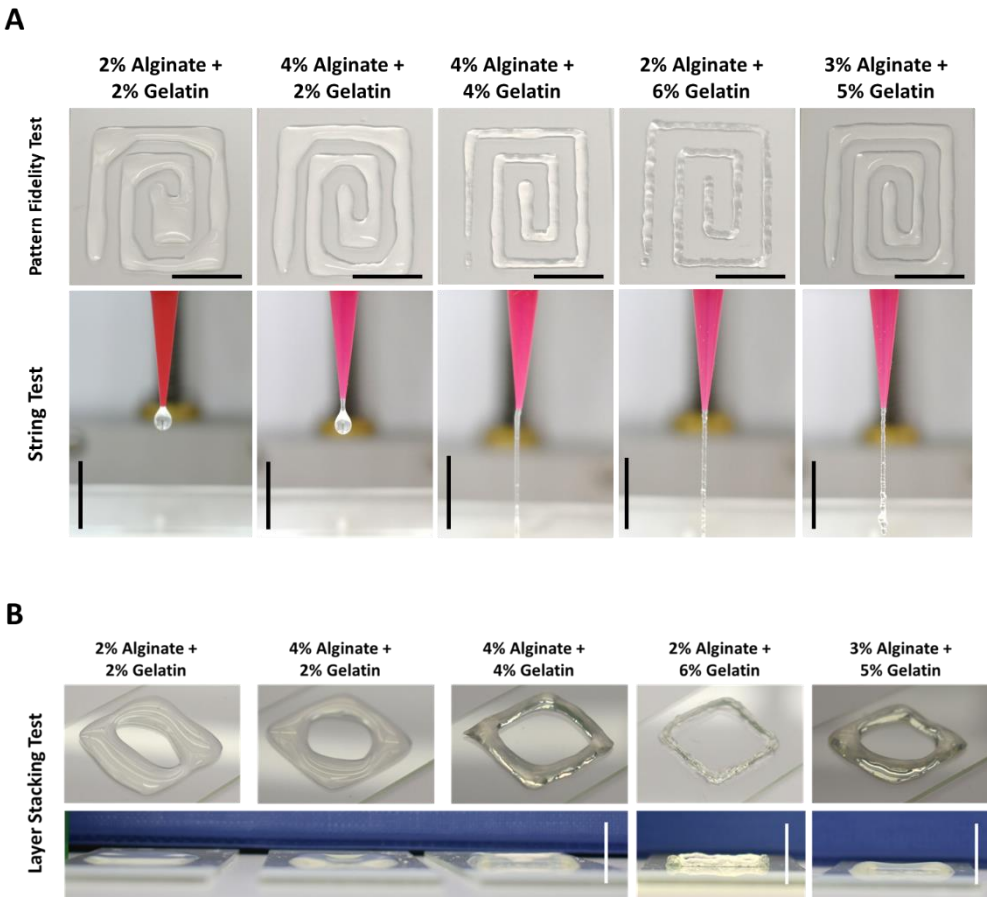

Fig 5-7: Bioprinting characteristics of alginate and gelatin composite bioinks. (**A**) Pattern fidelity and string test assays of each blended material. (**B**) Layer stacking assays of each biomaterial composition. Scale bars represent 10mm.

5.3.3 Formation of Neural Tissue Constructs Using Coaxial Bioprinting

As well as mono-axial bioprinting techniques, where a single material is deposited in a single filament; coaxial printing methodologies can combine two separate bioink formulations into a single extruded strand. Its applicability to neural tissue engineering relates to the generally low viscosity, low modulus hydrogels conducive to neural cell differentiation being unsuitable for the majority of free-standing extrusion bioprinting processes shown above. However, by separating a neural cell-laden "core" material that maintains the appropriate modulus and biophysical interactions to allow for neural differentiation to take place, and surrounding it concentrically with a "shell" material that maintains the structural support and pattern fidelity of the bioprinted scaffold, then *de novo* neural tissue scaffolds can be designed.

To accomplish this, we utilised a coaxial printing nozzle that was generated through selective laser melting of titanium 6Al4V alloy. This coaxial system was developed internally and has been utilised for precursor cartilage bioprinting (O'Connell *et al.*, 2016; Duchi *et al.*, 2017). The "shell" material chosen for coaxial printing tests was a 3% alginate and 5% gelatin composite bioink (A3G5), as determined by the positive printability characteristics displayed in Section 5.3.2. Initial "core" material tests for bioprinting capabilities used a coloured water solution in place of a bioink to assess the stability and sealed nature of the core/shell structure. However, the low viscosity core continuity was easily disturbed through the printing process (data not shown) and so future experiments utilised a collagen (0.4mg/ml) and 1% HA core material in order to represent the true printing format of neural cells and increase the viscosity of the core to a level that would not be disrupted through the bioprinting process (Fig 5-8).

These bioink formulations extruded through the coaxial nozzle maintained segregation of core and shell components and could generate free standing string formations (Fig 5-8 A). Furthermore, this process could derive coaxial printed scaffolds to a pre-determined two-layer print design and maintained the core/shell separation (Fig 5-8 B). Following *in situ* crosslinking, the printed scaffold could be handled easily. This was also seen after 24 hours in cell culture conditions at 37^{o}C. This retention of integrity was due to the alginate component of the shell bioink which retained ionic crosslinking properties in cell culture media, whereas the non-crosslinked nature of the gelatin component would undergo gel-sol transition at physiological temperatures. Steric entanglement of gelatin

molecules within the alginate scaffold however, may act to retain some gelatin composition.

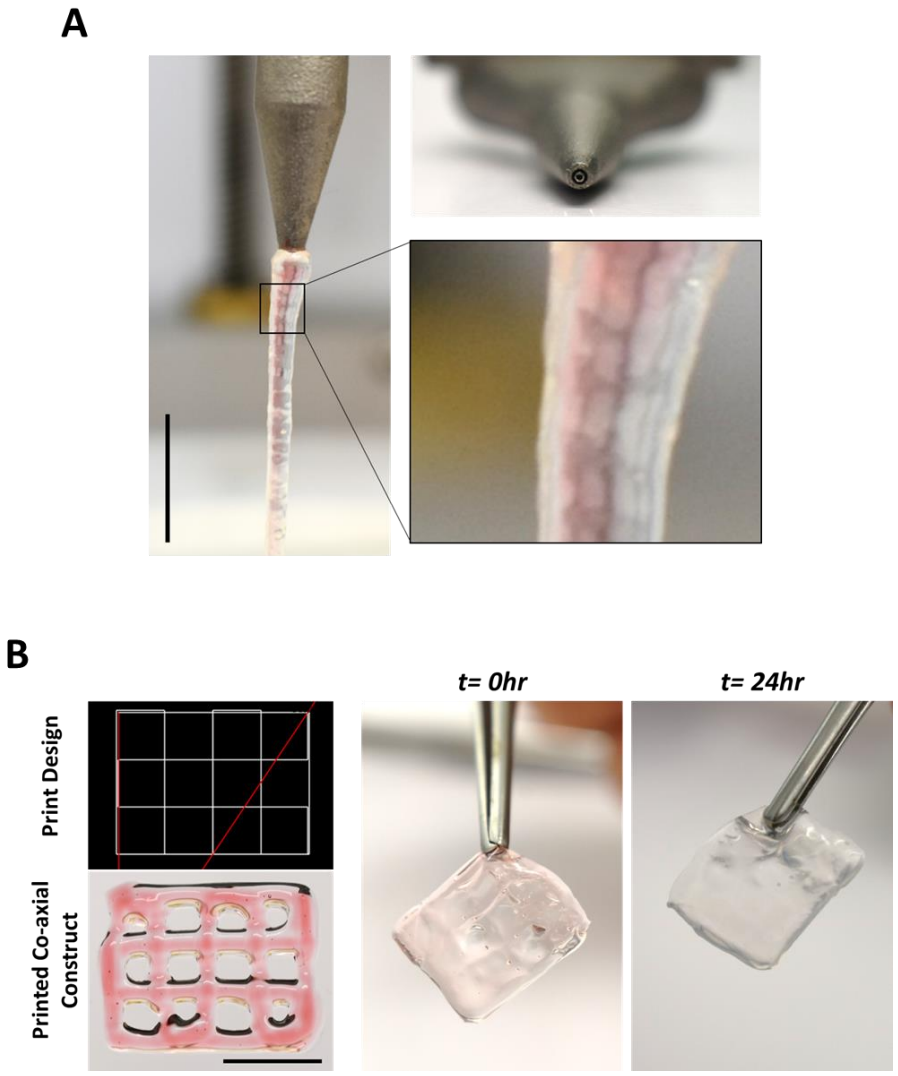

Fig 5-8: Coaxial bioprinting of 3% alginate/5% gelatin shell materials and collagen/HA core materials. (**A**) Coaxial separation of core and shell is maintained throughout the printing process together with string formation. The geometry of the coaxial nozzle is also shown. (**B**) Bioprinting of the coaxial bioink formulations can be made to specific design patterns that maintain structural integrity. Scale bars represent 10mm.

To further demonstrate the segregated nature of the core and shell elements after the printing process, the core material was combined with fluorescently-labelled beads while the shell material was left "empty". Fig 5-9 shows that 24 hours after printing and maintenance in cell culture conditions, fluorescent beads were present only in the core of

each coaxial filament. The total filament size ranged from 1-2mm in diameter with the core representing approximately 500-750µm of this width. This process has therefore generated a construct in which the core biomaterial composition could not ostensibly be generated into a multi-layer bioprinted construct using conventional mono-axial printing alone. But through the combination of a non-cytotoxic structural support material and coaxial design, successful generation of a large-scale scaffold can be generated.

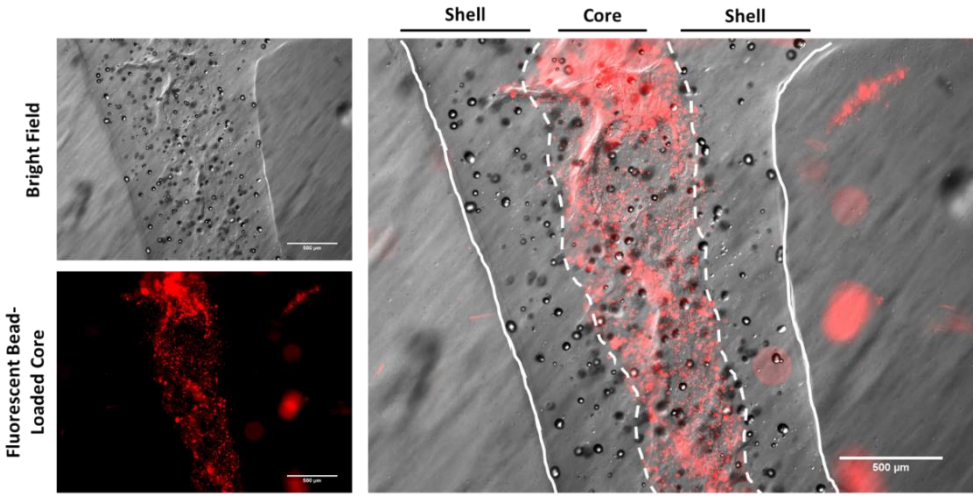

Fig 5-9: Demonstration of core/shell filament formation from coaxial bioprinting. The core material was mixed with fluorescently-labelled beads (Red) to show separation of core and shell bioinks. Images were taken 24 hours post-print. Scale bars represent 500µm.

The next element of study for coaxial neural tissue bioprinting was to assay whether encapsulated neural cells retained viability after the formation of bioprinted scaffold or underwent irreparable damage in the extrusion process. A neural cell line was encapsulated in physiologically buffered core material of the same composition as assayed above. Coaxial bioprinting of the cell-laden core and shell material was completed to the same design as seen in Fig 5-8. A Calcein-AM and Ethidium homodimer cell viability dye assay demonstrated a very high proportion of viable cells four days post-print (Fig 5-10, Green), whereas cells displaying positive ethidium homodimer fluorescence (dead cells) were barely present throughout the construct. This illustrates that the coaxial printing process itself, crosslinking process, and maintenance in neural cell differentiating conditions does not have detrimental effects on cell survival.

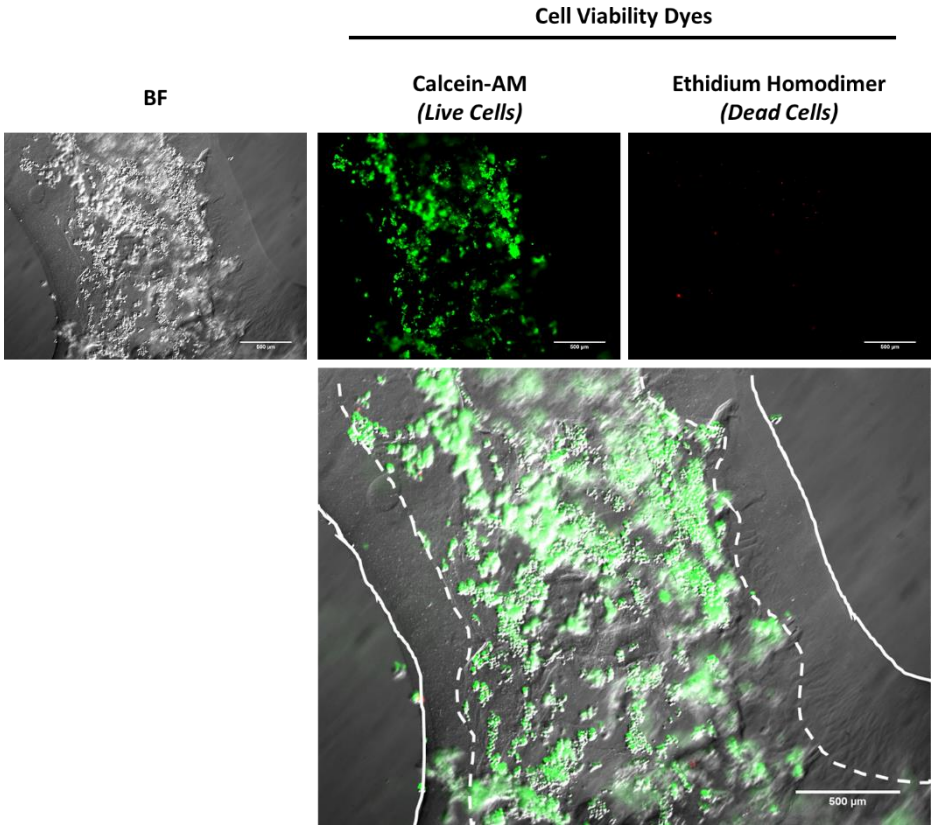

Fig 5-10: Cell viability assay of encapsulated neural cells in coaxial bioprinted structures. Calcein-AM staining of viable cells are shown in green, whereas ethidium homodimer staining (red) highlights dead cells. All cells were loaded in the core of the construct. BF; Bright field. Scale bars represent 500µm.

Finally, after demonstrating high retention of neural cell viability within the core of the bioprinted construct, it was necessary to determine whether neural differentiation characteristics such as neuritogenesis was also preserved within this collagen-based core material. Live cell imaging of the scaffolds after one week of neural differentiation displayed widespread neuritogenesis of cells within the construct (Fig 5-11). The neurites extended into the core biomaterial itself and were not restricted to cellular aggregates, displaying the successful interaction between the neural cells and the encapsulating matrix.

This not only demonstrates the efficacy of bioprinting a structurally sound neural-tissue construct from multiple bioinks, but that principles of neural cell differentiation, within conducive hydrogel scaffolds in simple cast-gel formats, can be translated into bioprinting methodologies.

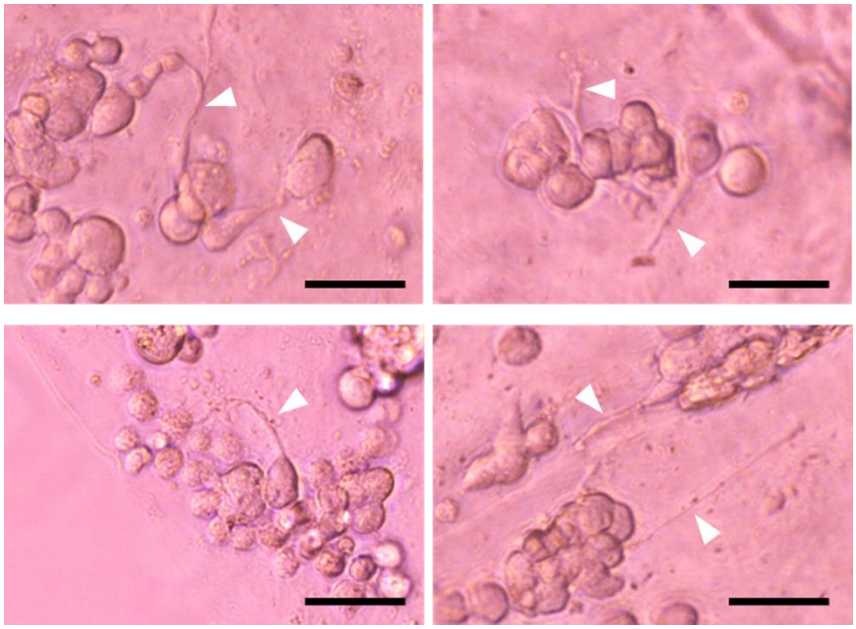

Fig 5-11: Live cell imaging of encapsulated neural cells undergoing neuritogenesis within the bioprinted core material after 7 days of differentiation. The neural cells displayed widespread propensity for neurite extensions (white arrow heads). Scale bars represent 50µm.

5.4 Discussion and Conclusions

The rise of bioprinting technology as a catalyst for tissue-engineering and regenerative medicine studies in recent years has generated much hope for the future of personalised medicine (Zhang *et al.*, 2017). Compared to standard 3D encapsulation-based cell culture, bioprinting of cells in tailored biomaterials has many advantages to its use. Through the printing of cell-laden filaments in particular arrangements it has been shown that a pseudovasculature-like system can be generated that allows for extensive nutrient and oxygen diffusion in large, clinically-relevant sized 3D constructs (Kang *et al.*, 2016). This is an inherent limitation in simple cast-gel cell culture techniques where an increase in scaffold volume limits the surface area by which to adequately diffuse nutrients. This also limits possible cell densities within these constructs, as cell density is increased to tissue-like levels, so does the demand for oxygen and metabolic components. To obtain 3D neural cell cultures with cell densities approaching that of native tissue, the only way of achieving this in static culture is to limit construct size (Frampton *et al.*, 2011).

The ability to design and control bioprinted scaffold complexity not only allows for tissue-like cellular composition and increased overall size of the scaffolds, but can also form complex structures that recapitulate elements of native-tissue morphology. For the printing of neural tissue, this has included the laminar layered composition of the cortex (Lozano *et al.*, 2015). As well as the ability to mimic tissue composition and structure, such bioprinting techniques could be used to segregate or combine specific neural cell types within the same construct, but in a controlled manner. This would mirror the mixing of glial and neuronal lineages in iPSC-derived neural functionality assays (Odawara *et al.*, 2016).

Successful reports of neural tissue extrusion-bioprinting are beginning to increase in frequency, with a wide array of polysaccharide- and protein-based polymers utilised in the production of neural tissue constructs (Thomas and Willerth, 2017; Knowlton *et al.*, 2018). However, the biomaterials used within these positive reports tend to lack high filament resolution or display limited interaction between embedded neural cells and the hydrogel scaffold i.e. low neuritogenesis. Here we have shown that biomaterial formulations shown to be conducive to positive neural differentiation and neuritogenesis in simple cast-gel formats (Chapters 2 and 4) were not amenable to the generation of free-standing bioprinted neural constructs. As such, we focused on the modification of these materials by which to attempt to maintain positive neural cell viability and differentiation but also allow for the printability of the scaffolds.

Low concentration alginate and collagen scaffolds failed all used printability tests including pattern fidelity, string formation and multi-layer stacking. Even at very high alginate concentrations (8% w/v) this material failed to adequately generate a free-standing string under extrusion and was unable to stack layered filaments without collapse and pooling. Pattern fidelity in a single layer did show promise, although this is not enough to conclude that base alginate alone is a suitable bioink. This mirrors similar methods of alginate bioprinting that form either composite blends with gelatin (Chung *et al.*, 2013) or other polysaccharide polymers (Gu *et al.*, 2017).

Preliminary tests of blending the mammalian glycosaminoglycan hyaluronic acid (HA) within collagen hydrogel formulations, did improve markers of printability. Pattern fidelity and string formation was greatly improved with 4% w/v addition of HA, albeit with lower multi-layer stacking outcomes. However, the soluble and non-crosslinked nature of HA within these scaffolds and the inherent increase in viscosity generated may adversely

affect scaffold stability under long term cell culture conditions and the ability of neural cells to undergo neuritogenesis in this modified collagen-based biomaterial.

To overcome this limitation, we employed the use of coaxial bioprinting, by which to segregate a neural-conducive inner core collagen-based biomaterial, and an outer shell support material based on alginate hydrogel formation. This coaxial technology has already been utilised to generate precursor cartilage tissue through separation of stabilising supporting material and the cell-laden biomaterial cargo, although with different bioink formulations (O'Connell *et al.*, 2016; Duchi *et al.*, 2017). Composite blends of alginate and gelatin bioinks were assayed for their printability characteristics and a final formulation that appeared promising for bioprinting applications was deduced (3% alginate and 5% gelatin concentration). This was combined with a modified collagen-based core material, that contained a 1% HA concentration to slightly increase bioink viscosity, to make it more amenable to the flow characteristics of coaxial extrusion bioprinting.

Assays of the combined coaxial printing process demonstrated clear separation of shell and core during extrusion, and a maintenance of free-standing string formation. Coaxial printing of an *in silico* designed two-layer grid pattern was recapitulated by the printing process, and the core/shell segregation was maintained throughout the printed construct. Ionic crosslinking of the alginate polymer within the shell material, through addition of calcium cations, resulted in a construct that could be handled and manipulated easily by hand. The gelatin component of the shell bioink was non-crosslinked into the hydrogel itself and undergoes sol-gel transition at physiological temperatures. However, after 24 hours within cell culture growth conditions (37^{o}C, 5% CO_2) the structural integrity of the construct was maintained. This demonstrates that the alginate component of the shell is widespread and robust enough after crosslinking to maintain scaffold shape fidelity, even after the possible solubilisation of the gelatin portion of the shell bioink. It is also a possibility that some level of gelatin retention is enabled through steric entangling of the gelatin and alginate chains during crosslinking. Either outcome is non-detrimental, as residual gelatin components would add to the stability of the construct, whereas any solubilised gelatin may increase the porosity of the shell hydrogel and allow for increased levels of nutrient diffusion. That being said, further work will need to be undertaken to ensure the stability of the scaffold during differentiation assays of hiPSC-derived neurons, that takes place over the course of months and not days. However, this initial data is a promising result in this endeavour.

The maintenance of core/shell separation was further shown after printing through the use of fluorescently-labelled beads that indicated the location of core printed material. This result demonstrates the limited mixing and of core and shell components during the printing process and shows the limited turbulence generated under this method of coaxial bioprinting.

To determine how these bioink formulations and the coaxial printing process itself affected encapsulated neural cell viability, bioprinted constructs containing a neural cell line were produced to the same specifications as the bead-loaded scaffold. After four days post-printing, an assay of cell viability of the encapsulated neural cells revealed almost complete retention of living cells within the core bioink. This demonstrates that not only is the printing process itself amenable to high levels of cell survival, but as is the crosslinking process and the diffusion level of nutrients within the scaffold. Such a result is integral for forming constructs of increased cell density approaching that of native neural tissue. Another implication of this result is that the level of shear stress imposed on the encapsulated cells during the extrusion printing process is well tolerated. High shear stress has previously been shown to have detrimental effects on cell survival (Blaeser *et al.*, 2016), which is not seen under these bioprinting conditions.

Finally, to ensure that the collagen-based core bioink retained its ability to support neuritogenesis of encapsulated neural cells under differentiation conditions, we assayed whether neurite extension occurred after 7 days of neural differentiation within the coaxially printed scaffold. Live cell imaging did reveal neuritogenesis throughout the core of the scaffolds which indicates the favourable neural differentiation conditions within this core bioink formulation. Comparing this outcome to other published (although limited) neural-tissue bioinks would give valuable information on the practicality and efficacy of this bioink for neural tissue engineering.

Taken together, these data show the development of a coaxial format of generating self-supporting 3D bioprinted neural tissue scaffolds. Each element of the core and shell bioinks could further be tailored depending on design specifications or desired printing resolution, but form a strong foundation stone on which future bioprinted neural constructs can be fabricated. The retention of neural cell viability and the ability to undergo neuritogenesis within these scaffolds are a key factor in the progression of these techniques and must be at the forefront of future bioink formulations. The cell-based functionality of the desired tissue type is the true goal of experiments such as these, and so

a bioink that retains highly printable characteristics but loses cell functionality is an unacceptable outcome.

Projected future work from these experimental findings would be far reaching, but ultimately crucial to the development of higher resolution neural tissue models. Long term culture of such scaffolds must be shown to maintain sufficient integrity for confluent neural tissue formation to take place. The effect of temperature controlled extrusion can have striking repercussions on the printing characteristics of bioinks (Chung *et al.*, 2013) and may be yet another method of modifying scaffold formation and resolution.

Furthermore, assessing the limits of cell densities possible within designed scaffolds such as this, will allow for the formation of more brain-tissue representative *in vitro* modelling practices. By combining this technology with long-term differentiation of hiPSC-derived neural cultures it will begin to be possible to generate more tailored and representative tissue morphologies that ultimately will push forward the frontiers of modern neuroscience.

5.4.1 Summary of Chapter Findings

- Low concentration collagen and alginate hydrogel solutions show poor bioprinting traits.
- Increasing alginate concentrations has positive effects on pattern fidelity of a single printed layer but displays limited string formation and poor filament stacking properties.
- Composite bioinks of collagen and hyaluronic acid show improved bioprinting traits, although the soluble nature of hyaluronic acid and increased viscosity of the bioink would make them poor single component bioink for neural tissue engineering.
- Alginate and gelatin composite bioinks show differential printing characteristics heavily dependent on concentration and ratio to each other. A 3% alginate and 5% gelatin mix was found to have promising properties for a bio-printable material.
- Coaxial printing of a collagen-based core material designed to be amenable to neural cell differentiation, and an alginate-gelatin shell bioink surrounding the core adding to the structural integrity of the scaffold, was developed.

- Core/shell separation was conserved throughout the printing process and could form two-layer *in silico* designed grid structures.
- Acellular versions of the scaffold construct could be handled manually, and maintained structural integrity after storage under physiological conditions.
- Separation of core and shell biomaterial components was demonstrated through fluorescent-bead loading of the core material, which displayed continued core/shell separation after maintenance at 37^{o}C.
- Neural cell encapsulation and growth within the bioprinted core component of the coaxial scaffold demonstrated the retention of high cell viability by day four post-printing.
- Neuritogenesis was prevalent by day 7 of differentiation post-print within the coaxial scaffold. Demonstrating conduciveness to neural differentiation within the core collagen-based bioink.

5.4.2 Acknowledgements

We would like to acknowledge the help of Dr. Cathal O'Connell (BioFab3D, St. Vincent's Hospital Melbourne) for his workshops and training on 3D printing and generation of G-Code designs. We would also like to thank members of the Cartilage Regeneration Group (Dept. of Surgery, University of Melbourne) for access to the coaxial print nozzles. We are also grateful to research teams within the ANFF (Australian National Fabrication Facility) and Intelligent Polymer Research Institute (IPRI) who developed and fabricated the coaxial nozzle design.

Chapter 6: Overall Conclusions and Future Directions

The broad aim of this thesis was to study and develop multiple aspects of *in vitro* three-dimensional forebrain neural tissue constructs from human stem cells. The main components of this goal were to; assay and analyse candidate biomaterial hydrogels as potential cell carriers for neural cell differentiation; to successfully differentiate and compare markers of neural maturation of dorsal and ventral forebrain neural cell identities from hiPSCs; to demonstrate the effects of a pro-neuritogenic hydrogel scaffold on hiPSC-neural differentiation; and lastly, to modify and develop bioprinting techniques that allow for the generation of 3D neural tissue constructs through additive fabrication technologies.

Stem cell lineage specification is known to be driven strongly by the substrate stiffness of the materials in contact with the cells (Engler *et al.*, 2006). Neural tissue modelling applications have therefore benefitted from matching the moduli of cell culture substrates to those of native brain tissue (Banerjee *et al.*, 2009; Teixeira *et al.*, 2009; McKinnon, Kloxin and Anseth, 2013). In this body of work, both alginate- and collagen type I-based candidate hydrogels displayed storage moduli lower than that recorded for native brain tissue, and both preserved cell viability of neural cells after encapsulation and over the course of differentiation. However, only collagen-based scaffolds allowed for neuritogenic events to occur. Alginate hydrogels covalently modified with neural matrix metalloproteinase (MMP)-cleavable motifs and laminin-binding moieties also failed to induce neurite extension morphology, although did elicit changes in neural marker protein expression, demonstrating a direct effect of hydrogel composition and modification on protein expression during neural differentiation. As a further direction of research, it would be valuable to assay whether other functionalisation groups (such as other MMP-sensitive motifs) elicit a similar effect on encapsulated neural cells, or whether modified reaction conditions, that would generate higher degrees of functionalisation, may overcome the steric hindrance imposed by the alginate environment and allow neuritogenesis to occur. In a similar vein, it would be crucial to understand whether this process is indeed relative to the covalently-bonded peptide moieties themselves, or whether the loss of carboxyl-

groups used for the carbodiimide chemistry, impacts polymer chain ionic-crosslinking. It is possible that this effect mimics the sub-stoichiometric conditions seen in recent positive polysaccharide hydrogel neural tissue studies (Palazzolo *et al.*, 2015). Indeed, it is entirely possible that a synergistic effect between restricted ionic cross-linking sites and native peptide motifs may take place.

Some canonical neuronal marker expression profiles did show upregulation during the differentiation of encapsulated neural cells, but this upregulation did not reflect the level of neuritogenesis within the scaffold. This is an intriguing finding, as the upregulation of many standard neuronal markers has been used to demonstrate the success of a hydrogel scaffold's composition for neural tissue engineering purposes in many published studies. This thesis shows however, that with a panel of cytoskeletal-associated markers, striking differences can be seen within protein marker expression profiles from neural cells in pro-neuritogenic and non-neuritogenic environments. However, it should be noted that the patterns of marker expression from pro-neuritogenic environments do not intrinsically follow those of planar culture differentiation. This suggests a strong interplay between the three-dimensional environment itself on neural differentiation kinetics and the ability to generate neurites within the hydrogel scaffold, that differs to planar culture. Further investigation to see if this holds true with other neural cell types, and with extended panels of markers will allow improved resolution of early neural differentiation responses in three-dimensional environments.

A possible limitation in the analytical power of the alginate and collagen hydrogel assays outlined in Chapter 2 relates to the constitutively high gene expression of many neuronal markers even under proliferative conditions of the neural cell line. Although protein marker expression showed clear and distinct patterns between culture conditions, gene marker expression fold-changes were very low over the course of differentiation. This may be related to the type of neural cell line used, which may employ post-transcriptional regulation of differentiation-associated genes to generate the neuritogenic phenotype (Lindenbaum *et al.*, 1988; Perrone-Bizzozero, Cansino and Kohn, 1993). Other primary cells or neural cell lines may therefore show more robust gene expression changes during differentiation, but would also require longer periods of time in culture to generate a mature neural phenotype. As Chapter 2 was primarily based on biomaterial-suitability for future three-dimensional culture of iPSCs-derived neural cells and less an understanding of a specific neural cell line differentiation processes: the accelerated speed of differentiation

and neuritogenesis of PC12s under differentiating conditions was advantageous. From these results, the collagen-based hydrogel scaffold as a pro-neuritogenic environment was selected as the scaffold for downstream three-dimensional iPSC-based neural differentiation (Chapter 4).

Accurate *in vitro* human forebrain modelling, be it for developmental or disease-based study, requires the accurate recapitulation of *in vivo* cellular content. Forebrain cortical tissue is derived from both dorsal- and ventral-neural tube structures, with the development of complete cortical tissue driven by the tangential migration of ventrally-derived cells into dorsal regions. *In vitro* "patterning" of iPSC-derived forebrain neural cultures however would predominantly generate either dorsal *or* ventral neural cell types. Therefore, to understand the timings and maturation events of ventrally-patterned and dorsally-patterned neural cell types derived from hiPSCs, we undertook parallel differentiation strategies to directly compare molecular and functional components of the differentiation process. Understanding the details of these processes will lead to more accurate and representative combinations of cell types from both pathways as is seen *in vivo*. The work in this thesis demonstrated that NPC pools from both patterned differentiation strategies were generated in comparable amounts early in the differentiation timeline, but that stark differences in expression existed between the dorsal-specific and ventral-specific NPC markers (*PAX6* and *NKX2.1* respectively) between neural cells from dorsal and ventral patterned differentiation pathways in planar culture. This separation of dorsal and ventral identity widened over the time-course of neural maturation with the segregated expression of pre-synaptic ventral-GABAergic markers and dorsal-glutamatergic markers dependent on the differentiation strategy. Interestingly, there was a consistent trend of upregulated neural marker gene and protein expression in ventrally-patterned hiPSC-derived neural cultures compared to dorsal-cultures. This may be indicative of an accelerated level of differentiation of cells derived from this pathway or a possible enrichment of neuronal cells. However, preliminary functional assays of neuronal electrophysiological activity demonstrated a more functionally-mature phenotype in ventrally-patterned neural cells, verified by higher numbers of induced action potentials following current stimulation, and larger sodium and potassium currents during invoked activity. Initial experiments to observe spontaneous activity of neural cell cultures via extracellular recordings, displayed activity in a subset of ventrally-patterned hiPSC-neural cultures that was not seen in cells from dorsal inductions. However, this induction of

functionally mature behaviour was only achieved through the use of media formulations previously shown to enhance electrical maturation of various neuronal cell types (Bardy *et al.*, 2015). This reveals the potential for acceleration of other maturation processes within hiPSC-derived neural cells through media composition alone, and may be another tool by which to generate and modulate derived neuronal cell activity.

This difference in neuronal marker expression and functional maturity can now act as a guide to understand how different combinations of these patterned neural cell types will interact when matured together in controlled mixed differentiation cultures. Perhaps through substrate patterning or other segregation methods, co-culture models based on these induction strategies can then generate truly representative models of complete human forebrain cytoarchitecture.

To understand whether differentiation within pro-neuritogenic three-dimensional hydrogel environments had positive or negative effects on the efficiency or speed of neural maturation, hiPSC-derived NPCs (both dorsally- and ventrally-patterned) were encapsulated in collagen-based scaffolds. As was seen in Chapter 2 with differentiation studies on PC12s, hiPSC-derived neural cells were able to undergo extensive neuritogenesis throughout collagen scaffolds in all three directional axes. Early significant peaks of both NPC and mature neural marker expression were recorded from ventrally-patterned three-dimensional neural cultures, whereas this accelerated maturation was not observed in cells from dorsally-patterned inductions. This accelerated upregulation of neural differentiation markers was also significantly higher than that seen from planar ventrally-patterned inductions. This is suggestive of a system by which the same scaffold environment may elicit differing effects on neural maturation depending on neural subtype specificity. It was also demonstrated that the hydrogel environment itself did not alter the patterning of differentiating neural cells themselves, and the morphogen driven separation of ventral and dorsal lineages was preserved within the three-dimensional scaffolds.

However, markers of maturation at later time points in differentiation appeared lower in neural cells in three-dimensional scaffolds than was seen in planar culture. One possible explanation is the necessity of high neural cell densities by which to trigger the expression of genes associated with neuronal and synaptic maturation. The cell densities in this study were utilised to minimise cell death derived from low diffusion rates of oxygen and nutrients into the solid cast-gel constructs. This compromise to maintain cell viability may have negative effects on functional neural network formation. Other studies using

more tissue-representative cell densities, but employing smaller construct sizes or bioprinted grid structures to maintain viability, have shown promising results from three-dimensional neural scaffolds (Frampton *et al.*, 2011; Gu *et al.*, 2017).

Therefore, to overcome issues of cell density limitation within cast-formed three-dimensional scaffolds, bioprinting strategies for additive fabrication of neural tissue formation were developed. The low biomaterial content of the hydrogels that show successful pro-neuritogenic neural differentiation results in low pre-gelation viscosities which make them unsuited for use as free-standing bioprinting inks or "bioinks". To overcome this, a coaxial system using a pro-neuritogenic cell-laden collagen-based "core" and a structurally reinforcing outer "shell" of alginate and gelatin composite hydrogel, was developed to generate multilayered printed structures. These structures allowed for the successful segregation of cell-laden and acellular supportive elements that maintained a protected core structure of consistent diameter. Neural cell lines printed within this core retained high cell survival rates and displayed neurite extensions after 7 days of neural differentiation.

Although in this instance only a two-layered grid structure was formed, this methodology can be further developed to generate much more complex tissue construct designs in a multi-layered fashion. The modification of grid-like print designs to introduce elements of pseudovasculature would also enable the increase of neural cell densities within bioprinted culture systems. To this end, the scaling up of *in vitro* neurological models to sizes relevant for human clinical translation may be possible. Further tailoring and refinement of the shell bioinks used in this study may also aid with the porosity of the scaffold, as the gelatin component of the bioink used was non-crosslinked with the alginate polymer, other than steric retention. It would therefore be necessary to observe the long-term stability of such constructs and to modulate this with the alginate network forming the shell structure.

Another advantage of using multiple bioink printing capabilities is the ability to localise and place specific neural cell types in known three-dimensional arrangements. Precise neurological models could then be developed to mimic specific brain tissue morphologies and cellular content. However, enhanced printing resolution would need to be developed to ensure that cellular placement and fibre arrangement was on the scale seen *in vivo*. Current methodologies of cellular placement and arrangement are quite crude by comparison. The refinement of these models could then easily be analysed through

assays of neural network formation and functionality and be used as the basis for highly representative neurological-disease models that stem from hiPSC-based modelling. In combination, the synergy of bioprinting methodologies and hiPSC-modelling of human neural development make a potent toolkit to further the study of neuroscience through purely *in vitro* study.

In conclusion, this thesis has covered the development and biological assays of candidate biomaterials for neural tissue engineering. The major cellular subtype components of human forebrain formation have been generated from hiPSCs and the time-lines of maturation and functionality directly compared. The same processes were modelled within three-dimensional environments that elicited changes in neuronal maturation rates dependent on subtype composition. Finally, pro-neuritogenic hydrogel scaffolds were adapted to bioprinting methodologies in order to increase the complexity of neural tissue architecture, and as a method of maintaining high cell viability with higher cell densities. This body of work will help inform the next generation of *in vitro* neurological modelling studies, with the hope of better understanding human brain development and disease.

References

Aasen, T. *et al.* (2008) 'Efficient and rapid generation of induced pluripotent stem cells from human keratinocytes.', *Nature biotechnology*, 26(11), pp. 1276–84. doi: 10.1038/nbt.1503.

Addae, C. *et al.* (2012) 'All-trans-retinoid acid induces the differentiation of encapsulated mouse embryonic stem cells into GABAergic neurons.', *Differentiation; research in biological diversity*. Elsevier, 83(5), pp. 233–41. doi: 10.1016/j.diff.2012.03.001.

Alenina, N., Bashammakh, S. and Bader, M. (2006) 'Specification and differentiation of serotonergic neurons.', *Stem cell reviews*, 2(1), pp. 5–10. doi: 10.1007/s12015-006-0002-2.

Allodi, I. and Hedlund, E. (2014) 'Directed midbrain and spinal cord neurogenesis from pluripotent stem cells to model development and disease in a dish.', *Frontiers in neuroscience*, 8(May), p. 109. doi: 10.3389/fnins.2014.00109.

Alvarez-Perez, M. A. *et al.* (2010) 'Influence of gelatin cues in PCL electrospun membranes on nerve outgrowth.', *Biomacromolecules*, 11(9), pp. 2238–46. doi: 10.1021/bm100221h.

Van den Ameele, J. *et al.* (2014) 'Thinking out of the dish: What to learn about cortical development using pluripotent stem cells', *Trends in Neurosciences*. Elsevier Ltd, 37(6), pp. 334–342. doi: 10.1016/j.tins.2014.03.005.

Ananiev, G. *et al.* (2011) 'Isogenic pairs of wild type and mutant induced pluripotent stem cell (iPSC) lines from rett syndrome patients as In Vitro disease model', *PLoS ONE*, 6(9). doi: 10.1371/journal.pone.0025255.

Andersen, T., Auk-Emblem, P. and Dornish, M. (2015) '3D Cell Culture in Alginate Hydrogels', *Microarrays*, 4(2), pp. 133–161. doi: 10.3390/microarrays4020133.

Anderson, S. and Vanderhaeghen, P. (2014) 'Cortical neurogenesis from pluripotent stem cells: complexity emerging from simplicity.', *Current opinion in neurobiology*. Elsevier Ltd, 27, pp. 151–7. doi: 10.1016/j.conb.2014.03.012.

Antoine, E. E., Vlachos, P. P. and Rylander, M. N. (2014) 'Review of Collagen I Hydrogels for Bioengineered Tissue Microenvironments: Characterization of Mechanics, Structure, and Transport', *Tissue Engineering Part B: Reviews*, 20(6), pp. 683–696. doi: 10.1089/ten.teb.2014.0086.

Arber, C. and Li, M. (2013) 'Cortical interneurons from human pluripotent stem cells:

prospects for neurological and psychiatric disease.', *Frontiers in cellular neuroscience*, 7(March), p. 10. doi: 10.3389/fncel.2013.00010.

Azevedo, F. a C. *et al.* (2009) 'Equal numbers of neuronal and nonneuronal cells make the human brain an isometrically scaled-up primate brain.', *The Journal of comparative neurology*, 513(5), pp. 532–41. doi: 10.1002/cne.21974.

Balgude, A. P. *et al.* (2001) 'Agarose gel stiffness determines rate of DRG neurite extension in 3D cultures.', *Biomaterials*, 22(10), pp. 1077–84.

Banerjee, A. *et al.* (2009) 'The influence of hydrogel modulus on the proliferation and differentiation of encapsulated neural stem cells.', *Biomaterials*. Elsevier Ltd, 30(27), pp. 4695–9. doi: 10.1016/j.biomaterials.2009.05.050.

Barateiro, A. and Fernandes, A. (2014) 'Temporal oligodendrocyte lineage progression: in vitro models of proliferation, differentiation and myelination.', *Biochimica et biophysica acta*. Elsevier B.V., 1843(9), pp. 1917–29. doi: 10.1016/j.bbamcr.2014.04.018.

Barberi, T. *et al.* (2003) 'Neural subtype specification of fertilization and nuclear transfer embryonic stem cells and application in parkinsonian mice.', *Nature biotechnology*, 21(10), pp. 1200–7. doi: 10.1038/nbt870.

Bardy, C. *et al.* (2015) 'Neuronal medium that supports basic synaptic functions and activity of human neurons in vitro', *Proceedings of the National Academy of Sciences*, 112(20), pp. E2725–E2734. doi: 10.1073/pnas.1504393112.

Bayart, E. and Cohen-Haguenauer, O. (2013) 'Technological overview of iPS induction from human adult somatic cells.', *Current gene therapy*, 13(2), pp. 73–92.

Beltrão-Braga, P. C. B. *et al.* (2011) 'Feeder-free derivation of induced pluripotent stem cells from human immature dental pulp stem cells.', *Cell transplantation*, 20(11–12), pp. 1707–19. doi: 10.3727/096368911X566235.

Bissonnette, C. J. *et al.* (2011) 'The controlled generation of functional basal forebrain cholinergic neurons from human embryonic stem cells.', *Stem cells (Dayton, Ohio)*, 29(5), pp. 802–11. doi: 10.1002/stem.626.

Blaeser, A. *et al.* (2016) 'Controlling Shear Stress in 3D Bioprinting is a Key Factor to Balance Printing Resolution and Stem Cell Integrity', *Advanced Healthcare Materials*, 5(3), pp. 326–333. doi: 10.1002/adhm.201500677.

Bonaguidi, M. a *et al.* (2005) 'LIF and BMP signaling generate separate and discrete types of GFAP-expressing cells.', *Development (Cambridge, England)*, 132(24), pp. 5503–14. doi: 10.1242/dev.02166.

Borghese, L. *et al.* (2010) 'Inhibition of notch signaling in human embryonic stem cell-derived neural stem cells delays G1/S phase transition and accelerates neuronal differentiation in vitro and in vivo.', *Stem cells (Dayton, Ohio)*, 28(5), pp. 955–64. doi: 10.1002/stem.408.

Bourke, J. L. *et al.* (2014) 'Neuronal electrophysiological function and control of neurite outgrowth on electrospun polymer nanofibers are cell type dependent.', *Tissue engineering. Part A*, 20(5–6), pp. 1089–95. doi: 10.1089/ten.TEA.2013.0295.

Bozza, A. *et al.* (2014) 'Neural differentiation of pluripotent cells in 3D alginate-based cultures.', *Biomaterials*. Elsevier Ltd, 35(16), pp. 4636–45. doi: 10.1016/j.biomaterials.2014.02.039.

Brännvall, K. *et al.* (2007) 'Enhanced neuronal differentiation in a three-dimensional collagen-hyaluronan matrix', *Journal of Neuroscience Research*, 85(10), pp. 2138–2146. doi: 10.1002/jnr.21358.

Brennand, K. J. *et al.* (2015) 'Creating Patient-Specific Neural Cells for the in Vitro Study of Brain Disorders', *Stem Cell Reports*, 5(6), pp. 933–945. doi: 10.1016/j.stemcr.2015.10.011.

Briscoe, J. and Ericson, J. (2001) 'Specification of neuronal fates in the ventral neural tube.', *Current opinion in neurobiology*, 11(1), pp. 43–9.

Brodski, C. *et al.* (2003) 'Location and size of dopaminergic and serotonergic cell populations are controlled by the position of the midbrain-hindbrain organizer.', *The Journal of neuroscience : the official journal of the Society for Neuroscience*, 23(10), pp. 4199–207.

Busskamp, V. *et al.* (2014) 'Rapid neurogenesis through transcriptional activation in human stem cells.', *Molecular systems biology*, 10, p. 760.

Cambray, S. *et al.* (2012) 'Activin induces cortical interneuron identity and differentiation in embryonic stem cell-derived telencephalic neural precursors', *Nature Communications*, 3(May), p. 841. doi: 10.1038/ncomms1817.

Camp, J. G. *et al.* (2015) 'Human cerebral organoids recapitulate gene expression programs

of fetal neocortex development.', *Proceedings of the National Academy of Sciences of the United States of America*, 112(51), pp. 15672–7. doi: 10.1073/pnas.1520760112.

Carey, B. W. *et al.* (2009) 'Reprogramming of murine and human somatic cells using a single polycistronic vector.', *Proceedings of the National Academy of Sciences of the United States of America*, 106(1), pp. 157–62. doi: 10.1073/pnas.0811426106.

Chambers, S. M. *et al.* (2009) 'Highly efficient neural conversion of human ES and iPS cells by dual inhibition of SMAD signaling.', *Nature biotechnology*, 27(3), pp. 275–80. doi: 10.1038/nbt.1529.

Chanda, S. *et al.* (2014) 'Generation of induced neuronal cells by the single reprogramming factor ASCL1.', *Stem cell reports*, 3(2), pp. 282–96. doi: 10.1016/j.stemcr.2014.05.020.

Chang, C.-W. *et al.* (2009) 'Polycistronic lentiviral vector for "hit and run" reprogramming of adult skin fibroblasts to induced pluripotent stem cells.', *Stem cells (Dayton, Ohio)*, 27(5), pp. 1042–9. doi: 10.1002/stem.39.

Chatzi, C. *et al.* (2009) 'Derivation of homogeneous GABAergic neurons from mouse embryonic stem cells.', *Experimental neurology*. Elsevier Inc., 217(2), pp. 407–16. doi: 10.1016/j.expneurol.2009.03.032.

Chen, W. *et al.* (2014) 'Generation of the SCN1A epilepsy mutation in hiPS cells using the TALEN technique', *Scientific Reports*, 4, pp. 1–8. doi: 10.1038/srep05404.

Cheung, A. Y. L. *et al.* (2011) 'Isolation of MECP2-null Rett Syndrome patient hiPS cells and isogenic controls through X-chromosome inactivation', *Human Molecular Genetics*, 20(11), pp. 2103–2115. doi: 10.1093/hmg/ddr093.

Choi, S. H. *et al.* (2014) 'A three-dimensional human neural cell culture model of Alzheimer's disease', *Nature*. Nature Publishing Group, 515(7526), pp. 274–8. doi: 10.1038/nature13800.

Christopherson, K. S. *et al.* (2005) 'Thrombospondins are astrocyte-secreted proteins that promote CNS synaptogenesis.', *Cell*, 120(3), pp. 421–33. doi: 10.1016/j.cell.2004.12.020.

Chung, J. H. Y. *et al.* (2013) 'Bio-ink properties and printability for extrusion printing living cells', *Biomaterials Science*, 1(7), p. 763. doi: 10.1039/c3bm00012e.

Chwalek, K. *et al.* (2015) 'In vitro bioengineered model of cortical brain tissue.', *Nature*

protocols, 10(9), pp. 1362–73. doi: 10.1038/nprot.2015.091.

Clarke, L. E. and Barres, B. a (2013) 'Emerging roles of astrocytes in neural circuit development.', *Nature reviews. Neuroscience*, 14(5), pp. 311–21. doi: 10.1038/nrn3484.

Compagnucci, C. *et al.* (2014) 'In vitro neurogenesis: development and functional implications of iPSC technology.', *Cellular and molecular life sciences : CMLS*, 71(9), pp. 1623–39. doi: 10.1007/s00018-013-1511-1.

Cornock, R. *et al.* (2014) 'Coaxial additive manufacture of biomaterial composite scaffolds for tissue engineering.', *Biofabrication*, 6(2), p. 025002. doi: 10.1088/1758-5082/6/2/025002.

Corti, S. *et al.* (2012) 'Genetic correction of human induced pluripotent stem cells from patients with spinal muscular atrophy', *Sci Transl Med*, 4, p. 165ra162. doi: 10.1126/scitranslmed.3004108.

Crawford, T. Q. and Roelink, H. (2007) 'The notch response inhibitor DAPT enhances neuronal differentiation in embryonic stem cell-derived embryoid bodies independently of sonic hedgehog signaling.', *Developmental dynamics : an official publication of the American Association of Anatomists*, 236(3), pp. 886–92. doi: 10.1002/dvdy.21083.

Crompton, K. E. *et al.* (2007) 'Polylysine-functionalised thermoresponsive chitosan hydrogel for neural tissue engineering', *Biomaterials*, 28(3), pp. 441–449. doi: 10.1016/j.biomaterials.2006.08.044.

Crompton, L. a *et al.* (2013) 'Stepwise, non-adherent differentiation of human pluripotent stem cells to generate basal forebrain cholinergic neurons via hedgehog signaling.', *Stem cell research*. Elsevier B.V., 11(3), pp. 1206–21. doi: 10.1016/j.scr.2013.08.002.

Cullen, D. K. *et al.* (2007) 'Microfluidic engineered high cell density three-dimensional neural cultures.', *Journal of neural engineering*, 4(2), pp. 159–172. doi: 10.1088/1741-2560/4/2/015.

Cunningham, M. *et al.* (2014) 'hPSC-Derived Maturing GABAergic Interneurons Ameliorate Seizures and Abnormal Behavior in Epileptic Mice', *Cell Stem Cell*. Elsevier Inc., 15(5), pp. 559–573. doi: 10.1016/j.stem.2014.10.006.

Czepiel, M. *et al.* (2011) 'Differentiation of induced pluripotent stem cells into functional oligodendrocytes', *Glia*, 59(6), pp. 882–892. doi: 10.1002/glia.21159.

Dajani, R. *et al.* (2013) 'Investigation of Rett syndrome using pluripotent stem cells.', *Journal of cellular biochemistry*, 114(11), pp. 2446–53. doi: 10.1002/jcb.24597.

Danjo, T. *et al.* (2011) 'Subregional Specification of Embryonic Stem Cell-Derived Ventral Telencephalic Tissues by Timed and Combinatory Treatment with Extrinsic Signals', *Journal of Neuroscience*, 31(5), pp. 1919–1933. doi: 10.1523/JNEUROSCI.5128-10.2011.

Das, K. P., Freudenrich, T. M. and Mundy, W. R. (2004) 'Assessment of PC12 cell differentiation and neurite growth: A comparison of morphological and neurochemical measures', *Neurotoxicology and Teratology*, 26(3), pp. 397–406. doi: 10.1016/j.ntt.2004.02.006.

DeQuach, J. a *et al.* (2011) 'Decellularized porcine brain matrix for cell culture and tissue engineering scaffolds.', *Tissue engineering. Part A*, 17(21–22), pp. 2583–92. doi: 10.1089/ten.TEA.2010.0724.

DeRosa, B. a. *et al.* (2015) 'hVGAT-mCherry: A novel molecular tool for analysis of GABAergic neurons derived from human pluripotent stem cells.', *Molecular and cellular neurosciences*. Elsevier B.V., 68, pp. 244–57. doi: 10.1016/j.mcn.2015.08.007.

Discher, D. E., Janmey, P. and Wang, Y.-L. (2005) 'Tissue cells feel and respond to the stiffness of their substrate.', *Science (New York, N.Y.)*, 310(5751), pp. 1139–1143. doi: 10.1126/science.1116995.

Dowell-Mesfin, N. M. *et al.* (2004) 'Topographically modified surfaces affect orientation and growth of hippocampal neurons.', *Journal of neural engineering*, 1(2), pp. 78–90. doi: 10.1088/1741-2560/1/2/003.

Le Dréau, G. and Martí, E. (2012) 'Dorsal-ventral patterning of the neural tube: a tale of three signals.', *Developmental neurobiology*, 72(12), pp. 1471–81. doi: 10.1002/dneu.22015.

Drury, J. L. and Mooney, D. J. (2003) 'Hydrogels for tissue engineering: Scaffold design variables and applications', *Biomaterials*, 24(24), pp. 4337–4351. doi: 10.1016/S0142-9612(03)00340-5.

Du, X. and Parent, J. M. (2015) 'Using Patient-Derived Induced Pluripotent Stem Cells to Model and Treat Epilepsies.', *Current neurology and neuroscience reports*, 15(10), p. 71. doi: 10.1007/s11910-015-0588-3.

Duan, L. *et al.* (2014) 'Stem cell derived basal forebrain cholinergic neurons from Alzheimer's disease patients are more susceptible to cell death.', *Molecular neurodegeneration*, 9, p. 3. doi: 10.1186/1750-1326-9-3.

Duchi, S. *et al.* (2017) 'Handheld Co-Axial Bioprinting: Application to in situ surgical cartilage repair', *Scientific Reports*, 7(1), pp. 1–12. doi: 10.1038/s41598-017-05699-x.

Ebert, A. D. *et al.* (2009) 'Induced pluripotent stem cells from a spinal muscular atrophy patient.', *Nature*. Nature Publishing Group, 457(7227), pp. 277–80. doi: 10.1038/nature07677.

Eiraku, M. *et al.* (2008) 'Self-Organized Formation of Polarized Cortical Tissues from ESCs and Its Active Manipulation by Extrinsic??Signals', *Cell Stem Cell*. Elsevier Inc., 3(5), pp. 519–532. doi: 10.1016/j.stem.2008.09.002.

Elkabetz, Y. *et al.* (2008) 'Human ES cell-derived neural rosettes reveal a functionally distinct early neural stem cell stage.', *Genes & development*, 22(2), pp. 152–65. doi: 10.1101/gad.1616208.

Emdad, L. *et al.* (2012) 'Efficient Differentiation of Human Embryonic and Induced Pluripotent Stem Cells into Functional Astrocytes', *Stem Cells and Development*, 21(3), pp. 404–410. doi: 10.1089/scd.2010.0560.

Engler, A. J. *et al.* (2006) 'Matrix Elasticity Directs Stem Cell Lineage Specification', *Cell*, 126(4), pp. 677–689. doi: 10.1016/j.cell.2006.06.044.

Erceg, S. *et al.* (2012) 'Derivation of cerebellar neurons from human pluripotent stem cells.', *Current protocols in stem cell biology*, Chapter 1(March), p. Unit 1H.5. doi: 10.1002/9780470151808.sc01h05s20.

Espuny-Camacho, I. *et al.* (2013) 'Pyramidal Neurons Derived from Human Pluripotent Stem Cells Integrate Efficiently into Mouse Brain Circuits In Vivo', *Neuron*, 77(3), pp. 440–456. doi: 10.1016/j.neuron.2012.12.011.

Falk, A. *et al.* (2012) 'Capture of neuroepithelial-like stem cells from pluripotent stem cells provides a versatile system for in vitro production of human neurons.', *PloS one*, 7(1), p. e29597. doi: 10.1371/journal.pone.0029597.

Farra, N. *et al.* (2012) 'Rett syndrome induced pluripotent stem cell-derived neurons reveal novel neurophysiological alterations.', *Molecular psychiatry*. Nature Publishing Group,

17(12), pp. 1261–71. doi: 10.1038/mp.2011.180.

Ferris, C. J. *et al.* (2015) 'Peptide modification of purified gellan gum', *J. Mater. Chem. B*, 3(6), pp. 1106–1115. doi: 10.1039/C4TB01727G.

Fonseca, K. B. *et al.* (2011) 'Molecularly designed alginate hydrogels susceptible to local proteolysis as three-dimensional cellular microenvironments', *Acta Biomaterialia*. Acta Materialia Inc., 7(4), pp. 1674–1682. doi: 10.1016/j.actbio.2010.12.029.

Frampton, J. P. *et al.* (2011) 'Fabrication and optimization of alginate hydrogel constructs for use in 3D neural cell culture.', *Biomedical materials (Bristol, England)*, 6(1), p. 015002. doi: 10.1088/1748-6041/6/1/015002.

Franke, W. W., Grund, C. and Achtstatter, T. (1986) 'Co-expression of cytokeratins and neurofilament proteins in a permanent cell line: Cultured rat PC12 cells combine neuronal and epithelial features', *Journal of Cell Biology*, 103(5), pp. 1933–1943. doi: 10.1083/jcb.103.5.1933.

Frega, M. *et al.* (2015) 'Network dynamics of 3D engineered neuronal cultures: a new experimental model for in-vitro electrophysiology', *Scientific Reports*, 4(1), p. 5489. doi: 10.1038/srep05489.

Freudenberg, U. *et al.* (2009) 'A star-PEG-heparin hydrogel platform to aid cell replacement therapies for neurodegenerative diseases.', *Biomaterials*. Elsevier Ltd, 30(28), pp. 5049–60. doi: 10.1016/j.biomaterials.2009.06.002.

Friling, S. *et al.* (2009) 'Efficient production of mesencephalic dopamine neurons by Lmx1a expression in embryonic stem cells.', *Proceedings of the National Academy of Sciences of the United States of America*, 106(18), pp. 7613–8. doi: 10.1073/pnas.0902396106.

Frotscher, M. *et al.* (2009) 'Role of Reelin in the development and maintenance of cortical lamination', *Journal of Neural Transmission*, 116, pp. 1451–1455. doi: 10.1007/s00702-009-0228-7.

Fusaki, N. *et al.* (2009) 'Efficient induction of transgene-free human pluripotent stem cells using a vector based on Sendai virus, an RNA virus that does not integrate into the host genome', *Proceedings of the Japan Academy, Series B*, 85(8), pp. 348–362. doi: 10.2183/pjab.85.348.

Ganat, Y. *et al.* (2012) 'Identification of embryonic stem cell–derived midbrain

dopaminergic neurons for engraftment', *The Journal of clinical Investigation*, 122(8), pp. 2928–2939. doi: 10.1172/JCI58767DS1.

Gaspard, N. *et al.* (2008) 'An intrinsic mechanism of corticogenesis from embryonic stem cells.', *Nature*, 455(7211), pp. 351–7. doi: 10.1038/nature07287.

Gelain, F. *et al.* (2006) 'Designer self-assembling peptide nanofiber scaffolds for adult mouse neural stem cell 3-dimensional cultures.', *PloS one*, 1(1), p. e119. doi: 10.1371/journal.pone.0000119.

Georges, P. C. *et al.* (2006) 'Matrices with compliance comparable to that of brain tissue select neuronal over glial growth in mixed cortical cultures.', *Biophysical journal*. Elsevier, 90(8), pp. 3012–3018. doi: 10.1529/biophysj.105.073114.

Di Giorgio, F. P. *et al.* (2008) 'Human embryonic stem cell-derived motor neurons are sensitive to the toxic effect of glial cells carrying an ALS-causing mutation.', *Cell stem cell*. Elsevier Inc., 3(6), pp. 637–48. doi: 10.1016/j.stem.2008.09.017.

Gomez, N. *et al.* (2007) 'Micropatterned polypyrrole: A combination of electrical and topographical characteristics for the stimulation of cells', *Advanced Functional Materials*, 17(10), pp. 1645–1653. doi: 10.1002/adfm.200600669.

Gomez, N. and Schmidt, C. E. (2007) 'Nerve growth factor-immobilized polypyrrole: Bioactive electrically conducting polymer for enhanced neurite extension', *Journal of Biomedical Materials Research - Part A*, 81(1), pp. 135–149. doi: 10.1002/jbm.a.31047.

González, F., Boué, S. and Izpisúa Belmonte, J. C. (2011) 'Methods for making induced pluripotent stem cells: reprogramming à la carte.', *Nature reviews. Genetics*. Nature Publishing Group, 12(4), pp. 231–42. doi: 10.1038/nrg2937.

Goridis, C. and Rohrer, H. (2002) 'Specification of catecholaminergic and serotonergic neurons.', *Nature reviews. Neuroscience*, 3(7), pp. 531–41. doi: 10.1038/nrn871.

Gorris, R. *et al.* (2015) 'Pluripotent stem cell-derived radial glia-like cells as stable intermediate for efficient generation of human oligodendrocytes', *Glia*, 63(12), pp. 2152–2167. doi: 10.1002/glia.22882.

Goulburn, A. L. *et al.* (2011) 'A targeted NKX2.1 human embryonic stem cell reporter line enables identification of human basal forebrain derivatives', *Stem Cells*, 29(3), pp. 462–473. doi: 10.1002/stem.587.

Goulburn, A. L. *et al.* (2012) 'Generating GABAergic cerebral cortical interneurons from mouse and human embryonic stem cells', *Stem Cell Research*. Elsevier B.V., 8(3), pp. 416–426. doi: 10.1016/j.scr.2011.12.002.

Grade, S., Bernardino, L. and Malva, J. O. (2013) 'Oligodendrogenesis from neural stem cells: perspectives for remyelinating strategies.', *International journal of developmental neuroscience : the official journal of the International Society for Developmental Neuroscience*. International Society for Developmental Neuroscience, 31(7), pp. 692–700. doi: 10.1016/j.ijdevneu.2013.01.004.

Gu, Q. *et al.* (2017) '3D Bioprinting Human Induced Pluripotent Stem Cell Constructs for In Situ Cell Proliferation and Successive Multilineage Differentiation', *Advanced Healthcare Materials*, 6(17), pp. 1–11. doi: 10.1002/adhm.201700175.

Gupta, K. *et al.* (2012) 'Human embryonic stem cell derived astrocytes mediate non-cell-autonomous neuroprotection through endogenous and drug-induced mechanisms', *Cell Death and Differentiation*. Nature Publishing Group, 19(5), pp. 779–787. doi: 10.1038/cdd.2011.154.

Hansen, D. V., Rubenstein, J. L. R. and Kriegstein, A. R. (2011) 'Deriving Excitatory Neurons of the Neocortex from Pluripotent Stem Cells', *Neuron*. Elsevier Inc., 70(4), pp. 645–660. doi: 10.1016/j.neuron.2011.05.006.

Hanson, J. N. *et al.* (2009) 'Textural guidance cues for controlling process outgrowth of mammalian neurons.', *Lab on a chip*, 9(1), pp. 122–131. doi: 10.1039/b803595d.

Hartfield, E. M. *et al.* (2014) 'Physiological characterisation of human iPS-derived dopaminergic neurons.', *PloS one*, 9(2), p. e87388. doi: 10.1371/journal.pone.0087388.

Higurashi, N. *et al.* (2013) 'A human Dravet syndrome model from patient induced pluripotent stem cells.', *Molecular brain*, 6, p. 19. doi: 10.1186/1756-6606-6-19.

Ho, S.-M. *et al.* (2016) 'Rapid Ngn2-induction of excitatory neurons from hiPSC-derived neural progenitor cells.', *Methods (San Diego, Calif.)*. Elsevier Inc., 101, pp. 113–24. doi: 10.1016/j.ymeth.2015.11.019.

Hoffman-Kim, D., Mitchel, J. a and Bellamkonda, R. V (2010) 'Topography, cell response, and nerve regeneration.', *Annual review of biomedical engineering*, 12, pp. 203–31. doi: 10.1146/annurev-bioeng-070909-105351.

Hosseinkhani, H. *et al.* (2013) 'Engineering three-dimensional collagen-IKVAV matrix to mimic neural microenvironment.', *ACS chemical neuroscience*, 4(8), pp. 1229–35. doi: 10.1021/cn400075h.

Hu, B.-Y. *et al.* (2009) 'Human oligodendrocytes from embryonic stem cells: conserved SHH signaling networks and divergent FGF effects.', *Development (Cambridge, England)*, 136(9), pp. 1443–52. doi: 10.1242/dev.029447.

Hu, B.-Y. *et al.* (2010) 'Neural differentiation of human induced pluripotent stem cells follows developmental principles but with variable potency.', *Proceedings of the National Academy of Sciences of the United States of America*, 107(9), pp. 4335–40. doi: 10.1073/pnas.0910012107.

Hu, B.-Y., Du, Z.-W. and Zhang, S.-C. (2009) 'Differentiation of human oligodendrocytes from pluripotent stem cells.', *Nature protocols*. Nature Publishing Group, 4(11), pp. 1614–22. doi: 10.1038/nprot.2009.186.

Hu, B.-Y. and Zhang, S.-C. (2009) 'Differentiation of spinal motor neurons from pluripotent human stem cells.', *Nature protocols*, 4(9), pp. 1295–304. doi: 10.1038/nprot.2009.127.

Hu, M. *et al.* (2009) 'Cell immobilization in gelatin-hydroxyphenylpropionic acid hydrogel fibers', *Biomaterials*. Elsevier Ltd, 30(21), pp. 3523–3531. doi: 10.1016/j.biomaterials.2009.03.004.

Hu, R. *et al.* (2007) 'Astrocyte-derived estrogen enhances synapse formation and synaptic transmission between cultured neonatal rat cortical neurons.', *Neuroscience*, 144(4), pp. 1229–40. doi: 10.1016/j.neuroscience.2006.09.056.

Huch, M. and Koo, B. (2015) 'Modeling mouse and human development using organoid cultures.', *Development (Cambridge, England)*, 142(18), pp. 3113–25. doi: 10.1242/dev.118570.

Hughes, E. G., Elmariah, S. B. and Balice-Gordon, R. J. (2010) 'Astrocyte secreted proteins selectively increase hippocampal GABAergic axon length, branching, and synaptogenesis.', *Molecular and cellular neurosciences*. Elsevier Inc., 43(1), pp. 136–45. doi: 10.1016/j.mcn.2009.10.004.

Imaizumi, Y. and Okano, H. (2014) 'Modeling human neurological disorders with induced pluripotent stem cells.', *Journal of neurochemistry*, 129(3), pp. 388–99. doi:

10.1111/jnc.12625.

Imayoshi, I. and Kageyama, R. (2014) 'bHLH factors in self-renewal, multipotency, and fate choice of neural progenitor cells.', *Neuron*. Elsevier Inc., 82(1), pp. 9–23. doi: 10.1016/j.neuron.2014.03.018.

Irons, H. R. *et al.* (2008) 'Three-dimensional neural constructs: a novel platform for neurophysiological investigation.', *Journal of neural engineering*, 5(3), pp. 333–41. doi: 10.1088/1741-2560/5/3/006.

Israel, M. a *et al.* (2012) 'Probing sporadic and familial Alzheimer's disease using induced pluripotent stem cells.', *Nature*. Nature Publishing Group, 482(7384), pp. 216–20. doi: 10.1038/nature10821.

Izrael, M. *et al.* (2007) 'Human oligodendrocytes derived from embryonic stem cells: Effect of noggin on phenotypic differentiation in vitro and on myelination in vivo', *Molecular and Cellular Neuroscience*, 34(3), pp. 310–323. doi: 10.1016/j.mcn.2006.11.008.

Jessell, T. M. (2000) 'Neuronal specification in the spinal cord: inductive signals and transcriptional codes.', *Nature reviews. Genetics*, 1(1), pp. 20–9. doi: 10.1038/35049541.

Jiao, J. *et al.* (2013) 'Modeling Dravet syndrome using induced pluripotent stem cells (iPSCs) and directly converted neurons', *Human Molecular Genetics*, 22(21), pp. 4241–4252. doi: 10.1093/hmg/ddt275.

Jo, J. *et al.* (2016) 'Midbrain-like Organoids from Human Pluripotent Stem Cells Contain Functional Dopaminergic and Neuromelanin-Producing Neurons.', *Cell stem cell*, 19(2), pp. 248–257. doi: 10.1016/j.stem.2016.07.005.

Juopperi, T. a *et al.* (2012) 'Astrocytes generated from patient induced pluripotent stem cells recapitulate features of Huntington's disease patient cells.', *Molecular brain*. Molecular Brain, 5(1), p. 17. doi: 10.1186/1756-6606-5-17.

Kachouie, N. N. *et al.* (2010) 'Directed assembly of cell-laden hydrogels for engineering functional tissues.', *Organogenesis*, 6(4), pp. 234–244. doi: 10.4161/org.6.4.12650.

Kadoshima, T. *et al.* (2013) 'Self-organization of axial polarity, inside-out layer pattern, and species-specific progenitor dynamics in human ES cell-derived neocortex.', *Proceedings of the National Academy of Sciences of the United States of America*, 110(50), pp. 20284–9. doi: 10.1073/pnas.1315710110.

Kaneko, A. and Sankai, Y. (2014) 'Long-term culture of rat hippocampal neurons at low density in serum-free medium: combination of the sandwich culture technique with the three-dimensional nanofibrous hydrogel PuraMatrix.', *PloS one*, 9(7), p. e102703. doi: 10.1371/journal.pone.0102703.

Kang, H.-W. *et al.* (2016) 'A 3D bioprinting system to produce human-scale tissue constructs with structural integrity.', *Nature biotechnology*. Nature Publishing Group, 34(3), pp. 312–9. doi: 10.1038/nbt.3413.

Kang, S.-M. *et al.* (2007) 'Efficient induction of oligodendrocytes from human embryonic stem cells.', *Stem cells (Dayton, Ohio)*, 25(2), pp. 419–24. doi: 10.1634/stemcells.2005-0482.

Kanski, R. *et al.* (2014) 'A star is born: new insights into the mechanism of astrogenesis.', *Cellular and molecular life sciences : CMLS*, 71(3), pp. 433–47. doi: 10.1007/s00018-013-1435-9.

Karumbayaram, S. *et al.* (2009) 'Directed differentiation of human-induced pluripotent stem cells generates active motor neurons.', *Stem cells (Dayton, Ohio)*, 27(4), pp. 806–11. doi: 10.1002/stem.31.

Karus, M., Blaess, S. and Brüstle, O. (2014) 'Self-organization of neural tissue architectures from pluripotent stem cells.', *The Journal of comparative neurology*, 522(12), pp. 2831–44. doi: 10.1002/cne.23608.

Kawasaki, H. *et al.* (2000) 'Induction of midbrain dopaminergic neurons from ES cells by stromal cell-derived inducing activity.', *Neuron*, 28(1), pp. 31–40. doi: 10.1016/S0896-6273(00)00083-0.

Kelava, I. and Lancaster, M. A. (2016) 'Stem Cell Models of Human Brain Development', *Cell Stem Cell*. Elsevier Inc., 18(6), pp. 736–748. doi: 10.1016/j.stem.2016.05.022.

Keung, A. J. *et al.* (2012) 'Soft microenvironments promote the early neurogenic differentiation but not self-renewal of human pluripotent stem cells.', *Integrative biology : quantitative biosciences from nano to macro*, 4(9), pp. 1049–58. doi: 10.1039/c2ib20083j.

Kikuchi, T. *et al.* (2011) 'Survival of human induced pluripotent stem cell-derived midbrain dopaminergic neurons in the brain of a primate model of Parkinson's disease.', *Journal of Parkinson's disease*, 1(4), pp. 395–412. doi: 10.3233/JPD-2011-11070.

Kim, D. *et al.* (2009) 'Generation of human induced pluripotent stem cells by direct delivery of reprogramming proteins.', *Cell stem cell*. Elsevier Inc., 4(6), pp. 472–6. doi: 10.1016/j.stem.2009.05.005.

Kim, J.-E. *et al.* (2011) 'Investigating synapse formation and function using human pluripotent stem cell-derived neurons.', *Proceedings of the National Academy of Sciences of the United States of America*, 108(7), pp. 3005–10. doi: 10.1073/pnas.1007753108.

Kim, J., Sachdev, P. and Sidhu, K. (2013) 'Alginate microcapsule as a 3D platform for the efficient differentiation of human embryonic stem cells to dopamine neurons.', *Stem cell research*. Elsevier B.V., 11(3), pp. 978–89. doi: 10.1016/j.scr.2013.06.005.

Kim, K. *et al.* (2011) 'Donor cell type can influence the epigenome and differentiation potential of human induced pluripotent stem cells.', *Nature biotechnology*, 29(12), pp. 1117–9. doi: 10.1038/nbt.2052.

Kim, K. Y., Hysolli, E. and Park, I. H. (2011) 'Neuronal maturation defect in induced pluripotent stem cells from patients with Rett syndrome', *Proc Natl Acad Sci U S A*, 108(34), pp. 14169–14174. doi: 10.1073/pnas.1018979108.

Kim, T. G. *et al.* (2014) 'Efficient specification of interneurons from human pluripotent stem cells by dorsoventral and rostrocaudal modulation', *Stem Cells*, 32, pp. 1789–1804. doi: 10.1002/stem.1704.

Kim, Y. H. *et al.* (2015) 'A 3D human neural cell culture system for modeling Alzheimer's disease.', *Nature protocols*, 10(7), pp. 985–1006. doi: 10.1038/nprot.2015.065.

Kim, Y. T. *et al.* (2008) 'The role of aligned polymer fiber-based constructs in the bridging of long peripheral nerve gaps', *Biomaterials*, 29(21), pp. 3117–3127. doi: 10.1016/j.biomaterials.2008.03.042.

Kirwan, P. *et al.* (2015) 'Development and function of human cerebral cortex neural networks from pluripotent stem cells in vitro', *Development*, 142(18), pp. 3178–3187. doi: 10.1242/dev.123851.

Knowlton, S. *et al.* (2018) 'Bioprinting for Neural Tissue Engineering.', *Trends in neurosciences*. Elsevier Ltd, 41(1), pp. 31–46. doi: 10.1016/j.tins.2017.11.001.

Koch, P. *et al.* (2009) 'A rosette-type, self-renewing human ES cell-derived neural stem cell with potential for in vitro instruction and synaptic integration.', *Proceedings of the National*

Academy of Sciences of the United States of America, 106(9), pp. 3225–30. doi: 10.1073/pnas.0808387106.

Kondo, T. *et al.* (2014) 'Focal Transplantation of Human iPSC-Derived Glial-Rich Neural Progenitors Improves Lifespan of ALS Mice', *Stem Cell Reports*. The Authors, 3(2), pp. 242–249. doi: 10.1016/j.stemcr.2014.05.017.

Kotwal, A. and Schmidt, C. E. (2001) 'Electrical stimulation alters protein adsorption and nerve cell interactions with electrically conducting biomaterials', *Biomaterials*, 22(10), pp. 1055–1064. doi: 10.1016/S0142-9612(00)00344-6.

Koutsopoulos, S. and Zhang, S. (2013) 'Long-term three-dimensional neural tissue cultures in functionalized self-assembling peptide hydrogels, matrigel and collagen I.', *Acta biomaterialia*. Acta Materialia Inc., 9(2), pp. 5162–9. doi: 10.1016/j.actbio.2012.09.010.

Krencik, R. *et al.* (2011) 'Specification of transplantable astroglial subtypes from human pluripotent stem cells.', *Nature biotechnology*. Nature Publishing Group, 29(6), pp. 528–34. doi: 10.1038/nbt.1877.

Kriks, S. *et al.* (2011) 'Dopamine neurons derived from human ES cells efficiently engraft in animal models of Parkinson's disease.', *Nature*. Nature Publishing Group, 480(7378), pp. 547–51. doi: 10.1038/nature10648.

Kucukdereli, H. *et al.* (2011) 'Control of excitatory CNS synaptogenesis by astrocyte-secreted proteins Hevin and SPARC.', *Proceedings of the National Academy of Sciences of the United States of America*, 108(32), pp. E440-9. doi: 10.1073/pnas.1104977108.

Kunze, A. *et al.* (2011) 'Micropatterning neural cell cultures in 3D with a multi-layered scaffold', *Biomaterials*. Elsevier Ltd, 32(8), pp. 2088–2098. doi: 10.1016/j.biomaterials.2010.11.047.

Kuo, Y.-C. and Chang, Y.-H. (2013) 'Differentiation of induced pluripotent stem cells toward neurons in hydrogel biomaterials.', *Colloids and surfaces. B, Biointerfaces*. Elsevier B.V., 102, pp. 405–11. doi: 10.1016/j.colsurfb.2012.08.061.

Lancaster, M. a. and Knoblich, J. a. (2014) 'Organogenesis in a dish: modeling development and disease using organoid technologies.', *Science (New York, N.Y.)*, 345, p. 1247125. doi: 10.1126/science.1247125.

Lancaster, M. a *et al.* (2013) 'Cerebral organoids model human brain development and

microcephaly.', *Nature*. Nature Publishing Group, 501(7467), pp. 373–9. doi: 10.1038/nature12517.

LaPlaca, M. C. *et al.* (2010) 'Three-dimensional neuronal cultures', in Berthiaume, F. and Morgan, J. (eds) *Methods in Bioengineering: 3D Tissue Engineering*. Artech House, pp. 187–204.

Lee, H. *et al.* (2007) 'Directed differentiation and transplantation of human embryonic stem cell-derived motoneurons.', *Stem cells (Dayton, Ohio)*, 25(8), pp. 1931–9. doi: 10.1634/stemcells.2007-0097.

Lee, J. Y. *et al.* (2009) 'Polypyrrole-coated electrospun PLGA nanofibers for neural tissue applications', *Biomaterials*. Elsevier Ltd, 30(26), pp. 4325–4335. doi: 10.1016/j.biomaterials.2009.04.042.

Lee, M. K. *et al.* (2015) 'A bio-inspired, microchanneled hydrogel with controlled spacing of cell adhesion ligands regulates 3D spatial organization of cells and tissue.', *Biomaterials*. Elsevier Ltd, 58, pp. 26–34. doi: 10.1016/j.biomaterials.2015.04.014.

Leipzig, N. D. *et al.* (2011) 'Differentiation of neural stem cells in three-dimensional growth factor-immobilized chitosan hydrogel scaffolds.', *Biomaterials*. Elsevier Ltd, 32(1), pp. 57–64. doi: 10.1016/j.biomaterials.2010.09.031.

Li, H., Wijekoon, A. and Leipzig, N. D. (2012) '3D differentiation of neural stem cells in macroporous photopolymerizable hydrogel scaffolds.', *PloS one*, 7(11), p. e48824. doi: 10.1371/journal.pone.0048824.

Li, H., Wijekoon, A. and Leipzig, N. D. (2014) 'Encapsulated neural stem cell neuronal differentiation in fluorinated methacrylamide chitosan hydrogels.', *Annals of biomedical engineering*, 42(7), pp. 1456–69. doi: 10.1007/s10439-013-0925-0.

Li, L. *et al.* (2011) 'Neural lineage differentiation of embryonic stem cells within alginate microbeads.', *Biomaterials*. Elsevier Ltd, 32(20), pp. 4489–97. doi: 10.1016/j.biomaterials.2011.03.019.

Li, Q. and Chau, Y. (2010) 'Neural differentiation directed by self-assembling peptide scaffolds presenting laminin-derived epitopes', *Journal of Biomedical Materials Research - Part A*, 94, pp. 688–699. doi: 10.1002/jbm.a.32707.

Li, Q., Chow, K. L. and Chau, Y. (2014) 'Three-dimensional self-assembling peptide matrix

enhances the formation of embryoid bodies and their neuronal differentiation.', *Journal of biomedical materials research. Part A*, 102(6), pp. 1991–2000. doi: 10.1002/jbm.a.34876.

Li, X.-J. *et al.* (2008) 'Directed differentiation of ventral spinal progenitors and motor neurons from human embryonic stem cells by small molecules.', *Stem cells (Dayton, Ohio)*, 26(4), pp. 886–93. doi: 10.1634/stemcells.2007-0620.

Li, X.-J. *et al.* (2009) 'Coordination of sonic hedgehog and Wnt signaling determines ventral and dorsal telencephalic neuron types from human embryonic stem cells.', *Development (Cambridge, England)*, 136(23), pp. 4055–63. doi: 10.1242/dev.036624.

Lindenbaum, M. H. *et al.* (1988) 'Transcriptional and post-transcriptional effects of nerve growth factor on expression of the three neurofilament subunits in PC-12 cells.', *The Journal of Bological Chemistry*, 263(12), pp. 5662–5667.

Liu, H. *et al.* (2010) 'Generation of endoderm-derived human induced pluripotent stem cells from primary hepatocytes.', *Hepatology (Baltimore, Md.)*, 51(5), pp. 1810–9. doi: 10.1002/hep.23626.

Liu, Q. *et al.* (2004) 'Neurofilament proteins in neurodegenerative diseases', *Cellular and Molecular Life Sciences*, 61(24), pp. 3057–3075. doi: 10.1007/s00018-004-4268-8.

Liu, Y. *et al.* (2013) 'Directed differentiation of forebrain GABA interneurons from human pluripotent stem cells.', *Nature protocols*, 8(9), pp. 1670–9. doi: 10.1038/nprot.2013.106.

Liu, Y. *et al.* (2013) 'Dravet syndrome patient-derived neurons suggest a novel epilepsy mechanism', *Annals of Neurology*, 74(1), pp. 128–139. doi: 10.1002/ana.23897.

Lozano, R. *et al.* (2015) '3D printing of layered brain-like structures using peptide modified gellan gum substrates.', *Biomaterials*, 67, pp. 264–73. doi: 10.1016/j.biomaterials.2015.07.022.

Lu, H. F. *et al.* (2012) 'Efficient neuronal differentiation and maturation of human pluripotent stem cells encapsulated in 3D microfibrous scaffolds.', *Biomaterials*. Elsevier Ltd, 33(36), pp. 9179–87. doi: 10.1016/j.biomaterials.2012.09.006.

Ma, L. *et al.* (2012) 'Human embryonic stem cell-derived GABA neurons correct locomotion deficits in quinolinic acid-lesioned mice', *Cell Stem Cell*. Elsevier Inc., 10(4), pp. 455–464. doi: 10.1016/j.stem.2012.01.021.

Ma, W. *et al.* (2004) 'CNS stem and progenitor cell differentiation into functional neuronal circuits in three-dimensional collagen gels', *Experimental Neurology*, 190(2), pp. 276–288. doi: 10.1016/j.expneurol.2003.10.016.

Mack, A. a *et al.* (2011) 'Generation of induced pluripotent stem cells from CD34+ cells across blood drawn from multiple donors with non-integrating episomal vectors.', *PloS one*, 6(11), p. e27956. doi: 10.1371/journal.pone.0027956.

Maden, M. (2006) 'Retinoids and spinal cord development.', *Journal of neurobiology*, 66(7), pp. 726–38. doi: 10.1002/neu.20248.

Maeda, H. *et al.* (2016) 'Establishment of isogenic iPSCs from an individual with SCN1A mutation mosaicism as a model for investigating neurocognitive impairment in Dravet syndrome.', *Journal of human genetics*. Nature Publishing Group, (January), pp. 1–5. doi: 10.1038/jhg.2016.5.

Maherali, N. and Hochedlinger, K. (2008) 'Guidelines and techniques for the generation of induced pluripotent stem cells.', *Cell stem cell*. Elsevier Inc., 3(6), pp. 595–605. doi: 10.1016/j.stem.2008.11.008.

Mallamaci, A. (2013) 'Developmental control of cortico-cerebral astrogenesis.', *The International journal of developmental biology*, 57(9–10), pp. 689–706. doi: 10.1387/ijdb.130148am.

Marchetto, M. C. *et al.* (2011) 'Induced pluripotent stem cells (iPSCs) and neurological disease modeling: progress and promises.', *Human molecular genetics*, 20(R2), pp. R109-15. doi: 10.1093/hmg/ddr336.

Marchetto, M. C. *et al.* (2017) 'Altered proliferation and networks in neural cells derived from idiopathic autistic individuals.', *Molecular psychiatry*, 22(6), pp. 820–835. doi: 10.1038/mp.2016.95.

Marchetto, M. C. N. *et al.* (2010) 'A model for neural development and treatment of rett syndrome using human induced pluripotent stem cells', *Cell*. Elsevier Ltd, 143(4), pp. 527–539. doi: 10.1016/j.cell.2010.10.016.

Mariani, J. *et al.* (2012) 'Modeling human cortical development in vitro using induced pluripotent stem cells', *Proceedings of the National Academy of Sciences*, 109(31), pp. 12770–12775. doi: 10.1073/pnas.1202944109/-

/DCSupplemental.www.pnas.org/cgi/doi/10.1073/pnas.1202944109.

Mariani, J. *et al.* (2015) 'FOXG1-Dependent Dysregulation of GABA/Glutamate Neuron Differentiation in Autism Spectrum Disorders.', *Cell*, 162(2), pp. 375–90. doi: 10.1016/j.cell.2015.06.034.

Maroof, A. M. *et al.* (2010) 'Prospective isolation of cortical interneuron precursors from mouse embryonic stem cells.', *The Journal of neuroscience : the official journal of the Society for Neuroscience*, 30(13), pp. 4667–75. doi: 10.1523/JNEUROSCI.4255-09.2010.

Matthews, K. *et al.* (2005) 'Animal models of depression: Navigating through the clinical fog', *Neuroscience and Biobehavioral Reviews*, 29(4–5), pp. 503–513. doi: 10.1016/j.neubiorev.2005.03.005.

Mattis, V. B. and Svendsen, C. N. (2011) 'Induced pluripotent stem cells: a new revolution for clinical neurology?', *The Lancet. Neurology*. Elsevier Ltd, 10(4), pp. 383–94. doi: 10.1016/S1474-4422(11)70022-9.

Matyash, M. *et al.* (2012) 'Novel soft alginate hydrogel strongly supports neurite growth and protects neurons against oxidative stress.', *Tissue engineering. Part A*, 18(1–2), pp. 55–66. doi: 10.1089/ten.TEA.2011.0097.

Matyash, M. *et al.* (2014) 'Swelling and mechanical properties of alginate hydrogels with respect to promotion of neural growth.', *Tissue engineering. Part C, Methods*, 20(5), pp. 401–11. doi: 10.1089/ten.TEC.2013.0252.

Mayshar, Y. *et al.* (2010) 'Identification and classification of chromosomal aberrations in human induced pluripotent stem cells.', *Cell stem cell*. Elsevier Inc., 7(4), pp. 521–31. doi: 10.1016/j.stem.2010.07.017.

Mazzoni, E. O. *et al.* (2013) 'Synergistic binding of transcription factors to cell-specific enhancers programs motor neuron identity.', *Nature neuroscience*, 16(9), pp. 1219–27. doi: 10.1038/nn.3467.

McKinnon, D. D., Kloxin, A. M. and Anseth, K. S. (2013) 'Synthetic hydrogel platform for three-dimensional culture of embryonic stem cell-derived motor neurons', *Biomaterials Science*, 1(5), p. 460. doi: 10.1039/c3bm00166k.

McMurtrey, R. J. (2014) 'Patterned and functionalized nanofiber scaffolds in three-dimensional hydrogel constructs enhance neurite outgrowth and directional control.',

Journal of neural engineering. IOP Publishing, 11(6), p. 066009. doi: 10.1088/1741-2560/11/6/066009.

Meinhardt, A. *et al.* (2014) '3D reconstitution of the patterned neural tube from embryonic stem cells.', *Stem cell reports*, 3(6), pp. 987–99. doi: 10.1016/j.stemcr.2014.09.020.

Meli, L. *et al.* (2014) 'Three dimensional cellular microarray platform for human neural stem cell differentiation and toxicology.', *Stem cell research*. Elsevier B.V., 13(1), pp. 36–47. doi: 10.1016/j.scr.2014.04.004.

Miller, J. D. *et al.* (2013) 'Human iPSC-based modeling of late-onset disease via progerin-induced aging.', *Cell stem cell*. Elsevier Inc., 13(6), pp. 691–705. doi: 10.1016/j.stem.2013.11.006.

Millet, L. J. and Gillette, M. U. (2012) 'Over a century of neuron culture: from the hanging drop to microfluidic devices.', *The Yale journal of biology and medicine*, 85(4), pp. 501–21.

Mironi-Harpaz, I. *et al.* (2012) 'Photopolymerization of cell-encapsulating hydrogels: Crosslinking efficiency versus cytotoxicity', *Acta Biomaterialia*. Acta Materialia Inc., 8(5), pp. 1838–1848. doi: 10.1016/j.actbio.2011.12.034.

Mong, J. *et al.* (2014) 'Transcription factor-induced lineage programming of noradrenaline and motor neurons from embryonic stem cells', *Stem Cells*, 32(3), pp. 609–622. doi: 10.1002/stem.1585.

Montgomery, A. *et al.* (2015) 'Engineering personalized neural tissue by combining induced pluripotent stem cells with fibrin scaffolds', *Biomater. Sci.* Royal Society of Chemistry, 3(2), pp. 401–413. doi: 10.1039/C4BM00299G.

Moreno, E. L. *et al.* (2015) 'Differentiation of neuroepithelial stem cells into functional dopaminergic neurons in 3D microfluidic cell culture.', *Lab on a chip*. Royal Society of Chemistry, 15(11), pp. 2419–28. doi: 10.1039/c5lc00180c.

Muchkaeva, I. A. *et al.* (2014) 'Generation of iPS cells from human hair follice dermal papilla cells', *Acta Naturae*, 6(20), pp. 45–53.

Muguruma, K. *et al.* (2015) 'Self-organization of polarized cerebellar tissue in 3D culture of human pluripotent stem cells.', *Cell reports*. The Authors, 10(4), pp. 537–50. doi: 10.1016/j.celrep.2014.12.051.

Mukhatyar, V. J. *et al.* (2011) 'Role of fibronectin in topographical guidance of neurite extension on electrospun fibers.', *Biomaterials*. Elsevier Ltd, 32(16), pp. 3958–68. doi: 10.1016/j.biomaterials.2011.02.015.

Mungenast, A. E., Siegert, S. and Tsai, L.-H. (2016) 'Modeling Alzheimer's disease with human induced pluripotent stem (iPS) cells.', *Molecular and cellular neurosciences*. Elsevier B.V., 73, pp. 13–31. doi: 10.1016/j.mcn.2015.11.010.

Muratore, C. R. *et al.* (2014) 'Comparison and Optimization of hiPSC Forebrain Cortical Differentiation Protocols.', *PloS one*, 9(8), p. e105807. doi: 10.1371/journal.pone.0105807.

Nagashima, F. *et al.* (2014) 'Novel and robust transplantation reveals the acquisition of polarized processes by cortical cells derived from mouse and human pluripotent stem cells.', *Stem cells and development*, 23(18), pp. 2129–42. doi: 10.1089/scd.2013.0251.

Nakaji-Hirabayashi, T., Kato, K. and Iwata, H. (2012) 'Improvement of neural stem cell survival in collagen hydrogels by incorporating laminin-derived cell adhesive polypeptides', *Bioconjugate Chemistry*, 23(2), pp. 212–221. doi: 10.1021/bc200481v.

Naujock, M. *et al.* (2014) 'Molecular and functional analyses of motor neurons generated from human cord-blood-derived induced pluripotent stem cells.', *Stem cells and development*, 23(24), pp. 3011–20. doi: 10.1089/scd.2014.0180.

Needham, K. *et al.* (2014) 'ScienceDirect Electrophysiological properties of neurosensory progenitors derived from human embryonic stem cells', *Stem Cell Research*, 12(1), pp. 241–249. doi: 10.1016/j.scr.2013.10.011.

Nemati, S. *et al.* (2011) 'Long-term self-renewable feeder-free human induced pluripotent stem cell-derived neural progenitors.', *Stem cells and development*, 20(3), pp. 503–14. doi: 10.1089/scd.2010.0143.

Ni, N. *et al.* (2013) 'Self-assembling peptide nanofiber scaffolds enhance dopaminergic differentiation of mouse pluripotent stem cells in 3-dimensional culture.', *PloS one*, 8(12), p. e84504. doi: 10.1371/journal.pone.0084504.

Nieweg, K. *et al.* (2015) 'Alzheimer's disease-related amyloid-β induces synaptotoxicity in human iPS cell-derived neurons.', *Cell death & disease*, 6, p. e1709. doi: 10.1038/cddis.2015.72.

Nikouei, K., Muñoz-Manchado, A. B. and Hjerling-Leffler, J. (2016) 'BCL11B/CTIP2 is highly

expressed in GABAergic interneurons of the mouse somatosensory cortex.', *Journal of chemical neuroanatomy*, 71, pp. 1–5. doi: 10.1016/j.jchemneu.2015.12.004.

Nistor, G. I. *et al.* (2005) 'Human embryonic stem cells differentiate into oligodendrocytes in high purity and myelinate after spinal cord transplantation', *Glia*, 49(3), pp. 385–396. doi: 10.1002/glia.20127.

Noebels, J. (2015) 'Pathway-driven discovery of epilepsy genes.', *Nature neuroscience*, 18(3), pp. 344–350. doi: 10.1038/nn.3933.

Novikova, L. N. *et al.* (2006) 'Alginate hydrogel and matrigel as potential cell carriers for neurotransplantation.', *Journal of biomedical materials research. Part A*, 77(2), pp. 242–52. doi: 10.1002/jbm.a.30603.

O'Connell, C. D. *et al.* (2016) 'Development of the Biopen: A handheld device for surgical printing of adipose stem cells at a chondral wound site', *Biofabrication*. IOP Publishing, 8(1). doi: 10.1088/1758-5090/8/1/015019.

O'Connor, S. M. *et al.* (2000) 'Primary neural precursor cell expansion, differentiation and cytosolic Ca2+ response in three-dimensional collagen gel', *Journal of Neuroscience Methods*, 102(2), pp. 187–195. doi: 10.1016/S0165-0270(00)00303-4.

O'Connor, S. M. *et al.* (2001) 'Survival and neurite outgrowth of rat cortical neurons in three-dimensional agarose and collagen gel matrices', *Neuroscience Letters*, 304(3), pp. 189–193. doi: 10.1016/S0304-3940(01)01769-4.

Odawara, A. *et al.* (2016) 'Physiological maturation and drug responses of human induced pluripotent stem cell-derived cortical neuronal networks in long-term culture.', *Scientific reports*. Nature Publishing Group, 6(April), p. 26181. doi: 10.1038/srep26181.

Odawara, A., Gotoh, M. and Suzuki, I. (2013) 'A three-dimensional neuronal culture technique that controls the direction of neurite elongation and the position of soma to mimic the layered structure of the brain', *RSC Advances*, 3(45), p. 23620. doi: 10.1039/c3ra44757j.

Ohuchi, T. *et al.* (2002) 'Assay-based quantitative analysis of PC12 cell differentiation.', *Journal of neuroscience methods*, 118(1), pp. 1–8.

Okabe, S. *et al.* (1996) 'Development of neuronal precursor cells and functional postmitotic neurons from embryonic stem cells in vitro', *Mechanisms of Development*, 59(1), pp. 89–

102. doi: 10.1016/0925-4773(96)00572-2.

Okada, Y. *et al.* (2004) 'Retinoic-acid-concentration-dependent acquisition of neural cell identity during in vitro differentiation of mouse embryonic stem cells.', *Developmental biology*, 275(1), pp. 124–42. doi: 10.1016/j.ydbio.2004.07.038.

Okano, H. and Yamanaka, S. (2014) 'iPS cell technologies: significance and applications to CNS regeneration and disease.', *Molecular brain*. Molecular Brain, 7(1), p. 22. doi: 10.1186/1756-6606-7-22.

Okita, K. *et al.* (2008) 'Generation of mouse induced pluripotent stem cells without viral vectors.', *Science (New York, N.Y.)*, 322(5903), pp. 949–53. doi: 10.1126/science.1164270.

Okita, K. *et al.* (2013) 'An efficient nonviral method to generate integration-free human-induced pluripotent stem cells from cord blood and peripheral blood cells.', *Stem cells (Dayton, Ohio)*, 31(3), pp. 458–66. doi: 10.1002/stem.1293.

Ono, Y. *et al.* (2007) 'Differences in neurogenic potential in floor plate cells along an anteroposterior location: midbrain dopaminergic neurons originate from mesencephalic floor plate cells.', *Development (Cambridge, England)*, 134(17), pp. 3213–25. doi: 10.1242/dev.02879.

Pakkenberg, B. *et al.* (2003) 'Aging and the human neocortex', *Experimental Gerontology*, 38(1–2), pp. 95–99. doi: 10.1016/S0531-5565(02)00151-1.

Palazzolo, G. *et al.* (2015) 'Ultrasoft Alginate Hydrogels Support Long-Term Three-Dimensional Functional Neuronal Networks.', *Tissue engineering. Part A*, 21(15–16), pp. 2177–85. doi: 10.1089/ten.TEA.2014.0518.

Pamies, D., Hartung, T. and Hogberg, H. T. (2014) 'Biological and medical applications of a brain-on-a-chip.', *Experimental biology and medicine (Maywood, N.J.)*, 239(9), pp. 1096–107. doi: 10.1177/1535370214537738.

Pang, Z. P. *et al.* (2011) 'Induction of human neuronal cells by defined transcription factors.', *Nature*, 476(7359), pp. 220–3. doi: 10.1038/nature10202.

Panman, L. *et al.* (2011) 'Transcription factor-induced lineage selection of stem-cell-derived neural progenitor cells.', *Cell stem cell*. Elsevier Inc., 8(6), pp. 663–75. doi: 10.1016/j.stem.2011.04.001.

Parent, J. M. and Anderson, S. a (2015) 'Reprogramming patient-derived cells to study the epilepsies.', *Nature neuroscience*, 18(3), pp. 360–6. doi: 10.1038/nn.3944.

Park, I.-H. *et al.* (2008) 'Disease-specific induced pluripotent stem cells.', *Cell*, 134(5), pp. 877–86. doi: 10.1016/j.cell.2008.07.041.

Parmar, M. and Li, M. (2007) 'Early specification of dopaminergic phenotype during ES cell differentiation.', *BMC developmental biology*, 7, p. 86. doi: 10.1186/1471-213X-7-86.

Paşca, A. M. *et al.* (2015) 'Functional cortical neurons and astrocytes from human pluripotent stem cells in 3D culture', *Nat Methods.*, 12(7), pp. 671–678. doi: 10.1038/nmeth.3415.

Patel, N. and Poo, M. M. (1982) 'Orientation of neurite growth by extracellular electric fields.', *The Journal of neuroscience : the official journal of the Society for Neuroscience*, 2(4), pp. 483–496.

Pautot, S., Wyart, C. and Isacoff, E. Y. (2008) 'Colloid-guided assembly of oriented 3D neuronal networks.', *Nature methods*, 5(8), pp. 735–40. doi: 10.1038/nmeth.1236.

Perrier, A. L. *et al.* (2004) 'Derivation of midbrain dopamine neurons from human embryonic stem cells.', *Proceedings of the National Academy of Sciences*, 101(11), pp. 12543–12548. doi: 10.1073/pnas.0404700101.

Perrone-Bizzozero, N. I., Cansino, V. V and Kohn, D. T. (1993) 'Posttranscriptional regulation of GAP-43 gene expression in PC12 cells through protein kinase C-dependent stabilization of the mRNA.', *The Journal of cell biology*, 120(5), pp. 1263–70.

Petros, T. J., Tyson, J. a and Anderson, S. a (2011) 'Pluripotent stem cells for the study of CNS development.', *Frontiers in molecular neuroscience*, 4(October), p. 30. doi: 10.3389/fnmol.2011.00030.

Pierani, A. *et al.* (1999) 'A sonic hedgehog-independent, retinoid-activated pathway of neurogenesis in the ventral spinal cord.', *Cell*, 97(7), pp. 903–15.

Prè, D. *et al.* (2014) 'A Time Course Analysis of the Electrophysiological Properties of Neurons Differentiated from Human Induced Pluripotent Stem Cells (iPSCs).', *PloS one*, 9(7), p. e103418. doi: 10.1371/journal.pone.0103418.

Qian, X. *et al.* (2016) 'Brain-Region-Specific Organoids Using Mini-bioreactors for Modeling

ZIKV Exposure', *Cell*. Elsevier Inc., 165(5), pp. 1238–1254. doi: 10.1016/j.cell.2016.04.032.

Rajnicek, a, Britland, S. and McCaig, C. (1997) 'Contact guidance of CNS neurites on grooved quartz: influence of groove dimensions, neuronal age and cell type.', *Journal of cell science*, 110 (Pt 2, pp. 2905–2913.

Reynolds, B. a and Rietze, R. L. (2005) 'Neural stem cells and neurospheres--re-evaluating the relationship.', *Nature methods*, 2(5), pp. 333–6. doi: 10.1038/nmeth758.

Robinson, M., Douglas, S. and Michelle Willerth, S. (2017) 'Mechanically stable fibrin scaffolds promote viability and induce neurite outgrowth in neural aggregates derived from human induced pluripotent stem cells', *Scientific Reports*, 7(1), p. 6250. doi: 10.1038/s41598-017-06570-9.

Rowley, J. a., Madlambayan, G. and Mooney, D. J. (1999) 'Alginate hydrogels as synthetic extracellular matrix materials', *Biomaterials*, 20(1), pp. 45–53. doi: 10.1016/S0142-9612(98)00107-0.

Sakaguchi, H. *et al.* (2015) 'Generation of functional hippocampal neurons from self-organizing human embryonic stem cell-derived dorsomedial telencephalic tissue.', *Nat Commun.* Nature Publishing Group, 6, p. 8896. doi: 10.1038/ncomms9896.

Salero, E. and Hatten, M. E. (2007) 'Differentiation of ES cells into cerebellar neurons.', *Proceedings of the National Academy of Sciences of the United States of America*, 104, pp. 2997–3002. doi: 10.1073/pnas.0610879104.

Sánchez, C., Díaz-Nido, J. and Avila, J. (2000) 'Phosphorylation of microtubule-associated protein 2 (MAP2) and its relevance for the regulation of the neuronal cytoskeleton function', *Progress in Neurobiology*, 61(2), pp. 133–168. doi: 10.1016/S0301-0082(99)00046-5.

Schmidt, C. E. *et al.* (1997) 'Stimulation of neurite outgrowth using an electrically conducting polymer.', *Proceedings of the National Academy of Sciences of the United States of America*, 94(17), pp. 8948–8953. doi: 10.1073/pnas.94.17.8948.

Schuurman, W. *et al.* (2013) 'Gelatin-methacrylamide hydrogels as potential biomaterials for fabrication of tissue-engineered cartilage constructs', *Macromolecular Bioscience*, 13(5), pp. 551–561. doi: 10.1002/mabi.201200471.

Schwab, A. J. and Ebert, A. D. (2015) 'Neurite Aggregation and Calcium Dysfunction in iPSC-

Derived Sensory Neurons with Parkinson's Disease-Related LRRK2 G2019S Mutation', *Stem Cell Reports*. The Authors, 5(6), pp. 1039–1052. doi: 10.1016/j.stemcr.2015.11.004.

Shaltouki, A. *et al.* (2013) 'Efficient generation of astrocytes from human pluripotent stem cells in defined conditions', *Stem Cells*, 31(5), pp. 941–952. doi: 10.1002/stem.1334.

Shi, Y. *et al.* (2012) 'Human cerebral cortex development from pluripotent stem cells to functional excitatory synapses.', *Nature neuroscience*. Nature Publishing Group, 15(3), pp. 477–86, S1. doi: 10.1038/nn.3041.

Shi, Y., Kirwan, P. and Livesey, F. J. (2012) 'Directed differentiation of human pluripotent stem cells to cerebral cortex neurons and neural networks.', *Nature protocols*, 7(10), pp. 1836–46. doi: 10.1038/nprot.2012.116.

Shimada, T. *et al.* (2012) 'A simplified method to generate serotonergic neurons from mouse embryonic stem and induced pluripotent stem cells.', *Journal of neurochemistry*, 122(1), pp. 81–93. doi: 10.1111/j.1471-4159.2012.07724.x.

Shin, S. *et al.* (2006) 'Long-term proliferation of human embryonic stem cell-derived neuroepithelial cells using defined adherent culture conditions.', *Stem cells (Dayton, Ohio)*, 24(1), pp. 125–38. doi: 10.1634/stemcells.2004-0150.

Smith, J. R. *et al.* (2008) 'Inhibition of Activin/Nodal signaling promotes specification of human embryonic stem cells into neuroectoderm.', *Developmental biology*, 313(1), pp. 107–17. doi: 10.1016/j.ydbio.2007.10.003.

Soldner, F. *et al.* (2009) 'Parkinson's Disease Patient-Derived Induced Pluripotent Stem Cells Free of Viral Reprogramming Factors', *Cell*. Elsevier Ltd, 136(5), pp. 964–977. doi: 10.1016/j.cell.2009.02.013.

Somaa, F. A. *et al.* (2017) 'Peptide-Based Scaffolds Support Human Cortical Progenitor Graft Integration to Reduce Atrophy and Promote Functional Repair in a Model of Stroke', *Cell Reports*. ElsevierCompany., 20(8), pp. 1964–1977. doi: 10.1016/j.celrep.2017.07.069.

Song, K. *et al.* (2014) 'In vitro culture and oxygen consumption of NSCs in size-controlled neurospheres of Ca-alginate/gelatin microbead.', *Materials science & engineering. C, Materials for biological applications*. Elsevier B.V., 40, pp. 197–203. doi: 10.1016/j.msec.2014.03.028.

Sood, D. *et al.* (2016) 'Fetal brain extracellular matrix boosts neuronal network formation in

3D bioengineered model of cortical brain tissue.', *ACS biomaterials science & engineering*, 2(1), pp. 131–140. doi: 10.1021/acsbiomaterials.5b00446.

Soundararajan, P. *et al.* (2007) 'Easy and rapid differentiation of embryonic stem cells into functional motoneurons using sonic hedgehog-producing cells.', *Stem cells (Dayton, Ohio)*, 25(7), pp. 1697–706. doi: 10.1634/stemcells.2006-0654.

Stadtfeld, M. *et al.* (2008) 'Induced pluripotent stem cells generated without viral integration.', *Science (New York, N.Y.)*, 322(5903), pp. 945–9. doi: 10.1126/science.1162494.

Stanslowsky, N. *et al.* (2014) 'Functional differentiation of midbrain neurons from human cord blood-derived induced pluripotent stem cells.', *Stem cell research & therapy*. Stem Cell Research & Therapy, 5(2), p. 35. doi: 10.1186/scrt423.

Su, H.-L. *et al.* (2006) 'Generation of cerebellar neuron precursors from embryonic stem cells.', *Developmental biology*, 290(2), pp. 287–96. doi: 10.1016/j.ydbio.2005.11.010.

Sundararaghavan, H. G. *et al.* (2009) 'Neurite growth in 3D collagen gels with gradients of mechanical properties.', *Biotechnology and bioengineering*, 102(2), pp. 632–43. doi: 10.1002/bit.22074.

Sundberg, M. *et al.* (2010) 'Production and isolation of NG2+ oligodendrocyte precursors from human embryonic stem cells in defined serum-free medium.', *Stem cell research*. Elsevier B.V., 5(2), pp. 91–103. doi: 10.1016/j.scr.2010.04.005.

Swindle-Reilly, K. E. *et al.* (2012) 'The impact of laminin on 3D neurite extension in collagen gels', *Journal of Neural Engineering*, 9(4), p. 046007. doi: 10.1088/1741-2560/9/4/046007.

Swistowski, A. *et al.* (2010) 'Efficient generation of functional dopaminergic neurons from human induced pluripotent stem cells under defined conditions.', *Stem cells (Dayton, Ohio)*, 28(10), pp. 1893–904. doi: 10.1002/stem.499.

Takahashi, K. *et al.* (2007) 'Induction of pluripotent stem cells from adult human fibroblasts by defined factors.', *Cell*, 131(5), pp. 861–72. doi: 10.1016/j.cell.2007.11.019.

Takahashi, K. and Yamanaka, S. (2006) 'Induction of pluripotent stem cells from mouse embryonic and adult fibroblast cultures by defined factors.', *Cell*, 126(4), pp. 663–76. doi: 10.1016/j.cell.2006.07.024.

Tamaoki, N. *et al.* (2010) 'Dental pulp cells for induced pluripotent stem cell banking.', *Journal of dental research*, 89(8), pp. 773–8. doi: 10.1177/0022034510366846.

Tang-Schomer, M. D. *et al.* (2014) 'Bioengineered functional brain-like cortical tissue', *Proceedings of the National Academy of Sciences*, 111(38), pp. 13811–13816. doi: 10.1073/pnas.1324214111.

Teixeira, A. I. *et al.* (2009) 'The promotion of neuronal maturation on soft substrates.', *Biomaterials*, 30(27), pp. 4567–72. doi: 10.1016/j.biomaterials.2009.05.013.

Theka, I. *et al.* (2013) 'Rapid generation of functional dopaminergic neurons from human induced pluripotent stem cells through a single-step procedure using cell lineage transcription factors.', *Stem cells translational medicine*, 2(6), pp. 473–9. doi: 10.5966/sctm.2012-0133.

Thomas, M. and Willerth, S. M. (2017) '3-D Bioprinting of Neural Tissue for Applications in Cell Therapy and Drug Screening', *Frontiers in Bioengineering and Biotechnology*, 5(November), pp. 1–11. doi: 10.3389/fbioe.2017.00069.

Thompson, B. C. *et al.* (2010) 'Conducting polymers, dual neurotrophins and pulsed electrical stimulation - Dramatic effects on neurite outgrowth', *Journal of Controlled Release*. Elsevier B.V., 141(2), pp. 161–167. doi: 10.1016/j.jconrel.2009.09.016.

Thomson, J. A. *et al.* (1998) 'Embryonic stem cell lines derived from human blastocysts.', *Science (New York, N.Y.)*, 282(5391), pp. 1145–7.

Vazin, T. *et al.* (2009) 'A novel combination of factors, termed SPIE, which promotes dopaminergic neuron differentiation from human embryonic stem cells.', *PloS one*, 4(8), p. e6606. doi: 10.1371/journal.pone.0006606.

Velasco, I. *et al.* (2014) 'Concise Review: Generation of Neurons From Somatic Cells of Healthy Individuals and Neurological Patients Through Induced Pluripotency or Direct Conversion', *Stem Cells*, 32(11), pp. 2811–2817. doi: 10.1002/stem.1782.

Vierbuchen, T. *et al.* (2010) 'Direct conversion of fibroblasts to functional neurons by defined factors.', *Nature*, 463(7284), pp. 1035–41. doi: 10.1038/nature08797.

Wang, H. B. *et al.* (2010) 'Varying the diameter of aligned electrospun fibers alters neurite outgrowth and Schwann cell migration.', *Acta biomaterialia*, 6(8), pp. 2970–8. doi: 10.1016/j.actbio.2010.02.020.

Wang, L. *et al.* (2013) 'Generation of integration-free neural progenitor cells from cells in human urine.', *Nature methods*, 10(1), pp. 84–9. doi: 10.1038/nmeth.2283.

Wang, T.-W. and Spector, M. (2009) 'Development of hyaluronic acid-based scaffolds for brain tissue engineering.', *Acta biomaterialia*. Acta Materialia Inc., 5(7), pp. 2371–84. doi: 10.1016/j.actbio.2009.03.033.

Warren, L. *et al.* (2010) 'Highly efficient reprogramming to pluripotency and directed differentiation of human cells with synthetic modified mRNA.', *Cell stem cell*, 7(5), pp. 618–30. doi: 10.1016/j.stem.2010.08.012.

Watanabe, K. *et al.* (2005) 'Directed differentiation of telencephalic precursors from embryonic stem cells', *Nat Neurosci*, 8(3), pp. 288–296. doi: 10.1038/nn1402.

Williams, C. G. *et al.* (2005) 'Variable cytocompatibility of six cell lines with photoinitiators used for polymerizing hydrogels and cell encapsulation', *Biomaterials*, 26(11), pp. 1211–1218. doi: 10.1016/j.biomaterials.2004.04.024.

Williams, E. C. *et al.* (2014) 'Mutant astrocytes differentiated from Rett syndrome patients-specific iPSCs have adverse effects on wildtype neurons', *Human Molecular Genetics*, 23(11), pp. 2968–2980. doi: 10.1093/hmg/ddu008.

Won, J. H. *et al.* (2015) 'DA-9801 promotes neurite outgrowth via ERK1/2-CREB pathway in PC12 cells.', *Biological & pharmaceutical bulletin*, 38(2), pp. 169–78. doi: 10.1248/bpb.b14-00236.

Xia, H. *et al.* (2014) 'Directed neurite growth of rat dorsal root ganglion neurons and increased colocalization with Schwann cells on aligned poly(methyl methacrylate) electrospun nanofibers.', *Brain research*. Elsevier, 1565, pp. 18–27. doi: 10.1016/j.brainres.2014.04.002.

Xie, J. *et al.* (2010) 'Electrospun nanofibers for neural tissue engineering.', *Nanoscale*, 2(1), pp. 35–44. doi: 10.1039/b9nr00243j.

Xing, D., Ma, L. and Gao, C. (2014) 'Synthesis of functionalized poly(ester carbonate) with laminin-derived peptide for promoting neurite outgrowth of PC12 cells.', *Macromolecular bioscience*, 14(10), pp. 1429–36. doi: 10.1002/mabi.201400186.

Xu, T. *et al.* (2009) 'Electrophysiological characterization of embryonic hippocampal neurons cultured in a 3D collagen hydrogel', *Biomaterials*. Elsevier Ltd, 30(26), pp. 4377–

4383. doi: 10.1016/j.biomaterials.2009.04.047.

Xue, Y. *et al.* (2013) 'Generating a non-integrating human induced pluripotent stem cell bank from urine-derived cells.', *PloS one*, 8(8), p. e70573. doi: 10.1371/journal.pone.0070573.

Yamaguchi, T. P. (2001) 'Heads or tails: Wnts and anterior-posterior patterning.', *Current biology : CB*, 11(17), pp. R713-24. doi: 10.1016/S0960-9822(01)00417-1.

Yang, F. *et al.* (2005) 'Electrospinning of nano/micro scale poly(l-lactic acid) aligned fibers and their potential in neural tissue engineering', *Biomaterials*, 26(15), pp. 2603–2610. doi: 10.1016/j.biomaterials.2004.06.051.

Yang, K. *et al.* (2014) 'Multiscale, hierarchically patterned topography for directing human neural stem cells into functional neurons.', *ACS nano*, 8(8), pp. 7809–22. doi: 10.1021/nn501182f.

Ye, W. *et al.* (1998) 'FGF and Shh signals control dopaminergic and serotonergic cell fate in the anterior neural plate.', *Cell*, 93(5), pp. 755–66. doi: 10.1016/S0092-8674(00)81437-3.

Ylä-Outinen, L. *et al.* (2014) 'Three-dimensional growth matrix for human embryonic stem cell-derived neuronal cells.', *Journal of tissue engineering and regenerative medicine*, 8(3), pp. 186–94. doi: 10.1002/term.1512.

Yu, D. X. *et al.* (2014) 'Modeling hippocampal neurogenesis using human pluripotent stem cells', *Stem Cell Reports*. The Authors, 2(3), pp. 295–310. doi: 10.1016/j.stemcr.2014.01.009.

Yu, D. X., Marchetto, M. C. and Gage, F. H. (2014) 'How to make a hippocampal dentate gyrus granule neuron.', *Development (Cambridge, England)*, 141(12), pp. 2366–75. doi: 10.1242/dev.096776.

Yu, J. *et al.* (2007) 'Induced pluripotent stem cell lines derived from human somatic cells.', *Science (New York, N.Y.)*, 318(5858), pp. 1917–20. doi: 10.1126/science.1151526.

Yu, J. *et al.* (2009) 'Human induced pluripotent stem cells free of vector and transgene sequences.', *Science (New York, N.Y.)*, 324(5928), pp. 797–801. doi: 10.1126/science.1172482.

Yuan, S. H. *et al.* (2011) 'Cell-surface marker signatures for the isolation of neural stem

cells, glia and neurons derived from human pluripotent stem cells.', *PloS one*, 6(3), p. e17540. doi: 10.1371/journal.pone.0017540.

Zeng, H. *et al.* (2010) 'Specification of region-specific neurons including forebrain glutamatergic neurons from human induced pluripotent stem cells.', *PloS one*, 5(7), p. e11853. doi: 10.1371/journal.pone.0011853.

Zeng, X. *et al.* (2004) 'Dopaminergic differentiation of human embryonic stem cells.', *Stem cells (Dayton, Ohio)*, 22(6), pp. 925–40. doi: 10.1634/stemcells.22-6-925.

Zhang, D. *et al.* (2014) 'A 3D Alzheimer's disease culture model and the induction of P21-activated kinase mediated sensing in iPSC derived neurons.', *Biomaterials*. Elsevier Ltd, 35(5), pp. 1420–8. doi: 10.1016/j.biomaterials.2013.11.028.

Zhang, M. *et al.* (2016) 'Pharmacological Reprogramming of Fibroblasts into Neural Stem Cells by Signaling-Directed Transcriptional Activation.', *Cell stem cell*, 18(5), pp. 653–67. doi: 10.1016/j.stem.2016.03.020.

Zhang, Q.-Y. *et al.* (2014) 'Stiff substrates enhance cultured neuronal network activity.', *Scientific reports*, 4, p. 6215. doi: 10.1038/srep06215.

Zhang, X. *et al.* (2010) 'Pax6 is a human neuroectoderm cell fate determinant', *Cell Stem Cell*. Elsevier Ltd, 7(1), pp. 90–100. doi: 10.1016/j.stem.2010.04.017.

Zhang, Y. *et al.* (2013) 'Rapid single-step induction of functional neurons from human pluripotent stem cells.', *Neuron*, 78(5), pp. 785–98. doi: 10.1016/j.neuron.2013.05.029.

Zhang, Y. S. *et al.* (2017) '3D Bioprinting for Tissue and Organ Fabrication.', *Annals of biomedical engineering*, 45(1), pp. 148–163. doi: 10.1007/s10439-016-1612-8.

Zhang, Z.-N. *et al.* (2016) 'Layered hydrogels accelerate iPSC-derived neuronal maturation and reveal migration defects caused by MeCP2 dysfunction', *Proceedings of the National Academy of Sciences*, 113(12), p. 201521255. doi: 10.1073/pnas.1521255113.

Zhou, H. *et al.* (2009) 'Generation of induced pluripotent stem cells using recombinant proteins.', *Cell stem cell*, 4(5), pp. 381–4. doi: 10.1016/j.stem.2009.04.005.

Zhou, S. *et al.* (2016) 'The positional identity of iPSC-derived neural progenitor cells along the anterior-posterior axis is controlled in a dosage-dependent manner by bFGF and EGF.', *Differentiation; research in biological diversity*. Elsevier, 92(4), pp. 183–194. doi:

10.1016/j.diff.2016.06.002.

Zhou, T. *et al.* (2012) 'Generation of human induced pluripotent stem cells from urine samples.', *Nature protocols*, 7(12), pp. 2080–9. doi: 10.1038/nprot.2012.115.

Zhou, W. and Freed, C. R. (2009) 'Adenoviral gene delivery can reprogram human fibroblasts to induced pluripotent stem cells.', *Stem cells (Dayton, Ohio)*, 27(11), pp. 2667–74. doi: 10.1002/stem.201.